PHYSICOCHEMICAL STUDY OF INCLUSION OF DRUG MOLECULES IN CYCLODEXTRINS

by

Devric Reginald Dodds

Thesis Presented for the Degree of
DOCTOR OF PHILOSOPHY
in the Department of Chemistry
Faculty of Science
UNIVERSITY OF CAPE TOWN

February 1999

ACKNOWLEDGEMENTS

My special thanks to :

Professor Mino Caira, for being an excellent and inspiring supervisor, as well as providing dedicated and invaluable guidance throughout my doctoral studies

Professor Luigi Nassimbeni for being a perennial source of enthusiasm and new ideas

Dr. Anita Coetzee for data-collections on the CAD4 diffractometer and for training me to operate the Kappa CCD diffractometer

Dr. Vivienne Griffith for sharing her wealth of experience with me in the early stages of my degree

The Foundation for Research and Development, the University of Cape Town and South African Druggists International for financial support

My parents, Reginald and Cheryl and brother, Donovan for their love and support at all times

PUBLICATIONS, PATENTS AND CONFERENCES

Parts of this thesis have been published :

1.) Inclusion of nonopiate drugs in cyclodextrins. I. X-ray structure of a 1:1 β-cyclodextrin-*p*-bromoacetanilide complex.
M. R. Caira and D. R. Dodds, *J. Inclusion Phenom. Mol. Recognit.* 1999, Vol. 5, in press.

2.) Inclusion of nonopiate analgesic drugs in cyclodextrins. II. X-ray structure of a 1:1 β-cyclodextrin-acetaminophen complex.
M. R. Caira and D. R. Dodds, *J. Inclusion Phenom. Mol. Recognit.*
Under review, May 1999.

Parts of this thesis have been included in the following patent application :

1.) L. J. Penkler and D. R. Dodds, Cyclodextrin-cyclizine complexes, SA Patent Application 99/2097, 16 March 1999, 15 pp.

Parts of this thesis have been presented at the following conferences :

1.) *The First International Conference on Pharmaceutical and Pharmacological Sciences (South Africa), Midrand, Gauteng*, 22-25 September 1996.
M. R. Caira, D. R. Dodds and L. R. Nassimbeni, Inclusion of Phenacetin, Paracetamol and *p*-Bromoacetanilide in β-Cyclodextrin : Thermal Analysis and X-Ray Diffraction.
Lecture for the Farmacia Upjohn Young Scientist Award.

2.) *Pharmaceutical Applications of Cyclodextrins Conference, Lawrence, Kansas, U.S.A.*, 29 June-2 July 1997.
M. R. Caira, D. R. Dodds and L. R. Nassimbeni, Solid State Structures and Properties of β-Cyclodextrin Complexes of Three Nonopiate Analgesic Drugs.

3.) *Molecular Design and Synthesis, U.C.T. Research Conference, University of Cape Town*, 3-4 April 1997.

D. R. Dodds, Cyclodextrin Inclusion of Analgesics.

4.) The 19th Annual Conference of the Academy of Pharmaceutical Sciences, Durban, South Africa, 28 June - 1 July 1998.

D. R. Dodds, M. R. Caira and L. R. Nassimbeni, Thermal, X-ray and Solubility Studies of β-cyclodextrin Complexes of Paracetamol and Paracetamol Acetate.

Lecture for the Farmacia Upjohn Young Scientist Award.

5.) *The 7th International Chemistry Conference in Africa & The 34th Convention of the South African Chemical Institute, Durban, South Africa*, 6 - 10 July 1998.

D. R. Dodds, M. R. Caira and L. R. Nassimbeni, Analgesics as Guests in Cyclodextrin Inclusion: Physicochemical and Structural Characterisation of Solid Inclusion Complexes.

ABSTRACT

Inclusion of drug molecules in cyclodextrins can significantly improve various aspects of their performance and has resulted in the use of cyclodextrins (CDs) for a wide variety of pharmaceutical applications. Consequently, the cyclodextrin inclusion of drugs has received great interest in the pharmaceutical and chemical fields.

For this study the inclusion of nine pharmaceutical drugs with CDs was investigated in the solid state. The objectives of the study were i.) the preparation, ii.) determination of the chemical composition, iii.) analysis of thermal behaviour and iv.) investigation of the solid state features of the complexes. Ultraviolet spectrophotometry, elemental analysis and thermogravimetric analysis were the principal techniques used for determination of composition. Hot stage microscopy, differential scanning calorimetry and thermogravimetric analysis were the principal techniques used for the analysis of thermal behaviour. Single crystal x-ray diffraction and x-ray powder diffraction were the principal techniques used for investigation of structural features.

This thesis reports the preparation by crystallisation from solution of eight beta cyclodextrin (β-CD) and four gamma cyclodextrin (γ-CD) inclusion complexes with selected drugs as guests, as well as the determination of their chemical compositions and analysis of their thermal behaviours. Investigation of the structural features of these complexes includes the determination of the crystal structures of five β-CD complexes and one γ-CD complex. The preparation of hydroxypropyl-β-CD complexes by kneading and co-grinding is also reported.

The β-CD complexes with the analgesic/antipyretic drugs acetaminophen, *p*-bromoacetanilide, diacetamate and phenacetin were prepared. The dissolution rates of acetaminophen and diacetamate were increased for the CD complexes compared to the free drugs and physical mixtures. Thermal analysis of the four complexes showed differences in thermal behaviour and stability. The complexes were all 1:1 host to guest complexes but the crystal structures revealed different modes of inclusion and

packing arrangements for the four structurally related *para*-substituted acetanilides. The included guests were disordered in various ways and their disordered arrangements were successfully modelled.

Crystalline inclusion complexes of the anti-ulcerative drugs cimetidine, famotidine and ranitidine, with β- and γ-cyclodextrin were prepared. The β-CD complexes are all 2:1 β-CD:drug complexes while the complexes with γ-CD were all 3:2 γ-CD:drug complexes. The thermal behaviours of the complexes suggest that the stability of the complexes is dependent on the stability of the included drug molecules. XRD and DSC techniques were principally used to investigate solid state properties of the complexes which were observed in all cases to differ from physical mixtures of their constituents.

The solid state preparation of hydroxypropyl-β-cyclodextrin (HP-β-CD) complexes with salbutamol laurate by manual co-grinding, mechanical co-grinding and kneading is reported. The HP-β-CD complex of this new salt of salbutamol is intended for commercial application as a sublingual dosage form. The characterisation of two polymorphic forms of salbutamol laurate and interaction of the drug with HP-β-CD were demonstrated by various physicochemical techniques.

The β- and γ-cyclodextrin complexes with the antiemetic cyclizine were prepared. The thermal behaviours of the two complexes were found to be very similar. The β-cyclodextrin complex displayed the unusual stoichiometric ratio of three cyclizine molecules to four β-cyclodextrin molecules. The piperazine ring is embedded in the β-cyclodextrin cavity; however, an unusual feature of the complex is that inclusion of the drug from both the primary and secondary ends of the β-CD molecule is observed. The γ-cyclodextrin complex crystallised as a trimer with the familiar channel-type packing arrangement and a stoichiometric ratio of one cyclizine molecule to three γ-cyclodextrin molecules. The cyclizine molecule displays disorder in the γ-cyclodextrin cavity; this disorder has been modelled appropriately. The piperazine ring of cyclizine is included from the wider secondary rim of the γ-CD cavity.

ABBREVIATIONS AND SYMBOLS

Drugs

ACE	:	Acetaminophen
BRO	:	*p*-Bromoacetanilide
PHE	:	Phenacetin
DIA	:	Diacetamate
CIM	:	Cimetidine
FAM	:	Famotidine
RAN	:	Ranitidine
SAL	:	Salbutamol laurate
CYC	:	Cyclizine

Cyclodextrins

CD	:	Cyclodextrin
β-CD	:	Beta-cyclodextrin
γ-CD	:	Gamma-cyclodextrin
HP-β-CD	:	Hydroxypropyl-beta-cyclodextrin

Drug-CD Complexes

ACEBCD	:	Acetaminophen-β-cyclodextrin complex
BROBCD	:	*p*-Bromoacetanilide-β-cyclodextrin complex
PHEBCD	:	Phenacetin-β-cyclodextrin complex
DIABCD	:	Diacetamate-β-cyclodextrin complex
CIMBCD	:	Cimetidine-β-cyclodextrin complex
CIMGCD	:	Cimetidine-γ-cyclodextrin complex
FAMBCD	:	Famotidine-β-cyclodextrin complex
FAMGCD	:	Famotidine-γ-cyclodextrin complex
RANBCD	:	Ranitidine-β-cyclodextrin complex
RANGCD	:	Ranitidine-γ-cyclodextrin complex
CYCBCD	:	Cyclizine-β-cyclodextrin complex
CYCGCD	:	Cyclizine-γ-cyclodextrin complex

Techniques

DSC	:	Differential scanning calorimetry
TGA	:	Thermogravimetric analysis
UV	:	Ultraviolet spectroscopy
IR	:	Infrared spectroscopy
HSM	:	Hot stage microscopy
XRD	:	X-ray powder diffraction
SEM	:	Scanning electron microscopy

Other Symbols

H	:	Host
G	:	Guest
W	:	Water
M_r	:	Molecular weight
T	:	Temperature
V	:	Volume of unit cell
Z	:	Number of formula units per unit cell
e.s.d.	:	estimated standard deviation
s.o.f.	:	site occupancy factor
RMS	:	Root-mean-squared deviation
CSD	:	Cambridge Structural Database

TABLE OF CONTENTS

CHAPTER 1 : INTRODUCTION

Natural origin of CDs

When the amylose fraction of starch is degraded by glucosyltransferases, some turns of the amylose helix are removed by hydrolysis and their ends joined together to form the cyclic oligosaccharides which have become known as cyclodextrins.[1] The enzymes are not very specific and thus produce a family of cycloamyloses containing different numbers of glucopyranose units. The most abundant of the cyclodextrins produced naturally are α-, β- and γ-cyclodextrin consisting of 6, 7 and 8 glucopyranose units respectively (Figure 1.1). The enzyme which produces cyclodextrins is a bacterial amylase called cyclodextrin glucosyltransferase (CGTase) which was first isolated from *Bacillus macerans*. Naturally occurring cyclodextrins consisting of 9(δ-CD), 10(ε-CD), 12(η-CD), 14(ι-CD) and even exceeding 17 glucopyranose units have been isolated from the action of various bacterial enzymes characterised.[2] Smaller cyclodextrins than α-CD would be sterically strained and are therefore not produced by the glucosyltransferase enzymes.

Historical overview of CDs

Discovery and Structure of CDs (1891-1930s)

1891 First reference to a substance, later found to be a cyclodextrin, published by Villiers[3]

1904 Schardinger notes the presence of two crystalline dextrins produced upon the degradation of starch by a microbe, which he isolates and names *Bacillus macerans*[4]

1904-1911 Schardinger publishes the fundamentals of cyclodextrin chemistry and characterises α- and β-dextrins[5-7]

1911-1935 Pringsheim publishes extensively on cyclodextrin chemistry and notes the high tendency of these molecules to form complexes with various organic compounds[8,9]

Study of CDs and their chemical and inclusion properties (1930s-1970s)

1930s Freudenberg et al. conclude that crystalline α- and β-dextrins consist of α-1,4-glycosidically linked glucopyranose units[10,11]

1936 Freudenberg et al. postulate the cyclic structure of these crystalline dextrins[12]

1948 γ-CD is discovered and its structure elucidated[13]

1953 Freudenberg, Cramer and Plieninger obtain first patent on CDs and describe the principles of CD application in drug formulations[14]

1954 Cramer publishes work on inclusion complex formation with CDs[15]

1957 French publishes the first review on CD chemistry including a reference to the alleged high toxicity of CDs[16]

1965 Monograph by Thoma and Stewart[17]

1968 Review of CD chemistry published by Caesar[18]

1960s Industrial possibilities of CDs show promise for a variety of applications

1957-1972 Many scientists deterred from developing CD-containing products for human use as a result of 1957 reference to the toxicity of cyclodextrins.

Industrial Production and Widespread Application of CDs (1970s onwards)

1970s Adequate toxicological studies show that there is no inherent toxicity of CDs and subsequent explosion in CD research

1972 Chinoin Pharmaceutical and Chemical Works (Hungary) launches a long-term CD research project

1981 First International Symposium on Cyclodextrins in Budapest which is followed by International CD symposium held every second year[19-27]

1988 Dr. József Szejtli establishes Cyclolab, the first company to exclusively produce and research cyclodextrins

1998 Number of CD-related publications exceeds 15000 and CD production is in excess of 1000 tons/year

2000 onwards The actual and potential uses of CDs in the pharmaceutical, food, cosmetics, chemical products and technological fields is predicted to show a steady increase. Significant new applications in the use of CDs are expected in biotechnology and in several other new industrial areas, such as the textile industry.[28]

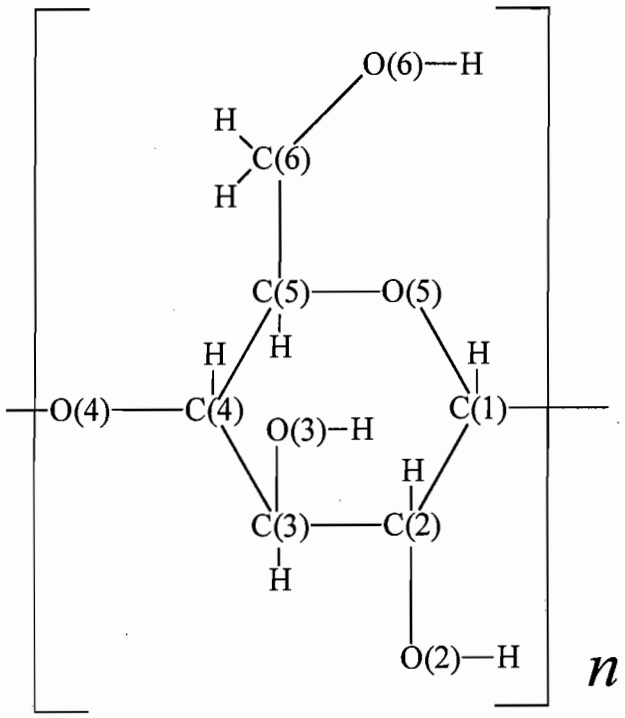

(a)

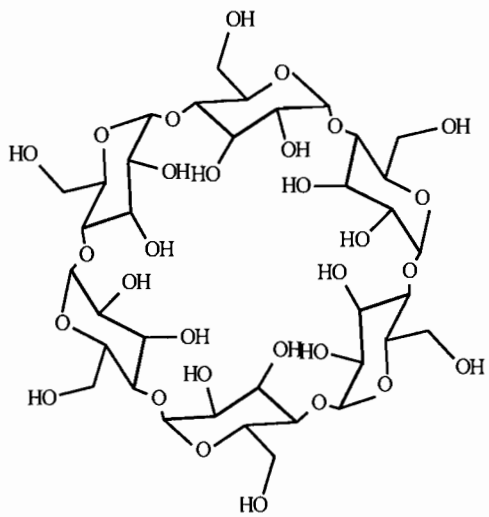

(b)

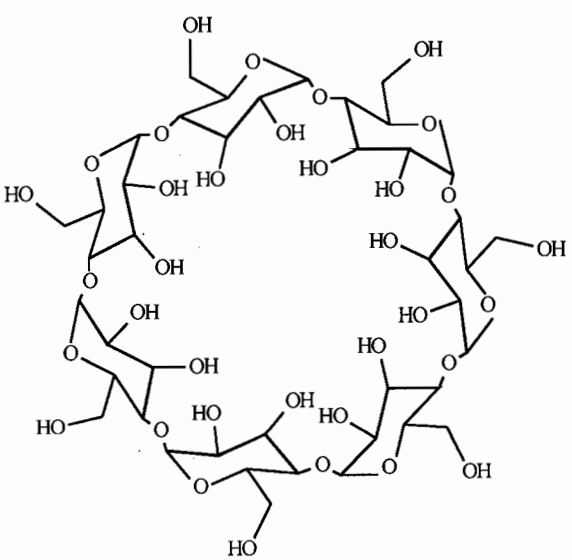

(c)

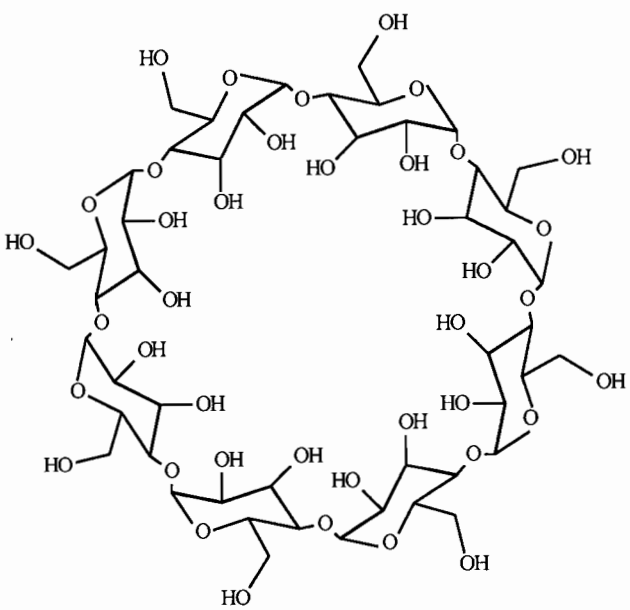

(d)

Figure 1.1 (a) The glucopyranose building block of CDs (n = 6, 7 and 8 for α-, β- and γ-CD respectively), (b) α-CD, (c) β-CD, (d) γ-CD

Structural features of CDs

The structural features of CDs will be discussed in terms of the three most commonly occurring native CDs. As already mentioned α-, β- and γ-CD are composed of 6, 7 and 8 glucose residues respectively. The glucose monomers are linked by α(1→4) glycosidic linkages and the pyranose rings all adopt the $^4C_1$ chair conformation.

A.) Principal torsion angles of CDs

The glucose monomers can be considered as fairly rigid building blocks; the only real conformational flexibility is the rotational freedom of the O6-H hydroxyl group around the axis of the C5-C6 bond and the limited rotational movements around the C1(n)-O4(n-1)-C4(n-1) glucosidic link (Figure 1.2).

Primary hydroxyl torsion angle

The primary hydroxyl or O5-C5-C6-O6 torsion angle (ω) can adopt three orientations namely (+)-*gauche*, (-)-*gauche* or *trans* conformations. The (-)-*gauche* orientation (ω = -60°) with the O6-H pointing away from the centre of the CD cavity is largely preferred; the (+)-*gauche* (ω = +60°) with the O6-H pointing toward the centre of the CD cavity is observed where a hydrogen bond is formed between the O6 hydroxyl group and an included guest molecule, while the *trans* orientation (ω = 180°) has not been observed for CD structures probably due to the adverse steric interactions which might occur between O6-H and atoms of the adjacent glucose residue. The absolute mean values of ω, as determined from x-ray diffraction studies, are listed for α-, β- and γ-CD in Table 1.1. The values are based on an analysis of the available crystal structures of the native CDs.[29]

Glycosidic torsion angles

The torsion angles around the C1(n)-O4(n-1)-C4(n-1) glycosidic linkage are referred to as the glycosidic torsion angles. The glycosidic torsion angles are defined as Φ = O5(n)-C1(n)-O4(n-1)-C4(n-1) and Ψ = C1(n)-O4(n-1)-C4(n-1)-C3(n-1). The mean values of these angles for α-, β- and γ-CD are listed in Table 1.1.

Pyranoid torsion angles

The two pyranoid torsion angles Θ1 (C2-C3-C4-C5) and Θ2 (C3-C4-C5-O5) can be used to describe the conformational relationships around the C4 atom of each glucose residue. The glucopyranose units invariably adopt the $^4C_1$ chair conformation with very small deviations from the ideal, undistorted values for a glucose residue (Table 1.1).

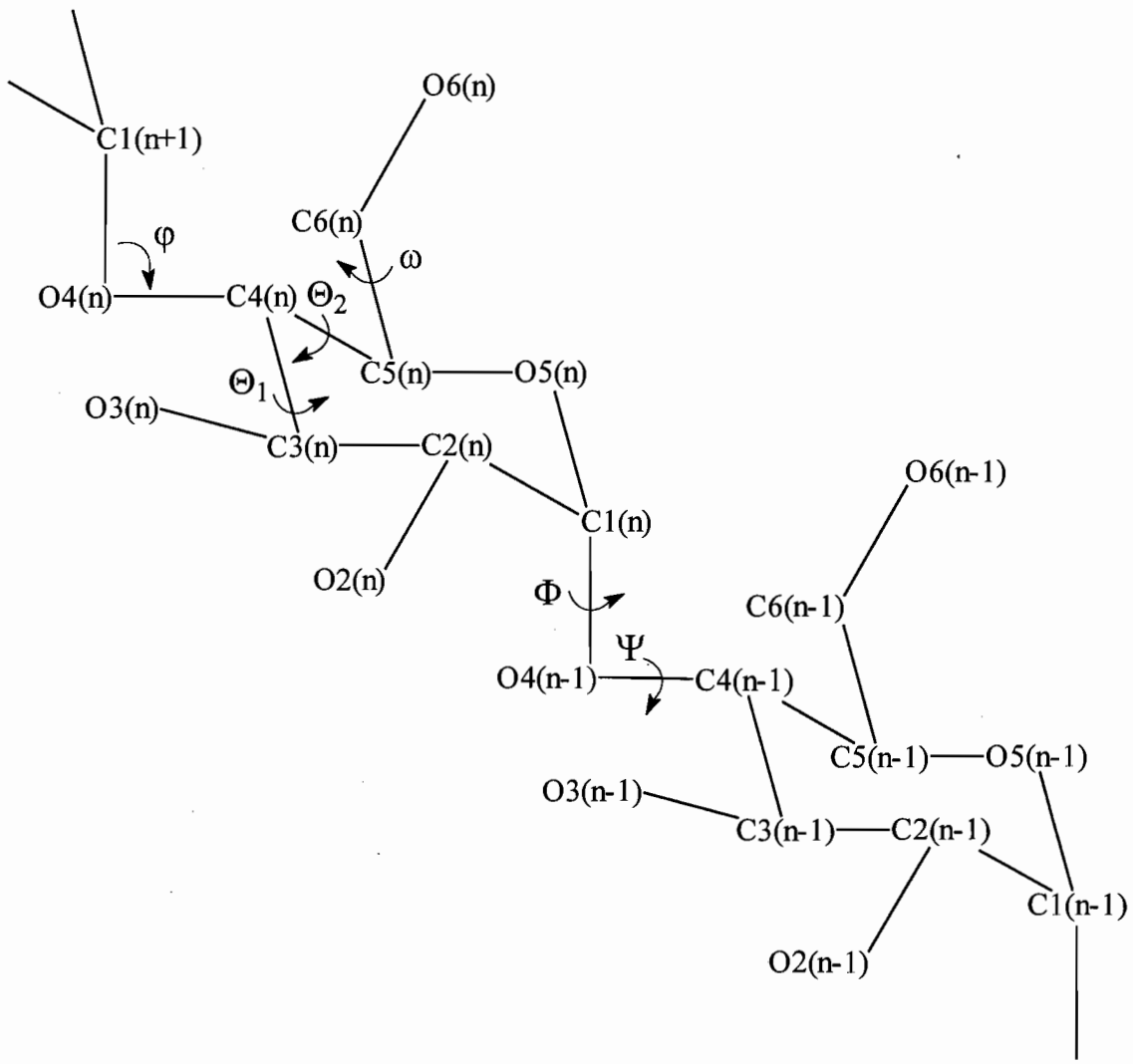

Figure 1.2 Numbering scheme and principal torsion angles of CD structures

Table 1.1 Mean values for principal torsion angles of CDs

CD	|ω| (°)[29]	Φ (°)[30]	Ψ (°)[30]	Θ_1 (°)[30]	Θ_2 (°)[30]
α	68	108	130	+52	-53
β	64	112	128	+56	-56
γ	68	110	130	+62	-62

B.) O4 Polygon

Polygons, composed of 6, 7 or 8 glycosidic O4 atoms offer a good model for describing the macrocyclic structures of α-, β- and γ-CD.

Figure 1.3 illustrates the various geometrical parameters of the O4 polygon. The side lengths (*l*) of the O4 polygon are the distances between O4(n) and O4(n+1), where O4(n+1) is the O4 atom of the next glucose unit. The radii (*r*) of the macrocycle are measured from the centre of gravity (C) of all O4 atoms to each O4 atom. The angle (*a*) is the O4(n)···O4(n+1)···O4(n+2) angle.

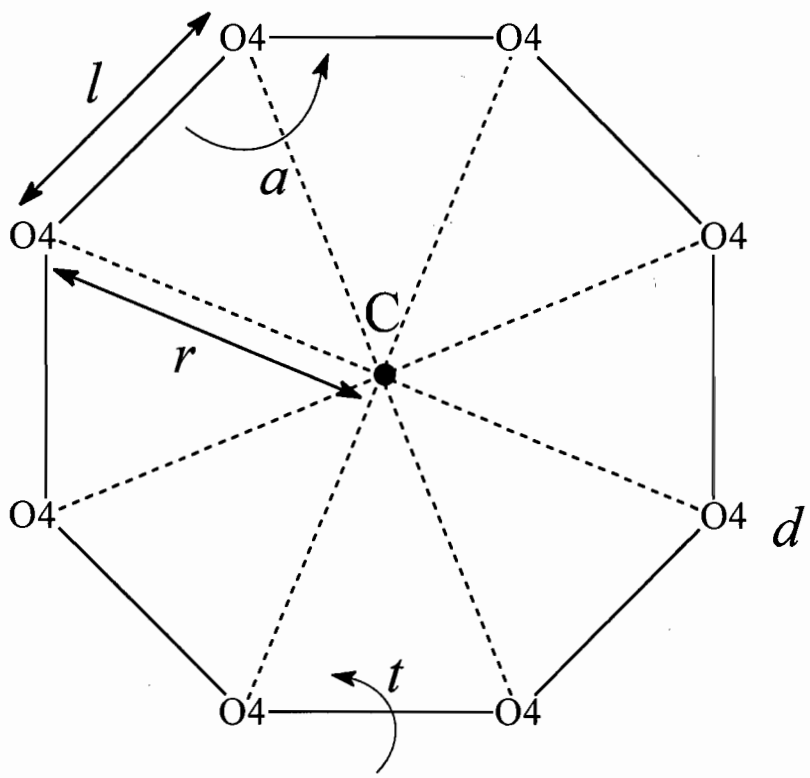

Figure 1.3 Principal geometrical parameters of the O4 polygon

The O4 polygons also offer a means to evaluate (i) the symmetry of the macrocylic structure and (ii) the planarity of the macrocylic ring.

Macrocyclic symmetry

If the macrocyclic structure of α-, β- and γ-CD showed perfect C_6, C_7, C_8 symmetry then the O4···O4 side lengths (*l*) would all be equal, as would the radii (*r*). The O4···O4···O4 angles would be exactly 120°, 128° and 132° for α-, β- and γ-CD respectively.

Coplanarity of macrocycle

The coplanarity of the macrocyclic structure is best assessed by the coplanarity of the O4 linker atoms of the O4 polygon. This can be evaluated by the deviation from planarity (*d*) of each O4 atom from the mean plane of all the O4 atoms, and the O4···O4···O4···O4 torsion angles (*t*) (Figure 1.3). For a planar macrocycle the deviation of each O4 from the mean plane of the macrocycle would be zero and the O4···O4···O4···O4 torsion angles (*t*) would all be 0°.

The mean values of the principal geometrical parameters of the O4 polygons for α-, β- and γ-CD are shown in Table 1.2.

Table 1.2 The mean values of the principal geometrical parameters of the O4 polygon

CD	*r* (Å)[31]	*l* (Å)[31]	*a* (°)[29]	| *d* | (Å)[29]	| *t* | (°)[29]
α	4.2	4.2	120	0.07	5
β	5.0	4.3	128	0.08	5
γ	5.9	4.5	132	0.02	2

C.) Important conformational descriptors for CDs

Intersaccharidic bond angles

The intersaccharidic bond angle (φ) is defined as φ = C1(n+1)-O4(n)-C4(n) (Figure 1.2). The value of φ decreases in the order φ(α-CD) > φ(β-CD) > φ(γ-CD) as the number of glucose residues making up the macrocycle increases (Table 1.3).

Intramolecular O2(n)···O3(n-1) hydrogen bonds

The structural rigidity of the CD seems to be mainly due to a ring of intramolecular hydrogen bonds between the secondary hydroxyl groups (labelled O2-H and O3-H) of adjacent glucose units which are orientated *cis*. These O2(n)···O3(n-1) hydrogen bonds stabilise the macrocyclic conformation and limit the conformational freedom of the glucosidic bond. The mean O2(n)···O3(n-1) distances become smaller on increasing the macrocyclic ring size from six to seven to eight glucose units (Table 1.3).

Tilt angle

The tilt angle is described as a measure of the inclination of the glucose units with respect to the mean macrocyclic plane defined by the O4 linker atoms. Two definitions of the tilt angle are considered. The tilt-angle (τ_1) is defined as the angle made between the mean plane through the six pyranoid ring atoms (labelled C1, C2, C3, C4, C5 and O5) of each glucose unit and the normal to the O4 mean plane. The tilt angle, τ_1, is schematically illustrated in Figure 1.4 with the glucose residue and appropriate mean planes all viewed edge on. The tilt angle (τ_2) is defined as the angle made between the mean plane through O4, C4, C1 and O4` atoms and the O4 mean plane. The tilt angle, τ_2, is schematically illustrated in Figure 1.4 with the glucose residue and appropriate mean planes all viewed edge on. In theory, if the glucose residues were completely undistorted from ideal conformation then the two definitions of the tilt angle would produce identical values. In practice, however, the tilt angles obtained from these two definitions differ from one another because the formation of the macrocycle somewhat distorts the conformation around the glycosidic linkages. The tilt angle (τ_2) has been traditionally reported for a large number of crystallographic investigations of CD structures.

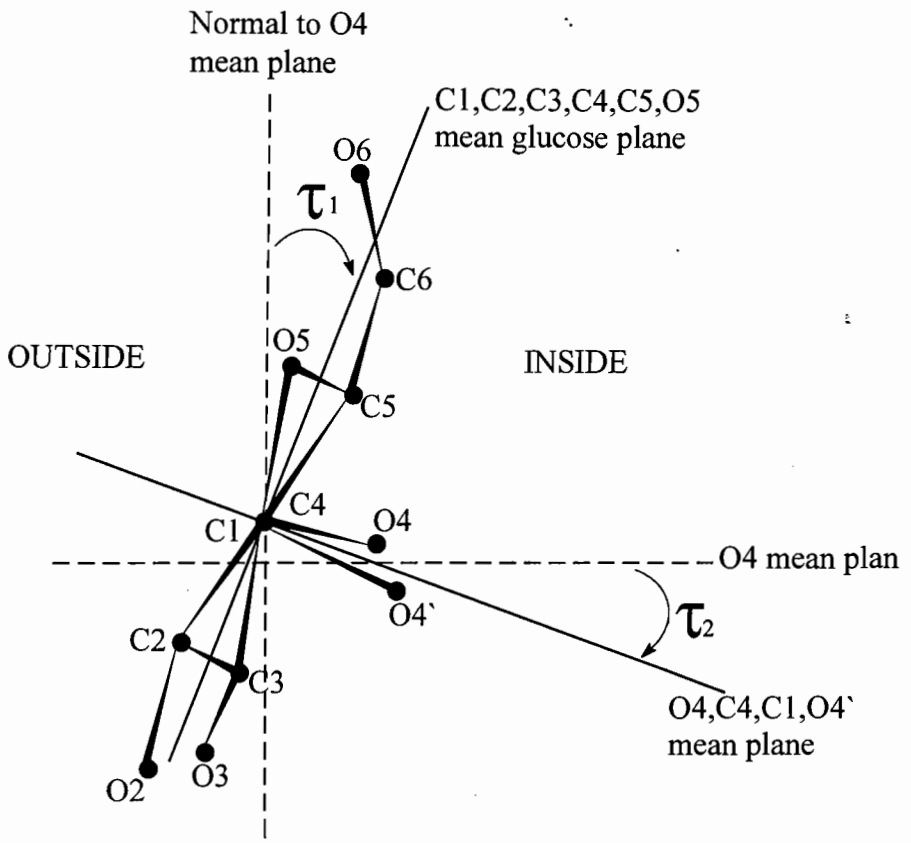

Figure 1.4 Schematic representation of the tilt angles τ_1 and τ_2 (the glucose and various mean planes are all viewed edge on)

Each glucose unit is not orthogonal to the mean O4 plane, but is inclined with the O6 side towards the inside or outside of the macrocycle. A positive tilt angle denotes that the glucose unit is inclined with the O6 side towards the inside of the macrocyclic cavity (as in Figure 1.4) while a negative tilt angle denotes that the glucose unit is inclined with the O6 side towards the outside of the macrocyclic cavity. For α-, β- and γ-CD the tilt angles are mostly positive and the result is that the O6 end is truncated for these CDs.

Table 1.3 Mean values of the intersaccharidic bond angle, O2(n)···O3(n-1) distances and the tilt angle for α-, β- and γ-CD

CD	φ (°)[30]	O2(n)···O3(n-1) (Å)[30]	τ_1 (°)[30]
α	118.4	3.05	+ 11.4
β	117.7	2.92	+ 9.5
γ	115.0	2.84	+ 14.5

Hydrophobic cavity

The three-dimensional shape of the CD is that of a hollow, truncated cone with the wide side being the secondary rim and the narrow side the primary rim. One of the most important properties of the cyclodextrin results from the distribution of hydrophilic and hydrophobic groups on the "doughnut-shaped" structure. The O6-H primary hydroxyl groups occupy the primary rim and O2-H and O3-H secondary hydroxyl groups occupy the secondary rim (Figure 1.5). These hydroxyl groups render the CD soluble in aqueous solution. The internal cavity of the macrocycle, however, is lined with C3-H, C5-H and C6-H2 hydrogen atoms and by the ethereal O4 oxygen atoms. The result is that the cavity of the molecule assumes a hydrophobic character.

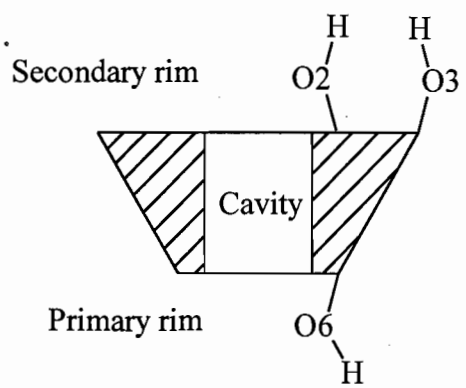

Figure 1.5 Schematic diagram of CD showing the cavity, primary and secondary faces and the distribution of primary and secondary hydroxyl groups on the two CD faces.

Guest inclusion

This hydrophobic cavity has the ability to include guest molecules with lower polarity than water, with the only requirement that the guest molecule must be of the appropriate shape and size to fit into the cavity, even if only partially. The pyranose conformation is affected by the interaction of included guest molecules, although it is difficult to detect significant changes in bond distances, angles and torsion angles. No covalent bonds are formed or broken during the formation of a guest-cyclodextrin

complex and in aqueous solution the complexes are readily dissociated. One of the main driving forces of complexation could be the release of high enthalpy water molecules from the cyclodextrin cavity. The energy of the system is lowered when these enthalpy-rich water molecules are replaced in the cyclodextrin cavity by a suitable guest molecule (Figure 1.6).

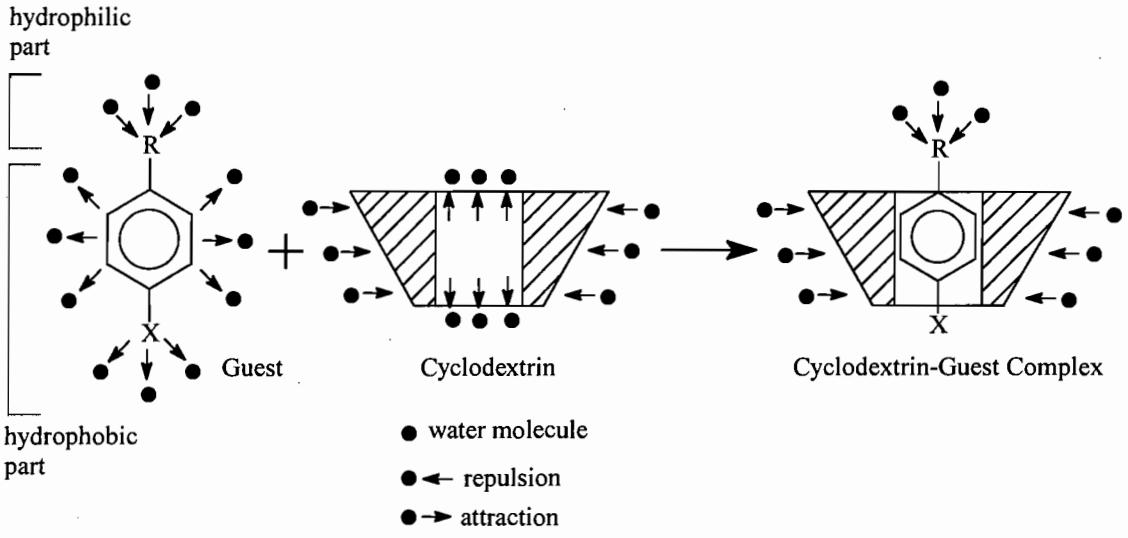

Figure 1.6 Guest inclusion by cyclodextrins and expulsion of water from CD cavity.

Enthalpic and entropic changes upon complexation enable distinction between complexation driven by van der Waals interactions or hydrophobic interactions. If there were no interaction between CD and guest, one should expect this to result in zero ΔH and zero ΔS. If van der Waals interactions are mainly responsible for driving complexation, one should expect this to result in a large negative ΔH and a zero ΔS, whereas if hydrophobic interactions play the major role, one should expect this to result in zero ΔH and a large positive ΔS. Complexation of guests with α- and β-CD usually produces values of ΔH and ΔS which suggest that van der Waals interactions play a major role while complexation with γ-CD shows values of ΔH and ΔS that are consistent with classical hydrophobic interactions. The interaction of a guest with a CD depends on the chemical properties of the respective CD and guest and the driving force for complexation can be due to a number of interactions or combinations thereof. However, the interactions of greatest importance are van der Waals interactions, hydrogen bonding, hydrophobic interactions, release of high-energy cavity water, release of macrocyclic ring strain and the effects of solvent-surface tension.

Orientation of guest in CD cavity

Size and shape

The primary factor determining the orientation and fit of a guest molecule in the cyclodextrin cavity is that the guest must be able to fit into the cavity even if only partially included. The physical dimensions and cavity volumes of α-, β- and γ-CD are presented in Figure 1.7. CDs are somewhat flexible hosts which can adapt to the topologies of the guests embedded in their cavities. The macrocyclic host adjusts its geometry to the topology of the guest during complex formation in a process that can best be envisaged to occur via an induced-fit type mechanism.

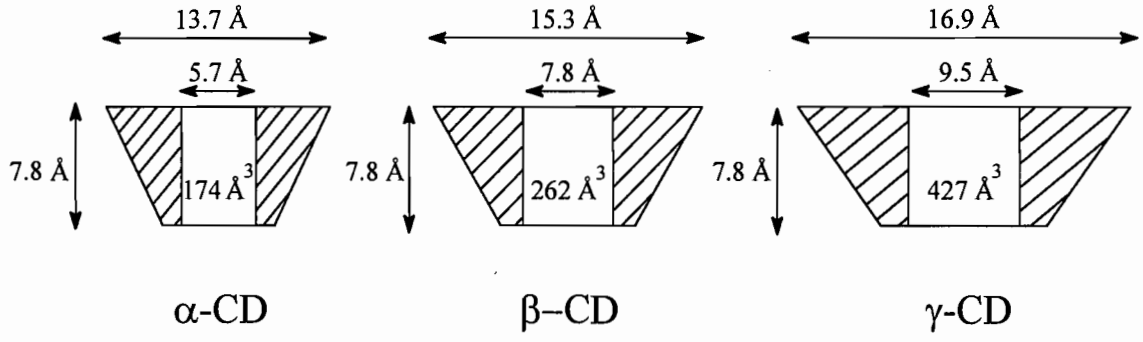

Figure 1.7 The physical dimensions of α-, β- and γ-CD[28]

Dipole moment alignments

Large values of the dipole moments have been calculated for α-, β- and γ-cyclodextrin using the x-ray structures of the three CDs. The relative strengths are in the order α–CD < β–CD < γ–CD, which is expected as the number of glucosyl residues in the macrocycle increases. The dipole moments are of the order of 10-20 Debye and are directed with the positive end of the dipole at the primary hydroxyl end and the negative end at the secondary hydroxyl rim.[32] In the inclusion complexes of CDs with aromatic molecules, the guest dipole moment has been noted to adopt an anti-parallel direction to that of the CD.[33,34]

The overall electric field of CDs is expressed strongly within the cavity of the macrocycle and the dipole moment of a CD is therefore thought to strongly influence the orientation of polar guest compounds in the CD cavity.

The direction of the cyclodextrin dipole moment can be expressed as the tilting angle, ϖ between the dipole moment vector and the axis of the cavity. If ϖ is sufficiently smaller then 90° then the dipole moment is directed from the secondary to the primary hydroxyl side, and this is the case for all CDs that have been studied thus far. The direction of the guest dipole moment can be expressed as Ω, the angle between the vector of the CD dipole moment and the vector of the guest dipole moment (Figure 1.8). When these two vectors are anti-parallel the angle Ω is 180°.

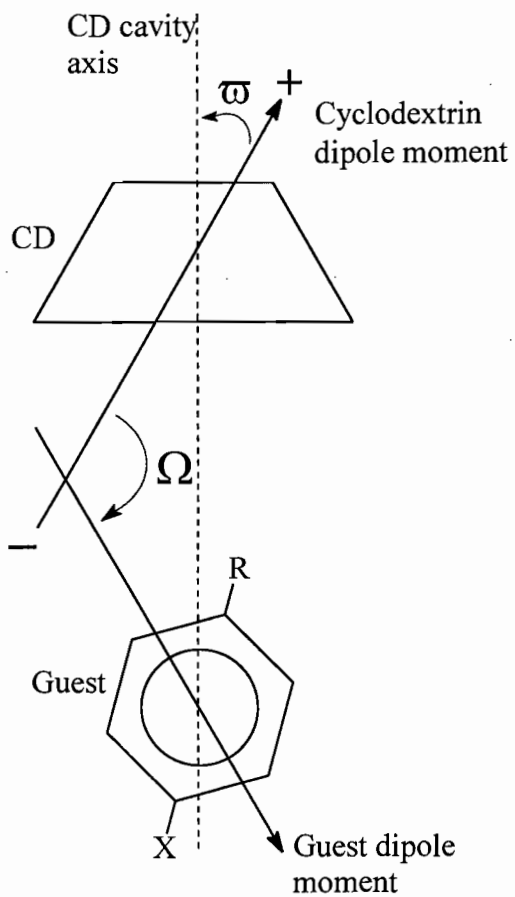

Figure 1.8 The relationships between the cyclodextrin and guest dipole moments (adapted from reference 32)

Hydrophobic attractions

A detailed analysis of computer-generated molecular lipophilicity patterns (MLPs) of cyclodextrin inclusion complexes has revealed that there is a close spatial relationship and complementarity between the hydrophobic and hydrophilic surface areas of cyclodextrins and guest molecules which they include.[35]

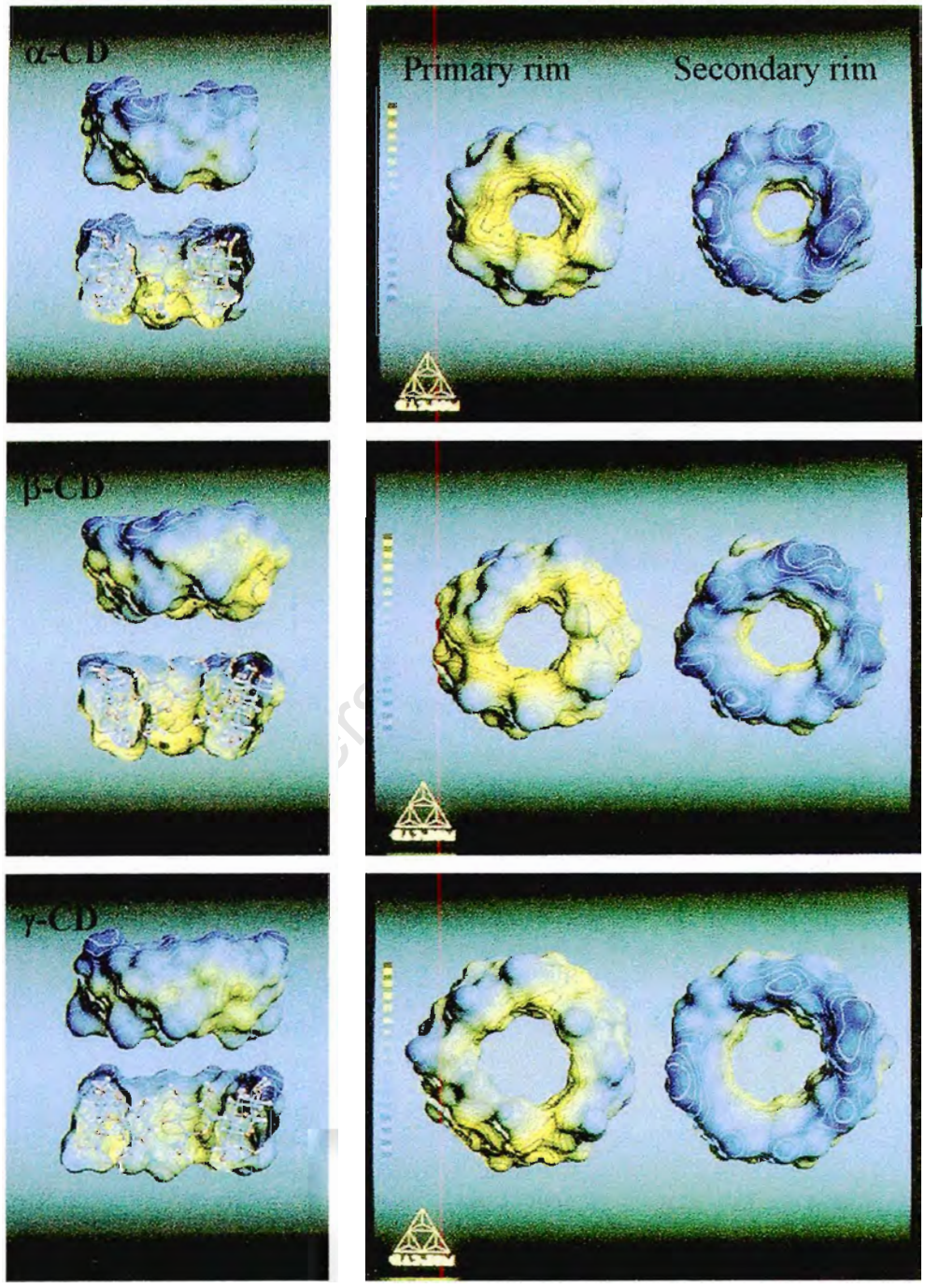

Figure 1.9 MLPs of α-(top), β-(middle) and γ-CD (bottom), side views (left) in closed and bisected form each with secondary rim aligned upwards, views onto primary and secondary rims (right) (taken from reference 30)

Figure 1.9 shows the MLPs for α-, β- and γ-CDs with the colour code ranging from dark blue for intensely hydrophilic portions to full yellow for the most hydrophobic regions. For these native CDs the MLPs reveal that the larger opening of the secondary rim of the macrocycle carrying the 2-OH and 3-OH hydroxyl groups is intensely hydrophilic. The opposite, narrower opening of the primary rim carries the 6-OH hydroxyl groups and is considerably less hydrophilic and partially permeated by hydrophobic regions. The bulk of the intensely hydrophobic regions is concentrated on the inner regions of the CD cavities. The hydrophobic portions of the included guest will therefore tend to be concentrated in the hydrophobic inner surface of the CD cavity and around the primary hydroxyl rim while the hydrophilic portions of a guest will tend to be aligned with the hydrophilic secondary hydroxyl rim. This tendency to optimise the occurrence of hydrophobic and hydrophilic domains at the host-guest interface is thought to be important in orientating the guest in the cavity and determining the stability of the complex. The per-O-methylated CDs show an inverse hydrophobicity pattern to the native CDs and the result is that the orientations of the guests are reversed from the orientations they adopt in the cavities of the native CDs.[36] These hydrophobic attractions are especially important in cases where the guest is devoid of polar groups. If polar groups are present then dipole-dipole alignments and the need for solvation of polar groups may diminish the importance of hydrophobic attractions for orientating and stabilising a guest in a CD cavity.

Cyclodextrin Structures in the Solid state

A useful and widely used technique for studying CDs and their complexes in the solid state is single crystal x-ray analysis. This technique provides valuable information regarding structural aspects of the CD and included guests and the nature of their interactions in the solid state.[31,37,38] Recent reviews[2,39] present comprehensive and updated discussions of the structural aspects of CD complexes as determined from crystallographic studies.

The author of this thesis carried out a search of the Cambridge Structural Database (Version 5.12, October 1998)[40] which yielded 74 β-CD and 11 γ-CD crystal structures, after re-determinations of the same structure had been eliminated. The structures have been surveyed and grouped into categories according to their unit cell parameters and packing arrangements.

β-CD crystal structures

Monomeric Structures

1.) Herringbone type (HB) e.g. β-CD hydrate ($P2_1$)

The monomeric herringbone packing arrangement (Figure 1.10 (a)) allows for very efficient packing of the β-CD molecules and this arrangement is preferred with small guest molecules that do not protrude from the β-CD cavity. The structures with this type of packing arrangement are found to have the space group $P2_1$ with the β-CD molecules stacked along the two-fold screw axis to form the characteristic herringbone pattern. The cavity of a β-CD molecule is blocked on one end by a β-CD molecule related by a screw axis and on the other end by a β-CD molecule related by translation along the *b*-axis. β-CD structures of HB type are listed in Table 1.4.

Table 1.4 β-CD monomeric structures of the herringbone (HB) type (space group $P2_1$)

Guest	H: G : Water†	a (Å)	b (Å)	c (Å)	α (°)	β (°)	γ (°)	Refcode
Hydrate[41-45]	1 : 0 : 12	21.29	10.33	15.10	90	112.4	90	BCDEXD
Hydrogen iodide[46]	1 : 2 : 8	21.25	10.28	15.30	90	113.25	90	BOBPEN
Methanol[46]	1 : 1 : 6.5	21.03	10.11	15.33	90	111.02	90	BOBPIR
Hydrate[43,44]	1 : 0 : 11	21.085	10.212	15.123	90	111.66	90	BUVSEQ
Nicotinamide[47]	1 : 1 : 6	20.433	10.367	15.373	90	110.46	90	CACCOY
Benzyl alcohol[48]	1 : 1 : 5	21.287	10.101	15.356	90	112.81	90	DEBGOG
Hexamethylenetetramine[49]	1 : 1 : 6	20.118	10.345	15.285	90	102.14	90	DIRVOP
Potassium hydroxide[50,51]	1 : 1 : 9	20.204	10.578	15.223	90	102.14	90	KOBRIC
1,4-Butanediol[52]	1 : 1 : 6.25	21.199	9.973	15.271	90	110.87	90	KUTKOZ
Ethylene glycol[53]	1 : 1 : 8	21.212	10.021	15.208	90	111.47	90	PIJGIY
Glycerol[53]	1 : 1 : 7.2	21.322	9.954	15.251	90	111.20	90	PIJGOE
Hydrate[44]	1 : 0 : 9.35	20.857	10.158	15.140	90	110.94	90	POBRON
Hydrate[44]	1 : 0 : 1	21.227	10.288	15.116	90	112.18	90	POBRUT
Diethanolamine[54]	1 : 1 : 6.4	21.310	9.987	15.247	90	111.85	90	YIYSII
But-2-yne 1,4 diol[54]	1 : 1 : 6.2	21.451	10.014	15.420	90	111.25	90	YIYSOO
Diethylene glycol[54]	1 : 1 : 6	21.288	9.969	15.276	90	111.62	90	YIYSUU
Propane-1,3-diol[54]	1 : 1 : 7	21.116	9.976	15.274	90	110.88	90	YIYTAB
1,5-Pentanediol[55]	1 : 1 : 6.2	20.988	10.092	15.223	90	110.30	90	ZIGZIY
Hydrate[56]	1 : 0 : x	21.12	10.25	15.18	90	111.6	90	ZZZBVA
Hydrochloride[56]	1 : 1.8 : x	20.75	10.27	15.04	90	109.0	90	ZZZBVD

† x in the second column refers to an unknown number of water molecules in the complex

2.) Zigzag type (ZZ) e.g. β-CD-calcium chloride ($P2_12_12_1$)

The β-CD monomers are arranged in the form of a zigzag-like chain which runs parallel to the *a*-axis (Figure 1.10 (b)). The symmetry of the structure produces a second zigzag-like chain with an anti-parallel orientation to the first. Each of the adjacent chains is extended to form sheets parallel to the *ab*-plane. These two anti-parallel sheets are stacked alternately along the *c*-axis. Structures of the ZZ type are listed in Table 1.5.

Table 1.5 β-CD monomeric structures of the zigzag (ZZ) type (space group $P2_12_12_1$)

Guest	H : G : Water	a (Å)	b (Å)	c (Å)	α (°)	β (°)	γ (°)	Refcode
Calcium chloride[57]	1 : 2 : 11.25	15.875	17.583	24.270	90	90	90	HIDZAV
Hexa-aqua-magnesium chloride[58]	1 : 2 : 3.5	15.947	18.610	23.361	90	90	90	ZEZTED

3.) Brickwork type (BW) e.g. β-CD-pyridine ($P2_1$)

The β-CD monomers are arranged with alternating orientations along the direction *c*` (*c*` = 2*a* - *c*) as shown in Figure 1.10 (c). The first β-CD molecule has the secondary hydroxyl group facing upwards while the adjacent molecule has the secondary hydroxyl side facing downwards. This arrangement is extended to form a layer parallel to the *bc*`-plane. A second layer is generated by the symmetry and is offset from the first layer to form a brickwork type of packing of the layers. The layers stack on top of one another in the direction roughly parallel to *a*` (*a*` = *a* + *c*).
β-CD structures of the BW type are listed in Table 1.6.

Table 1.6 β-CD monomeric structures of the brickwork (BW) type (space group $P2_1$)

Guest	H : G : Water	a (Å)	b (Å)	c (Å)	α (°)	β (°)	γ (°)	Refcode
Pyridine[59]	1 : 8 : 3	14.700	14.742	21.784	90	101.87	90	KUFHOI
Pyridine[59]	1 : 8 : 0	14.551	15.224	20.854	90	104.96	90	KUFHUO

4.) Layer type (LY) e.g. β-CD-sulfathiazole ($P2_1$)

In the layer packing arrangement the β-CD molecules are arranged in layers parallel to the *ac*-plane of the crystal structure with the β-CD molecules inclined by approximately 10° in the plane of the layers (Figure 1.10 (d)). The layers stack in the *b*-axis direction and two layers are offset with respect to one another by about the radius of a β-CD molecule. The result is that both ends of the β-CD cavity are nearly closed off by β-CD molecules of adjacent layers. β-CD structures of the LY type are listed in Table 1.7.

Table 1.7 β-CD monomeric structures of the layer (LY) type (space group $P2_1$)

Guest	H : G : Water	a (Å)	b (Å)	c (Å)	α (°)	β (°)	γ (°)	Refcode
1,4-diazabicyclo(2.2.2)octane[60]	1 : 1 : 13	15.395	16.598	15.441	90	117.35	90	BISTAY
Sulfathiazole[61]	1 : 1 : 8	15.264	16.500	15.559	90	117.29	90	LILLUN

5.) Helical channel type (HC) e.g. β-CD-diclofenac sodium ($P6_1$)

In the helical channel packing arrangement the β-CD molecules are stacked head-to-tail along a 6-fold screw axis to form a helically extended tube (Figure 1.10 (e)). Each β-CD molecule is rotated by 60° around the *c*-axis and extended by translation in layers parallel to the *ab*-plane. β-CD structures of the HC type are listed in Table 1.8.

Table 1.8 β-CD monomeric structures of helical channel (HC) (space group $P6_1$)

Guest	H : G : Water	a (Å)	b (Å)	c (Å)	α (°)	β (°)	γ (°)	Refcode
Sodium diclofenac[62]	1 : 1 : 11	15.956	15.956	50.95	90	90	120	HEHJEJ

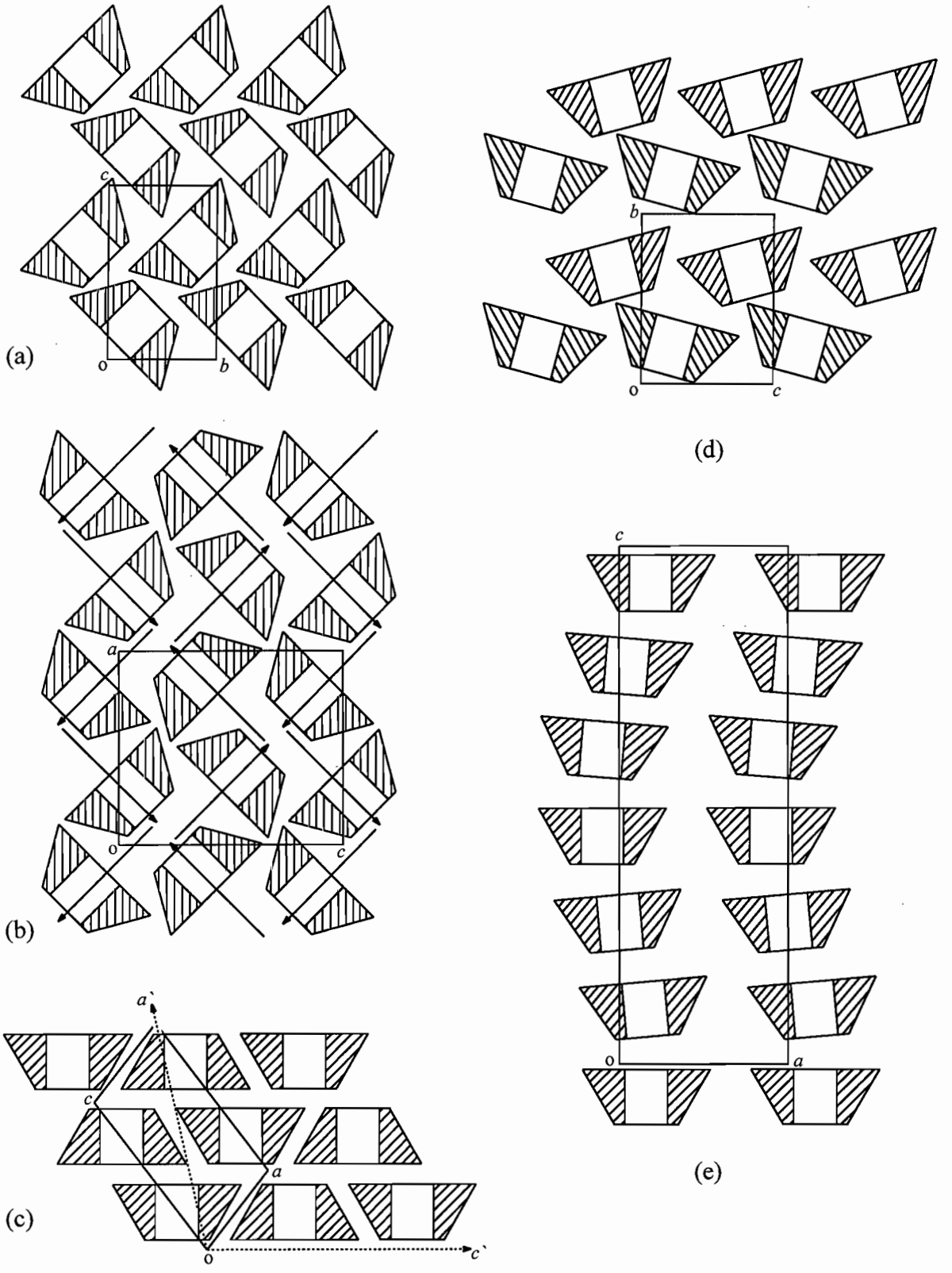

Figure 1.10 The packing arrangements of β-CD monomers : (a) Herringbone (HB), (b) Zigzag (ZZ), (c) Brickwork (BW), (d) Layer (LY) and (e) Helical Channel (HC)

Dimeric Structures

The dimeric β-CD structures pack in "infinitely" extended dimeric layers and the relative settings of these dimeric layers lead to the classification of four classes of molecular packing.[96] CH structures crystallise in the space groups C2 or P1 and the CB, IM and SC structures in the space groups $C222_1$, P1 and $P2_1$ respectively.

1.) Channel type (CH) e.g. β-CD-*p*-nitroacetanilide (P1), β-CD-spiroacetal (C2)

The dimeric layers are parallel to the *ab*-plane and the dimers are stacked on top of each other to form channels parallel to the *c*-axis (Figure 1.11 (a)). There is only a slight deformation of the linearity of the channels at the interdimeric interface. The average shift between the centres of consecutive dimers, when viewed perpendicular to their O4 heptagons, is 2.7 (2) Å (3.1 (2) Å for structures in the space group P1). β-CD structures of the CH type are listed in Table 1.9 (a) and (b).

Table 1.9 (a) β-CD dimeric structures of the channel (CH) type (space group C2)

Guest	H : G : Water†	a (Å)	b (Å)	c (Å)	α (°)	β (°)	γ (°)	Refcode
Ethyl *p*-amino benzoate[63]	2 : 2 : 15	18.746	24.528	15.658	90	110.21	90	BIHJEH
Potassium heptaiodide[64]	2 : 1 : 9	19.609	24.513	15.745	90	109.50	90	COCMIQ
Sodium polyiodide[65]	2 : 2 : 16	19.58	24.44	15.75	90	109.3	90	CYDXTF
Benzophenone[66]	2 : 2 : x	19.24	24.56	15.94	90	109.5	90	DEVTED
Biphenyl[66]	2 : 2 : x	19.34	24.49	15.80	90	109.8	90	DEVTIH
2-bromo-5-*t*-butylphenol[67]	2 : 2 : 18	19.235	24.662	16.018	90	108.9	90	HAMBZB
2,5-di-iodobenzoic acid[68]	2 : 2 : 16	19.192	24.759	15.739	90	109.6	90	HPAMIB
Cylcopentadienyl mesitylene iron hexafluorophosphate[69]	2 : 1 : 1	19.241	24.415	15.768	90	109.55	90	KOGLIB
Cyclopentadienyl biphenyl iron hexafluorophosphate[69]	2 : I : 1	19.206	24.334	15.674	90	108.88	90	KOGLOH
Spiroacetal[70]	2 : 2 : 18	19.368	24.45	15.94	90	108.72	90	TEMCIX
3,3-dimethylbutylamine[71,72]	2 : 2 : 22	19.187	24.56	15.893	90	108.77	90	VIJXAN
(*Z*)-9-dodecen-1-ol ethanol[73]	2 : 1 : 19.2	19.238	24.477	15.790	90	109.52	90	ZUZXOH

Table 1.9 (b) β-CD dimeric structures of the channel (CH) (space group P1)

Guest	H : G : Water†	a (Å)	b (Å)	c (Å)	α (°)	β (°)	γ (°)	Refcode
n-propanol (phase II)[74]	2 : 6 : 18	15.461	15.575	15.316	103.98	100.92	104.23	BCYDPR
p-nitroacetanilide[75]	2 : 2 : x	15.13	15.54	15.69	88.65	98.16	103.14	CHANAO
1,7-dioxaspiro-5,5-undecane[76]	2 : 2 : x	15.60	15.72	15.93	101.4	101.7	103.2	FERCOU
4-*t*-butyl toluene[77], ISS	2 : 2 : 17	15.562	15.564	15.835	102.11	102.15	103.64	KUTJUE
3,5-dimethylbenzoic acid[78], ISS	2 : 1.88 : 18.2	15.707	15.694	15.999	101.50	101.56	103.81	YOVVIO

† x in the second column refers to an unknown number of water molecules in the complex

2.) Intermediate type (IM) e.g. β-CD-(+)-flurbiprofen (P1)

The dimeric layers are parallel to the *bc*-plane and the dimers are stacked on top of each other along the direction of the *a*-axis (Figure 1.11 (b)). The average shift between the centres of consecutive dimers, when viewed perpendicular to their O4 heptagons, is 6.0 (2) Å, which is larger than the average radius of a β-CD heptagon (5.1 Å). This shift between consecutive dimers results in a significant discontinuity of the channel. β-CD structures of the IM type are listed in Table 1.10.

Table 1.10 β-CD dimeric structures of the intermediate (IM) type (space group P1)

Guest	H : G : Water†	a (Å)	b (Å)	c (Å)	α (°)	β (°)	γ (°)	Refcode
p-iodophenol[79]	2 : 3 : 24	17.985	15.352	15.363	102.8	113.1	99.4	BCDIPH
m-methyl phenol[80]	2 : 4 : 20	17.887	15.327	15.366	102.64	113.07	99.68	BCDMPH
n-propanol (phase I)[79]	2 : 3 : 24	17.980	15.424	15.299	103.0	113.5	99.4	BCDNPR
Ethyl cinnamate[81]	2 : 1 : 17.5	18.186	15.486	15.392	107.78	113.61	99.74	BIDMOQ
1-adamantane carboxylic acid[82]	2 : 2 : 30	17.747	15.255	15.491	102.54	113.54	98.87	BOGCAB
2-propanol[83]	2 : 1 : x	17.980	15.424	15.299	103.0	113.5	99.4	BULFIX
n-propanol[74]	2 : 4 : 24	17.980	15.424	15.229	103.0	113.5	99.4	CDEXPR
(±)-flurbiprofen[84]	2 : 2 : 20	18.033	15.420	15.490	103.05	113.63	99.36	CEDMUT
(+)-flurbiprofen[85,86]	2 : 2 : 21	18.107	15.446	15.513	102.89	113.52	99.32	CIGXOF
Barbital (form I)[87]	2 : 2 : 31	19.716	15.497	15.549	103.63	116.65	104.56	DEVVAB
Acetylsalicylic acid / Salicylic acid[88]	2 : 2 : 23.3	19.777	15.247	15.475	102.63	116.96	104.12	DIFHOP
N-acetylphenylamine[89]	2 : 2 : 26	18.129	15.411	15.585	103.97	112.89	98.79	DOCVUM
R,S-(±)-methyl-*p*-tolylsulfoxide[90,91]	2 : 3 : 34	19.618	15.432	15.476	102.98	117.70	104.30	GESVUV
4-*t*-butylbenzoic acid[92]	2 : 2 : 26.8	18.244	15.476	15.417	102.94	113.08	99.69	HEGXUM
Nonanoic acid[93]	2 : 1.6 : 23.9	18.056	15.446	15.452	103.16	112.99	99.35	TEJHAR

† x in the second column refers to an unknown number of water molecules in the complex

3.) Chessboard type (CB) e.g. β-CD-4-tert-butylbenzyl alcohol ($C222_1$)

The dimeric layers are parallel to the *ab*-plane and the layers are stacked on top of one another along the *c*-axis direction (Figure 1.11 (c)). The displacement of the centres of successive dimers, projected on the *ab*-plane, is 8.7 (2) Å. There is almost no overlap of the dimers of adjacent layers when looking normal to the *ab*-plane. Each dimer is located above the interdimer space of the layer below resulting in a three-dimensional chessboard-like arrangement. β-CD structures of the CB type are listed in Table 1.11.

Table 1.11 β-CD dimeric structures of the chessboard (CB) type (space group $C222_1$)

Guest	H : G : Water†	a (Å)	b (Å)	c (Å)	α (°)	β (°)	γ (°)	Refcode
Benzil[66]	2 : 2 : x	19.58	24.00	32.84	90	90	90	DEVTON
Phenyl-ethyl malonic acid[66]	2 : 2 : x	19.09	24.27	32.58	90	90	90	DEVTUT
1-hydroxymethyl-adamantane[94]	2 : 2 : 22	19.162	23.965	32.597	90	90	90	DUTLIN
Transaminedichlorotrimethyl Phosphine platinum[95]	2 : 2 : 11	19.431	24.082	32.503	90	90	90	GIPFEQ
4-*t*-butylbenzyl alcohol[96]	2 : 2 : 20	19.196	24.393	32.808	90	90	90	KOFJEU
2-methyl-2,4-pentanediol[97]	2 : 2 : 23	19.685	24.133	36.614	90	90	90	TECYIJ

† x in the second column refers to an unknown number of water molecules in the complex

4.) Screw Channel type (SC) e.g. β-CD-fenoprofen ($P2_1$)

The dimeric layers are parallel to the *ac*-plane and consecutive layers are stacked along the direction of the *b*-axis, with adjacent layers related by a screw axis parallel to the *b*-axis (Figure 1.11 (d)). The average displacement of centres of consecutive dimers projected on the *ac*-plane is 2.6 (2) Å, which is similar to that for the channel (CH) packing mode. However, the channel has a screw-like appearance because consecutive dimers are not parallel to one another, but tilted with respect to their layer planes. The dimers of each layer are tilted by about 10° to the normal of their layer planes, alternatively clockwise and anticlockwise for successive layers along the *b*-axis direction. β-CD structures of the SC type are listed in Table 1.12.

Table 1.12 β-CD dimeric structures of the screw channel (SC) type (space group $P2_1$)

Guest	H : G : Water	a (Å)	B (Å)	c (Å)	α (°)	β (°)	γ (°)	Refcode
p-ethylaniline[98]	2 : 2 : 32	15.300	32.311	15.584	90	102.40	90	CDETAN
Phenobarbital[99]	2 : 2 : 27	15.562	33.189	15.229	90	104.85	90	CIVBUE
R,S-(±)-fenoprofen[100,101]	2 : 2 : 25	15.277	32.232	15.316	90	101.18	90	DUTLIN
R-(-)-fenoprofen[102]	2 : 2 : 26	15.26	32.76	15.35	90	101.5	90	GETPAW
S-(+)-fenoprofen[102]	2 : 2 : 25	15.310	32.124	15.277	90	100.76	90	GETPEA
(*L*)-menthol[103]	2 : 2 : 29	15.342	32.54	15.324	90	102.44	90	NIZGUY
Carmofur[104]	2 : 2 : 19.4	15.507	35.307	15.495	90	102.68	90	SAJPIC

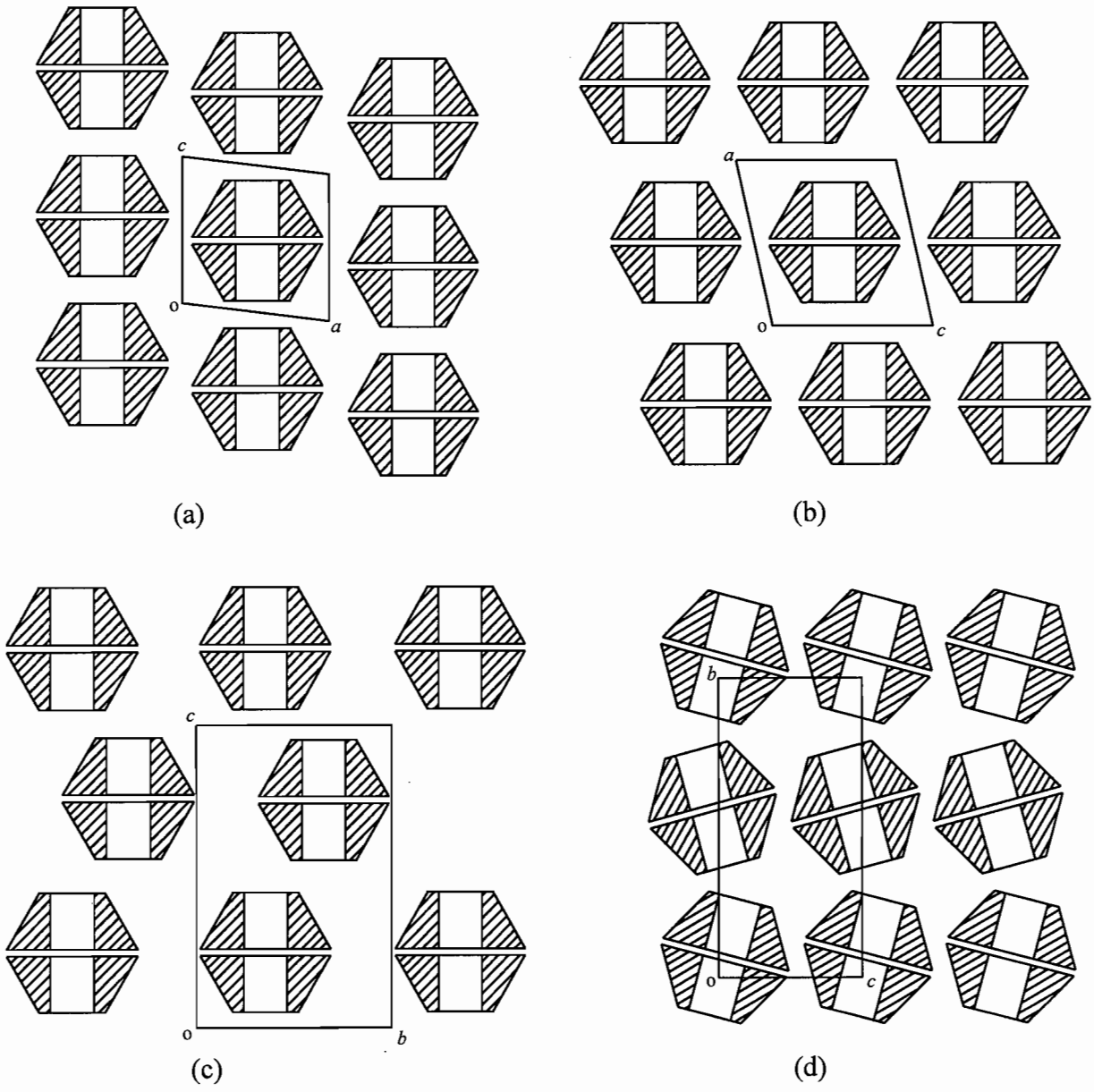

Figure 1.11 The packing arrangements of β-CD dimers : (a) Channel (CH), (b) Intermediate (IM), (c) Chessboard (CB), (d) Screw Channel (SC)

Tetrameric Structures

1.) Tetrameric intermediate type (TI) e.g. β-CD-barbital (P1)

Two dimers are arranged to form a tetrameric channel (Figure 1.12 (a)). The tetrameric layers are parallel to the *bc*-plane and tetramers stack along the *a*-axis direction. The consecutive tetramers are arranged according to the IM packing mode crystallising in space group P1. β-CD structures of TI type are listed in Table 1.13.

Table 1.13 β-CD tetrameric structures of the intermediate (TC) (space group P1)

Guest	H : G : Water	a (Å)	b (Å)	c (Å)	α (°)	β (°)	γ (°)	Refcode
Barbital (form II)[87]	4 : 4 : 50	34.341	15.497	15.568	103.82	100.58	106.67	DEVVEF

2.) Tetrameric chessboard type (TC) e.g. β-CD-*S*-(-)-methyl-*p*-tolylsulfoxide ($P2_1$)

Two dimers are arranged to form a tetrameric channel (Figure 1.12 (b)). The tetrameric layers are parallel to the *ac*-plane and tetramers stack along the *b*-axis direction. The consecutive tetramers are stacked in the CB packing mode crystallising in space group $P2_1$. β-CD structures of TC type are listed in Table 1.14.

Table 1.14 β-CD tetrameric structures of the chessboard (TC) type (space group $P2_1$)

Guest	H : G : Water	a (Å)	b (Å)	c (Å)	α (°)	β (°)	γ (°)	Refcode
S-(-)-methyl-*p*-tolylsulfoxide[90,91]	4 : 4 : 68	15.495	65.04	15.471	90	102.60	90	GESWAC

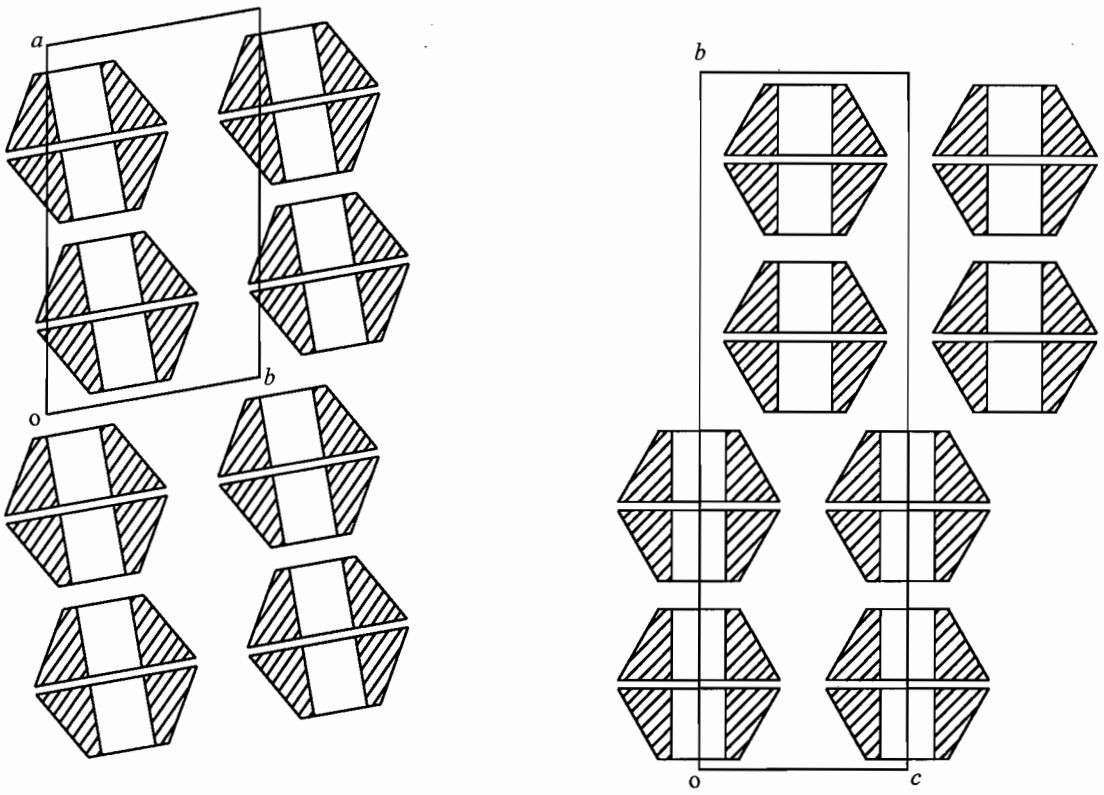

(a) (b)

Figure 1.12 The packing arrangements of β-CD tetramers : (a) tetrameric intermediate (TI), (b) tetrameric chessboard (TC)

γ-CD structures

1.) Herringbone type (HB) e.g. γ-CD-hydrate ($P2_1$)

In this type of monomeric packing arrangement a cage-type structure is formed where two glucose units from an adjacent γ-CD molecule are partially inserted into the cavity of the γ-CD molecule from the secondary hydroxyl side (Figure 1.13 (a)). This type of packing arrangement has been observed only for the γ-CD hydrate. γ-CD structures of the HB type are listed in Table 1.15.

Table 1.15 γ-CD monomeric structures of the herringbone (HB) type (space group $P2_1$)

Guest	H : G : Water†	a (Å)	b (Å)	c (Å)	α (°)	β (°)	γ (°)	Refcode
Hydrate[105]	1 : 0 : 11	20.287	22.079	16.858	90	105.07	90	CIMSAS
Hydrate[106,107]	1 : 0 : 14	20.271	11.098	16.847	90	104.97	90	CIWMIE
Hydrate[108]	1 : 0 : 17	20.253	10.494	16.892	90	105.32	90	CYOCAM
Hydrate[109]	1 : 0 : x	19.84	11.13	16.76	90	104.00	90	ZZZKHW

† x in the second column refers to an unknown number of water molecules in the complex

2.) Channel type (CH) e.g. γ-CD-*n*-propanol ($P42_12$)

In the channel type structure the γ-CD molecules with their inherent 8-fold (C_8) symmetry are stacked along a 4-fold axis to produce linear "infinite" channels (Figure 1.13 (b)). These channels are unique in that they have three γ-CD molecules in one asymmetric unit. The three crystallographically independent γ-CD molecules A,B,C form a trimer arranged in head-to-head (A-B), head-to-tail (B-C), and tail-to-tail (C-A`) relationships. The fourfold rotation axis runs through the centre of the γ-CD cavity and any guest molecule included in the cavity will of necessity be disordered around the fourfold axis, unless it possesses four-fold symmetry itself. This channel type packing mode has been observed for all γ-CD complexes containing guests, other than water, and therefore it has been suggested that there is no specific influence of the guest molecule in determining the packing arrangement of γ-CD complexes. γ-CD structures of the CH type are listed in Table 1.16.

Table 1.16 γ-CD trimeric structures of the channel packing (CH) type (space group $P42_12$)

Guest	H : G : Water†	a (Å)	b (Å)	c (Å)	α (°)	β (°)	γ (°)	Refcode
n-propanol[110]	3 : 3 : x	23.759	23.759	23.069	90	90	90	CYDXPL
12-crown-4[111]	3 : 3 : 27	23.808	23.808	23.175	90	90	90	DOCYID
Bis(12-crown-4) lithium 12-crown-4 isothiocyanate[112]	3 : 1 : 23.1	23.75	23.75	22.92	90	90	90	FEJFIJ
Bis(12-crown-4) potassium 12-crown-4 chloride[112]	3 : 1 : 27	23.842	23.842	23.132	90	90	90	FEJFOP
Bis(12-crown-4) sodium 12-crown-4 chloride[113]	3 : 1 : 23.1	23.816	23.816	23.072	90	90	90	SAJNAS
1-propanol[114]	3 : 3 : 51	23.840	23.840	23.227	90	90	90	SIBJES
1-propanol[114]	3 : 3 : 51.36	23.810	23.810	23.207	90	90	90	SIBJAO

† x in the second column refers to an unknown number of water molecules in the complex

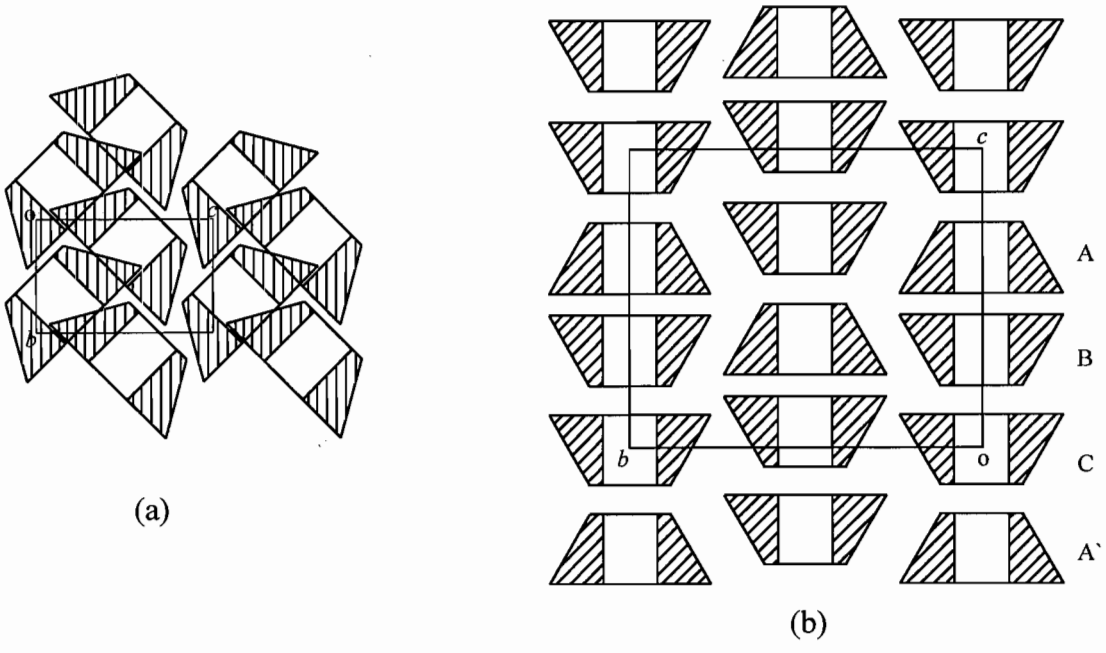

Figure 1.13 The packing arrangements of γ-CD structures : (a) herringbone (HB), (b) channel (CH)

The hydrogen bonded network of CD structures

A summary of the different hydrogen bonding interactions that may occur between CDs, included guests and the water molecules of crystallisation in a cyclodextrin inclusion complex is presented below :

1.) Cyclodextrin to cyclodextrin hydrogen bonds (CD-CD)
2.) Cyclodextrin to water hydrogen bonds (CD-W)
3.) Water to water hydrogen bonds (W-W)
4.) Guest to cyclodextrin hydrogen bonds (CD-G)
5.) Guest to water hydrogen bonds (G-W)
6.) Guest to guest hydrogen bonds (G-G)

The β-CD molecule almost always contains a ring of intramolecular O2···O3 hydrogen bonds which gives the macromolecular structure a rigid, cyclic shape. These consist of seven O2(n)···O3(n-1) intra-CD bonds. Neutron diffraction studies have shown that this type of hydrogen bonding is of the flip-flop nature in β- and γ-cyclodextrin with both O2(n)-H···O3(n-1) and O2(n)···H-O3(n-1) hydrogen bonds being observed.[115,116] The mean O2(n)···O3(n-1) distance is 2.92 Å for β-CD.

Although there are many examples of β-CD inclusion complexes which crystallise with a monomeric packing arrangement, most β-CD inclusion complexes crystallise as dimers with the dimers linked head-to-head by hydrogen bonds between the secondary hydroxyls and stacked in the crystal with their seven-fold axes approximately parallel.[117] The dimers are linked together in "infinite" two-dimensional layers held together by a dense network of hydrogen bonds.

The intra-dimer hydrogen bonds include O3···O3, O2···O2 and O3···O2 bonds between the two CDs of the dimer, of which the seven O3···O3 bonds are thought to be the most important. [118]

The layer interactions include the intra-layer and inter-layer hydrogen bond systems.

The intra-layer hydrogen bond system links dimers within a layer. These intra-layer hydrogen bonds include direct O2···O2, O2···O3, O3···O3 and O6···O6 bonds between dimers and those mediated by water molecules.

The inter-layer hydrogen bond system links two adjacent dimeric layers. These inter-layer hydrogen bonds include direct O6···O6 bonds between dimers and those mediated by water molecules.

As all the crystal structures of β-CD complexes investigated in this study are of the dimeric type, all hydrogen bonds and contacts within hydrogen bonding ranges will be categorised according to the following scheme :

β-CD (dimeric structures) hydrogen bonded network

A. Cyclodextrin interactions : O2(n)···O3(n-1)

B. Dimer interactions

Intra-dimer : O3···O3, O2···O2, O2···O3

C. Layer interactions

Intra-layer : O6···O6, O2···O2, O2···O3, O3···O3

Inter-layer : O6···O6

D. Guest interactions : G···CD, G···W, G···G

E. Water interactions : O2···W, O3···W, O6···W, W···W

For γ-CD structures, a ring of intramolecular O2(n)···O3(n-1) hydrogen bonds stabilises the macrocyclic structure. The mean O2(n)···O3(n-1) distance is 2.84 (6) Å for γ-CD.

Although the hydrates of γ-CD crystallise in a monomeric packing arrangement , all other γ-CD complexes crystallise as trimers linked in a head-to-head, head-to-tail and tail-to-tail arrangement. The head-to-head (A-B) arrangement displays the same secondary hydroxyl hydrogen bonded network as seen with β-CD dimers with O2···O2, O2···O3 and O3···O3 hydrogen bonds bridging the two CDs. The tail-to-tail (B-C) arrangement is characterised by direct O6···O6 hydrogen bonds and those mediated by water molecules. The head-to-tail (C-A`) arrangement is characterised by O2···O6, O3···O6 hydrogen bonds and those mediated by water. The trimers are arranged in "endless" linear channels parallel to the c-axis of the structure. The water molecules of crystallisation are associated with the cavity channel and the interstitial channel.

γ-CD (trimeric structures) hydrogen bonded network

A. Cyclodextrin interactions	:	O2(n)···O3(n-1)
B. Trimer interactions		
Head-to-head	:	O2···O3, O2···O2, O3···O3
Tail-to-tail	:	O6···O6
Head-to-tail	:	O2···O6, O3···O6
C. Inter-channel interactions	:	O2···O6, O3···O6, O6···O6, O2···O3, O2···O2, O3···O3
D. Water interactions	:	W···W, O6···W, O2···W, O3···W
E. Guest interactions	:	G···CD, G···W, G···G

Pharmaceutical aspects of cyclodextrins

Applications of CDs in Pharmacy

CDs have a wide variety of applications which are utilised in foods, cosmetics and toiletries, pesticides, biomedical products and pharmaceuticals. CDs also display useful applications in chemical technology, analytical chemistry and diagnostics.[119]

However, since the aim of this study was to investigate the interactions of various drug molecules with CDs, the pharmaceutical applications are most relevant.

The most notable uses of CDs in the pharmaceutical field include (i) increasing aqueous solubility, dissolution and release rates, bioavailability of various water-insoluble drugs and (ii) improving chemical stability of unstable drugs by providing increased protection from photodegradation, hydrolysis, decomposition, oxidation, racemization and isomerisation. In addition, the complexation may also suppress the volatility and unpleasant odours or tastes associated with the drug and avoid incompatibility problems with other drugs or excipients in a formulation, as well as reducing the local irritance and haemolysis caused by a drug.[120]

A review by Thompson[121] published in 1997 lists ten pharmaceutical products which are marketed as CD formulations; eight of these are marketed in Japan and two in Europe. Numerous clinical trials of CD-based drug formulations have also been completed or are in progress in the United States.

The use of CDs to address various formulation problems will be discussed using the various examples from the CD-based formulations that are already on the market.

Improvements in solubility, dissolution and bioavailability

Improvement of the aqueous solubility of poorly soluble drugs can improve oral bioavailability when solubility and dissolution rate limit the availability of the drug for absorption.

Formulation problems with the broad-spectrum, semi-synthetic cephalosporin antibiotic, cefotiam hexetil hydrochloride, prompted the development of CD formulation of the drug. The drug forms a gel with poor dissolution characteristics when it enters the acidic conditions of the gastric contents. Various excipients were screened, and formulation with α-CD afforded the best dissolution and solubility of the drug.[122,123] This formulation is currently marketed in Japan as Nitropen™.

The antiulcer and antigastritis drug, benexate hydrochloride, showed poor dissolution and solubility in spite of attempts to formulate the drug in a variety of methods. The result was that at acceptable doses only limited inhibition of gastric ulcers was observed *in vivo*. The 1:1 β-CD complex of the drug showed improved dissolution and inhibited ulceration at significantly lower doses.[124-126] The β-CD complexed form of the drug is marketed in Japan as Ulgat™ and Lonmiel™.

Reduction of unpleasant side effects

Improvements in solubility and dissolution rate of a drug can improve the rate of absorption which will in turn reduce the contact time between the drug and the tissue mucosa. This can be useful in the reduction of unpleasant side effects associated with tissue irritation.

Non-steroidal anti-inflammatory drugs (NSAIDs), such as piroxicam, show a degree of local irritation which results in a high incidence of gastrointestinal ulceration. A β-CD formulation of piroxicam was developed and *in vivo* tests showed that there were significantly fewer incidences of acute gastric lesions in patients receiving the CD formulation of the drug.[127-130] This CD formulation of piroxicam is currently marketed in Europe under the tradenames of Brexin™, Cycladol™ and Brexidol™. It is also the first CD formulation to be marketed in South Africa where it is marketed as Brexicam™.

Improvements in stability

The protected environment that is offered to a drug molecule when included by a CD can produce many favourable improvements in stability, often resulting in significant decreases in the degradation rate of the drug.

CD formulations of prostaglandin E_1 were developed in order to increase the stability of the drug. The drug is highly susceptible to dehydration which limits its shelf-life. The α-CD formulation significantly increased the stability and shelf-life of the drug, which is currently marketed in Germany and Japan under the tradenames of Prostavasin™ and Prostandin™ respectively.[131]

In addition to the three naturally occurring CDs, α-, β and γ-CD, the methyl, hydroxypropyl and sulfobutylether derivatives of β-CD are currently available for use in pharmaceutical products.[121]

Cyclodextrin derivatives

The O2, O3 and O6 hydroxyl groups represent the target of most modifications that have been made to the natural CDs. A wide variety of these modified cyclodextrins are known and certain groups of modified CD derivatives are of current pharmaceutical interest. They include (i) various methylated and alkylated CDs (e.g. 2,6-dimethyl-β-cyclodextrin (DM-β-CD), 2,3,6-trimethylated-β-CD (TM-β-CD) and randomly methylated β-CD (RM-β-CD)),[132,133] (ii) hydroxypropyl and hydroxyethyl CDs (e.g. 2-hydroxypropyl-β-CD (HP-β-CD)),[134-137] (iii) various branched CDs like glucosyl, diglucosyl, maltosyl and dimaltosyl CDs (e.g. 6-glucosyl-β-CD (G-β-CD)),[138-140] (iv) carboxyalkyl CDs and their derivatives[141-145] and (v) sulfoalkylether CDs (e.g. sulfobutylether β-CD (SBE-β-CD)).[146-153]

Cyclodextrin formulations for the parenteral, oral, nasal, ophthalmic, dermal, rectal, pulmonary and epidural administration and delivery of many types of drug substances have been investigated.[154]

Cyclodextrin metabolism and safety

CDs and their inclusion complexes are consumed by humans or animals in the form of orally administered pharmaceuticals or as food additives.[119] Upon ingestion into the stomach the gastric juice causes rapid dissociation of the complex and accelerated absorption of hydrophobic guest molecules. The CD serves as a carrier of the guest molecule, bringing it into solution, keeping it in the dissolved state and transporting it to the lipophilic cell membrane for absorption into the circulation. Although the mammalian organism cannot degrade CDs, specific cylodextrinase enzymes (including CTG-ase) are produced by micro-organisms and bacteria which inhabit the human colon. The primary metabolites (acyclic maltodextrins, glucose and maltose) are further metabolised, absorbed and finally excreted as CO_2 and H_2O.

A number of safety evaluations have shown that the three natural CDs (α-, β, and γ-CD) and some chemically modified CDs (HP-β-CD, DM-β-CD, SBE-β-CD and G-β-CD) are suitable for oral formulations.[155] In addition, γ-CD, HP-β-CD, SBE-β-CD and G-β-CDs are suitable for parenteral formulations.

Regulatory situation and future outlook

As already mentioned, oral formulations of β-CD complexes have already been marketed in Europe and Japan. A monograph for β-CD is present in the Japanese Pharmacopoeia and is due to appear in the European Pharmacopoeia shortly. In the United States a monograph for β-CD is available in the ~~Pharmacopoeia~~ National Formulary.[156,159] This is the first example of a citation for an excipient which is not yet present in a marketed product and it suggests that oral β-CD formulations are likely to be introduced to the U.S. market very shortly. Chemically modified CDs are also receiving much regulatory attention. A monograph for HP-β-CD is in preparation for the U.S. Pharmacopoeia and parenteral formulations containing this CD are currently completing preliminary and advanced clinical trials and are expected for commercial release within this year. Research studies exploring the pharmaceutical applications of CDs are growing exponentially and a growth in the number of commercial products containing CD-based formulations is predicted for the future.

Motivation for the selection of drugs

Ranitidine, cyclizine and salbutamol laurate were chosen for this investigation in consultation with industrial partners at South African Druggists International™ who had identified commercial applications for the cyclodextrin inclusion of these drugs. Cimetidine and famotidine are structurally related to ranitidine and were chosen mainly for comparative studies. The cyclodextrin inclusion of those two anti-ulcerative compounds could also be of much commercial interest.

Acetaminophen, *p*-bromoacetanilide, phenacetin and diacetamate were chosen as a series of structurally related compounds with analgesic and antipyretic activity. Literature surveys have indicated that the cyclodextrin complexation of non-steroidal anti-inflammatory, antipyretic and analgesic drugs is of interest to researchers and the pharmaceutical industry.[157] The β-CD complexation of acetaminophen, in particular, has received much attention in the literature although the solid state structure of a CD inclusion complex with this drug has hitherto not been determined.

More specific details of the rationale and motivation for the choice of drugs investigated in this study will be discussed under the relevant chapters.

Objectives for CD complexation of selected drugs

The investigation of the pharmaceutical applications of CD complexes is of great interest and reports from the literature suggest that the CD complexation of many of the drugs investigated in this study are of current interest. This investigation will primarily focus on i.) preparation, ii.) determination of chemical composition, iii.) analysis of thermal behaviour and iv.) investigation of the solid state features of the complexes with these drugs.

A detailed knowledge of the composition and properties is of growing importance to the regulatory approval of any CD-based formulations. Demonstration of the detailed nature of CD-drug interaction in the solid state is a powerful means of supporting the approval of a CD-based preparation. This study intends to draw attention to the features of CD-drug inclusion in the solid state.

References

1.) J. Szejtli, *Topics in Inclusion Science-Cyclodextrin Technology*, Kluwer Academic Publishers, Dordrecht, The Netherlands, **1988**.

2.) K. Harata, *Chem. Rev.*, **1998**, 98, 1803.

3.) A. Villiers, *Compt. Rend.*, **1891**, 112, 536.

4.) F. Z. Schardinger, *Unters. Nahr. U. Genussum.*, **1903**, 6, 865.

5.) F. Schardinger, *Wien. Klin. Wochenschr.*, **1904**, 17, 207.

6.) F. Schardinger, *Zentralbl. Bakteriol. Parasintenk. Abt. 2*, **1905**, 14, 772.

7.) F. Schardinger, *Zentralbl. Bakteriol. Parasintenk. Abt. 2*, **1911**, 29, 188.

8.) H. Pringsheim, *Chemistry of the Saccharides*, McGraw-Hill, New York, **1932**, p. 280.

9.) H. Pringsheim, *A Comprehensive Survey of Starch Chemistry*, ed. R. P. Walton, Chemical Catalogue Co. Inc., New York, **1928**, p. 35.

10.) K. Freudenberg and W. Rapp, *Ber. Dtsch. Chem. Ges.*, **1936**, 69, 2041.

11.) K. Freudenberg, H. Boppel and M. Meyer-Delius, *Naturwissenschaften*, **1938**, 26,123.

12.) K. Freudenberg, G. Blomquist, L. Ewald and K. Soff, *Ber. Dtsch. Chem. Ges.*, **1936**, 69, 1258.

13.) K. Freudenberg and F. Cramer, *Z. Naturforsch*, **1948**, 3b, 464.

14.) K. Freudenberg, F. Cramer and H. Plieninger, *Ger. Patent 895*, 769, **1953**.

15.) F. Cramer, Einschlussverbindungen (Inclusion Compounds), Springer-Verlag, Berlin, **1954**.

16.) D. French, *Adv. Carbohydr. Chem.*, **1957**, 12, 189.

17.) J. A. Thoma and L. Stewart, Starch : *Chemistry and Technology I.*, ed. R. L. Whistler and E. F. Paschall, Academic Press, New York, **1965**, p. 209.

18.) G. V. Caesar, *Starch and its Derivatives*, ed. J. A. Radley, Chapman and Hall, London, **1968**, Chapter 10, p. 290.

19.) J. Szejtli, Ed., *Proc. 1st Int. Symp. on Cyclodextrins, Budapest, 1981*, D. Reidel Publ. Co., Dordrecht, **1982**.

20.) J. L. Atwood, J. E. D. Davies, T. Osa, Eds., *Clathrate Compounds, Molecular*

Inclusion Phenomena and Cyclodextrins, Proc. of Third Int. Symp. on Clathrate Compounds and the Second Int. Symp. on Cyclodextrins, Tokyo, 1984, D. Reidel Publ. Co., Dordrecht, **1985**.

21.) J. L. Atwood and J. E. D. Davies, Eds., *Inclusion Phenomena in Inorganic, Organic and Organometallic Hosts, Proc. Third Int. Symp. on Inclusion Phenomena and the Third Int. Symp. on Cyclodextrins, Lancaster, 1986*, D. Reidel Publ. Co., Dordrecht, **1987**.

22.) O. Huber and J. Szejtli, Eds., *Proc. Fourth Int. Symp. on Cyclodextrins, Munich, 1988*, Kluwer Academic Publ., Dordrecht, **1988**.

23.) D. Duchene, Ed., *Minutes of the Fifth Int. Symp. on Cyclodextrins, Paris, 1990*, Editions de Santé, Paris, **1990**.

24.) A. R. Hedges, Ed., *Minutes of the Sixth Int. Symp. on Cyclodextrins, Chicago, 1992*, Editions de Santé, Paris, **1992**.

25.) T. Osa, Ed., *Proceedings of the Seventh International Cyclodextrin Symposium, Tokyo, 1994*, Publ. Office of Business Center for Academic Societies of Japan, **1994**.

26.) J. Szejtli and L. Szente, Eds., *Proceedings of the Eighth International Cyclodextrin Symposium, Budapest, 1996*, Kluwer Acad. Publ., Dordrecht, **1996**.

27.) *Proceedings of the Ninth International Cyclodextrin Symposium, Santiago de Compostela, 1998*, Kluwer Acad. Publ., Dordrecht, **1998**.

28.) J. Szejtli, *Chem. Rev.*, **1998**, 98, 1743.

29.) K. B. Lipkowitz, K. Green and J. Yang, *Chirality*, **1992**, 4, 205.

30.) F. W. Lichtenthaler and S. Immel, *Liebigs Ann.*, **1996**, 27.

31.) K. Harata, in *Inclusion Compounds*, ed. J. L. Atwood, J. E. D. Davies and D. D. MacNicol, Oxford University Press, London, **1984**, Vol. 5, Chapter 9.

32.) M. Sakurai, M. Kitagawa, H. Hoshi, Y. Inoue and R. Chûjô, *Carbohydr. Res.*, **1990**, 198, 181.

33.) M. Kitagawa, H. Hoshi, M. Sakurai, Y. Inoue and R. Chûjô, *Bull. Chem. Soc. Jpn.*, **1988**, 61, 4225.

34.) M. Sakurai, M. Kitagawa, H. Hoshi, Y. Inoue and R. Chûjô, *Chem. Lett.*, **1988**, 895.

35.) F. W. Lichtenthaler and S. Immel, *Starch*, **1996**, 48(4), 145.

36.) F. W. Lichtenthaler and S. Immel, *Starch*, **1996**, 48(6), 225.

37.) W. Saenger, *J. Inclusion Phenom.*, **1984**, 2, 445.

38.) W. Saenger, in *Inclusion Compounds*, ed. J. L. Atwood, J. E. D. Davies and D. D. MacNicol, Academic Press, London, **1984**, Vol. 2, Chapter 8.

39.) W. Saenger, J. Jacob, K. Gessler, T. Steiner, D. Hoffman, H. Sanbe, K. Koizumi, S. M. Smith and T. Takaha, *Chem. Rev.*, **1998**, 98, 1787

40.) *Cambridge Structural Database and Cambridge Structural Database System*, Version 5.12, October 1998, Cambridge Crystallographic Data Centre, University Chemical Laboratory, Cambridge, England.

41.) K. Lindner and W. Saenger, *Angew. Chem. Int. Ed. Engl.*, **1978**, 17, 694.

42.) J. J. Stezowski and J. M. Maclennan, *Am. Cryst. Assoc., Ser. 2*, **1980**, 7, 24.

43.) T. Fujiwara, M. Yamazaki, Y. Tomizu, R.Tokuoka, K.-I. Tomita, T. Matsuo, H. Suga, W. Saenger, *Nippon Kagaku Kaishi (J. Chem. Soc. Jpn.)*, **1983**, 181.

44.) T. Steiner and G. Koellner, *J. Am. Chem. Soc.*, **1994**, 116, 5122.

45.) K. Lindner and W. Saenger, *Carbohydr. Res.*, **1982**, 99, 103.

46.) K. Lindner and W. Saenger, *Carbohydr. Res.*, **1982**, 107, 7.

47.) K. Harata, K. Kawano, K. Fukunaga and Y. Ohtani, *Chem. Pharm. Bull.*, **1983**, 31, 1428.

48.) K. Harata, K. Uekama, M. Otagiri, F. Hirayama and Y. Ohtani, *Bull. Chem. Soc. Jpn.*, **1985**, 58, 1234.

49.) K. Harata, *Bull. Chem. Soc. Jpn.*, **1984**, 57, 2596.

50.) P. Charpin, I. Nicolis, F. Villian, C. de Rango and A. W. Coleman, *Acta Crystallogr., Sect. C*, **1991**, 47, 1829.

51.) I. Nicolis, P. Charpin, F. Villian, C. de Rango and A. W. Coleman, *Proc. Int. Symp. Cyclodextrins*, **1990**, 120.

52.) T. Steiner, G. Koellner and W. Saenger, *Cabohydr. Res.*, **1992**, 228, 321.

53.) K. Gessler, T. Steiner, G. Koellner and W. Saenger, *Carbohydr. Res.*, **1993**, 249, 327.

54.) T. Steiner, G. Koellner, K. Gessler and W. Saenger, *J. Chem. Soc., Chem. Commun.*, **1995**, 511.

55.) T. Steiner and W. Saenger, *J. Chem. Soc., Chem. Commun.*, **1995**, 2087.

56.) J. Szejtli and Z. Budai, *Acta Chim. Acad. Sci. Hung.*, **1977**, 94, 383.

57.) I. Nicolis, A. W. Coleman, P. Charpin and C. de Rango, *Acta Crystallogr., Sect. B*, **1996**, 52, 122.

58.) I. Nicolis, A. W. Coleman, P. Charpin and C. de Rango, *Angew. Chem. Int. Ed. Engl.*, **1995**, 34, 2381.

59.) C. de Rango, P. Charpin, J. Navaza, N. Keller, I. Nicolis, F. Villain and A. W. Coleman, *J. Am. Chem. Soc.*, **1992**, 114, 5475.

60.) K. Harata, *Bull. Chem. Soc. Jpn.*, **1982**, 55, 2315.

61.) M. R. Caira, V. J. Griffith, L. R. Nassimbeni and B. van Oudtshoorn, *J. Inclusion Phenom.*, **1994**, 17, 187.

62.) M. R. Caira, V. J. Griffith, L. R. Nassimbeni and B. van Oudtshoorn, *J. Chem. Soc., Chem. Commun.*, **1994**, 1061.

63.) J. A. Hamilton and M. N. Sabesan, *Carbohydr. Res.*, **1982**, 102, 31.

64.) C. Betzel, B. Hingerty, M. Noltemeyer, G. Weber, W. Saenger and J. A. Hamilton, *J. Inclusion. Phenom.*, **1983**, 1, 181.

65.) M. Noltemeyer and W. Saenger, *J. Am. Chem. Soc.*, **1980**, 102, 2710.

66.) G. le Bas, C. de Rango, N. Rysanek and G. Tsoucaris, *J. Inclusion Phenom.*, **1984**, 2, 861.

67.) J. A. Hamilton, M. N. Sabesan and L. K. Steinrauf, *Carbohydr. Res.*, **1981**, 89, 33.

68.) J. A. Hamilton, M. N. Sabesan, L. K. Steinrauf and A. Geddes, *Biochem. Biophys. Res. Commun.*, **1976**, 73, 659.

69.) B. Klingert and G. Rihs, *J. Chem. Soc., Dalton Trans.*, **1991**, 2749.

70.) N. Rysanek, G. le Bas, F. Villain and G. Tsoucaris, *Acta Crystallogr., Sect. C*, **1996**, 52, 2932.

71.) I. Moustakali-Mavridis, E. Hadjoudis and G. Tsoucaris, *Mol. Cryst. Liq. Cryst.*, **1990**, 186, 185.

72.) I. Mavridis, E. Hadjoudis and G. Tsoucaris, *Carbohydr. Res.*, **1991**, 220, 11.

73.) D. Mentzafos, I. M. Mavridis and M. B. Hursthouse, *Acta Crystallogr., Sect. C*, **1996**, 52, 1220.

74.) K. H. Jogun and J. J. Stezowski, *Nature (London)*, **1979**, 278, 667.

75.) M. M. Harding, J. M. Maclennan and R. M. Paton, *Nature (London)*, **1978**, 274, 621.

76.) G. Tsoucaris, G. le Bas, N. Rysanek and F. Villain, *J. Inclusion. Phenom.*, **1987**, 5, 77.

77.) I. M. Mavridis and E. Hadjoudis, *Carbohydr. Res.*, **1992**, 229, 1.

78.) A. Rontoyianni and I. M. Mavridis, *J. Inclusion Phenom.*, **1994**, 18, 211.

79.) J. J. Stezowski, K. H. Jogun, E. Eckle and K. Bartels, *Nature (London)*, **1978**, 274, 617.

80.) K. Jogun, J. M. Maclennan, J. J. Stezowski, *Eur. Cryst. Meeting*, **1979**, 5, 34.

81.) M. B. Hursthouse, C. Z. Smith, M. Thornton-Pett and J. H. P. Utley, *J. Chem. Soc., Chem. Commun.*, **1982**, 881.

82.) J. A. Hamilton and M. N. Sabesan, *Acta Crystallogr., Sect. B*, **1982**, 38, 3063.

83.) M. Czugler, G. Geiger and J. J. Stezowski, *Z. Kristallogr.*, **1983**, 162, 54.

84.) K. Uekama, F. Hirayama, T. Imai, M. Otagiri and K. Harata, *Chem. Pharm. Bull.*, **1983**, 31, 3363.

85.) K. Uekama, F. Hirayama, T. Imai, M. Otagiri and K. Harata, *Chem. Pharm. Bull.*, **1984**, 32, 1662.

86.) K. Harata, K. Uekama, M. Otagiri and F. Hirayama, *J. Inclusion Phenom.*, **1984**, 1, 279.

87.) I. Nakanishi, M. Arai, T. Fujiwara and K. Tomita, *J. Inclusion Phenom.*, **1984**, 2, 689.

88.) F. Nishioka, I. Nakanishi, T. Fujiwara and K. Tomita, *J. Inclusion Phenom.*, **1984**, 2, 701.

89.) J. J. Stezowski, *Trans. Am. Crystallogr. Assoc.*, **1985**, 20, 73.

90.) T. Fujiwara, K.-I. Tomita, I. Marseigne and J. Vicens, *Mol. Cryst. Liq. Cryst.*, **1988**, 156, 393.

91.) J. Vicens, T. Fujiwara and K.-I. Tomita, *J. Inclusion Phenom.*, **1988**, 6, 577.

92.) A. Rontoyianni, I. M. Mavridis, E. Hadjoudis, A. J. M. Duisenberg, *Carbohydr. Res.*, **1994**, 252, 19.

93.) A. Rontoyianni and I. M. Mavridis, *Acta Crystallogr., Sect. C*, **1996**, 52, 2277.

94.) J. A. Hamilton, *Carbohydr. Res.*, **1985**, 142, 21.

95.) D. R. Alston, A. M. Z. Slawin, J. F. Stoddart, D. J. Williams and R. Zarzycki, *Angew. Chem. Int. Ed. Engl.*, **1988**, 27, 1184.

96.) D. Mentzafos, I. M. Mavridis, G. le Bas and G. Tsoucaris, *Acta Crystallogr., Sect. B*, **1991**, 47, 746.

97.) N. E. Zhukhlistova, G. N. Tishchenko, I. P. Kuranova, B. K. Vainshtein, P. Mattson and T. Korpella, *Kristallografiya*, **1996**, 41, 97.

98.) R. Tokuoka, T. Fujiwara and K.-I. Tomita, *Acta Crystallogr., Sect. B*, **1981**, 37, 1158.

99.) I. Nakanishi, T. Fujiwara and K. Tomita, *Acta Crystallogr., Sect.A*, **1984**, 40, C78.

100.) J. A. Hamilton and L. Chen, *Am. Cryst. Assoc., Abstr. Papers (Winter)*, **1986**, 14, 50.

101.) J. A. Hamilton and L. Chen, *J. Am. Chem. Soc.*, **1988**, 110, 5833.

102.) J. A. Hamilton and L. Chen, *J. Am. Chem. Soc.*, **1988**, 110, 4379.

103.) M. R. Caira, V. J. Griffith, L. R. Nassimbeni and B. van Oudtshoorn, *Supramol. Chemistry*, **1996**, 7, 119.

104.) K. Harata, F. Hirayama, K. Uekama and G. Tsoucaris, *Chem. Lett.*, **1988**, 1585.

105.) B. E. Hingerty, C. Betzel and W. Saenger, *Am. Cryst. Assoc., Abstr. Papers (Winter)*, **1984**, 12, 37.

106.) K. Harata, *Chem. Lett.*, **1984**, 641.

107.) K. Harata, *Bull. Chem. Soc. Jpn.*, **1987**, 60, 2763.

108.) J. M. Maclennan and J. J. Stezowski, *Biochem. Biophys. Res. Commun.*, **1980**, 92, 926.

109.) Borchert, *Z. Naturforsch., Teil B*, **1948**, 3, 464.

110.) K. Lindner and W. Saenger, *Biochem. Biophys. Res. Commun.*, **1980**, 92, 933.

111.) S. Kamitori, K. Hirotsu and T. Higuchi, *J. Chem. Soc.,Chem. Commun.*, **1986**, 690.

112.) S. Kamitori, K. Hirotsu and T. Higuchi, *J. Chem. Soc.,Chem. Commun.*, **1987**, 109, 2409.

113.) S. Kamitori, K. Hirotsu and T. Higuchi, *Bull. Chem. Soc. Jpn.*, **1988**, 61, 3825.

114.) J. Ding, T. Steiner and W. Saenger, *Acta Crystallogr., Sect. B*, **1991**, 47, 731.

115.) W. Saenger, C. Betzel, G. Hingerty and G. M. Brown, *Nature*, **1982**, 296,581.

116.) W. Saenger, C. Betzel, G. Hingerty and G. M. Brown, *Angew. Chem. Int. Ed. Engl.*, **1983**, 22, 883.

117.) G. le Bas and G. Tsoucaris, *Mol. Cryst. Liq. Cryst.*, **1986**, 137, 287.

118.) G. le Bas and G. Tsoucaris, *Supramolecular Chemistry*, **1994**, 4, 13.

119.) K-H. Frömming and J. Szejtli, Topics in *Inclusion Science (Volume 5) : Cyclodextrins in Pharmacy*, Dordrecht, The Netherlands, ~~1988~~ 1993.

120.) K. Uekama and M. Otagiri, *CRC Crit. Rev. Ther. Drug Carrier Syst.*, **1987**, 3, 1.

121.) D. Thompson, *CRC Crit. Rev. Ther. Drug Carrier Syst.*, **1997**, 14(1), 1.

122.) S. Hirai in *Proceedings of the Seventh International Cyclodextrin Symposium, Tokyo, 1994*, T. Osa, Ed., Publ. Office of Business Center for Academic Societies of Japan, **1994**.

123.) S. Hirai, H. Koyama, T. Makino, N. Kitamori and H. Toguchi, Yakuzaigaku, **1988**, 48, 189.

124.) N. Muranushi, M. Yoshida, H. Kinoshita, F. Hirose, T. Fukuda, M. Doteuchi and H. Yamada, Nippon Yakurigaku Zasshi, 1988, 91, 377.

125.) Y. Suzuki, T. Tsukada, N. Nagafuji, Y. Tomoda, T. Hayashi, H. Tanaka, A. Fujimoto, C. Nakajima, K. Shima, T. Ogura and Y. Takagishi, Yakuzaigaku, 1993, 53, 201.

126.) K. Hirano and M. Shinoda in *Proceedings of the Seventh International Cyclodextrin Symposium, Tokyo, 1994*, T. Osa, Ed., Publ. Office of Business Center for Academic Societies of Japan, **1994**.

127.) R. Bettini, P. Santi, P. L. Catellani, G. Massimo, A. Bellottti, C. Barthelemy, A. M. Guyot-Hermann, F. Trublin and P. Colombo, *Eur. J. Pharm. Biopharm.*, **1992**, 38, 203.

128.) L. Santucci, S. Fiorucci, S. Chiucchiu, A. Sicilia, L. Bufalino and A. Morelli, *Digest. Dis. Sci.*, **1992**, 37, 1825.

129.) A. Nervetti, U. Ambanelli and G. Ugolotti, *J. Drug. Dev., Suppl.*, **1991**, 4, 39.

130.) L. Patoia, G. Clausi, F. Farroni, P. Alberti, P. Fugiani and L. Bufalino, *Eur. J. Clin. Pharmacol.*, **1989**, 36, 599.

131.) K. Inaba and J. Mizutani, *Yakuzaigaku*, **1986**, 46, 58.

132.) B. Casu, M. Reggiani and G. R. Sanderson, *Carbohydr. Res.*, **1979**, 76, 59.

133.) K. Harata, K. Uekama, M. Otagiri and F. Hirayama, *J. Inclusion Phenom.*, **1984**, 1, 279.

134.) C. T. Rao, H. M. Fales and J. Pitha, *Pharm. Res.*, **1990**, 7, 612.

135.) J. Pitha, J. Milecki, H. Fales, L. Pannell and K. Uekama, *Int. J. Pharm.*, **1986**, 29, 73.

136.) T. Irie, K. Fukunaga, A. Yoshida, K. Uekama, H. M. Fales and J. Pitha, *Pharm. Res.*, **1988**, 5, 713.

137.) A. Yoshida, M. Yamamoto, T. Irie, F. Hirayama and K. Uekama, *Chem. Pharm. Bull.*, **1989**, 37, 1059.

138.) Y. Okada, Y. Kubota, K. Koizumi, S. Hizukuri, T. Ohfuji and K. Ogata, *Chem. Pharm. Bull.*, **1988**, 36, 2176.

139.) M. Yamamoto, A. Yoshida, F. Hirayama and K. Uekama, *Int. J. Pharm.*, **1989**, 49, 163.

140.) M. Yamamoto, H. Aritori, T. Irie, F. Hirayama and K. Uekama, *S. T. P. Pharm. Sci.*, **1991**, 1, 397.

141.) K. Uekama, Y. Horiuchi, T. Irie and F. Hirayama, *Carbohydr. Res.*, **1989**, 192, 323.

142.) K. Uekama, T. Horikawa, Y. Horiuchi and F. Hirayama, *J. Controlled Rel.*, **1993**, 25, 99.

143.) T. Horikawa, K. Abe, F. Hirayama and K. Uekama, *J. Controlled Rel.*, **1991**, 15, 177.

144.) H. Adachi, T. Irie, K. Uekama, T. Manako, T. Yano and M. Saita, *Eur. J. Pharm. Sci.*, **1993**, 1, 117.

145.) K. Uekama, H. Adachi, T. Irie, T. Yano, M. Saita and K. Noda, *J. Pharm. Pharmacol.*, **1992**, 44, 119.

146.) K. Okimoto, R. A. Rajewski, J. A. Jona and V. J. Stella, *Pharm. Res.*, **1995**, 12, 205.

147.) R. A. Rajewski, G. Traiger, J. Bresnahan, P. Jaberaboansari, V. J. Stella and D. O. Thompson, *J. Pharm. Sci.*, **1995**, 84, 927.

148.) K. Jarvinen, T. Jarvinen, D. O. Thompson and V. J. Stella, *Curr. Eye Res.*, **1994**, 13, 897.

149.) T. Jarvinen, K. Jarvinen, A. Urtti, D. Thompson and V. J. Stella, *J. Ocular Pharm. Therapeut.*, **1995**, 120, 197.

150.) T. Jarvinen, K. Jarvinen, N. Schwarting and V. J. Stella, *J. Pharm. Sci.*, **1995**, 84, 295.

151.) B. A. Gorecka, Y. D. Sanzgiri, D. S. Bindra and V. J. Stella, *Int. J. Pharm.*, **1995**, 125, 55.

152.) V. J. Stella, H. K. Lee and D. O. Thompson, *Int. J. Pharm.*, 120, 189, **1995**.

153.) V. J. Stella, H. K. Lee and D. O. Thompson, *Int. J. Pharm.*, 120, 197, **1995**.

154.) R. A. Rajewski and V. Stella, *J. Pharm. Sci.*, **1996**, 85(11), 1142.

155.) T. Irie and K. Uekama, *J. Pharm. Sci.*, **1997**, 86(2), 147.

156.) T. Loftsson and M. E. Brewster, *J. Pharm. Sci.*, **1996**, 85(10), 1017.

157.) W. Saenger, *Angew. Chem., Int. Ed. Engl.*, **1980**, 19, 344

158.) Herbstein and Marsh, Acta Cryst. B54, 1998, 677.

159.) USP 23 | NF 18, United States Pharmacopeal Convention, Inc., Rockville, MD, 1994, 2220.

CHAPTER 2 : EXPERIMENTAL MATERIALS AND METHODS

Host Compounds

β-cyclodextrin and γ-cyclodextrin were obtained from Cyclolab, Hungary. Hydroxypropyl-β-cyclodextrin was supplied by South African Druggists International. All were used as received.

Guest Compounds

Acetaminophen, phenacetin, cimetidine and famotidine were obtained from Sigma Chemical Company (U.S.A.). *p*-Bromoacetanilide was obtained from Fluka Chemika (Germany). Ranitidine was supplied by South African Druggists International. Cyclizine was prepared from cyclizine hydrochloride, also supplied by South African Druggists International. Diacetamate was synthesised from acetaminophen as starting material. Details of the synthesis of cyclizine and diacetamate are given in the appropriate chapters. Salbutamol laurate was supplied by South African Druggists International.

Inclusion complex preparation and crystal growth

Inclusion complexes of β- and γ-cyclodextrin with the various drugs were obtained by dissolving host and guest in fixed molar ratios and concentrations in distilled water at elevated temperatures. Crystalline samples were obtained by slow cooling or slow evaporation of these aqueous solutions. Inclusion complexes of hydroxypropyl-β-cyclodextrin with salbutamol laurate were prepared by the manual co-grinding, kneading or mechanical co-grinding of the CD and drug. Full details of the preparation of individual complexes are given in the appropriate chapters.

Scanning Electron Microscopy (SEM)

Scanning electron microscopy was carried out on a Leica Stereoscan 440I scanning electron microscope. An accelerating potential of 10kV and a probe current of 75mA were used. The working distance was 25mm and scans were recorded at magnifications of 50x and 2000x.

UV Spectrophotometry (UV)

UV spectra were recorded on a Philips PU8700 series UV/visible spectrophotometer over a wavelength range of 190nm to 600nm at a scanning rate of 250nm/min. All samples were dissolved in distilled water or 0.1M hydrochloric acid. The samples were placed in 10mm quartz cuvettes (Pye Unicam) and the concentrations were suitably adjusted such that all absorbance readings were taken between zero and one absorbance unit. Calibration curves for the various drugs were constructed using the λ_{max} value of the appropriate drug. The absorbance of a solution of an inclusion complex with an accurately known concentration was determined. The percentage weight of the drug in the inclusion complex could then be determined. Together with the percentage weight of water in the inclusion complex, obtained from TGA, the stoichiometry of the inclusion complex was expressed in terms of the cyclodextrin:drug:water ratio.

Microanalysis

Elemental analyses were performed in duplicate on all the prepared inclusion compounds on a Carlo Erba elemental analyser Model 1106. Samples were dried under vacuum for one hour to remove the water content from the complexes. The samples were then placed in vials containing magnesium sulphate as a drying agent to prevent re-absorption of water. The residual water content was established by TGA and the percentages of the various elemental constituents were calculated. In all cases C and H elemental analyses were performed, and where appropriate, the N and/or S elemental analyses were also done. Microanalysis of the inclusion compounds under these conditions served to confirm the stoichiometric ratio of CD:drug in all cases.

IR Spectrophotometry (IR)

IR spectra were obtained using a Perkin-Elmer 983 IR spectrophotometer. Samples were run as nujol mulls over the range of 600–4000cm^{-1} (unless otherwise stated). Percentage transmittance was recorded against frequency. For the CD complexes, shifts in certain characteristic bands of the appropriate drug molecule were indicative of interaction between the CD and drug.

Hot Stage Microscopy (HSM)

The inclusion complexes that were prepared were examined under a Nikon SMZ-10 microscope during heating at a constant rate on a Linkam THMS 600 hot stage linked to a Linkam TP92 temperature-controlling unit. Observations of thermal events occurring under the microscope were recorded photographically using a Nikon AFX-II exposure-controlling unit together with a Nikon FX-35 dark box. The cyclodextrin and drugs were also examined under the same conditions. This proved useful for preliminary identification of inclusion complexes and allowed one to distinguish, at an early stage, the differences between preparations that contained an inclusion complex versus preparations that contained the crystalline cyclodextrin, the crystalline drug or a mixture of the two.

Thermogravimetric Analysis (TGA)

Thermogravimetric analysis was performed on a Perkin-Elmer PC-7 series thermal analysis system at a scanning rate of 10°C/min (unless otherwise stated) under N_2 gas purge with a flow rate of 30cm^3/min. Temperature ranges over which the traces were recorded were 30-350°C for β-CD and γ-CD complexes. Sample masses were in the range of 5–15mg. Samples were removed from mother liquor, dried under filter paper and crushed to an appropriate particle size and placed in an open platinum pan. The TG thermocouple and balance were calibrated using built-in procedures for the furnace and weight calibrations. A two-point standard temperature calibration was performed by measuring the Curie points of alumel (163°C) and nickel (354°C).

The temperature ranges over which weight loss occurred were determined from the first derivative of the trace and are quoted together with the associated weight loss. Weight losses observed in the TG traces are due to loss of water from the inclusion complexes over the temperature range of 30-150°C as well as decomposition of the complexes at higher temperatures. This decomposition of the inclusion complexes is often a complicated process which proceeds in multiple stages.

Differential Scanning Calorimetry (DSC)

Differential scanning calorimetry was performed on a Perkin-Elmer PC-7 series thermal analysis system at a scanning rate of 10°C/min (unless otherwise stated) under N_2 gas purge with a flow rate of 30cm^3/min. Temperature ranges over which the traces were recorded were 30-350°C for β-CD and γ-CD complexes. Sample masses were in the range of 5–15mg. Samples were removed from mother liquor, dried under filter paper and crushed to an appropriate particle size and sealed in a crimped, vented aluminium pan. A sealed and empty pan was used as a reference. The DSC analyser was calibrated by measuring the onset temperatures of the melting of indium (156.4°C) and zinc (419.5°C) while the heat flow was calibrated from the enthalpy of melting of indium (28.62J/g). Endothermic and exothermic peaks appearing in the DSC traces were analysed in terms of their onset temperatures, temperature range of the peak (determined from the first derivative of the trace) and the enthalpy of the peak (measured in J/g). The various endothermic and exothermic peaks observed in the DSC trace can be interpreted in conjunction with HSM and TGA to be associated with solvent loss, phase changes in the sample and decomposition. The decomposition of the inclusion complexes is a complicated and multi-stage process and is characterised by a number of thermal events observed with DSC.

Dissolution

Dissolution studies were conducted using the rotating basket method as described in the USPXXI.[1] Tablets were compressed with an IR punch (Perkin-Elmer) with a compressional force of 300kg/cm^2 with the mean tablet mass 500±1mg. Tablets were placed in the baskets and the rotational speed of the baskets was set at 100rpm. The dissolution medium was distilled water and the temperature of the medium was 37.0±0.5°C. Samples were present in triplicate and aliquots of each sample were removed at 15min intervals over a 150min period. The assay was by UV spectrophotometry at an appropriate wavelength for the active ingredient.

Crystal Structure Analysis

X-ray photography

Preliminary unit cell parameters and space group symmetry were determined by X-ray photography for all inclusion complexes for which sufficiently good crystals had been grown. Oscillation, Weissenberg, cone-axis, de Jong-Bouman and Buerger precession photographs were taken on Stöe goniometers using Ni-filtered CuKα radiation.

Data-collection

Suitable single crystals, typically between 0.2 and 0.5mm in all dimensions, were chosen for data-collection. Plane polarised light was used to confirm that the crystal chosen was indeed a single crystal. All crystals were unstable when removed from mother liquor and were therefore firmly wedged and sealed in 0.3 or 0.5mm diameter Lindemann capillary tubes containing mother liquor.

For data-collections at reduced temperature the crystals were cooled and maintained at 278K (5°C) by a constant stream of N_2 gas with a flow rate of $20cm^3$/min produced by a Cryostream cooler (Oxford Cryosystems). It was necessary, in the case of these data-collections, to maintain the temperature above the freezing point of water since the crystals were often submersed in aqueous mother liquor. Room-temperature data-collections were performed at 293 K (20°C).

For the inclusion complexes of ACEBCD, BROBCD and PHEBCD (Chapter 3), reflection intensities were collected on an Enraf-Nonius CAD-4 diffractometer with graphite-monochromated MoKα radiation (λ=0.71069Å). Intensity data were collected in the ω-2θ mode (max. scan time 80s per reflection). Accurate unit cell parameters were obtained by least-squares analysis of the setting angles of 24 reflections in the θ-range 16-17°. Three standard reflections were monitored at regular 60min intervals in order to monitor possible crystal decay while orientation control was performed after every 200 measured reflections. Data were corrected for Lorentz-polarisation and linear decay corrections applied if crystal decay was significant.

The data-collections for the DIABCD (Chapter 3), CYCBCD and CYCGCD complexes (Chapter 6) were performed by the author. In these cases, reflection intensities were collected on a Nonius Kappa-CCD diffractometer using graphite-monochromated MoKα radiation (λ=0.71069Å). Data were corrected for Lorentz-polarisation effects and cell refinement and data reduction were performed using the programs DENZO and SCALEPACK.[2]

Structure solution and refinement

The structures were solved either by the optimisation of a molecular fragment with the program PATSEE[3,4] or by isomorphous replacement methods, using the published co-ordinates for selected cyclodextrin atoms of an isomorphous structure. For those structures solved by isomorphous replacement, published coordinates for the skeleton CD atoms of an isomorphous complex were input for refinement in the programs SHELX-76[5] or SHELXL-93.[6] The refinement of all structures was completed with either SHELX-76 or SHELXL-93.

PATSEE

For the DIABCD (Chapter 3) and the CYCBCD complexes (Chapter 5) structure solution was achieved using the program PATSEE.

PATSEE attempts to combine the merits of both Patterson and direct methods techniques in order to position a fragment of known geometry in a unit cell.

The reflection data are processed with SHELXS[7] using the PSEE command to calculate the sharpened Patterson map and a set of the largest E-values. A fragment search is then performed with PATSEE. The fragment search consists of a rotational search for the best orientation of the fragment followed by a translational search.

The orientation of the search model is determined by a conventional but highly automated real-space Patterson rotation search. A comparison between the weights of a number of vectors (n) produced by the orientations of the search model (w_i) and the closest matching Patterson map vectors (P_i) is used to calculate rotational figures of merit (RFOMs).

$$RFOM = [\sum P_i/w_i] / n$$

The translational positions of a set of the fragments with the highest RFOM values is located by maximising the weighted sum of cosines of a small number of strong translational-sensitive triple-phase invariants.

$$TPRSUM = [\sum E_h E_k E_{-h-k} \cos(\varphi_h+\varphi_k+\varphi_{-h-k})] / [\sum E_h E_k E_{-h-k}]$$

For the solutions obtained, the correlation between the Patterson function and the intermolecular vector set is used to determine a translational figure of merit (TFOM), in an analogous manner to that for CFOM.

$$TFOM = [\sum P_i/w_i] / n$$

An R-index (R_E) based on E magnitudes is computed for sets of solutions with the best TFOM values.

$$R_E = [\sum \{|E_{obs}|-|E_{calc}| / p\}] / [\sum |E_{obs}|]$$

The best solutions are sorted according to a combined figure of merit (CFOM) based upon agreement with the Patterson function (TFOM), triple-phase consistency (TPRSUM) and the R-index involving E_{obs} and E_{calc} (R_E).

$$CFOM = [0.2 \times \{(RFOM+TFOM) / 2\} + \times TPRSUM^{1/2}] / R_E$$

PATSEE produces a list of the best solutions found for the fragment. The fractional coordinate sets of these positions can then be chosen for partial structure expansion in SHELXS. If the partial structure expansion is successful, atomic coordinates can be input for refinement.

SHELX-76

For the complexes ACEBCD, BROBCD and PHEBCD (Chapter 3) the refinements were completed using the SHELX-76 program. For this program minimisation of the function $\Sigma w(|F_o| - |kF_c|)^2$ is pursued by refinement using full-matrix or block-diagonal least squares techniques. The residual index, R_1, is a measure of the agreement between the observed structure factors obtained from the measured reflection intensities and the calculated structure factors computed from the model which is being refined.

$$R_1 = \Sigma (| |F_o|-|F_c| |) / \Sigma (|F_o|)$$

A weighted value of the residual index (R_w) is computed where the measured structure factors are weighted according to their reliability.

$$R_w = \Sigma (w^{1/2}(| |F_o|-|F_c| |) / \Sigma (w^{1/2}|F_o|))$$

where $w = 1 / [\sigma^2(F_o)+g(F_o)^2]$

The term g is chosen in the above weighting scheme to yield constant distributions of $w(|F_o|-|F_c|)^2$ with respect to $\sin\theta$ and $(F_o/F_{max})^{1/2}$.

The Goodness of Fit, S, represents another measure of the agreement between observed and calculated structure factors. The value of S is unity if there is perfect agreement.

$$S = [\Sigma w(|F_o|-|F_c|)^2 / (N-n_p)]^{1/2}$$

where N is the total number of reflections and n_p is the total number of parameters refined.

R_{int} is a measure of the agreement between all reflections for which more than one equivalent reflection has been measured.

$$R_{int} = \Sigma |(F_o-F_{o\,(mean)}| / \Sigma |F_o|$$

SHELXL-93

For the complexes DIABCD (Chapter 3), CYCBCD and CYCGCD (Chapter 6) structure refinement was completed using the SHELXL-93 program. For this program, minimisation of the function $\sum w(F_o^2-kF_c^2)^2$ is pursued by refinement using full-matrix least-squares techniques. The values of the weighted residual index (wR_2) obtained for refinement against F^2 are larger than the values of wR obtained for refinement against F. For comparison with refinements based on F, the conventional index R_1 based on observed F values larger than $4\sigma(F_o)$ is also calculated.

R_1 = as for SHELX-76

$$wR_2 = [\ \sum (w(F_o^2-F_c^2)^2) / \sum (w(F_o^2)^2)\ ]^{1/2}$$

where $w = 1 / [\sigma^2(F_o)^2+(aP)^2+(bP)]$

and $P = [\max(Fo^2,0) + 2F_c^2] / 3$

The terms a and b are chosen in the above weighting scheme to yield constant distributions of $(w(F_o^2-F_c^2)^2)$ with $\sin\theta$ and $(F_o/F_{max})^{1/2}$.

Refining against F^2 leads to greater deviations of the Goodness of Fit (S), from unity than refinement against F. These values are therefore not directly comparable to structures refined against F.

$$S = [\ \sum w(|F_o^2|-|F_c|^2)^2 / (N-np)\ ]^{1/2}$$

As for SHELX-76 R_{int} is a measure of the agreement between all equivalent reflections and is computed with F_o^2 for SHELXL-93.

$$R_{int} = \sum |F_o^2-F_o^2{}_{mean}| / \sum |F_o^2|$$

Further details of specific structure solutions and refinements are discussed under individual structures in the relevant chapters.

X-ray Powder Diffraction (XRD)

For all the crystalline inclusion complexes prepared with β- and γ-cyclodextrin, x-ray powder diffraction patterns were obtained using a Philips PW1050/25 goniometer with Ni-filtered CuKα-radiation (λ=1.5418Å) produced at 50kV and 40mA. The system was calibrated with a silicon standard which yielded peak positions 28.45±0.01° 2θ before and after each scan. The samples to be analysed were removed from mother liquor, dried under filter paper and crushed to a particle size of less than 100μm using a mortar and pestle. The samples were packed in Al sample holders and XRD traces (scan speed 1.0° 2θ/min, step size 0.1° 2θ) were recorded from 5 to 45° in 2θ.

For the co-ground and kneaded preparations containing salbutamol laurate and hydroxypropyl-β-cyclodextrin, x-ray powder diffraction patterns were obtained using a Philips PW1050/80 goniometer with a PW1394 motor control unit and PW1390 channel control unit mounted on a Philips PW1130/90 x-ray generator operating at 40kV and 25mA. The powdered samples were packed in aluminium sample holders. The samples were scanned with Ni-filtered CoKα radiation (λ=1.790Å) and step scans (0.1° 2θ, 1 second counting times) were performed from 4 to 40° in 2θ.

Calculated XRD powder patterns were produced using the POWDIS-POWUTL option of the OscailP Version 7 crystallography package.[8] In order to generate such an idealised x-ray powder pattern the cell parameters, space group symmetry, atomic coordinates and thermal parameters of the appropriate crystal structure were used as input for the program. Calculated powder patterns were compared with the corresponding experimental patterns to prove that the crystallographic model is correct. The calculated patterns can also be used to conveniently identify and assess the purity of a sample.

Additional resources

Molecular parameters and geometrical data with their associated e.s.d.s were calculated using the program PARST95.[9] Molecular and packing diagrams were drawn with the programs PLUTO[10] and PLATON.[11] CPK diagrams were constructed using the program Weblab ViewerPro Version 3.20.[12] Dipole moments for molecules were calculated using the MNDO potential function as part of the MOPAC utilities of program Chem3D Pro Version 3.5.[13] Non-bonded distances, angles and torsion angles were obtained from the program RES2INS.[14]

The Cambridge Structural Database (CSD)[15] was used to investigate published crystal data for comparison with structures reported in this study.

Files containing atomic coordinates, bond lengths, bond angles, torsion angles and structure factor tables for the solved structures have been deposited on computer diskettes attached to the inside back cover of the thesis (see Appendix A and B for details). The files have been saved as text files and can be opened in a text editor such as WORDPAD in Windows95 and Windows98. The files can also be opened in Microsoft Word 6.0 or Microsoft Word-97 as well as other word processing packages.

The PARST[9] files containing the atomic coordinates, displacement parameters, bond lengths, bond angles and torsion angles for each structure are saved under the abbreviation of the complex with the extension .lst (e.g. ACEBCD.LST). The structure factor tables are saved with the extension .sft or .fcf depending on whether the structure factors are based on F or F^2 respectively (e.g. ACEBCD.HKL). The Crystallographic Information Files are saved with the extension .cif (e.g. ACEBCD.CIF). The SHELX[6] type coordinate files are saved with the extension .res and are included for visualisation of the structures (e.g. ACEBCD.RES).

References

1.) *The United States Pharmacopoeia, Twenty-First Revision*, United States Pharmacopoeial Convention, Inc., Rockville, Maryland, **1985**.

2.) Z. Otwinowski and W. Minor, *Processing of X-ray Diffraction Data in Oscillation Mode in Methods in Enzymology*, ed. C. W. Carter and R. M. Sweet, Academic Press, New York, **1996**, Vol. 276, 307.

3.) E. Egert, *Acta Cryst.*, **1983**, A39, 936.

4.) E. Egert and G. M. Sheldrick, *Acta Cryst.*, **1985**, A41, 262.

5.) G. M. Sheldrick, *SHELX-76, Program for crystal structure determination*, University of Cambridge, England, **1976**.

6.) G. M. Sheldrick, *SHELXL-93, Program for the Refinement of Crystal Structures*, University of Göttingen, Germany, **1993**.

7.) G. M. Sheldrick, *Crystallographic Computing*, ed. G. M. Sheldrick, C. Krüger and R. Goddard, Oxford University Press, **1985**, Volume 3, 175.

8.) P. McArdle, *J. Appl. Cryst.*, **1998**, 31, in press.

9.) M. Nardelli, *J. Appl. Cryst.*, **1995**, 28, 659.

10.) W. D. S. Motherwell, *PLUTO89, program for plotting molecular and crystal structures*, University of Cambridge, England, **1989**.

11.) Spek, A. L., *Acta Cryst.*, **1990**, A46, C-34.

12.) *Weblab ViewerPro Version 3.20* (Copyright **1998** by Molecular Simulations Inc.).

13.) *Chem3D Pro Version 3.5.1* (Copyright **1986-1996** CambridgeSoft Corporation).

14.) L. J. Barbour, *J. Appl. Cryst.*, **1998**, 31, 963.

15.) *Cambridge Structural Database and Cambridge Structural Database System*, Version 5.12, October **1998**, Cambridge Crystallographic Data Centre, University Chemical Laboratory, Cambridge, England.

CHAPTER 3 : β-CD COMPLEXES WITH *PARA*-AMINOPHENOL DERIVATIVES

Introduction

Acetaminophen, *p*-bromoacetanilide, phenacetin and diacetamate are members of a group of compounds known as the *para*-aminophenol derivatives and this group forms part of the class of analgesic-antipyretic agents (Figure 3.1).

Acetanilide is the parent member of this group of drugs. It was introduced into medicine in 1886 under the name of antifebrin when its antipyretic action was discovered accidentally.[1] However, acetanilide proved to be excessively toxic. In the search for less toxic compounds, *para*-aminophenol was tried in the belief that the body oxidised acetanilide to this compound. Toxicity was not lessened; however, a number of chemical derivatives of *para*-aminophenol were then tested. One of the more satisfactory of these was phenacetin which was introduced into therapy in 1887 and was extensively employed in analgesic mixtures. Acetaminophen (or paracetamol) was first introduced in medicine in 1893. However it has gained popularity only since 1949 after it was recognised as the active metabolite of both acetanilide and phenacetin.

The antipyretic activity of these compounds resides in the aminobenzene structure. Introduction of other substituents onto the position *para* to the amino group and onto the free amino group reduces toxicity without loss of antipyretic action.[2] The best results are obtained with phenolic alkyl ethers (e.g. phenacetin) and with the amides (e.g. acetaminophen, phenacetin).

Acetaminophen and phenacetin have analgesic and antipyretic effects that do not differ significantly from those of aspirin (acetylsalicylic acid). However, they have only weak anti-inflammatory effects. Neither drug produces the gastric irritation, erosion or bleeding which may occur after administration of aspirin and other salicylates.[3]

The compounds selected for this study are all *para*-substituted acetanilides, namely acetaminophen (ACE), *p*-bromoacetanilide (BRO), phenacetin (PHE) and diacetamate (DIA), which are substituted with hydroxy, bromo, ethoxy and acetyloxy groups respectively. Figure 3.1 shows the chemical formulae and numbering schemes employed for the four drug molecules.

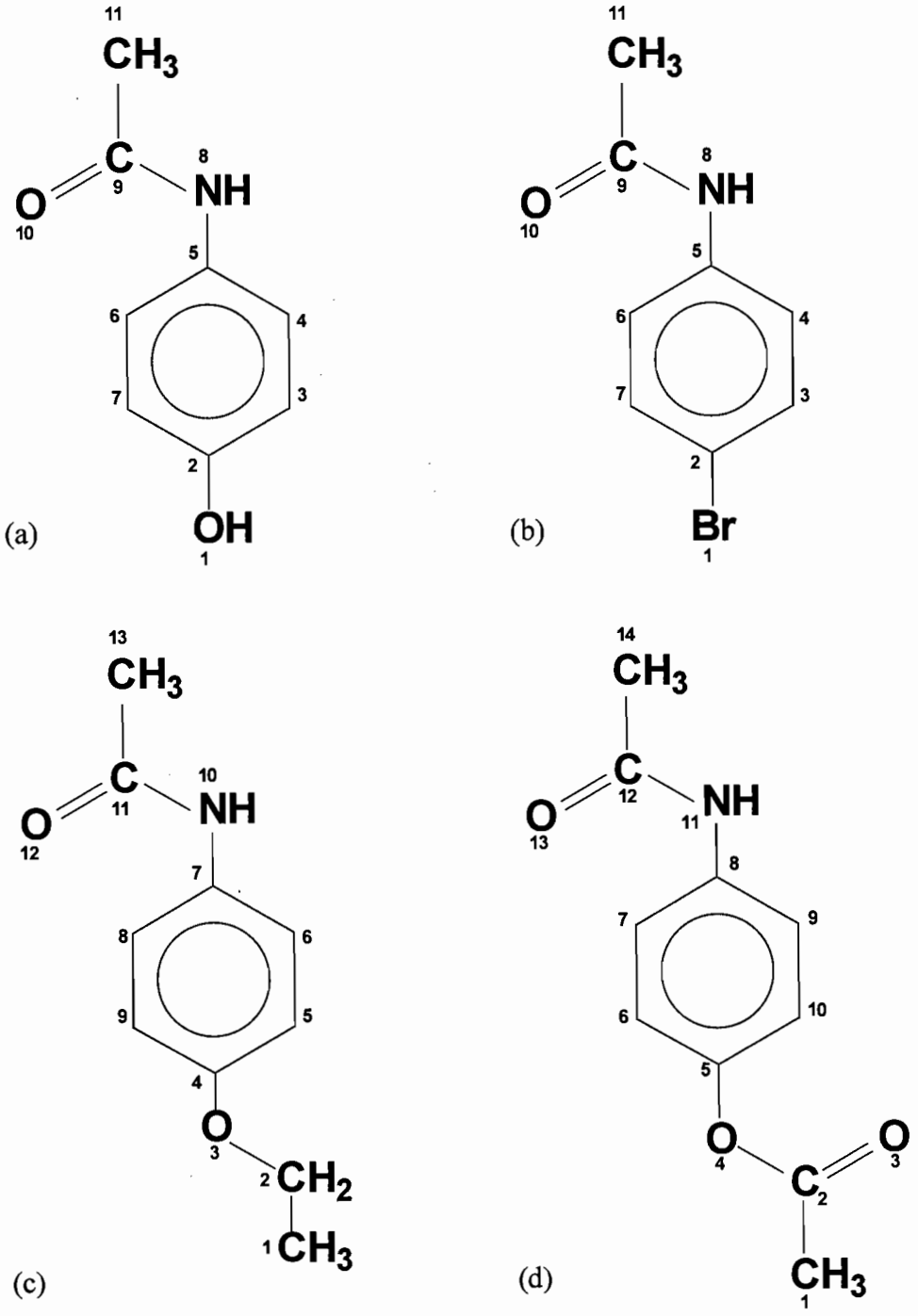

Figure 3.1 Chemical formulae and numbering schemes for (a) ACE, (b) BRO, (c) PHE and (d) DIA

Acetaminophen and phenacetin are widely used as antipyretic and analgesic agents. Acetaminophen formulations are marketed under a variety of names including PANADOL™ and TYLENOL™. Acetaminophen has been reported as being slightly soluble in water[4] while its acrid taste and unpleasant feeling in the mouth continue to provide problems in its use.[5,6] Phenacetin has also been reported to possess a low aqueous solubility.[4] The improvement of solubility and dissolution rate is the most popular reason for formulation of drugs as CD complexes. CD complexation of acetaminophen and phenacetin are likely to provide a favourable increase in these solution properties of the two drugs. The acrid taste of acetaminophen could be eliminated by CD inclusion of the drug, as has been the case with CD complexation of other bitter-tasting drug substances. This is achieved by the masking of the bitter taste of the drug and by the addition of the relatively sweet taste of the CD; for example, a β-CD solution of 2.5% is as sweet as a 1.7% sucrose solution.[7] The favourable granulation and tabletting properties of CD preparations are useful for the formulation of poorly compressible drug substances. It has been reported in a number of publications that the compression behaviour of acetaminophen is very poor.[8,9]

p-Bromoacetanilide was prepared, together with a number of other *para*-aminophenol derivatives, soon after the discovery of the activity of these compounds. Its analgesic and antipyretic activity was reported and it was marketed under the brand name of ANTISEPSIN™. However, it was surpassed by acetaminophen and phenacetin in use as an analgesic/antipyretic agent. *p*-Bromoacetanilide is reported to be practically insoluble in cold water.[4] CD complexation of this compound was investigated mainly for comparative reasons in this study, as human toxicity has been reported for it.

Diacetamate is the acetylated derivative of acetaminophen and is actively metabolised to acetaminophen. The results of studies indicated that diacetamate was completely converted to acetaminophen by pancreatic lipase in less than 15min.[10] Diacetamate was determined to be a good candidate for incorporation into chewable tablets, where the use of acetaminophen is restricted by its acrid taste.[5,6] The bioavailability of diacetamate was reported to be closely similar to that of acetaminophen.[11] However, diacetamate has been reported to possess low aqueous solubility[12] and poor flowability and compressibility.[10] CD complexation of diacetamate might provide a useful means for improving such properties of the drug.

A thorough search of Chemical Abstracts from 1972 to July 1998 produced 25 papers on the study and applications of acetaminophen with various CDs and 4 concerning the CD complexation of phenacetin. No publications reporting the study and applications of *p*-bromoacetanilide or diacetamate with CDs were found.

Thermoanalytical investigations of inclusion complexes of acetaminophen and β-CD concluded that DSC was a useful method for the detection of complexation. [13,14] These conclusions were based on the disappearance of the sharp melting endotherm of acetaminophen in the β-CD complex preparations.

Thermal analysis was employed as the main tool in the investigation of the interaction between acetaminophen and β-CD by powder compaction. The results obtained with a hydraulic press and single punch tablet machine showed that mixtures of included, amorphous and crystalline acetaminophen are formed.[15] DSC was used to determine the interaction and 1:1 stoichiometry of an acetaminophen-β-CD inclusion complex.[16,17] The same researchers also investigated the interaction of supercritical fluids (CO_2 in this case) with the acetaminophen-β-CD inclusion complex and physical mixture.[18] The influence of temperature, particle size and water content were tested and the conclusions were that the inclusion complex proved to be fairly stable under the experimental conditions adopted.

Lin et al.[19-27] reported a number of studies on the interaction of acetaminophen (ACE) with α- and β-CD. Solution studies reported that the solubility and partition rate of ACE were increased in the presence of CDs[19] while the partition coefficient and equivalence point of the conductimetric titration curve were decreased.[20] The changes were explained by the complexation of ACE with α- and β-CD. The stability constants of acetaminophen with α- and β-CD were determined kinetically and were found to be higher for the 1:1 ACE:β-CD complex than for the ACE:α-CD 1:1 complex.[19] The stability constant of the acetaminophen-α-CD inclusion complex was reported as 3.53 M^{-1} †. Increasing CD concentrations were reported to decrease the degradation of ACE.[21] Spray drying[23], co-grinding,[24,25] heating,[25] freeze-drying[25,26], mechanical grinding[26] and humidity[27] were investigated in their influence on the formation of inclusion complexes of ACE with α- and β-CD.

† The author is aware that the equilibrium constant is a unitless quantity; however, equilibrium constants obtained from the literature will be reported as they were in the original publication

Complexes were evaluated by DSC, X-ray diffraction and IR spectroscopy. All methods resulted in the formation of a β-CD complex with ACE while only heating was reported to lead to the formation of an α-CD complex. The dissolution rates of the ground and spray dried β-CD complexes with ACE were reported to be higher than for the physical mixtures and drug alone.[23,24] Based on the results of the IR spectra of the co-ground and freeze-dried preparations, Lin and Lee[26] postulated a structure for the acetaminophen-β-CD inclusion complex as shown in Figure 3.2. It was suggested that the shift of the C=O stretching vibration to a higher frequency was caused by dissociation of the intermolecular hydrogen bonds of ACE as a result of the formation of an inclusion complex. The band corresponding to the amido group of ACE was shifted to a lower frequency which was attributed to a possible intermolecular hydrogen bond between the amido group of acetaminophen and a hydroxyl group of the β-CD molecule.

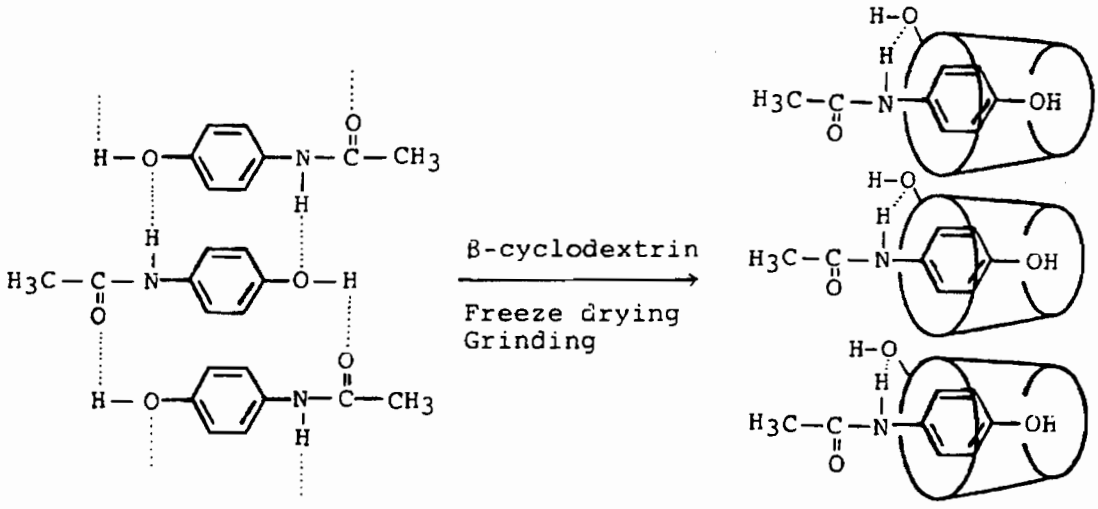

Figure 3.2 Schematic illustration of the proposed mode of inclusion in the ACE-β-CD complex (reproduced from Reference 26)

A patent ~~was filed~~ ~~for~~ the preparation of a HP-β-CD complex with acetaminophen.[28] The application cited an improvement of the relatively low water solubility and dissolution properties of the drug.

α-, β-, γ- and HP-β-CD were noted to enhance the migration of acetaminophen and other *p*-nitroanilines in an aqueous mobile phase on thin layer chromatography.[29] Equilibrium binding constants were determined for the drug-cyclodextrin complexes formed in the mobile phase. The stability constants of acetaminophen with β-CD were also determined by means of absorption and fluorescence spectroscopy.[30]

The stability constants of acetaminophen and phenacetin complexes with β-CD were determined spectrophotometrically at 20°C. The stability constants were reported as 179 M^{-1} and 106 M^{-1} for phenacetin and acetaminophen respectively.[31] The solubility and dissolution rate of phenacetin in aqueous solution were increased on complexation with β-CD.[32] The shift of the 2θ = 13° XRD peak for ~~pure~~ hydrated β-CD to a lower diffraction angle was reported to be intrinsic for complex formation. Phenacetin complexation with β-CD was tested in this manner, but could not be confirmed.[33] However, complexation was confirmed for a number of other drugs interacting with β-CD using this procedure. The formation of CD inclusion complexes by an agglomeration process has been patented and complexes with phenacetin and a number of other guest molecules were reported to be prepared by this process.[34] Sufficient agitation in the presence of a small amount of water was reported to result in complex formation and bonding into agglomerates.

UV visible spectrophotometric studies of the interaction of acetaminophen with β- and dimethyl-β-CD enabled the estimation of the stability constants of the inclusion complexes, which were determined to be 130 and 83 M^{-1} respectively.[35] The spectral changes associated with the interaction of acetaminophen and α- and γ-CD were too small for use in determining stability constants. From examination of the CPK models, the authors suggested that complete inclusion of the hydrophobic benzene ring into the α-CD cavity is not possible and would lead to unfavourable interactions between the excluded portion of the benzene ring and solvent water. Examination of the CPK models for the inclusion of acetaminophen into the cavities of β-CD and dimethyl-β-CD showed that the benzene ring can be totally included in either CD. Methylation of the β-CD molecule led to a decrease in the stability constant of acetaminophen for dimethyl-β-CD relative to β-CD. The explanation suggested for this observation was that in the β-CD complex the polar hydroxy and amide groups of the drug could interact with the hydroxy groups of the β-CD molecule or with solvent water. However, in the case of the dimethyl-β-CD, the number of hydroxy groups is reduced and the length of the hydrophobic cavity is extended, thus reducing the possibilities for interaction of the polar groups of acetaminophen with CD hydroxyl groups or solvent water, leading to a decrease in the stability of that complex. The benzene ring of acetaminophen was thought to be too small compared to the internal

diameter of the γ-CD annulus, leading to a very small tendency for formation of an inclusion complex.

Tasic et al.[36-38] reported that the solubility and dissolution rates of β-CD-acetaminophen dispersion powders (1:1 by weight) and tablets were increased compared to those of acetaminophen alone.[36] Scanning electron microscopy (SEM) was used to evaluate the texture, structure, compactibility and consolidation phenomenon in spray dried and kneaded acetaminophen-β-CD dispersion powders.[37] The results demonstrated that these tablets show good plastic deformation with strong cohesion and small elasticity of particles. The mechanism of cool sintering was proposed for the consolidation of these tablets. Acetaminophen alone and acetaminophen physical mixtures with β-CD showed poor compression behaviour and were compressed by the brittle fracture mechanism. The conclusions made were that β-CD has a positive influence on the compression properties and mechanism of consolidation. The evaluation of the compression behaviour of these acetaminophen-β-CD solid dispersions by the study of the energy parameters using force-displacement measurements further confirmed the conclusions drawn from the SEM study.[38]

It was reported by Weiszeiler and Szejtli[39] that the bitter taste of acetaminophen can be perfectly eliminated by complexation with β-CD. A medicated gum containing acetaminophen and β-CD was formulated and recently patented by researchers in industry in Switzerland. The chewing gum was reported to contain an acetaminophen-β-CD inclusion complex and to have a pleasant taste which was independent of this active ingredient.[40,102]

Objectives of the study

The aim of investigation was to prepare crystalline complexes of acetaminophen (ACE), *p*-bromoacetanilide (BRO), phenacetin (PHE) and diacetamate (DIA) with β-CD and provide a physicochemical characterisation of these complexes in the solid state.

Furthermore, this series of closely related drugs, differing only in the nature of the substituent *para* to the acetamide group, presents the opportunity for evaluating the effects of substituent variation on the nature and mode of drug inclusion in CDs.

Synthesis of Diacetamate

10g (66mmol) of acetaminophen was placed in a 500ml round-bottomed flask containing a mixture of 6.2ml (66mmol) of acetic anhydride, 1ml of reagent grade pyridine and 10ml isopropanol. The mixture was refluxed until a clear solution was obtained. It was then poured on 100g of crushed ice and filtered under vacuum. The precipitated diacetamate was washed with chilled water until free from pyridine and acetic acid. The white solid obtained was re-crystallised from isopropanol-water (40:60) yielding glossy, plate-like crystals. The melting behaviour was checked using DSC and found to have an onset temperature of 153°C and a peak at 155°C which corresponded to the melting temperature referred to in the literature.[10] The mass spectrum gave a molecular ion peak at m/e 193 which corresponds to the molecular weight. The C, H, and N microanalysis results are presented in Table 3.1.

Table 3.1 C, H, and N microanalysis results for DIA

	Calculated %			Experimental %		
	C	**H**	**N**	**C**	**H**	**N**
DIA	62.18	5.70	7.25	62.43	5.82	7.45

Complex preparation

Crystalline complexes of ACE, BRO, PHE and DIA with β-CD were obtained from slow cooling of hot aqueous solutions of CD and drug in 1:1 molar ratios. The solutions were prepared according to the concentrations listed in Table 3.2. The complexes of ACE, BRO, PHE, DIA with β-CD will be referred to hereafter as the ACEBCD, BROBCD, PHEBCD and DIABCD complexes. Photographs of crystals of the complexes taken on a microscope under plane polarised light at a magnification of 10x are shown in Figure 3.3.

Table 3.2 The details of the preparation of the ACEBCD, BROBCD, PHEBCD and DIABCD complexes

Complex	CD (mmol)	Drug (mmol)	Water (ml)
ACEBCD	0.70	0.70	4
BROBCD	0.53	0.53	4
PHEBCD	0.53	0.53	4
DIABCD	0.62	0.62	4

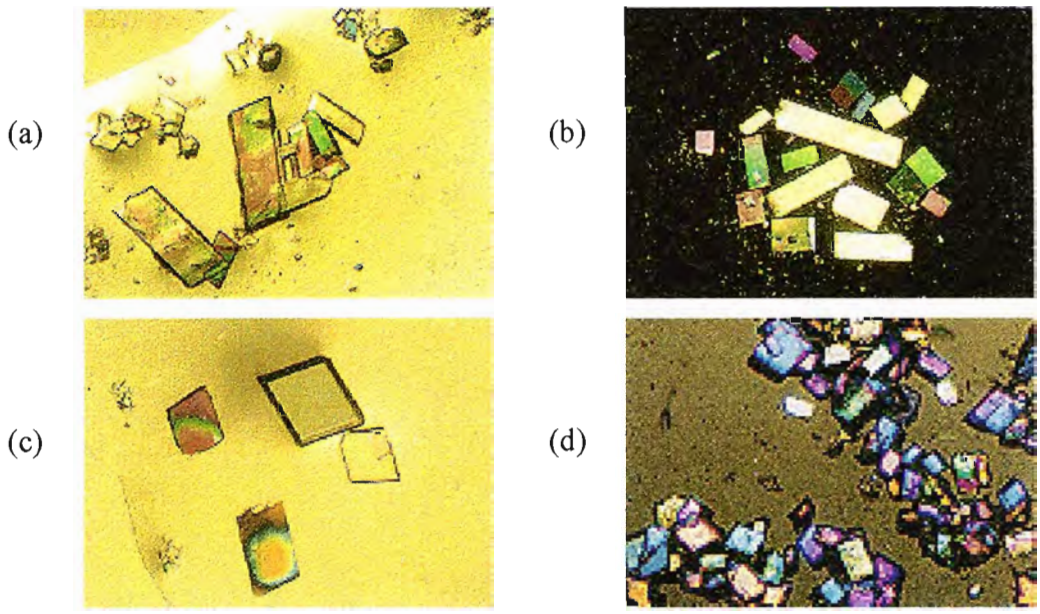

Figure 3.3 Photographs of the crystals taken under plane polarised light (at a magnification of 10x) (a) ACEBCD (b) BROBCD (c) PHEBCD (d) DIABCD

UV Spectrophotometry

The host:guest ratios were determined by UV spectrophotometry at 244, 248, 245 and 242nm in distilled water for the ACEBCD, BROBCD, PHEBCD and DIABCD complexes. The stoichiometric ratios obtained are shown in Table 3.3.

Table 3.3 The β-CD : drug ratios determined from UV spectrophotometry

Complex	ACEBCD	BROBCD	PHEBCD	DIABCD
Host : Guest ratio	1:1	1:1	1:1	1:1

Microanalysis

The host:guest ratios were confirmed by C, H and N microanalysis results. The complexes were dried under vacuum for 1 hour and thermogravimetric analysis was used to determine the residual water content of the samples to be analysed (Table 3.4).

Table 3.4 The C, H and N microanalysis results for the ACEBCD, BROBCD, PHEBCD and DIABCD complexes

Complex	Calculated (%)			Experimental (%)		
	C	H	N	C	H	N
ACEBCD.2H_2O	45.42	6.28	1.06	45.43	6.36	1.18
BROBCD.2H_2O	43.35	5.92	1.01	43.64	6.02	1.19
PHEBCD.2H_2O	46.26	6.45	1.04	46.59	6.50	1.22
DIABCD.2H_2O	45.78	6.24	1.03	46.22	6.33	1.23

Water content

The total water content of the complexes was calculated from the initial mass losses obtained from TGA traces of the ACEBCD, BROBCD, PHEBCD and DIABCD complexes (Table 3.5).

Table 3.5 The percentage water loss from the ACEBCD, BROBCD, PHEBCD and DIABCD complexes and the number of water molecules per CD molecule for each

Complex	% weight loss	Temperature range (°C)	No. of water molecules / CD
ACEBCD	15.7	30-150	13.3
BROBCD	15.4	30-150	13.5
PHEBCD	16.3	30-150	14.2
DIABCD	16.1	30-150	14.2

Stoichiometric formulae

The full stoichiometric formulae of the complexes obtained from the TGA, UV and microanalysis results are presented in Table 3.6.

Table 3.6 The H:G:Water ratios and stoichiometric formulae for ACEBCD, BROBCD, PHEBCD and DIABCD complexes

Complex	H : G : Water	Stoichiometric formula
ACEBCD	1 : 1 : 13.3	$1(C_{42}H_{70}O_{35})\cdot1(C_8H_9NO_2)\cdot13.3(H_2O)$
BROBCD	1 : 1 : 13.5	$1(C_{42}H_{70}O_{35})\cdot1(C_8H_8NOBr)\cdot13.5(H_2O)$
PHEBCD	1 : 1 : 14.2	$1(C_{42}H_{70}O_{35})\cdot1(C_{10}H_{13}NO_2)\cdot14.2(H_2O)$
DIABCD	1 : 1 : 14.2	$1(C_{42}H_{70}O_{35})\cdot1(C_{10}H_{11}NO_3)\cdot14.2(H_2O)$

Dissolution

Dissolution studies were conducted using the rotating basket method as described in Chapter 2. The dissolution profiles for the pure drug, 1:1 β-CD:drug physical mixture and inclusion complex are shown in Figures 3.4 and 3.5 for ACE and DIA respectively. The assays were done by UV spectrophotometry at 244 for ACE and 242nm for DIA.

The dissolution rates of the CD inclusion complexes were, in both cases, more rapid than those for the uncomplexed drugs and the 1:1 CD:drug physical mixtures. Both the ACEBCD and DIABCD complexes reached 50% dissolved drug after 10min, while the physical mixtures with ACE and DIA reached that stage after 20 and 25min

respectively. Uncomplexed ACE reached 50% dissolved drug after 25min while uncomplexed DIA only reached that stage after 150min.

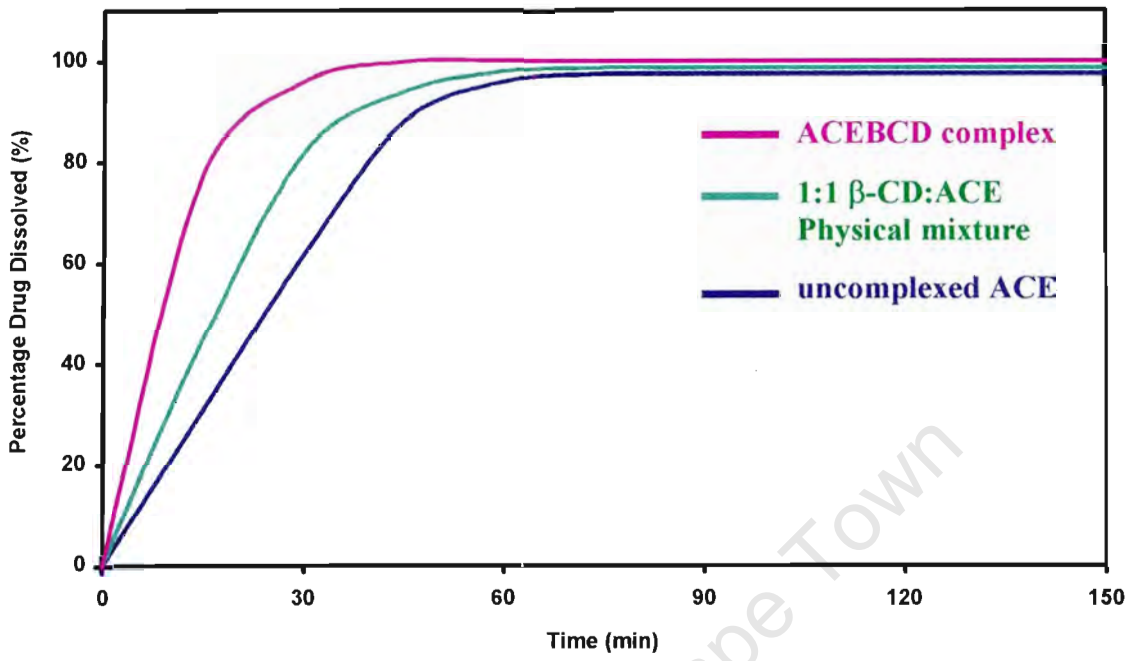

Figure 3.4 Dissolution profile for uncomplexed ACE, a 1:1 β-CD:ACE physical mixture and the ACEBCD complex

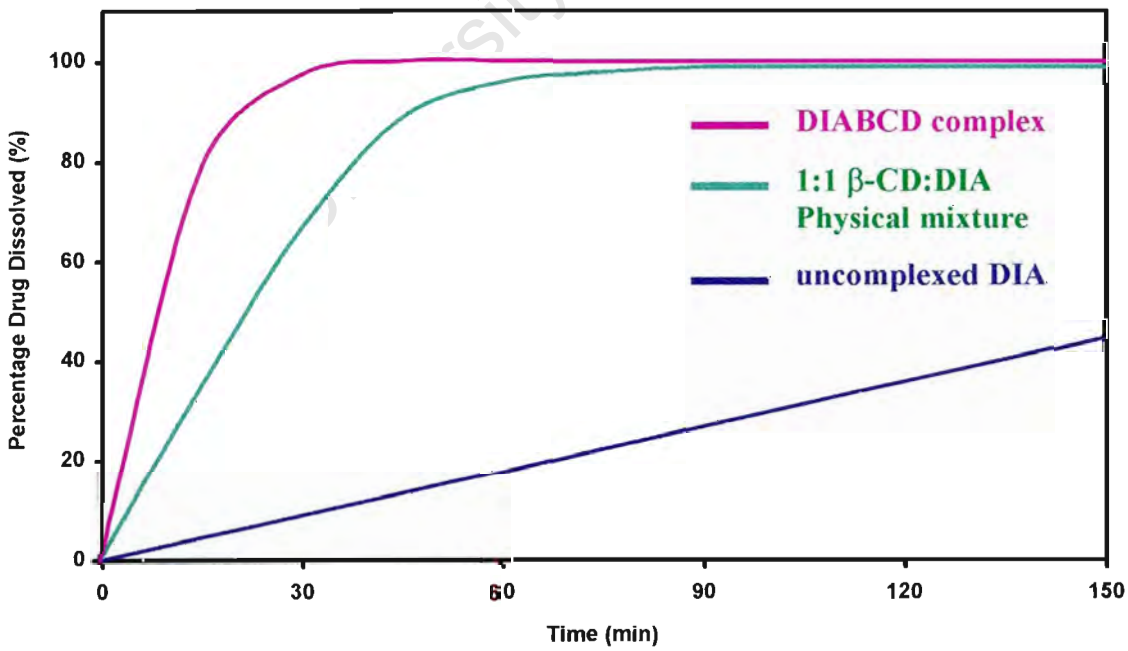

Figure 3.5 Dissolution profile for uncomplexed DIA, a 1:1 β-CD:DIA physical mixture and the DIABCD inclusion complex

HSM

HSM was used to analyse the thermal behaviour of the complexes upon heating at a constant rate of 10°C/min. The HSM results for ACEBCD, BROBCD, PHEBCD and DIABCD are presented in Figure 3.6. After removal from mother liquor, the crystals of the complexes displayed signs of cracking as they began to lose their water of crystallisation. By 150°C the complexes had become opaque. Significant cracking is evident in the crystals of the BROBCD and PHEBCD complexes. TGA results (Figures 3.7 (a), 3.7 (b), 3.8 (a) and 3.8 (b)) show that water loss is completed by 150°C for all four complexes. The crystals of the complexes remain unchanged from the completion of dehydration to shortly before 300°C. Decomposition begins at a much earlier temperature (as determined from TGA and DSC evidence) for all complexes but is only evident by discoloration of the crystals after 270°C during HSM studies. The stages of decomposition can be more clearly seen from the TGA results presented in Table 3.7. Between 300°C and 310°C the crystals of the four complexes show a pseudo-melt and liquefy somewhat. As decomposition continues the semi-fluid state of the crystals becomes black and charred and odours of the acrid acetanilide guests can be detected. By 350°C extensive decomposition of the complexes has taken place.

TGA

The TGA results for the ACEBCD, BROBCD, PHEBCD and DIABCD complexes are shown in Figures 3.7 (a), 3.7 (b), 3.8 (a), and 3.8 (b). A summary of the observed percentage weight losses over the temperature intervals between 30, 150, 250, 300 and 350°C is presented in Table 3.7.

Table 3.7 The percentage weight losses for the ACEBCD, BROBCD, PHEBCD and DIABCD complexes at various temperatures

Temperature (°C)	ACEBCD		BROBCD		PHEBCD		DIABCD	
	Sample weight (%)	Δ Weight loss (%)†	Sample weight (%)	Δ Weight loss (%)†	Sample weight (%)	Δ Weight loss (%)†	Sample weight (%)	Δ Weight loss (%)†
30	100	-	100	-	100	-	100	-
150	86.7	13.3	86.5	13.5	85.8	14.2	85.8	14.2
250	85.4	1.3	84.1	2.4	80.9	4.9	82.7	3.1
300	82.2	3.2	78.0	6.1	75.7	2.9	77.3	5.4
350	35.0	47.2	25.0	53.0	32.0	43.7	15.0	62.3

† ΔWeight loss (%) = [Sample weight (%) at temperature(n-1)] - [Sample weight (%) at temperature(n)]

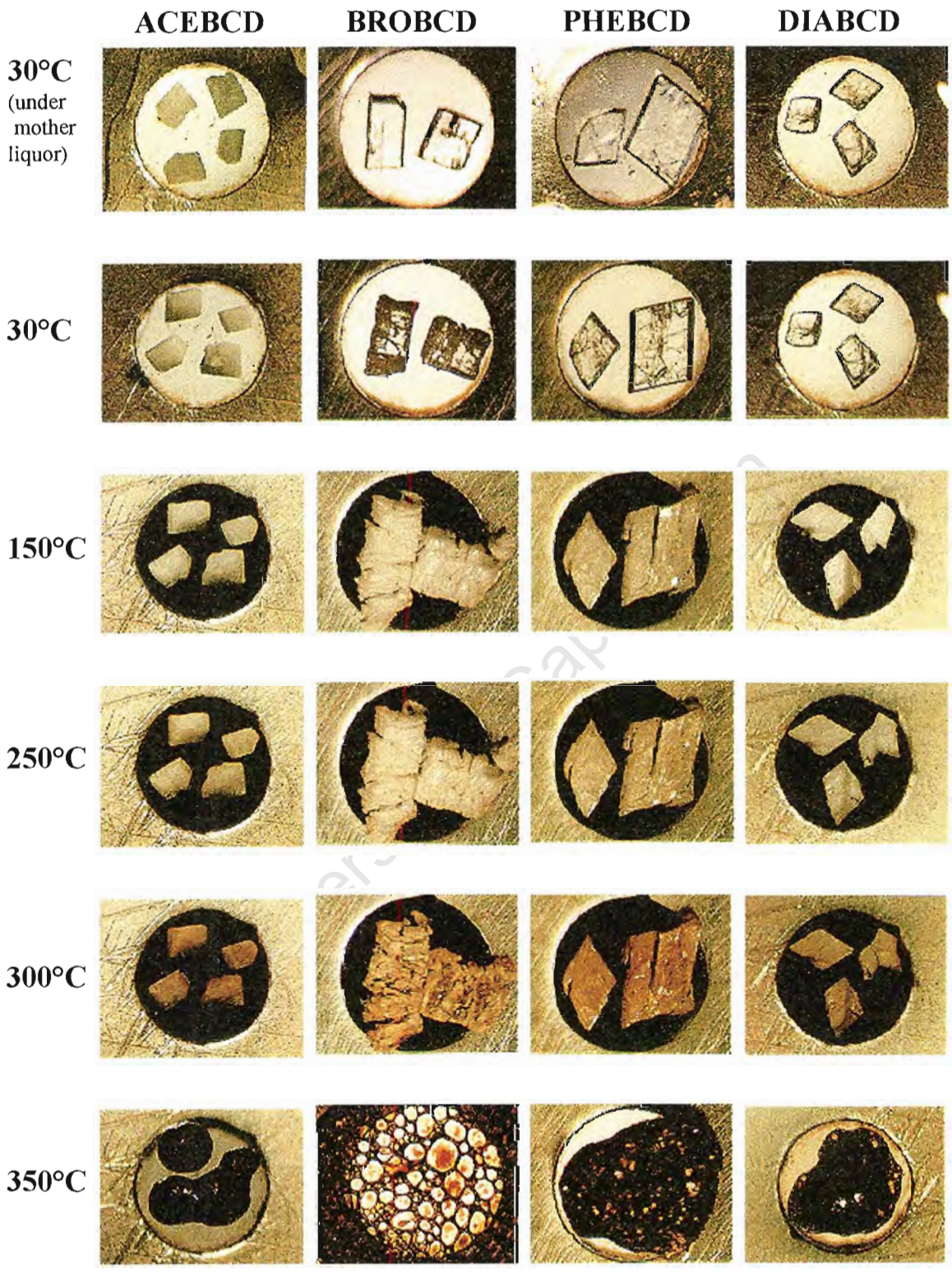

Figure 3.6 HSM photographs taken at various temperatures for crystals of the ACEBCD, BROBCD, PHEBCD and DIABCD complexes

DSC

The DSC and TGA traces for the ACEBCD, BROBCD, PHEBCD and DIABCD complexes are shown in Figures 3.7 (a), 3.7 (b), 3.8 (a) and 3.8 (b) respectively.

All complexes show endothermic events corresponding to water loss in the range 30 to 150°C. These endotherms cover the same range where water loss is observed from TGA (weight loss due to water loss is labelled A for the TGA traces). For ACEBCD the peak of the water loss endotherm (labelled A) occurs at 91°C. However, this peak contains a number of shoulders occurring at 100, 114, 121 and 142 °C indicating that water loss from this complex is clearly a multi-stage process. The water loss from the BROBCD complex displays a complex and highly reproducible sequence of endothermic events on DSC indicating that this complex follows a characteristic multi-stage dehydration process. The main endothermic peak (labelled A) occurs at a temperature of 80°C, with smaller but relatively distinct peaks at 56, 95, 102, 110, 120 and 142 °C. The PHEBCD and DIABCD complexes show a characteristic single dehydration endotherm (labelled A in each case) with peaks at 106 and 80 °C respectively. The presence of a single endotherm would indicate that water loss from these complexes occurs in a single step. However, both of these peaks are fairly asymmetrical, indicating that separate stages of water loss still occur. The traces show possible shouldering peaks at 80°C for PHEBCD and 100°C for DIABCD.

Smaller endotherms at 225, 187, 171 and 180°C for ACEBCD, BROBCD, PHEBCD and DIABCD (labelled B in each case) indicate the onset of decomposition for these complexes. The endotherm for BROBCD shows a distinct bimodal appearance with a second peak at 191°C. The onset temperatures of these endotherms correspond with the beginning of further mass loss on the TGA traces (labelled B). This decomposition begins in all cases well below the decomposition of the β-CD molecule, which occurs above 290°C, and is therefore associated with decomposition of the guest molecules included in the complexes. At 250°C the ACEBCD complex shows a sharp and characteristic exotherm (labelled C). This exotherm most likely indicates a phase change occurring in the already partially decomposing complex. A small bimodal peak 220°C for the PHEBCD complex is also associated with a phase change occurring during the decomposition.

The ACEBCD complex shows a sharp endotherm at 296°C (labelled D) which is attributed to a breakdown of the host framework of the complex. This corresponds with the decomposition of the β-CD molecule which begins above 290°C. For the BROBCD, PHEBCD and DIABCD complexes broader endotherms (labelled D in each case) characterise the region of the traces from 280 to 310°C.

The BROBCD complex shows a bimodal endotherm with peaks at 285 and 298°C while the PHEBCD and DIABCD complexes show single endotherms with peaks at 311 and 320°C respectively. The endotherms of the BROBCD trace are followed by a broad exotherm which is a further thermal event associated with the continuing decomposition of the complex. The PHEBCD complex also displays an exothermic event occurring above 320°C. Very large weight losses are observed in the TGA traces from 300°C onwards for all complexes (labelled D in all cases), confirming the decomposition of the β-CD molecules.

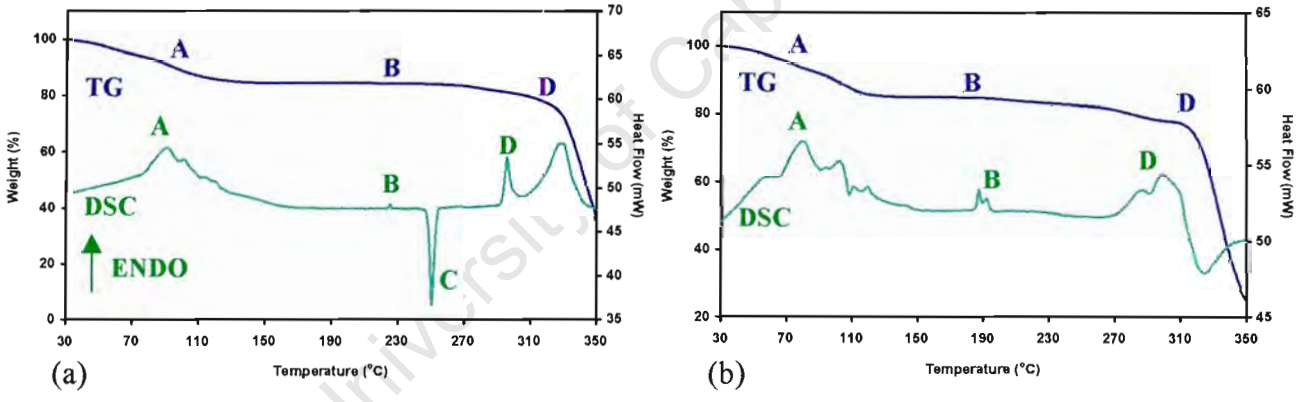

Figure 3.7 DSC and TGA traces of the (a) ACEBCD and (b) BROBCD complexes

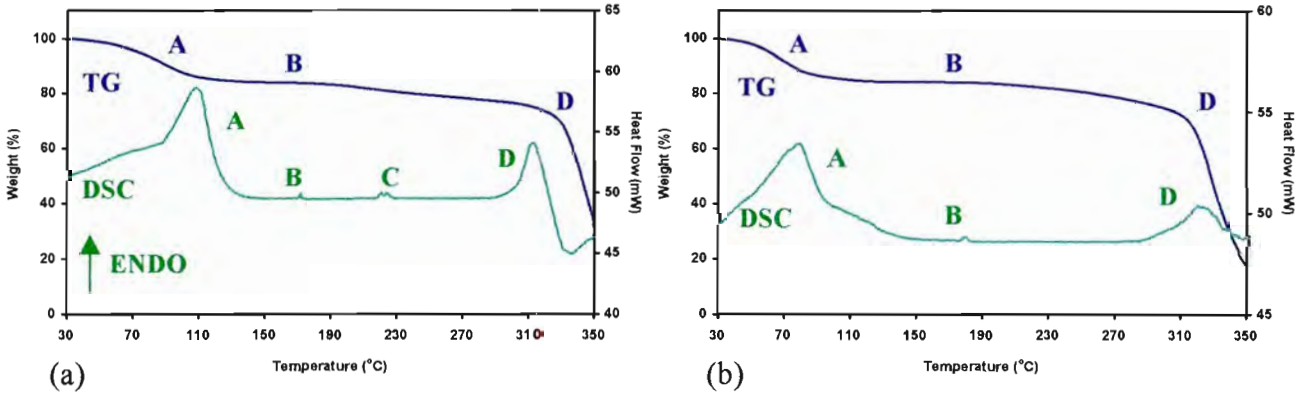

Figure 3.8 DSC and TGA traces of the (a) PHEBCD and (b) DIABCD complexes

X-ray crystallographic analysis of the ACEBCD structure

Data-collection

The preliminary cell parameters and space group for the ACEBCD structure (containing acetaminophen (ACE) as guest) were determined by x-ray photographic techniques. The latter revealed Laue 2/m symmetry and reflection conditions *hkl* : $h + k = 2n$, *h0l* : ($h = 2n$), and 0*k*0 : ($k = 2n$) which indicated the monoclinic space groups C2, C*m* or C2/*m*. Since the host is chiral, the former space group was chosen. During crystallisation from slow cooling the initially clear, translucent crystals of the ACEBCD complex became noticeably opaque once the temperature approached 20°C. The crystals of the complex were also very unstable when removed from mother liquor. In spite of some major difficulties in obtaining suitable crystals, data were collected for the ACEBCD complex for a crystal of the complex mounted under mother liquor. The data-collection was performed at 293K on an Enraf-Nonius CAD4 diffractometer. Three reference reflections were measured every hour to monitor crystal decay. All data were corrected for Lorentz-polarisation effects but not for absorption. The latter was considered negligible for the size of the crystal used. Crystal data are listed in Table 3.8 while data-collection parameters are listed in Table 3.9.

Table 3.8 Crystal data for the ACEBCD structure

Crystal data	
Molecular formula	$1(C_{42}H_{70}O_{35})\cdot1(C_8H_9NO_2)\cdot13.3(H_2O)$
M_r (g.mol^{-1})	1525.76
Crystal system	Monoclinic
Space group	C2
Z	4
a (Å)	19.207 (7)
b (Å)	24.48 (1)
c (Å)	15.700 (4)
α (°)	90
β (°)	109.52 (3)
γ (°)	90
V (Å^3)	6959 (5)
D_c (g.cm^{-3})	1.4563
F (000)	3260
μ (Mo Kα) (cm^{-1})	1.319
Crystal dimensions (mm)	0.4 x 0.4 x 0.4

Table 3.9 Data-collection parameters for the ACEBCD structure

Data-collection	
Diffractometer	Enraf-Nonius CAD4
Range scanned θ (°)	$1 \leq \theta \leq 25$
Index range	h : -18,18; k : 0,23; l : 0,15
Scan width (°)	0.8 + 0.35 tan θ
Aperture width (mm)	1.12 + 1.05 tan θ
Temperature	293 K
Radiation (λ)	Mo Kα (0.71069 Å)

Structure solution and refinement

The ACEBCD complex crystallises in the monoclinic space group C2 with a single β-CD molecule, a guest molecule and 13.3 water molecules comprising the asymmetric portion of the structure. The β-CD molecule is rotated through a diad parallel to the *b*-axis to produce the other half of a dimer. The structure was solved using the published coordinates for the non-hydrogen CD atoms (excluding primary hydroxyl oxygen atoms) of the isomorphous β-CD-ibuprofen complex.[41] The final refinement parameters are listed in Table 3.10.

After refinement in SHELX-76,[42] the difference Fourier map revealed the positions of some of the primary hydroxyl oxygen atoms. After further refinement it was found that three of these atoms had full site occupancy, while a further three were disordered over two major positions. The major position was assigned an occupancy of 0.6 in each case based on a comparison of peak heights in the electron density difference map. The remaining primary hydroxyl oxygen atom was disordered over three positions, each position in this case being assigned a site occupancy of 0.33. The isotropic temperature factors of the full site occupancy primary hydroxyl oxygen atoms vary from 0.07 to 0.13Å^2, while the corresponding figures for the disordered atoms are 0.06 to 0.19Å ^{2}. Refinement continued with the placement of water molecules , many of which were disordered.

Table 3.10 Refinement parameters for the ACEBCD structure

Refinement	
Refinement program	SHELX-76
No. of reflections collected	6472
No. of unique reflections	5103
R_{int}	0.0302
Reflections with $I > 3\sigma(I)$	2176
Number of L.S. parameters	458
R_1	0.1345
wR	0.1390
w	$[\sigma^2(F_o) + 1.452 \times 10^{-3} F_o^2]^{-1}$
S	7.60
$(\Delta\rho)_{max}$ final ($eÅ^{-3}$)	0.53
$(\Delta\rho)_{min}$ final ($eÅ^{-3}$)	-0.47

Only three of the 21 positions located for water molecules could be assigned a full site occupancy factor. Two water molecules, O1W and O15W, were located on the two-fold axis and were treated appropriately. The isotropic temperature factors of the three full site occupancy water molecules were in the range 0.10-0.14$Å^2$. The remaining water molecules, with the exception of O19W, were assigned a fixed isotropic temperature factor of 0.17$Å^2$ while the site occupancies were allowed to refine. The site occupancies of these 17 water molecules varied in the range 0.34-0.72, amounting to an additional 8.8 water molecules per asymmetric unit. The water oxygen atom, O19W, was associated with the acetaminophen guest molecule and was assigned a s.o.f. of 0.5, the reason for which will be discussed in the proceeding discussion on the location and modelling of the guest. This amounted to a total of 12.3 water molecules per asymmetric unit which were accounted for, as compared to the 13.3 water molecules expected from the TGA results presented earlier in this chapter. Hydrogen atoms were added in geometrically constrained positions to the carbon atoms of the CD, except for the C6 carbon atoms attached to disordered primary hydroxyl O atoms. The hydrogen atoms were refined using a common isotropic temperature factor to a final value of 0.09$Å^2$. All non-hydrogen atoms were refined with isotropic temperature factors. 2176 reflections with $F_o > 3\sigma(F_o)$ were used in the final refinement and 458 L.S. parameters were refined. The ratio of data to parameters confined all non-hydrogen atoms to refinement with isotropic temperature factors.

Modelling of the acetaminophen (ACE) guest

The UV spectrophotometric and microanalysis results presented earlier in the chapter indicated that a single ACE molecule was included per β-CD molecule. It became clear during the course of the refinement that this ACE molecule was disordered in the β-CD cavity. After careful inspection of the difference map, the two positions of the hydroxyl oxygen atoms of ACE were identified in the vicinity of the primary rim of the β-CD molecule. The two peaks, of approximately equal electron density, were assigned s.o.f. s of 0.5 each. Their identity was further confirmed by the O···O contact distances between their symmetry related positions which were all within hydrogen bonding distance (2.77-2.98Å). Careful and painstaking analysis of many electron density difference maps followed as refinement of the rest of the model proceeded. Finally, peaks in the difference map were identified that corresponded to two geometrically reasonable positions for the phenyl ring of ACE. The atoms of each phenyl ring were assigned s.o.f. s of 0.5 and the rings were constrained as rigid hexagons using the AFIX6 command. Refinement of these two positions for the hydroxy-phenyl fragment of the ACE was successful and produced a substantially clearer electron density map from which the two positions of the acetamino portion of the ACE molecule were evident. The two positions of the ACE molecule were refined with s.o.f. s of 0.5 each and distance constraints applied to the models. The two positions (labelled A and A`) for the ACE molecule can be seen in Figure 3.9 with the phenyl rings of each position approximately orthogonal to one another. A single isotropic temperature factor was used for the non-hydrogen atoms of each position and these refined to final values of 0.12 and 0.16Å$^2$ for A and A` respectively. Guest H atoms were included in geometrically calculated positions, with the exception of the hydroxyl hydrogen atom, which was omitted.

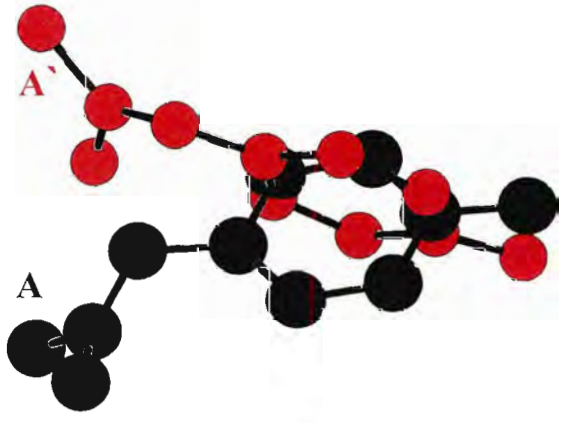

Figure 3.9 A plot of the two disordered positions (A and A`) of the ACE guest

Geometrical analysis of the ACEBCD structure

The asymmetric unit of the ACEBCD structure contains a single β-CD molecule, its associated guest molecule and 13.3 water molecules. The β-CD molecule will be referred to as CD(A) and its glucose units will be designated A1, A2, A3, A4, A5, A6 and A7. The ACE guest is disordered over two positions which will be referenced with the suffixes A and A`. Tables 3.11, 3.12 and 3.13 list the geometrical data for the β-CD molecule of the ACEBCD structure (e.s.d. s are in the range of 0.02-0.04Å for distances and 2-5° for angles). The glucose residues are all in the $^4C_1$ chair conformation and the values of the torsion angles are consistent with the average values obtained for β-CD structures. Table 3.11 lists selected torsion angles for the glucose units. These torsion angles are defined and illustrated on pages 4 and 5 of Chapter 1. The three primary hydroxyl groups with full s.o.f. s adopt the (-)-*gauche* orientation with an average value of ω = -64°. The primary hydroxyl groups of A1, A5 and A6 are disordered over two sites. The major position in each case adopts the (-)-*gauche* orientation while the minor positions adopt the (+)-*gauche* orientation. The primary hydroxyl group of A4 is disordered over three positions with two positions adopting the (-)-*gauche* orientation and one position adopting the (+)-*gauche* orientation. Disorder of the primary hydroxyl of A4 is necessitated since the major position for this primary hydroxyl group would be involved in an unacceptably short contact with its counterpart across the two-fold axis, at the interdimeric interface.

Table 3.11 Selected torsion angles for the ACEBCD structure

Glucose unit	ω (°)†	ω (°)†	ω (°)†	Φ (°)†	Ψ (°)†	Θ_1 (°)†	Θ_2 (°)†
A1	-63	+35	-	117	122	52	-53
A2	-64	-	-	117	129	51	-57
A3	-60	-	-	97	127	55	-54
A4	-74	+22	-51	115	132	49	-55
A5	-51	+71	-	114	128	54	-51
A6	-79	+41	-	116	128	53	-52
A7	-68	-	-	109	124	45	-45
A | mean |	**66**	**42**	**51**	**112**	**127**	**51**	**52**

† Refer to page 4,5 (Chapter 1) for definitions and descriptions of these quantities

The geometrical parameters of the O4 heptagon of the ACEBCD structure are listed in Table 3.12. These include the radii (*r*), side lengths (*l*), O4···O4···O4 angles (*a*), the deviation of each O4 from the mean O4 plane (*d*) and the O4···O4···O4···O4 torsion angles (*t*). These parameters are defined and illustrated on pages 6 and 7 of Chapter 1. Table 3.13 lists the other important features of the macrocyclic structure such as the intersaccharidic bond angle (φ), the O2(n)···O3(n-1) distances and the tilt angles (τ_1 and τ_2). These parameters are defined and illustrated on pages 8 and 9 of Chapter 1.

On the whole the macrocycles exhibit a highly planar and symmetrical conformation. Further discussion of the geometrical features of the ACEBCD structure will be dealt with presently in a comparison of the geometry of this structure with the three other β-CD structures.

Table 3.12 Geometrical parameters of the O4 heptagon for the ACEBCD structure

Glucose unit	*r* (Å)†	*l* (Å)†	*a* (°)†	*d* (Å)†	*t* (°)†
A1	4.98	4.35	125	+0.09	+1
A2	5.16	4.30	129	-0.04	+2
A3	5.00	4.42	131	-0.03	+0
A4	4.91	4.35	127	+0.05	-3
A5	5.08	4.36	127	+0.04	+2
A6	5.12	4.33	130	-0.08	+3
A7	4.94	4.46	130	0.00	-4
A | mean |	**5.03**	**4.37**	**129**	**0.05**	**2**

† Refer to page 6,7 (Chapter 1) for definitions and descriptions of these quantities

Table 3.13 φ , O2(n)···O3(n-1) distances, τ_1 and τ_2 for the ACEBCD structure

Glucose unit	φ (°)†	O2(n)···O3(n-1) (Å)†	τ_1 (°)†	τ_2 (°)†
A1	119	2.76	+7.1	+6.7
A2	121	2.85	+9.8	+16.7
A3	116	2.80	+5.8	+9.5
A4	117	2.94	+8.0	+12.7
A5	117	2.87	+4.8	+11.2
A6	120	2.80	+4.7	+8.7
A7	119	2.85	+3.1	+4.2
A | mean |	**118**	**2.84**	**6.2**	**10.0**

† Refer to page 8,9 (Chapter 1) for definitions and descriptions of these quantities

Guest interactions for the ACEBCD structure

Details of the disorder and guest interactions for the ACEBCD structure are shown schematically in Figure 3.10. Table 3.14 lists contact distances for the relevant interactions associated with the guest molecules (e.s.d. s are in the range 0.07-0.11Å).

Both the hydroxyl oxygen atoms of the disordered positions, ACE(A) and ACE(A`), are within hydrogen bonding contact of a primary hydroxyl oxygen atom of an adjacent CD. This oxygen atom is one of the disordered positions of the O6 atom of glucose residue A6, and has a (+)-*gauche* orientation. The O···O contact distances that it makes with the hydroxyl group of ACE(A) and ACE(A`) are 2.89 Å and 2.62 Å respectively. The O10(A`) atom of ACE(A`) makes a hydrogen bonded contact to a water molecule present in the secondary interface of the dimer. The water oxygen atom, O19W, also makes abnormally short contacts with the acetamino group of ACE(A) and the implication is that O19W is present in the dimer only in association with ACE(A`). The contacts made by the hydroxyl and acetamino groups of ACE to the CD hydroxyl groups and water are consistent with the suggestions made by Brown et al.[35] and Lin and Lee,[26] which were discussed on pages 4-7 of this chapter. The notable exception is that the amide N atom is not involved in any contacts to CD hydroxyl residues or solvent water as was suggested by Lin and Lee.[26]

Table 3.14 Guest interactions for the ACEBCD structure

Guest interaction	Distance (Å)	Equivalent positions
O1A···O6`A6	2.89	-x,y,-z
O1A`···O6`A6	2.62	-x,y,-z
O1A···O1A†	2.95	-x,y,-z
O1A···O1A`	2.98	-x,y,-z
O1A`···O1A`†	2.66	-x,y,-z
O10A`···O19W	2.77	

† Two-fold related counterpart

The hydroxyl oxygen atoms of ACE(A) and (A`) are all within hydrogen bonding contact of one another across the two-fold axis running between the primary faces of adjacent β-CD dimers. This implies that any combination of ACE(A) and ACE(A`) will form a single hydrogen bond across the primary rim interface in all disordered scenarios.

dimeric β-CD structures. The dimeric layers stack on top of one another with a single dimeric layer forming the repeating array of the structure.

Disorder of the included guest is often observed in structures of the channel (CH) type packing mode crystallising in the space group C2,[47-55] as was observed in the ACEBCD structure. Further discussion of the crystal packing of the ACEBCD structure will be included in a comparison of the four β-CD dimeric complexes.

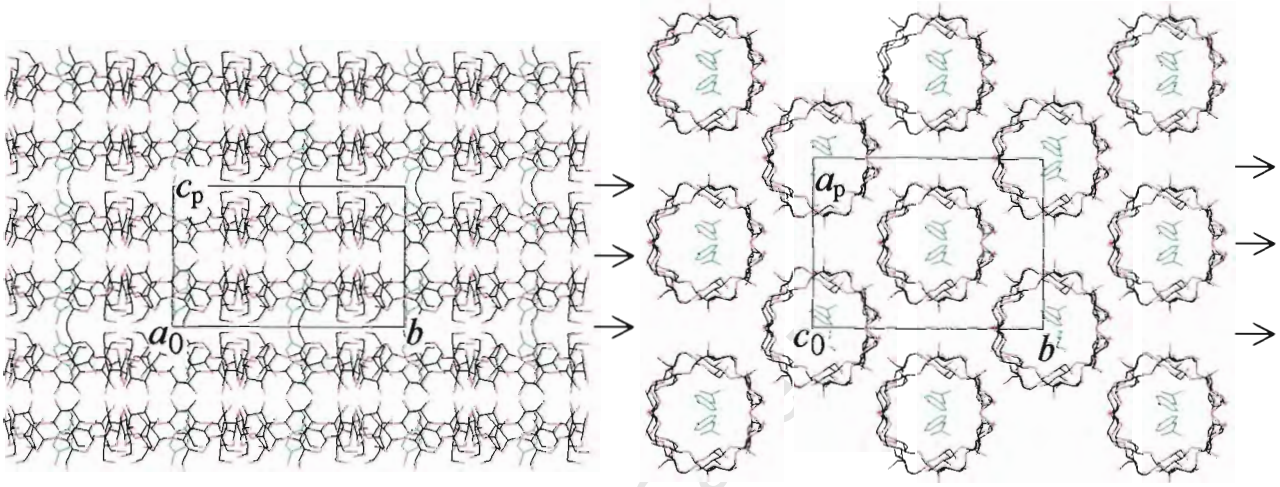

(a) (b)

Figure 3.14 Packing diagrams of the ACEBCD structure (a) *a*-axis projection and (b) *c*-axis projection

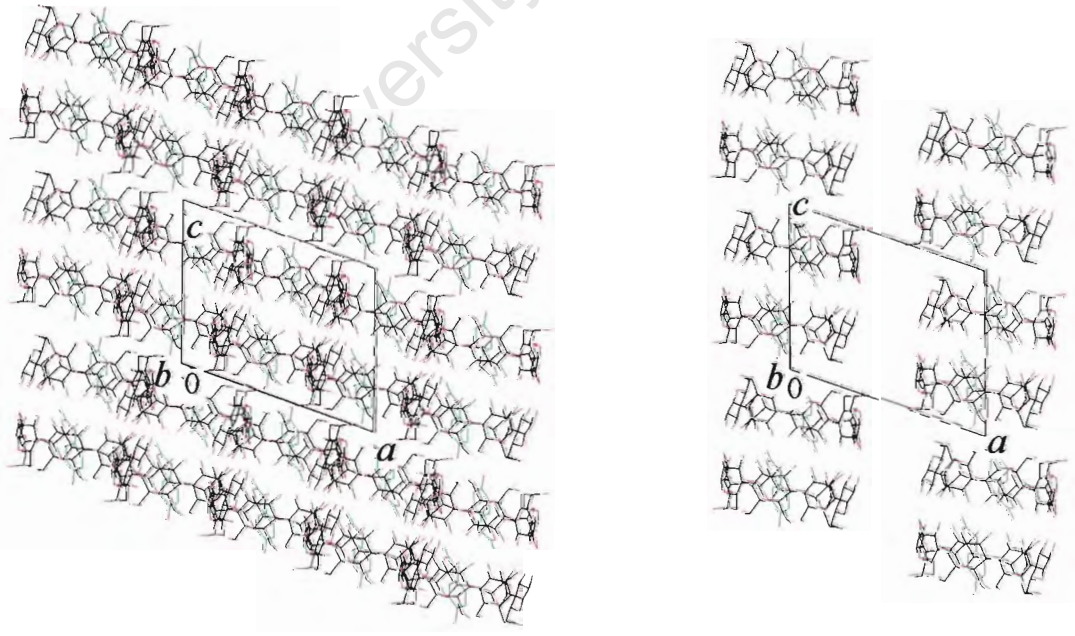

(a) (b)

Figure 3.15 Packing diagrams of the ACEBCD structure *b*-axis projection (a) with C-centred positions included (b) same projection with C-centred positions omitted

Hydrogen bonding interactions of the ACEBCD structure

Figure 3.16 (a) and (b) show the distribution of water molecules (shown as black spheres in the diagram) in the ACEBCD structure. The majority of the water molecules are present in the interstitial channels between the columns of β-CD dimers while a small number are positioned in the dimeric channels.

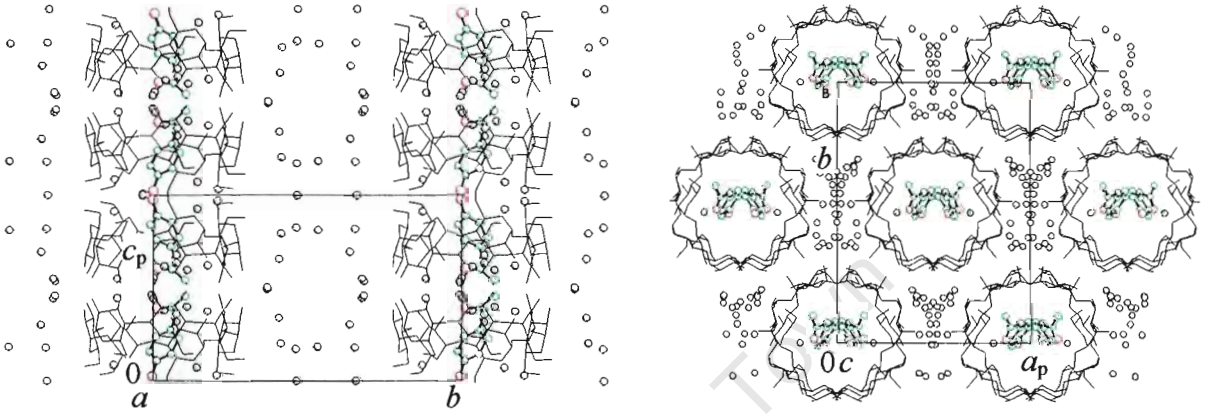

Figure 3.16 Diagrams showing the distribution of water molecules in the ACEBCD structure (a) *a*-axis projection (C-centred positions excluded) (b) *c*-axis projection

Tables 3.16, 3.17, 3.18 (a), 3.18 (b), 3.19 and 3.20 list summaries of the appropriate contacts for the cyclodextrin, dimer, intralayer, interlayer, guest and water hydrogen bonded interactions respectively. The listed contacts are all in the range of 2.50 to 3.20 Å and the e.s.d. s are in the range 0.03-0.09 Å for the cyclodextrin, dimer and layer interactions and in the range 0.04-0.16 Å for the guest and water interactions.

A.) Cyclodextrin interactions

Table 3.16 Cyclodextrin interactions for the ACEBCD structure

O2···O3	Number / CD	Range (Å)	Mean (Å)
A	7	2.76-2.94	2.84

B.) Dimer interactions

Table 3.17 Dimer interactions for the ACEBCD structure

Type	CDs	Number / dimer	Range (Å)	Mean (Å)
O3···O3	A-A†	7	2.74-2.87	2.80
O2···O2	A-A†	7	2.85-3.07	3.03
O2···O3	A-A†	12	3.01-3.17	3.08

† Two-fold related CD molecule

For many of the layer, guest and water interactions, disordered atoms are involved and this results in an apparent increase in the number of interactions present in the structure. Therefore, a normalised number of interactions will also be indicated to aid comparison between structures. The number of interactions of the aforementioned type will be adjusted by multiplication by a normalising factor, N †.

† N = [total occupancy of atoms involved in contacts] / [total number of sites of atoms involved in contacts]

C.) Layer interactions

Table 3.18 (a) Intra-layer interactions for the ACEBCD structure

Type	Number / dimer	(Number / dimer) x N	Range (Å)	Mean (Å)
O2···O2	2	2	2.83	2.83
O6···O6	8	5	2.76-3.11	2.89

Table 3.18 (b) Inter-layer interactions for the ACEBCD structure

Type	Number / dimer	(Number / dimer) x N	Range (Å)	Mean (Å)
O6···O6	8	5	2.76-2.83	2.79

D.) Guest interactions

Table 3.19 Guest interactions for the ACEBCD structure

Type	Guest	Number / dimer	(Number / dimer) x N	Mean (Å)
O1···O6	A	2	1	2.89
O1···O1	A	2	1	2.97
O1···O6	A`	2	1	2.62
O1···O1	A`	2	1	2.82
O10···OW	A`	2	1	2.77

E.) Water interactions

Table 3.20 Water interactions for the ACEBCD structure

Type	Number / dimer	(Number / dimer) x N	Range (Å)	Mean (Å)
O2···Water	18	12	2.59-3.19	2.86
O3···Water	18	12	2.66-3.18	2.92
O6···Water	22	13	2.70-3.18	2.82
Water···Water	66	39	2.58-3.19	2.89

X-ray crystallographic analysis of the BROBCD structure

Data-collection

The preliminary cell parameters and space group for the BROBCD structure (containing *p*-bromoacetanilide (BRO) as guest) were determined by x-ray photographic techniques. Laue symmetry $\bar{1}$ indicated the triclinic crystal system. The chiral nature of the CD molecule determined the space group as P1. The crystals of the complex were mounted under mother liquor in Lindemann capillaries on account of the instability of the crystals when removed from that medium. The data were collected at 273K on an Enraf-Nonius CAD4 diffractometer. Three reference reflections were measured every hour to monitor crystal decay. A fairly gradual linear decay of the intensities was observed over the 300 hour duration of the data-collection. Figure 3.17 shows the intensities of the three standard reflections against time. The intensity data were appropriately corrected for this effect by the author. A catastrophic decrease in intensity at the end of the data-collection signalled complete decay, preventing recording of further intensity measurements which could have been used to correct for absorption effects (estimated at ±5%). All data were corrected for Lorentz-polarisation effects. Crystal data are listed in Table 3.21 while data-collection parameters are listed in Table 3.22.

Table 3.21 Crystal data for the BROBCD structure

Molecular formula	$2(C_{42}H_{70}O_{35})\cdot2(C_8H_8NOBr)\cdot27(H_2O)$
M_r (g.mol^{-1})	3184.52
Crystal system	Triclinic
Space group	P1
Z	1
a (Å)	15.197 (3)
b (Å)	15.613 (2)
c (Å)	15.743 (4)
α (°)	87.16 (2)
β (°)	98.29 (2)
γ (°)	103.39 (1)
V (Å^3)	3595 (1)
D_c (g.cm^{-3})	1.4708
F (000)	1686
μ (Mo Kα) (cm^{-1})	6.825
Crystal dimensions (mm)	0.3 x 0.3 x 0.4

Table 3.22 Data-collection parameters for the BROBCD structure

Data-collection	
Diffractometer	Enraf-Nonius CAD4
Range scanned θ (°)	$1 \leq \theta \leq 25$
Index range	h -18,18; k –18,18; l 0,18
Scan width (°)	0.8 + 0.35 tan θ
Aperture width (mm)	1.12 + 1.05 tan θ
Temperature	273 K
Radiation (λ)	Mo Kα (0.71069 Å)

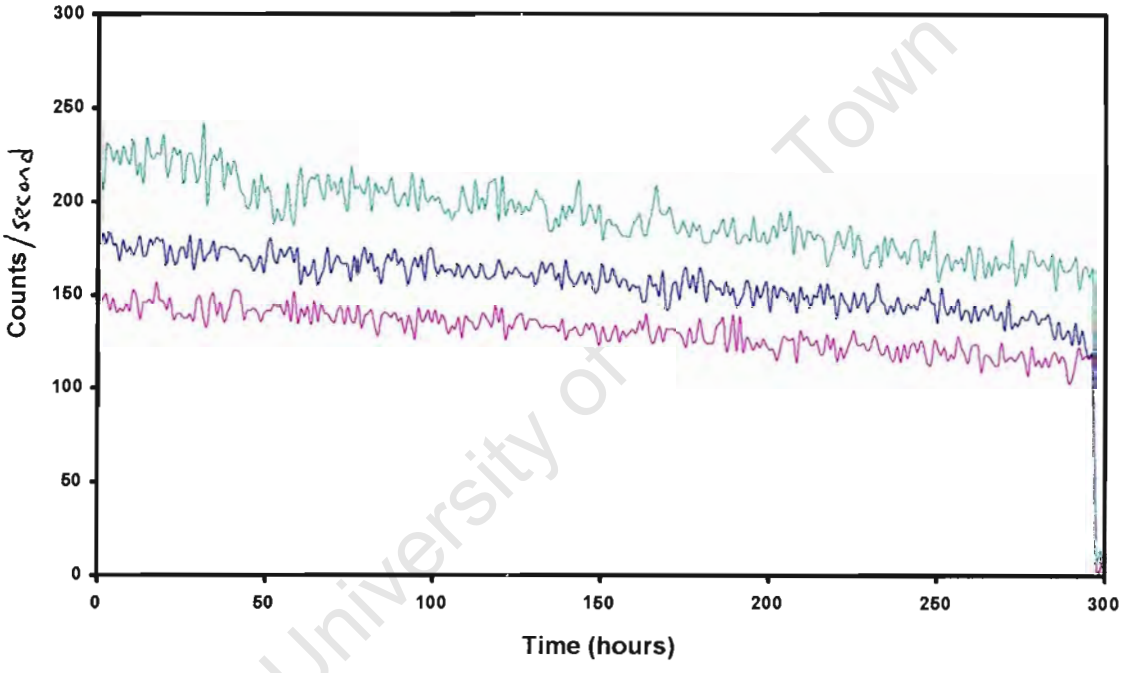

Figure 3.17 Plot of the intensities of the three reference reflections over the 300 hour period of the data-collection of the BROBCD structure

Structure solution and refinement

The BROBCD complex crystallises in the triclinic space group P1 with two crystallographically independent β-CD molecules, two guest molecules and 27 water molecules comprising the asymmetric portion of the structure. The structure was solved using coordinates of the non-hydrogen atoms (excluding primary hydroxyl O atoms) of the two independent β-CD molecules of the isomorphous β-CD-*p*-nitroacetanilide complex.[57] The final parameters for refinement of the structure in SHELX-76[42] are listed in Table 3.23.

Table 3.23 Refinement parameters for the BROBCD structure

Refinement	
Refinement program	SHELX-76
No. of reflections collected	13561
No. of unique reflections	11475
R_{int}	0.0506
Reflections with $I > 3\sigma(I)$	7351
Number of L.S. parameters	975
R_1	0.0948
wR	0.1011
w	$[\sigma^2(F_o) + 1.077 \times 10^{-3} F_o^2]^{-1}$
S	4.92
$(\Delta\rho)_{max}$ final ($eÅ^{-3}$)	0.36
$(\Delta\rho)_{min}$ final ($eÅ^{-3}$)	-0.30

The guest atoms, water molecules and remaining atoms of the host were located in successive difference electron density maps following least-squares refinements. The final cycles involved the blocked full-matrix technique with all atoms refining isotropically except the Br atoms which were assigned anisotropic thermal parameters. The function minimised was $\Sigma w(|F_o| - |kF_c|)^2$ with weights which yielded a constant distribution of $\Sigma(w\Delta F)^2$ with $\sin\theta/\lambda$ and $(F_o/F_{o,max})^{1/2}$. Four reflections (100, 010, 200, 020) displayed secondary extinction and were excluded from the refinement. The hydrogen atoms attached to carbon atoms of the β-CD molecules were inserted in geometrically calculated positions. The positions of the hydrogen atoms of CD hydroxyl groups were individually located in the electron density difference maps. One of the primary hydroxyl groups was found to be disordered over two sites with final refined s.o.f. s of 0.63 and 0.37. The final structural model included 21 water molecules with s.o.f. 1.00 each and 12 with s.o.f. in the range 0.41-0.59, accounting for a total of 27 H_2O molecules, or an average of 13.5 H_2O molecules per β-CD molecule, in agreement with the estimate from thermogravimetric analysis.

Modelling of the *p*-bromoacetanilide (BRO) guest

At an advanced stage of refinement, it became apparent from difference electron density maps that in each of the two independent guest molecules, the acetyl residue was disordered over two sites with the torsion angle around the C5-N8 bond (indicated by a red arrow in Figure 3.18), approximately 0° for one site and 180° for the other. The disordered acetyl residues are shown in Figure 3.18 with the acetyl residues labelled A and A` for BRO(A) and B and B` for BRO(B). Each of the four independent acetyl residues was included in the model with variable s.o.f. (initially set at 0.5 each, based on electron density peak heights) and a sufficient number of distance constraints was applied to ensure reasonable geometry. Further reduction of the number of least-squares variables was effected by treating the phenyl groups as regular hexagons and assigning two separate common variable U_{iso} values to the C atoms of the two phenyl rings. The guest H atoms were included in geometrically calculated positions at 1.00 Å from their parent atoms and were treated isotropically. The final refined s.o.f. s for atoms of the disordered acetyl residues were 0.58, 0.42 (guest molecule A) and 0.59, 0.41 (guest molecule B).

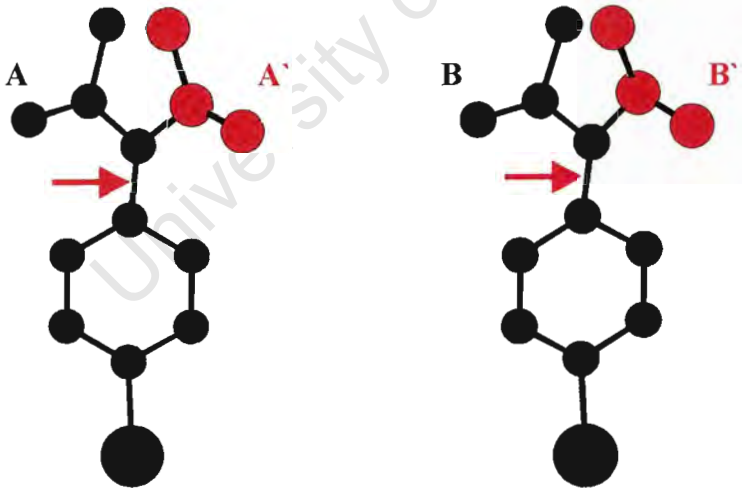

Figure 3.18 The guest molecules A and B showing their disordered acetyl groups

Geometrical analysis of the BROBCD structure

The asymmetric unit of the BROBCD structure contains two crystallographically independent β-CD molecules, their associated guests and 27 water molecules. The two CDs will be referred to as CD(A) and CD(B). The glucose residues of each of the CDs are numbered from one to seven, so that the glucose residues of CD(A) are A1, A2, A3, A4, A5, A6 and A7. The guest molecules associated with CD(A) and CD(B) will be referred to as BRO(A) and BRO(B) respectively. The atoms of their disordered acetyl groups will be referred to with the suffixes A and A` for BRO(A) and B and B` for BRO(B). Tables 3.24, 3.25 and 3.26 list the geometrical data for the two independent β-CD molecules of the BROBCD structure (e.s.d. s are of the order of 0.01Å for distances and 1° for angles). The geometrical data for BROBCD closely resemble those of the ACEBCD structure. A comparison of the geometrical data of these complexes will be made at the end of this chapter. The D-glucopyranose units are in the $^4C_1$ conformation and their torsion angles are consistent with the average values obtained for β-CD structures. The primary hydroxyl groups are all in the (-)-*gauche* conformation with the exception of the minor position of the disordered primary hydroxyl group of A4 which adopts the (+)-*gauche* orientation. On the whole the macrocycles exhibit a highly planar and symmetrical conformation

Table 3.24 Selected torsion angles for the BROBCD structure

Glucose unit	ω (°)†	ω (°)†	Φ (°)†	Ψ (°)†	Θ_1 (°)†	Θ_2 (°)†
A1	-69	-	118	130	54	-51
A2	-68	-	118	122	54	-49
A3	-65	-	113	124	58	-54
A4	-76	+40	116	126	54	-54
A5	-62	-	110	125	54	-52
A6	-66	-	115	133	60	-58
A7	-64	-	115	129	58	-55
A | mean |	**67**	**40**	**115**	**127**	**56**	**53**
B1	-66	-	119	127	57	-57
B2	-65	-	114	133	56	-53
B3	-66	-	114	126	50	-48
B4	-72	-	114	129	56	-51
B5	-64	-	114	124	56	-55
B6	-64	-	117	133	57	-53
B7	-65	-	109	120	53	-52
B | mean |	**66**	**-**	**114**	**127**	**55**	**53**

† Refer to page 4,5 (Chapter 1) for definitions and descriptions of these quantities

Table 3.25 Geometrical parameters for the O4 heptagons of the BROBCD structure

Glucose unit	*r* (Å)†	*l* (Å)†	*a* (°)†	*d* (Å)†	*t* (°)†
A1	5.11	4.29	126	+0.05	0
A2	5.17	4.40	131	-0.03	+2
A3	4.90	4.42	130	-0.03	-1
A4	4.96	4.38	125	+0.04	0
A5	5.22	4.26	129	0.00	-1
A6	5.03	4.47	132	-0.02	+3
A7	4.86	4.37	127	-0.02	-3
A | mean |	**5.04**	**4.37**	**129**	**0.03**	**1**
B1	5.09	4.41	132	0.00	+5
B2	4.86	4.39	128	+0.07	-2
B3	5.04	4.32	126	-0.06	-2
B4	5.16	4.33	129	-0.02	+3
B5	4.98	4.47	132	+0.06	-1
B6	4.89	4.34	126	-0.02	+1
B7	5.16	4.29	127	-0.03	-4
B | mean |	**5.03**	**4.36**	**129**	**0.04**	**3**

† Refer to page 6,7 (Chapter 1) for definitions and descriptions of these quantities

Table 3.26 φ , O2(n)···O3(n-1) distances, τ_1 and τ_2 for the BROBCD structure

Glucose unit	φ (°)†	O2(n)···O3(n-1) (Å)†	τ_1 (°)†	τ_2 (°)†
A1	116	2.78	+4.3	+8.0
A2	119	2.81	+0.9	+4.2
A3	118	2.70	+3.6	+6.3
A4	118	2.76	+4.5	+7.1
A5	118	2.80	+4.8	+8.3
A6	118	2.81	+11.3	+13.8
A7	119	2.83	+3.8	+7.0
A | mean |	**118**	**2.78**	**4.7**	**7.8**
B1	118	2.77	+12.9	+16.2
B2	117	2.78	+2.5	+5.6
B3	118	2.78	+0.8	+6.6
B4	119	2.76	+1.9	+7.9
B5	119	2.82	+8.6	+11.9
B6	118	2.77	+1.9	+6.0
B7	119	2.74	+1.8	+4.5
B | mean |	**118**	**2.77**	**4.3**	**8.4**

† Refer to page 8,9 (Chapter 1) for definitions and descriptions of these quantities

Guest interactions for the BROBCD structure

Details of the disorder and guest interactions are shown schematically in Figure 3.19 where the labels O10A, O10A` denote the two disordered positions of the carbonyl O atom for BRO(A) and labels O10B, O10B` denote those for BRO(B). It is significant that for each of the four disordered orientations found, a N-H···O(water) hydrogen bond occurs. Table 3.27 lists geometrical data for the N8···O(water) contacts, relevant O(water)···O(water) distances, as well as O10···O(water) distances, the latter indicating that all disordered guest carbonyl O atoms also engage in hydrogen bonding to water molecules (e.s.d. s are in the range 0.03-0.07Å).

The isomorphous β-CD-*p*-nitroacetanilide[57] complex also displays stabilisation of the acetylamino residues by N-H···O(water) hydrogen bonds to H_2O molecules inside the cavity in the region of the dimer interface. It is possible that analogous guest disorder occurs in that complex, since the reported structural analysis was incomplete (R = 17%) and the *p*-nitroacetanilide molecules were assigned a s.o.f. of 0.75 on the basis of peak heights in the electron density maps.

Table 3.27 Guest interactions for the BROBCD structure

Guest interaction	Distance (Å)
N8A···O29W	3.19
N8A···O31W	2.95
N8B···O30W	3.02
N8B···O32W	3.03
O10A···O33W	2.61
O10A`···O30W	2.66
O10B`···O29W	2.81
O10B···O33W	2.35†
O29W···O30W	2.68
O31W···O33W	2.88
O32W···O33W	2.75
O30W···O3B4	3.17
O32W···O3B2	2.93
O33W···O3A2	3.17

† disordered atoms involved in contact

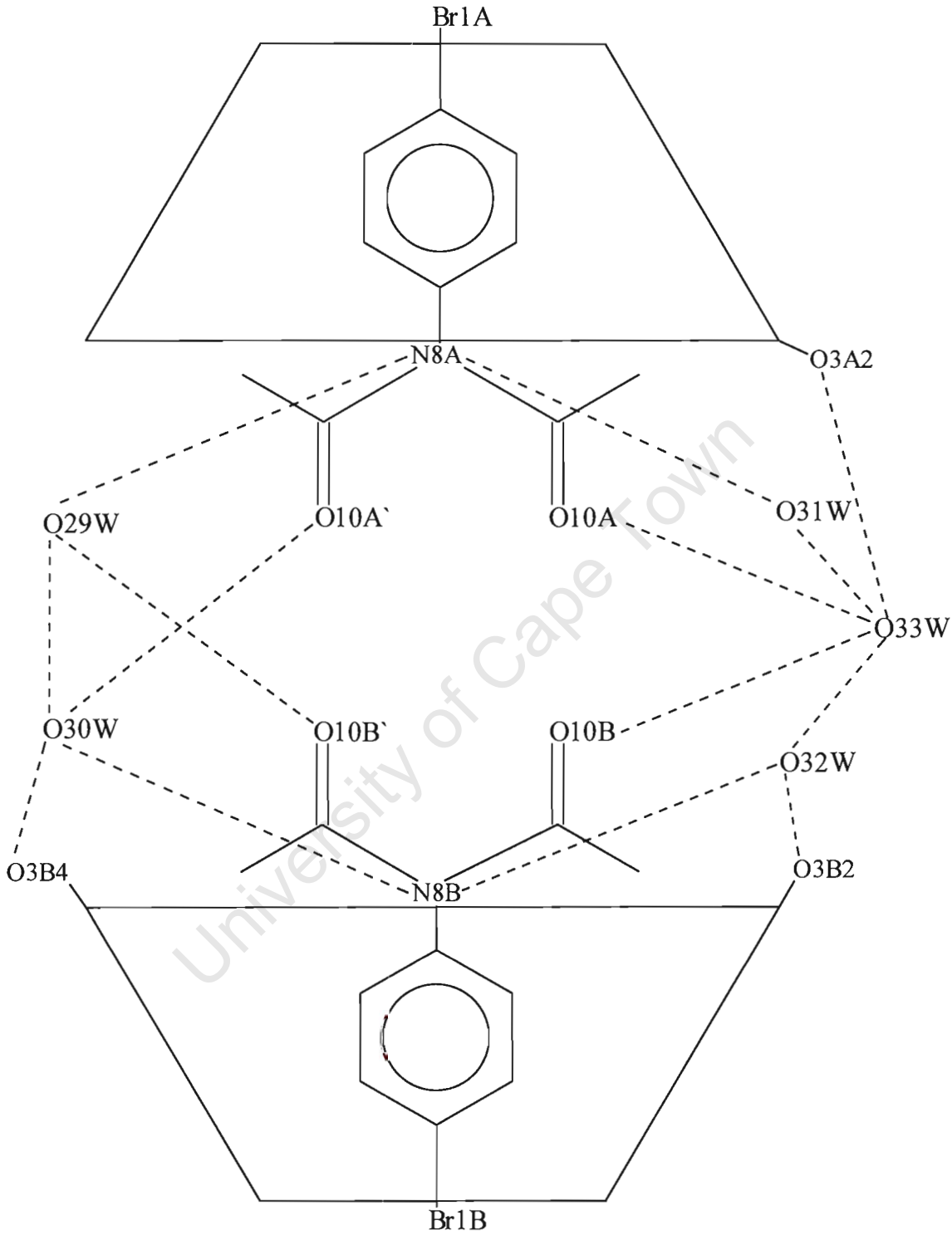

Figure 3.19 Schematic diagram showing guest interactions for the BROBCD structure

Overall description of the BROBCD structure

Figures 3.20 (a) and (b) show CPK diagrams for a dimer of the BROBCD structure. The dimer includes the A and B positions of the acetyl residues of BRO(A) and BRO(B) respectively. The colour codes used in these diagrams are as follows: β-CD: C (grey), O (red), H (white); BRO: C (green), H (yellow), N (blue), O (red), Br (purple); Water: O (light blue). Any hydrogen atoms of the host and guest that were not part of the final refined model have been inserted in geometrically sensible positions for these CPK diagrams. It is evident from Figure 3.20 (a) that bromine atoms protrude slightly from the primary rims of the β-CD dimer. However, the major portions of the two BRO guest molecules are contained within the dimer. This is achieved by tilting of the BRO molecules with respect to the mean O4 plane of the CD in which they are included. The mean planes of the phenyl rings of BRO(A) and BRO(B) make angles of 65(1)° and 62(1)°, with the mean O4 planes of CD(A) and CD(B) respectively. The bromine atoms of the two guests are situated in the vicinity of the primary rim with the acetamino portions contained within the secondary hydroxyl interface of the dimer. The association of O29W and O30W with the N atoms of BRO(A) and BRO(B) respectively is evident from Figure 3.20 (b), as well as the association of O33W with the carbonyl O atoms of BRO(A) and BRO(B).

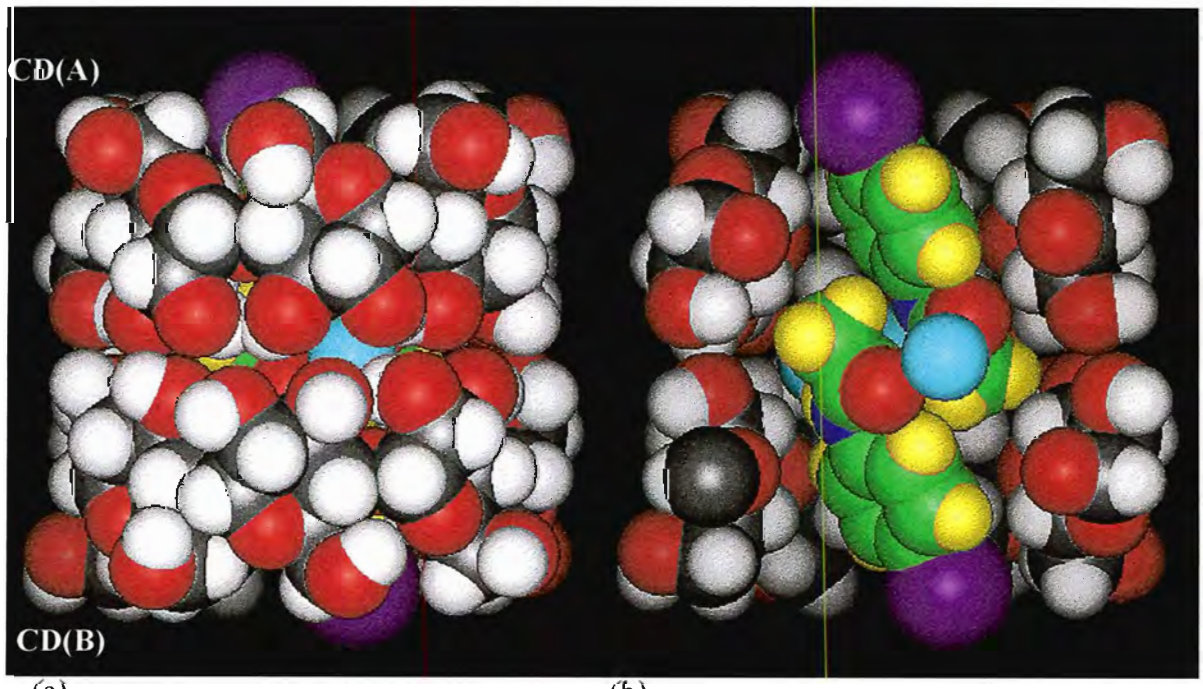

(a) (b)

Figure 3.20 CPK diagrams of the dimeric unit of the BROBCD complex (a) side view of dimer, (b) sectioned view of the same orientation

Atomic coordinates for the acetylaminobenzene portions of the *p*-bromoacetanilide guests are close to those for the same residue in the isomorphous β-CD complex containing *p*-nitroacetanilide,[57] showing that these different guests adopt the same degree of tilt with respect to the host molecules. This tilt permits the guests to occupy most of the available space in the cavity and is necessary to avoid abnormally close approach of the acetyl residues.

The BRO molecules adopt an approximately planar conformation which is stabilised by intramolecular (phenyl)C-H···O(carbonyl) hydrogen bonding with H···O in the range 2.05-2.34Å. A similar planar conformation is observed in the uncomplexed *p*-bromoacetanilide molecule (BRACTN),[58] where the torsion angles δ_1 and δ_2 (Figure 3.21) are 14° and -11° respectively (Table 3.28). This similarity in conformations of the BRO(A) and BRO(B) molecules with the uncomplexed molecule can be seen in the Br1 to C11 distances (*d*) (Table 3.28). An important feature of the present analysis is the finding that the acetyl residues of both BRO(A) and BRO(B) are disordered in two orientations. The relevant torsion angle, δ_1, has values of 6° and 169° for the two disordered sites in BRO(A) and -7° and 157° for BRO(B).

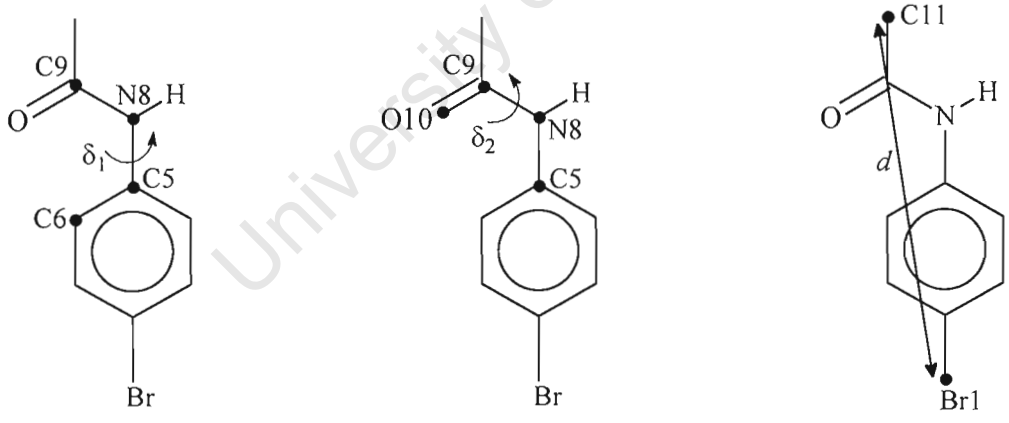

Figure 3.21 Torsion angles δ_1 and δ_2 of the acetamino group and the distance *d*

Table 3.28 Values of δ_1, δ_2 and *d* for BRO(A),(A`),(B),(B`) and BRACTN

***p*-Bromoacetanilide**	δ_1	δ_2	***d***
BRO(A)	6	-1	8.43
BRO(A`)	169	-18	8.35
BRO(B)	-7	-7	8.43
BRO(B`)	157	-16	8.48
BRACTN	14	-11	8.47

Crystal Packing of the BROBCD structure

Figure 3.22 shows a stereo diagram of a dimer of the BROBCD structure. The dimer is viewed parallel to the mean O4 planes.

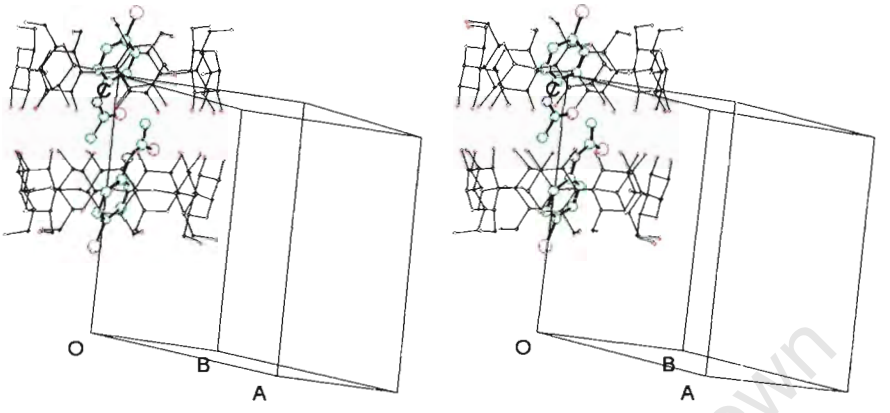

Figure 3.22 Stereo diagram of the dimer of the BROBCD structure

Figures 3.23 (a) and (b) are extended packing diagrams of the BROBCD structure showing projections as viewed down the *b*- and *a*-axes. Figure 3.23 (a) and (b) show the stacking of the dimers in columns parallel to the crystal *c*-axis. This stacking mode has been classified as the CH (for 'channel') type, which is characteristic for β-CD complexes crystallising in the space group C2 and for those crystallising in P1 with cell dimensions similar to those reported here (*viz.* with *a*, *b*, *c* each approximately 15Å). A number of structures with this packing motif have been described in the space group P1.[57,59-62] The packing of the β-CD dimers is analogous for the BROBCD structure and these isomorphous structures.

The channels are only slightly deformed at the interdimeric interface as a result of the central axis of the dimers not being exactly parallel to the channel axis, *c*. The relative average shift of consecutive dimers, when the dimers were viewed perpendicular to their mean O4 planes, is reported as 3.1(2) Å for CH type structures crystallising in the space group P1.[56] This value is only slightly larger then the value of 2.7(2) Å reported for CH type structures crystallising in the space group C2 (e.g. the structure of the ACEBCD complex). Figure 3.24 shows the "endless" channels produced by the cavities of the dimers.

From the packing diagrams it is evident that the dimers are arranged in layers parallel to the *ab*-plane of the structure. These dimeric layers are a characteristic feature of all dimeric β-CD structures. The BROBCD structure consists of a single dimeric layer which forms the repeating array of the structure by stacking along the c-axis of the structure. Further discussion of the BROBCD structure will be included in a comparison of the four β-CD complexes with *para*-substituted acetanilide guests at the end of this chapter.

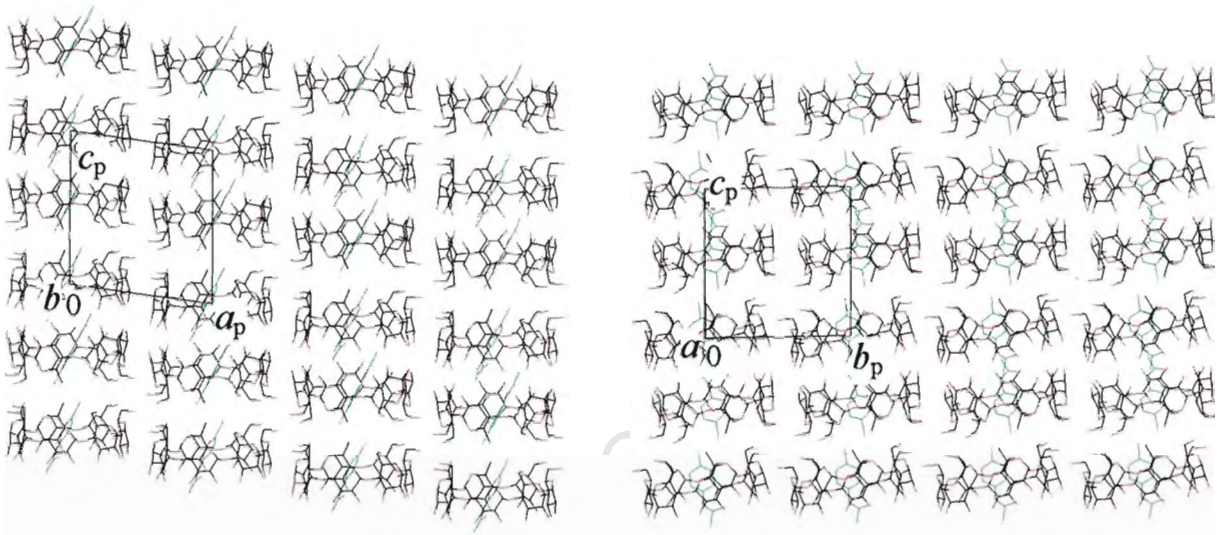

(a) (b)

Figure 3.23 Packing diagrams of the BROBCD structure (a) *b*-axis projection (b) *a*-axis projection

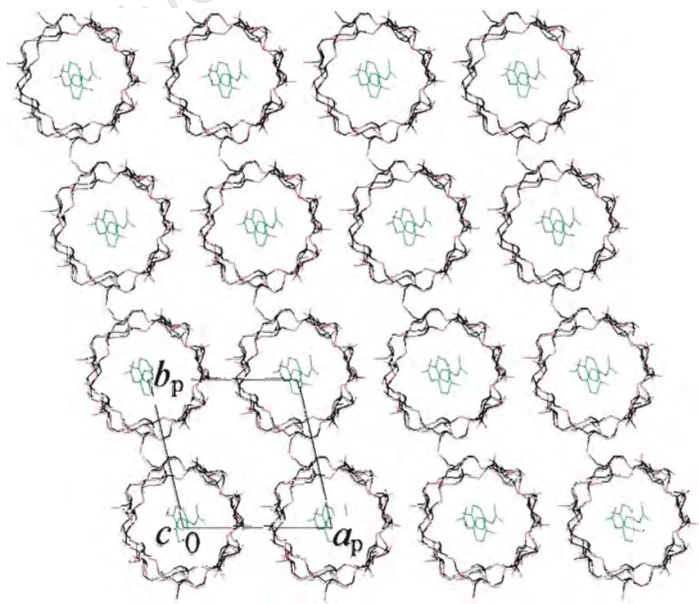

Figure 3.24 Packing diagram of the *c*-axis projection of the BROBCD structure

Hydrogen bonding interactions of the BROBCD structure

Figure 3.25 (a) and (b) show the distribution of water molecules (shown as black spheres in the diagrams) in the BROBCD structure. Figure 3.25 (b) shows that the majority of water molecules are present in the interstitial channels between the columns of β-CD dimers, while a small number are positioned in the dimeric channels. The latter are involved in contacts with the included guests.

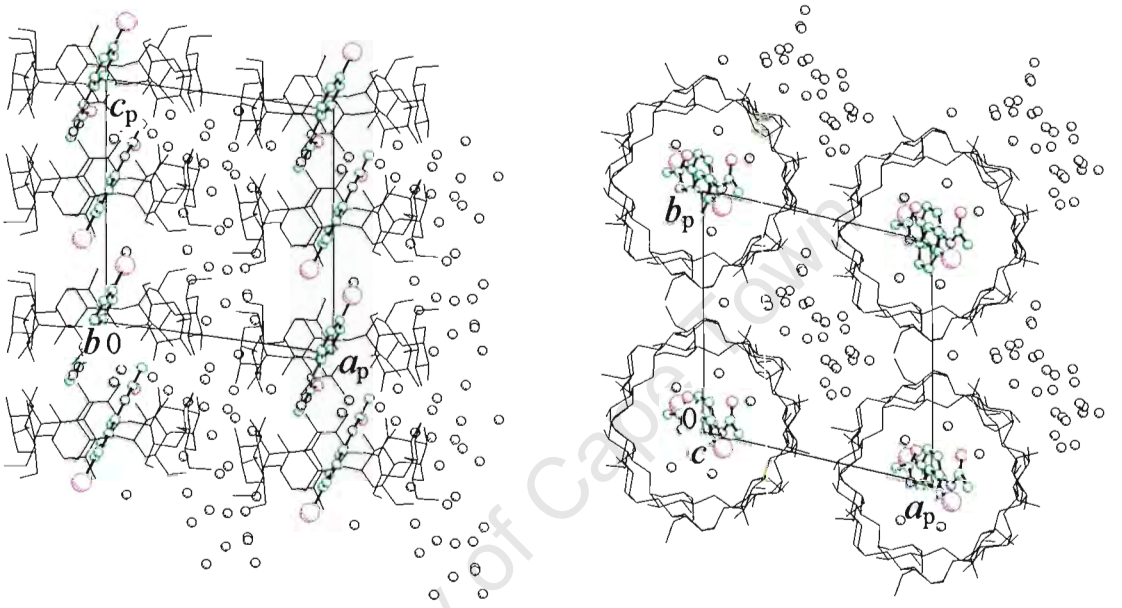

(a) (b)

Figure 3.25 Diagrams showing the distribution of water molecules in the BROBCD structure (a) *b*-axis projection (b) *c*-axis projection

Tables 3.29, 3.30, 3.31 (a), 3.31 (b), 3.32 and 3.33 list summaries of the appropriate contacts for the cyclodextrin, dimer, intralayer, interlayer, guest and water hydrogen bonded interactions respectively. The listed contacts are all in the range of 2.50 to 3.20 Å and the e.s.d. s are in the range 0.01-0.03 Å for the cyclodextrin, dimer and layer interactions and in the range 0.02-0.12 Å for the guest and water interactions.

A.) Cyclodextrin interactions

Table 3.29 Cyclodextrin interactions for the BROBCD structure

O2···O3	Number / CD	Range (Å)	Mean (Å)
A	7	2.70-2.83	2.78
B	7	2.74-2.82	2.77

References

1.) A. Goodman Gilman, T. W. Rall, A. S. Nies, P. Taylor, Eds., *Goodman and Gilman`s The Pharmaceutical Basis of Therapeutics Eighth Edition*, McGraw-Hill, Inc., New York, **1990**.

2.) *Pharmaceutical Business News*, 1 March 1991.

3.) W. Fischer and K. Klokkers, **PCT Int. Appl. WO 94 20,091** (Cl. 61K31/34), 15 Sep 1994, HU Appl. 93/9,306,024, 05 Mar 1993; 21 pp.

4.) L. J. Penkler, South African Druggists International, personal communication.

5.) L. J. Penkler and L. A. Glintenkamp, **PCT Int. Appl. WO 96 01,129** (Cl. A61K47/48), 18 Jan 1996, ZA Appl. 94/4,875, 6 Jul 1994; 44 pp.

6.) J. H. Coates, C. J. Easton, S. F. Lincoln, S. J. Van Eyk, B. L. May, M. L Williams, S. E. Brown, A. Lepore and M. L. Liao, **PCT Int. Appl. WO 91 13,100** (Cl. C08B37/16), 05 Sep 1991, AU Appl. 90/8,899, 02 Mar 1990; 179pp.

7.) T. Loftsson, H. Fridriksdottir, H. Olafsdottir and O. Gudmundsson, *Acta Pharm. Nord.*, **1991**, 3(4), 215.

8.) T. Loftsson, **Eur. Pat. Appl. EP 579,435** (Cl. A61K47/48), 19 Jan 1994, US Appl. 912,853, 14 Jul 1992; 46 pp.

9.) M. S. Islam and M. M. Narurkar, *Drug Dev. Ind. Pharm.*, **1991**, 17(9), 1229.

10.) M. A. Hussan and M. S. Suleiman, *Int. J. Pharm.*, **1990**, 58(1), 19.

11.) D. M. Mentzafos, I. R. Mavridis and M. B. Hursthouse, *Acta Crystallogr. Sect. C*, **1996**, 52, 1220.

Conclusion

DSC and XRD comparisons of inclusion complexes and the physical mixtures of their constituents revealed that this sort of approach is useful in demonstrating that inclusion complexes have been formed in the solid state.

The thermal stability of the complexes investigated in this chapter was found to be directly affected by the thermal stability of the included guest. These conclusions were drawn since the thermal stabilities of both the β- and γ-CD complexes increased with increasing decomposition temperatures of the guests they included.

The unit cell parameters and XRD trace of the CIMBCD complex was in close agreement with those of the ACEBCD complex (Chapter 3) indicating an analogous packing arrangement for the two complexes. The β-CD complexes with RAN and FAM crystallised with cell parameters that did not correspond to any presently known β-CD structures; however, the XRD trace of the RANBCD complex resembled that of the CIMBCD complex indicating a similar packing arrangement for the two complexes. Powder XRD and single crystal x-ray photographic information were used to show that the packing arrangements of the three γ-CD complexes are the same and analogous to that of the CYCGCD complex (Chapter 6).

Based on considerations of their crystallographic space groups and CD:drug stoichiometries the structures of all complexes, with the exception of the FAMBCD complex, would exhibit disorder of the guest molecule. However, if the single crystal x-ray structure solutions and guest modelling could be successfully achieved they would provide interesting insights into the inclusion of these conformationally flexible anti-ulcerative agents.

portions of the ranitidine molecules may protrude from the β-CD molecules in which they are included. The asymmetric volume for the FAMBCD complex is similar to that of the RANBCD complex. However, in the case of the FAMBCD complex the asymmetric unit of the structure contains two β-CD molecules. It is possible that the famotidine molecule may be ordered in this structure, since the 2:1 β-CD:drug ratio does not necessitate crystallographic disorder of the guest molecule.

Table 4.10 Asymmetric volumes for the CIMBCD, FAMBCD and RANBCD complexes

Complex	Space Group	β-CD : drug	V (Å^3)	Z	V/Z (Å^3)
CIMBCD	C2	2 : 1	7026	4	1757
FAMBCD	C2	2 : 1	15379	8	1922
RANBCD	$P2_12_12_1$	2 : 1	8594	4	2149

The γ-CD complexes with the three anti-ulceratives all crystallise in the space group $P42_12$ and display very closely matching cell parameters and asymmetric volumes. XRD evidence suggests that these structures would display an analogous packing arrangement to other γ-CD complexes with these cell parameters (e.g. CYCGCD in Chapter 6). γ-CD complexes of this type are positioned with the centre of the γ-CD molecules situated on a four-fold rotation axis. The guest molecules included in the cavities of these γ-CD molecules will inevitably be crystallographically disordered around this rotation axis by at least four-fold. In all three complexes two guest molecules are included per three γ-CD molecules. This suggests that the molecular dimensions of the included guests are too large for a single guest to be included in a single γ-CD molecule, despite the increase in cavity volume offered by a γ-CD molecule relative to a β-CD molecule. The average number of included guests per CD is, however, higher than for the corresponding β-CD complexes indicating that the increased physical dimensions of the γ-CD molecules are better able to accommodate these guest molecules.

Table 4.11 Asymmetric volumes for the CIMGCD, FAMGCD and RANGCD complexes

Complex	Space Group	γ-CD : drug	V (Å^3)	Z	V/Z (Å^3)
CIMGCD	$P42_12$	3 : 2	13080	6	2180
FAMGCD	$P42_12$	3 : 2	13153	6	2192
RANGCD	$P42_12$	3 : 2	13169	6	2195

However, the XRD trace of the RANBCD complex resembles that of the CIMBCD complex and the packing arrangement of those two structures are concluded to be similar.

The cell parameters of the CIMGCD, FAMGCD and RANGCD complexes are all closely matching and also show very close correspondence with the CYCGCD ~~CYGCD~~ complex (Chapter 6). In conjunction with the XRD findings, it can be concluded that the packing arrangements of the three γ-CD complexes with the anti-ulcerative agents are the same and analogous to that of the CYCGCD structure.

The details of the inclusion of these anti-ulcerative drugs is interesting since the drugs themselves can assume a number of different conformations. The conformations observed for these drugs and their salts can be grouped into two main categories : a U-shaped or a linear, extended conformation.

Penkler[2] showed by means of molecular modelling studies that the ranitidine molecule can be included in the β-CD molecule in its U-shaped conformation. This finding was supported by NMR evidence obtained for the solution structure of the β-CD-ranitidine complex.

The inclusion by β-CD of a linear molecule, (*Z*)-9-dodecen-1-ol, was investigated by Mentzafos et al.[11] The molecule has a chain length which is comparable to that of the three anti-ulcerative drugs investigated in this study. The β-CD:guest molecule ratio in this complex is also 2:1. The guest molecule is included in a β-CD dimeric motif and is disordered over two sites. The space group and cell parameters of this structure are also analogous to the CIMBCD structure. The asymmetric volume (*V/Z,* where *V* is the cell volume and *Z* is the number of CDs per unit cell) of the CIMBCD complex (Table 4.10) suggests that practically the entire cimetidine molecule may be included within a β-CD dimer with little protruding portions. It is likely that the disorder of the cimetidine molecule is similar to that observed in the (*Z*)-9-dodecen-1-ol-β-CD complex, possibly with the imidazole ring of each disordered position of cimetidine included in the β-CD cavity of one half of a dimeric unit and the bulky side chain extending into the other half of the dimer. A similar disordered scenario is speculated for the RANBCD complex where the asymmetric unit of the complex consists of a single β-CD molecule and the stoichiometry is, once again, 2:1 β-CD:drug. However, the higher asymmetric volume required for the RANBCD complex suggests that

Crystal data

Table 4.8 shows the crystal data for the CIMBCD, FAMBCD and RANBCD complexes. Table 4.9 shows the crystal data for the CIMGCD, FAMGCD and RANGCD complexes. The cell parameters and space groups were determined by x-ray photographic techniques.

Table 4.8 Crystal data for the CIMBCD, FAMBCD and RANBCD complexes

	CIMBCD	**FAMBCD**	**RANBCD**
Crystal system	Monoclinic	Monoclinic	Orthorhombic
Space group	C2	C2	$P2_12_12_1$
Z	4	8	4
a (Å)	19.22	37.72	15.10
b (Å)	24.57	15.50	15.37
c (Å)	15.75	26.91	37.03
α (°)	90	90	90
β (°)	109.1	102.2	90
γ (°)	90	90	90
V (Å^3)	7026	15379	8594

Table 4.9 Crystal data for the CIMGCD, FAMGCD and RANGCD complexes

	CIMGCD	**FAMGCD**	**RANGCD**
Crystal system	Tetragonal	Tetragonal	Tetragonal
Space group	$P42_12$	$P42_12$	$P42_12$
Z	6	6	6
a (Å)	23.77	23.80	23.82
b (Å)	23.77	23.80	23.82
c (Å)	23.15	23.22	23.21
α (°)	90	90	90
β (°)	90	90	90
γ (°)	90	90	90
V (Å^3)	13080	13153	13169

The cell parameters of the CIMBCD complex shown in Table 4.8 closely match those of the ACEBCD structure (Chapter 3). Together with the XRD results it can be concluded with certainty that the packing arrangement of this structure is analogous to that of the ACEBCD structure. The FAMBCD and RANBCD complexes have cell dimensions which do not correspond to any of the existing β-CD complexes.

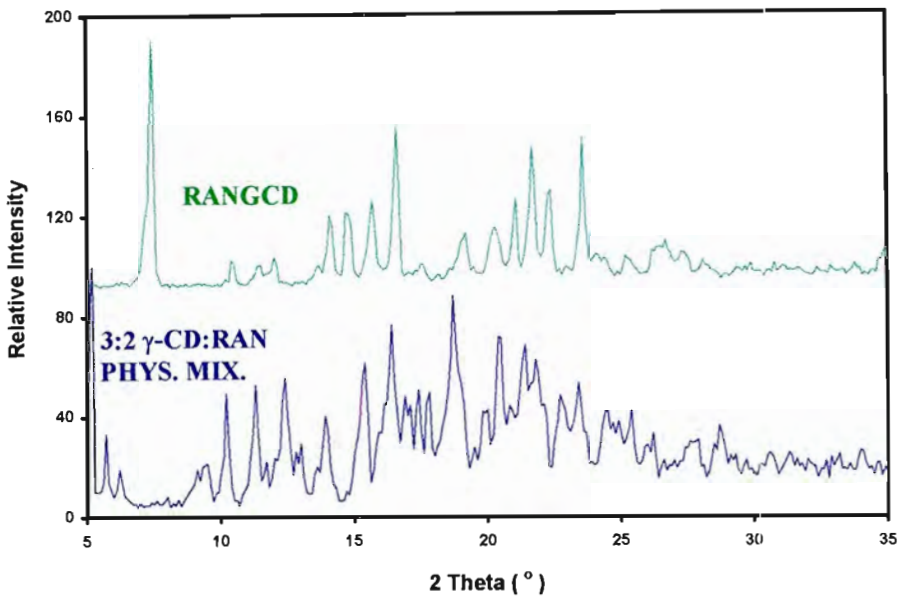

Figure 4.20 XRD patterns of the RANGCD complex and a 3:2 γ-CD:RAN physical mixture

The XRD patterns of all three complexes are closely matching and they can therefore be considered as isomorphous structures (Figure 4.21). The XRD patterns of the three γ-CD complexes also match that of the CYCGCD structure (Figure 6.27, Chapter 6) and the γ-CD complexes presented in this chapter are expected to display a similar packing to that complex.

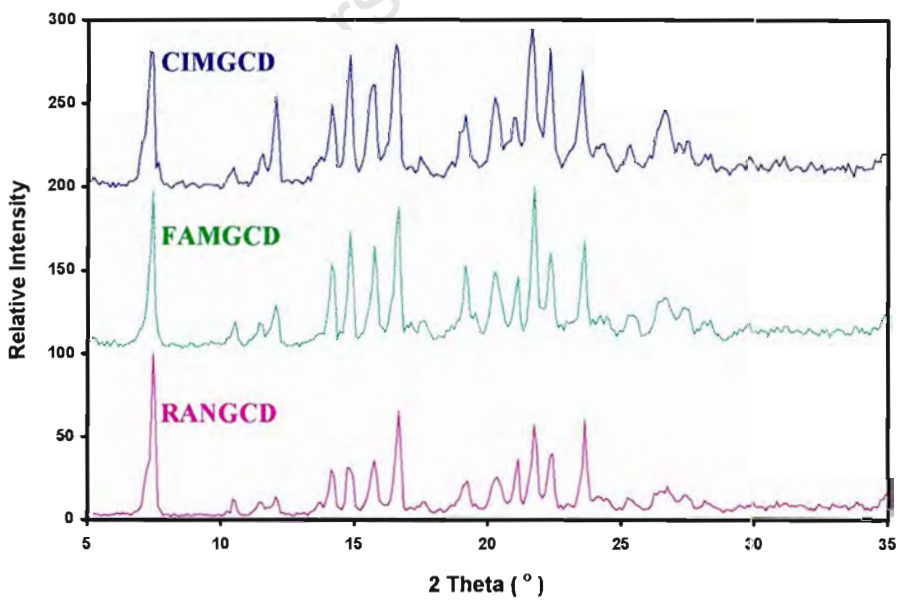

Figure 4.21 The XRD traces of the CIMGCD, FAMGCD and RANGCD complexes

Figures 4.18, 4.19 and 4.20 show the XRD patterns of the CIMGCD, FAMGCD and RANGCD complexes respectively together with the XRD patterns of the physical mixture of γ-CD with the appropriate drug. In all cases, the XRD pattern of the complex indicates a new crystalline phase distinct from the constituent γ-CD or drug, or any physical combination of those two phases.

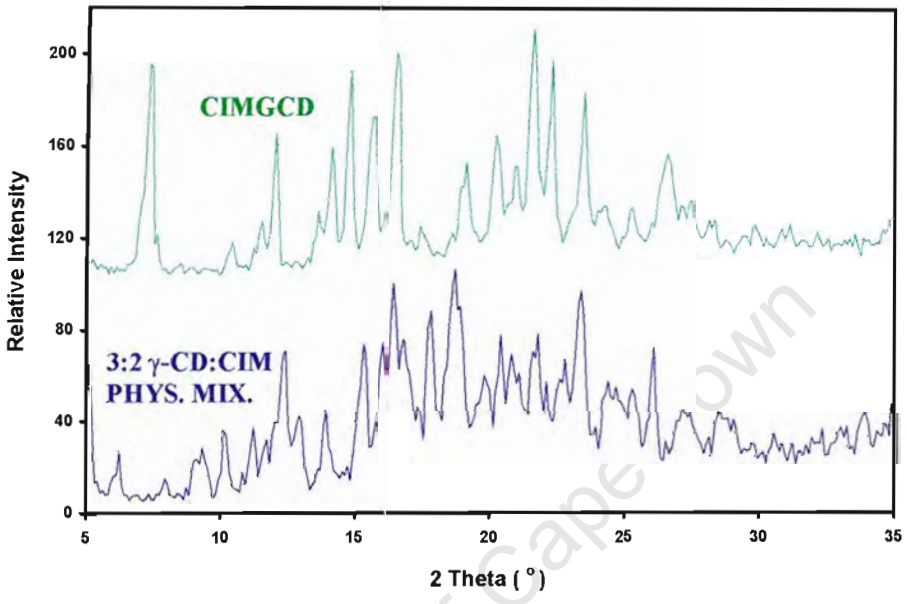

Figure 4.18 XRD patterns of the CIMGCD complex and a 3:2 γ-CD:CIM physical mixture

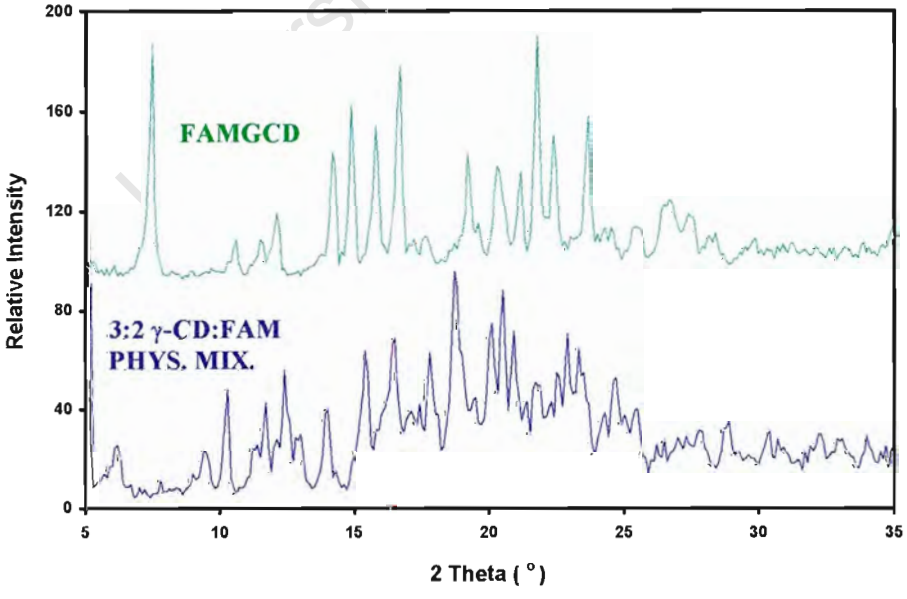

Figure 4.19 XRD patterns of the FAMGCD complex and a 3:2 γ-CD:FAM physical mixture

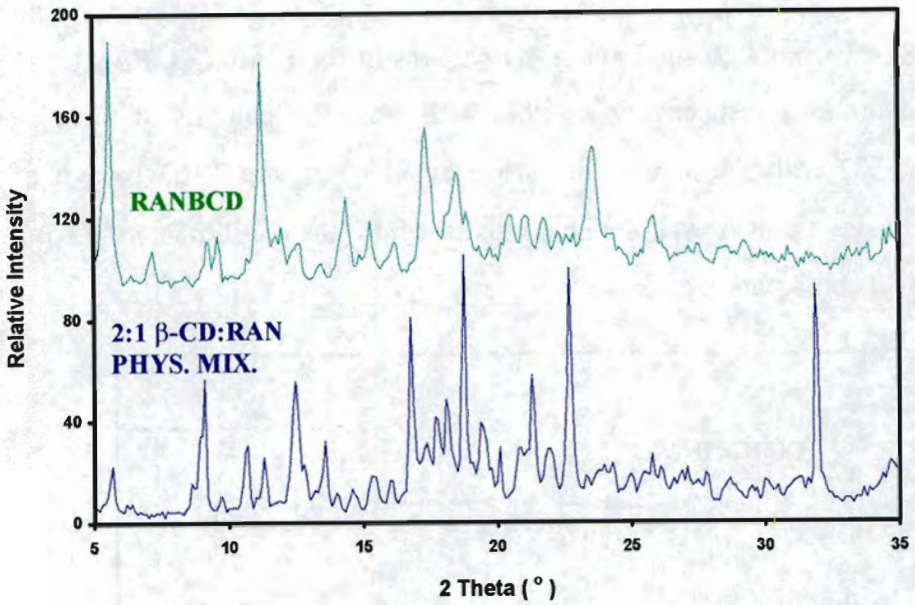

Figure 4.16 XRD patterns of the RANBCD complex and a 2:1 β-CD:RAN physical mixture

The CIMBCD complex referred to in Figure 4.14 has similar cell parameters to CH type dimeric β-CD structures (e.g. the ACEBCD structure discussed in Chapter 3). The XRD pattern of CIMBCD closely matches that of ACEBCD (Figure 4.17). This confirms that the CIMBCD structure is isomorphous with the ACEBCD structure and thus displays a similar packing of the β-CD molecules. The XRD trace of the RANBCD complex (Figure 4.16) displays an overall pattern which resembles that of the CIMBCD complex. These two complexes may therefore show a similar packing arrangement given the similarity of their XRD traces (Figure 4.17).

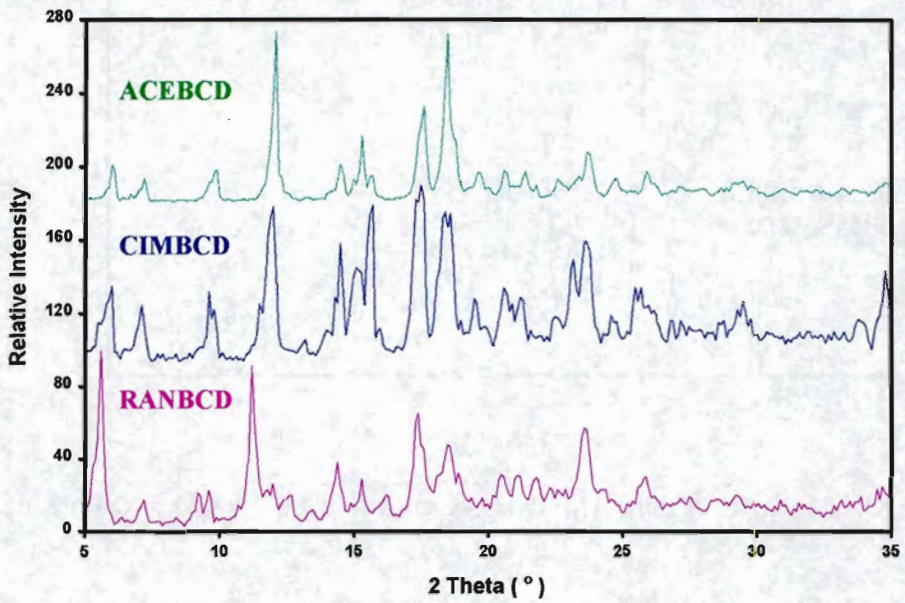

Figure 4.17 XRD patterns of the ACEBCD, CIMBCD and RANBCD complexes

XRD analysis of complexes and physical mixtures of their components

Figures 4.14, 4.15 and 4.16 show the XRD patterns of the CIMBCD, FAMBCD and RANBCD complexes respectively together with the XRD patterns of the physical mixture of β-CD with the appropriate drug. In all cases the appearance of a new crystalline phase, distinct from the constituent β-CD or drug, or any physical combination of those two phases, is evident.

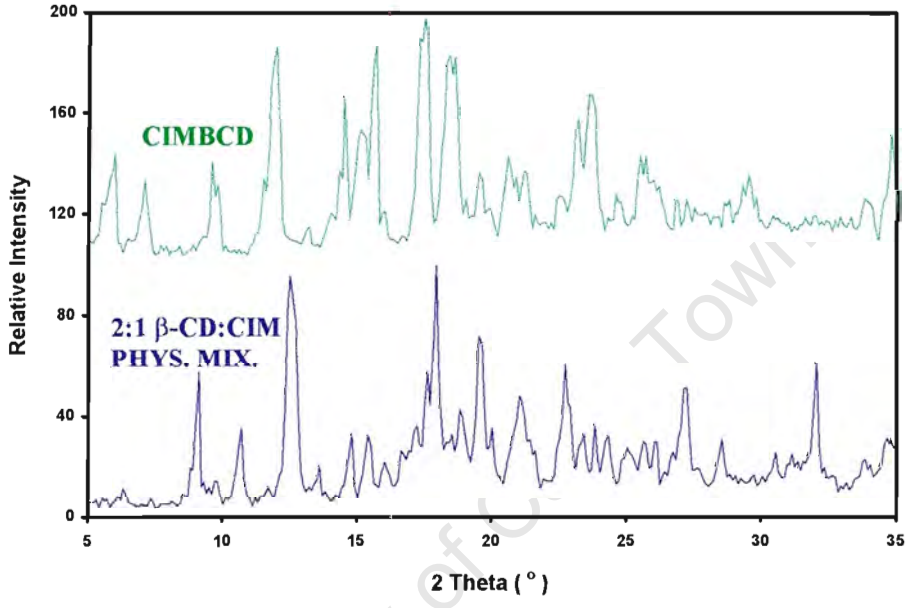

Figure 4.14 XRD patterns of the CIMBCD complex and a 2:1 β-CD:CIM physical mixture

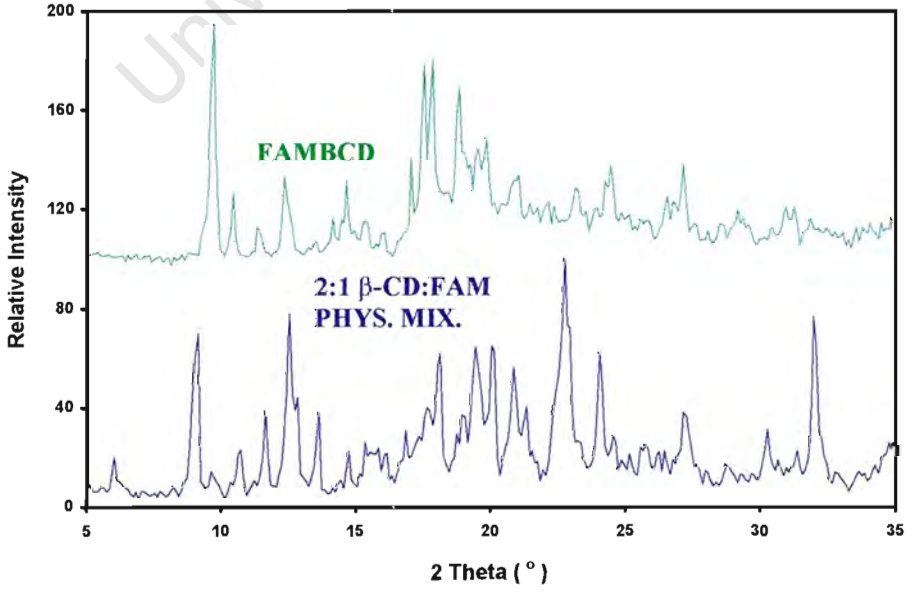

Figure 4.15 XRD patterns of the FAMBCD complex and a 2:1 β-CD:FAM physical mixture

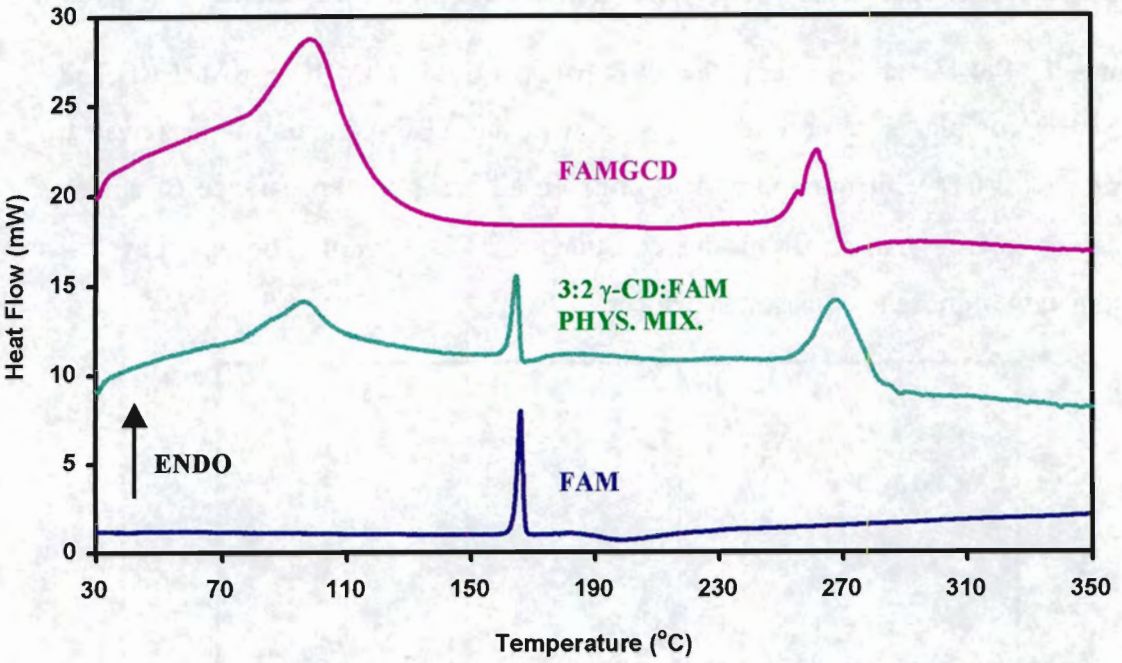

Figure 4.12 DSC traces of FAMGCD, 3:2 γ-CD:FAM physical mixture and uncomplexed FAM

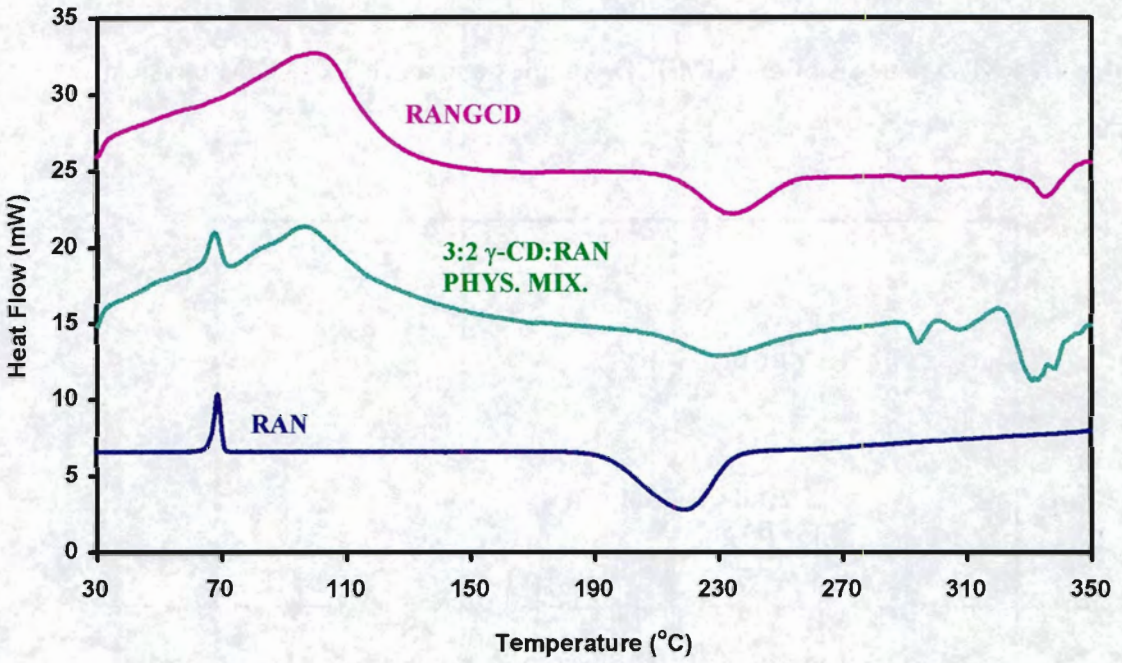

Figure 4.13 DSC traces of RANGCD, 3:2 γ-CD:RAN physical mixture and uncomplexed RAN

The DSC traces of the CIMGCD, FAMGCD and RANGCD complexes are shown in Figures 4.11, 4.12 and 4.13 together with the traces of the uncomplexed drugs and the 3:2 γ-CD:drug physical mixtures. As was observed for the β-CD complexes the characteristic melting endotherms of the CIM, FAM and RAN are clearly visible in the DSC traces of the uncomplexed drugs and the physical mixtures. In all cases disappearance of this fusion endotherm was observed in the DSC traces of the complexes. The disappearance of the drug endotherm indicates that an inclusion complex has been formed in the solid state. The decomposition temperatures of the uncomplexed drugs were determined from HSM, TGA and DSC investigations to be 180, 190 and 220°C for FAM, RAN and CIM respectively. The thermal stability of the inclusion complexes with these drugs was based on the analysis of the onset of decomposition for the complexes. It is noted earlier in this chapter that for the β-CD complexes, the thermal stability follows the order CIMBCD > RANBCD > FAMBCD and for the γ-CD complexes the order is CIMGCD > RANGCD > FAMGCD. The thermal stability of the inclusion complexes in both series seems to follow the order of the thermal stability of the drugs which they contain.

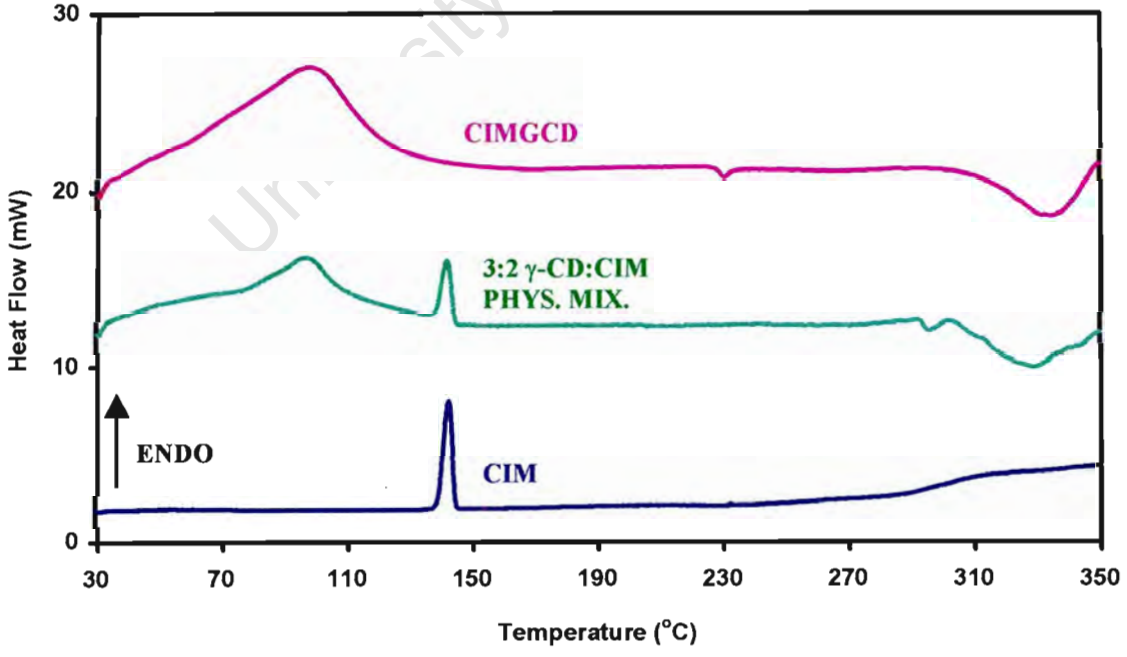

Figure 4.11 DSC traces of CIMGCD, 3:2 γ-CD:CIM physical mixture and uncomplexed CIM

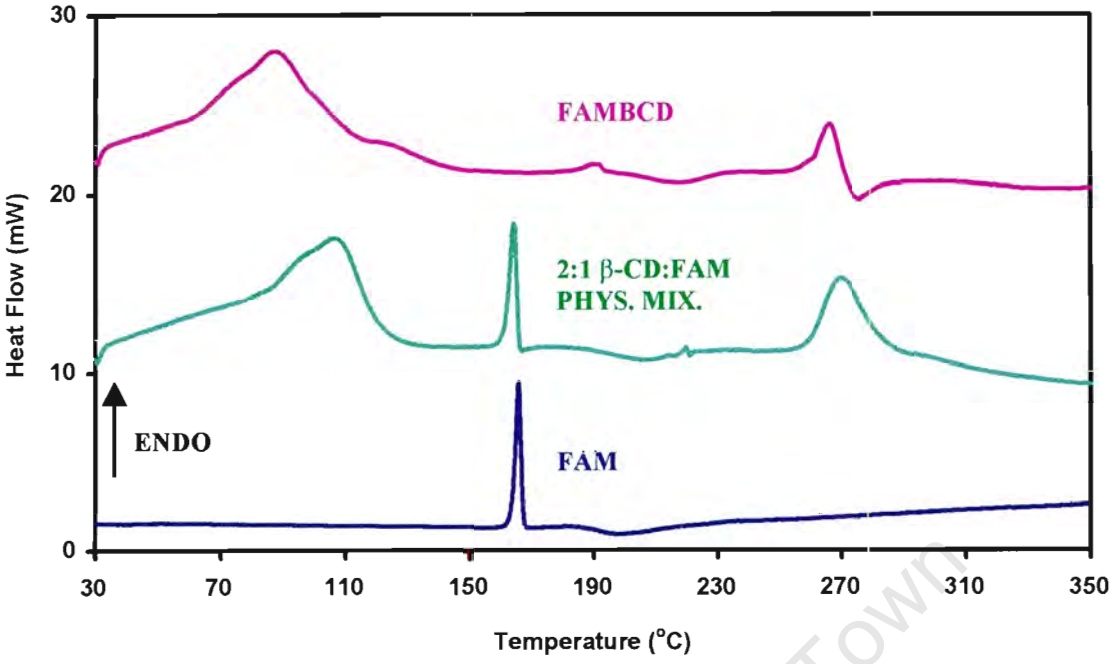

Figure 4.9 DSC traces of FAMBCD, 2:1 β-CD:FAM physical mixture and uncomplexed FAM

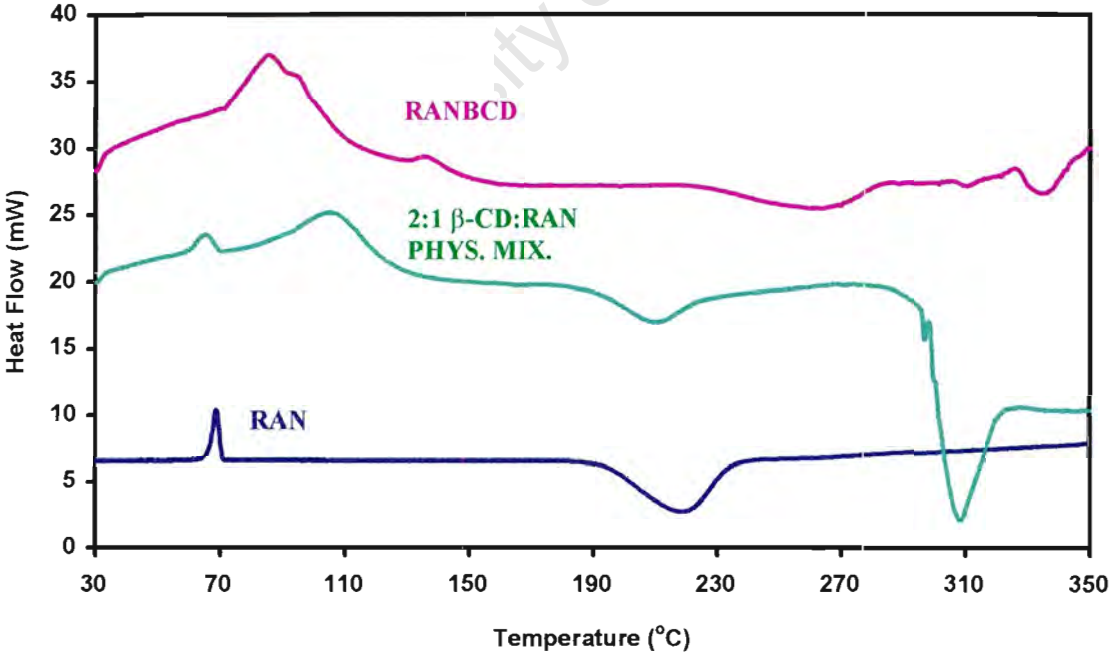

Figure 4.10 DSC traces of RANBCD, 2:1 β-CD:RAN physical mixture and uncomplexed RAN

DSC analysis of complexes and physical mixtures of their components

The DSC traces of the CIMBCD, FAMBCD and RANBCD complexes are shown in Figures 4.8, 4.9 and 4.10 together with the traces of the appropriate uncomplexed drug and the 2:1 β-CD:drug physical mixtures. The characteristic melting endotherms for uncomplexed CIM, FAM and RAN occur at temperatures of 141, 163 and 69°C. These fusion endotherms are clearly visible in the DSC traces of the uncomplexed drug and physical mixtures of these drugs with β-CD. In all cases disappearance of the fusion endotherm for the uncomplexed drug was observed for the inclusion complexes. Individual drug molecules are separated from one another and contained within the cavities of CD molecules and therefore will no longer exhibit the characteristics of their crystalline phase. The disappearance of the drug endotherm indicates that an inclusion complex has been formed in the solid state.

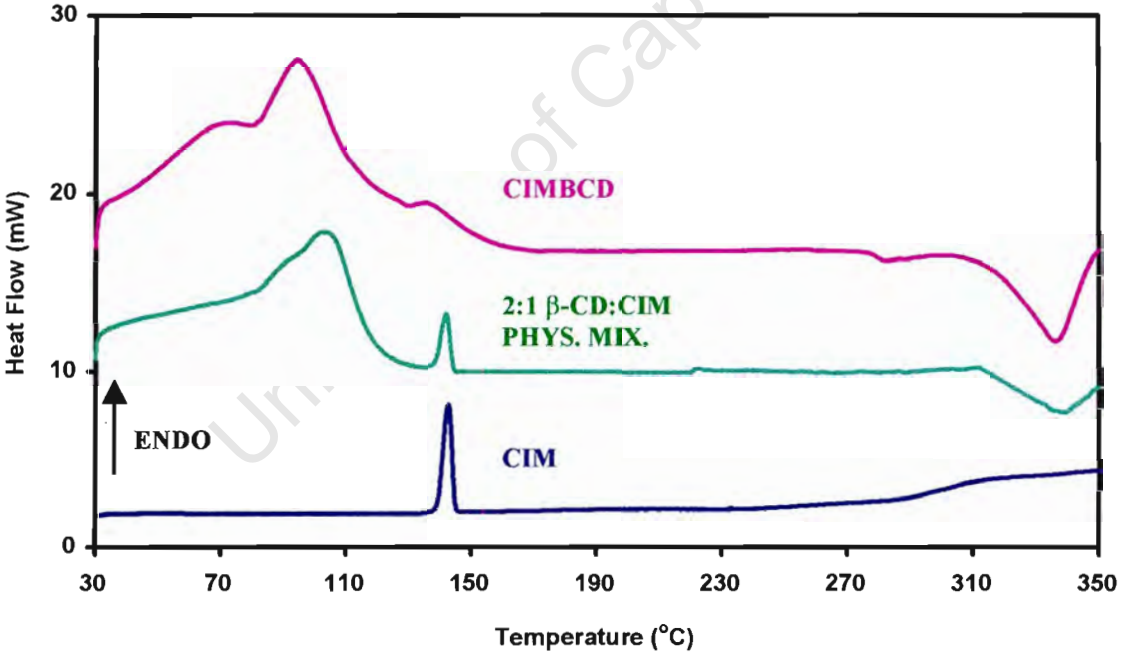

Figure 4.8 DSC traces of CIMBCD, 2:1 β-CD:CIM physical mixture and uncomplexed CIM

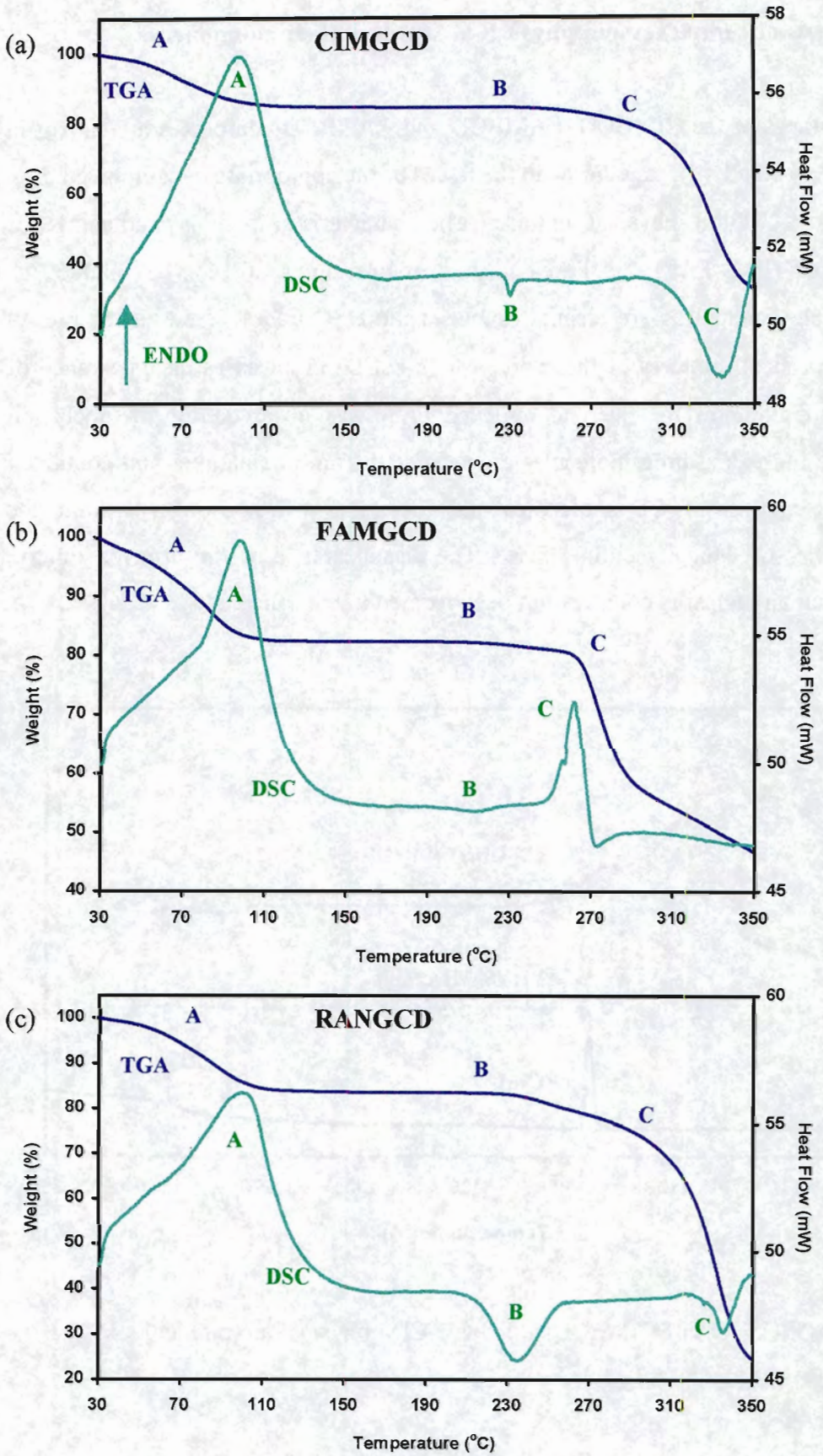

Figure 4.7 TGA and DSC traces for the (a) CIMGCD, (b) FAMGCD and (c) RANGCD complexes

DSC results for γ-CD complexes

The TGA traces of all three γ-CD complexes (Figures 4.7 (a), (b) and (c)) show water loss in the range 30 to 130°C (labelled A). This water loss is associated with broad endotherms on the DSC traces of the complexes. The major peak of the dehydration endotherm (labelled A) occurs at 100°C for all three complexes. The relatively symmetrical shape of the dehydration endotherms is an indication that water loss from these complexes occurs in a single step. The onset of decomposition (labelled B) at 230, 210 and 220°C for the CIMGCD, FAMGCD and RANGCD complexes is indicated by further mass loss on the TGA traces of the complexes. The onset of the decomposition closely corresponds with the onset of an exothermic thermal event (labelled B) for all three complexes. The peaks of these exotherms occur at 230, 215 and 235°C for the CIMGCD, FAMGCD and RANGCD complexes. This decomposition begins, in all cases, earlier than the decomposition of the γ-CD molecule, which occurs above 290°C, and is therefore associated with decomposition of the guest molecules. The final stages of decomposition are associated with a large exotherm for the CIMGCD and RANGCD complexes (labelled C in Figure 4.7 (a) and 4.7 (c) respectively). The FAMGCD complex behaves somewhat differently, displaying a fairly sharp endotherm (labelled C in Figure 4.7 (b)) followed by a shallow exotherm. The most rapid stages of weight loss, as observed from the TGA traces, occur above 290°C for the CIMGCD and RANBCD complexes (labelled C). The events indicate that decomposition of the γ-CD molecules is occurring. For the FAMGCD complex large weight losses are observed after 270°C. This significant decrease in sample mass occurs at a lower temperature than expected for the decomposition of the γ-CD host and the percentage weight loss suggests that the famotidine molecule was liberated from the complex during this stage of the decomposition.

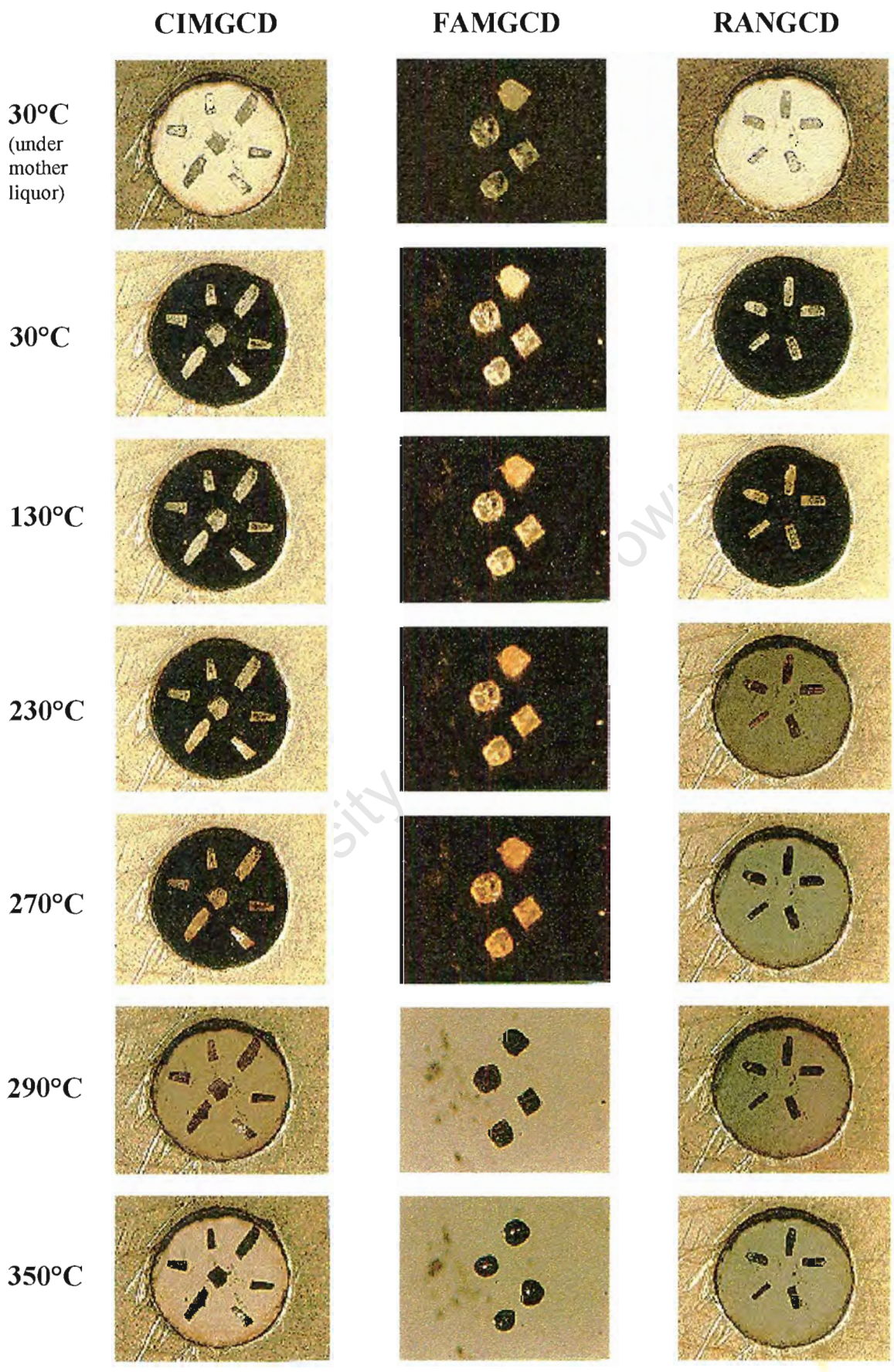

Figure 4.6 HSM photographs taken at various temperatures for crystals of the CIMGCD (10x), FAMGCD (40x) and RANGCD (10x) complexes

HSM results for γ-CD complexes

The HSM results for CIMGCD, FAMGCD and RANGCD are presented in Figure 4.6. Water loss from the complexes is visible by cracking of the crystals. Water loss is complete at 130°C for all three γ-CD complexes and the crystals of the complexes are largely opaque by this temperature. The temperature range of water loss is also clear from the TGA results (Figures 4.7 (a), (b) and (c)). The crystals of the complexes remain visibly unchanged from the end of water loss to the onset of decomposition. The crystals begin to become light brown in colour indicating the onset of decomposition for the CIMGCD, FAMGCD and CIMGCD complexes at temperatures of 230, 210 and 220°C. This is visible as further mass losses in the TGA traces of the complexes. At 350°C the crystals are completely black and charred. The CIMGCD complex displays the highest thermal stability while the thermal behaviours of the FAMGCD and RANGCD complexes show a fairly similar behaviour during HSM.

TGA results for γ-CD complexes

The TGA results for the CIMGCD, FAMGCD and RANGCD complexes are shown in Figures 4.7 (a), (b) and (c). A summary of the observed percentage weight losses is presented in Table 4.7. Weight losses from 30 to 130°C represent water loss from the complexes. From 130° to 210°C no significant weight loss is observed for any of the complexes. From 210°C onwards weight losses due to decomposition are observed.

Table 4.7 The percentage weight losses for the CIMGCD, FAMGCD and RANGCD complexes at various temperatures

	CIMGCD		FAMGCD		RANGCD	
Temperature (°C)	Sample weight (%)	ΔWeight loss† (%)	Sample weight (%)	Δ Weight loss† (%)	Sample weight (%)	Δ Weight loss† (%)
30	100	-	100	-	100	-
130	84.7	15.3	82.2	17.8	83.9	16.1
200	84.7	0.0	82.2	0.0	83.9	0.0
210	84.7	0.0	82.2	0.0	83.9	0.0
220	84.7	0.0	81.7	0.5	83.9	0.0
230	84.7	0.0	81.0	0.7	83.2	0.7
270	82.3	2.4	74.7	6.3	78.1	5.1
350	32.7	49.6	46.0	28.7	23.7	54.4

† ΔWeight loss (%) = [Sample weight (%) at temperature(n-1)] - [Sample weight (%) at temperature(n)]

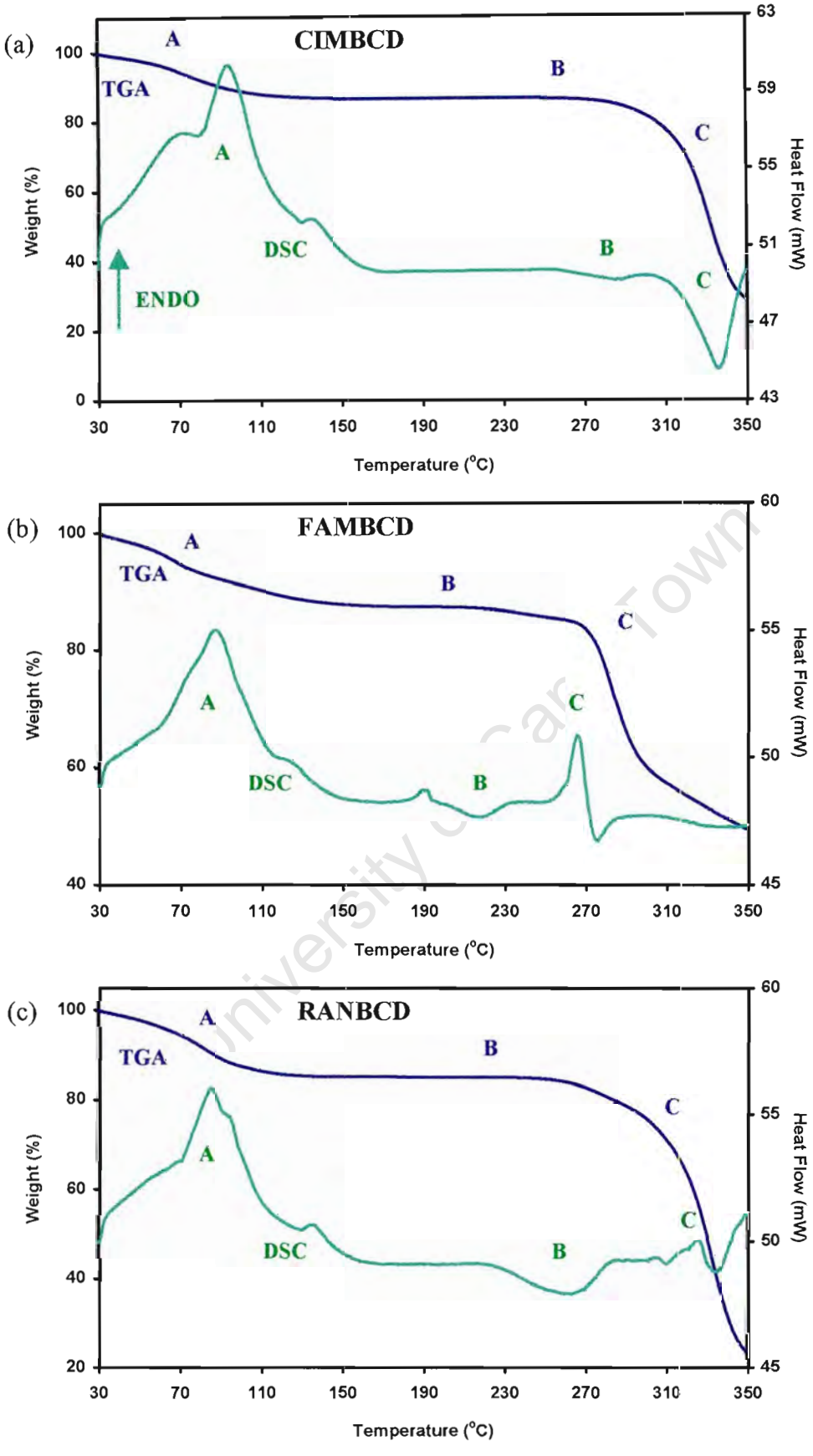

Figure 4.5 TGA and DSC traces for the (a) CIMBCD, (b) FAMBCD and (c) RANBCD complexes

DSC results for β-CD complexes

The three β-CD complexes show endothermic events corresponding to water loss in the range 30 to 160°C (Figures 4.5 (a), (b) and (c)). These endotherms cover the same range in which water loss is observed from the TGA traces (this weight loss is labelled A for the TGA traces). The dehydration endotherm has a major peak (labelled A) occurring at 97, 89 and 87°C for the CIMBCD, FAMBCD and RANBCD complexes. Each of the traces for the complexes also displays a shoulder to this peak at a higher temperature. The shoulders occur at 137, 126 and 136°C respectively indicating that a portion of the solvent water molecules requires more energy to be released from the complexes. The asymmetrical shape of the dehydration endotherms is an indication that water loss from these complexes is a multi-stage process. The onset of decomposition is indicated by further mass loss (labelled B on the TGA traces). The onset of decomposition occurs at 260, 200 and 220°C for the CIMBCD, FAMBCD and RANBCD complexes. The onset of the decomposition closely corresponds with the onset of a broad exotherm (labelled B in all cases) for all three complexes. The peaks of these exotherms occur at 282, 217 and 263°C for the CIMBCD, FAMBCD and RANBCD complexes. The FAMBCD complex displays a small endotherm at 191°C which is associated with a phase change in the complex that takes place shortly before the onset of decomposition. This decomposition begins in all cases well before the decomposition of the β-CD molecule, which occurs above 290°C, and is therefore associated with decomposition of the guest molecules. A large exotherm (labelled C in Figure 4.5 (a)) is associated with the final stages of decomposition of the CIMBCD complex. A sharp endotherm (labelled C in Figure 4.5 (b)) followed by an exotherm are associated with the final stages of decomposition of the FAMBCD complex. A weight loss of 17.2%, over the range 270-290°C, is observed for the TGA trace of the FAMBCD complex. This significant loss of sample mass occurs at a lower temperature than the decomposition of the β-CD host and suggests that the famotidine molecule is liberated from the complex during this stage of the decomposition. Large weight losses (labelled C) are observed in the TGA traces from 290°C onwards for all complexes, indicating that decomposition of the β-CD molecules is occurring.

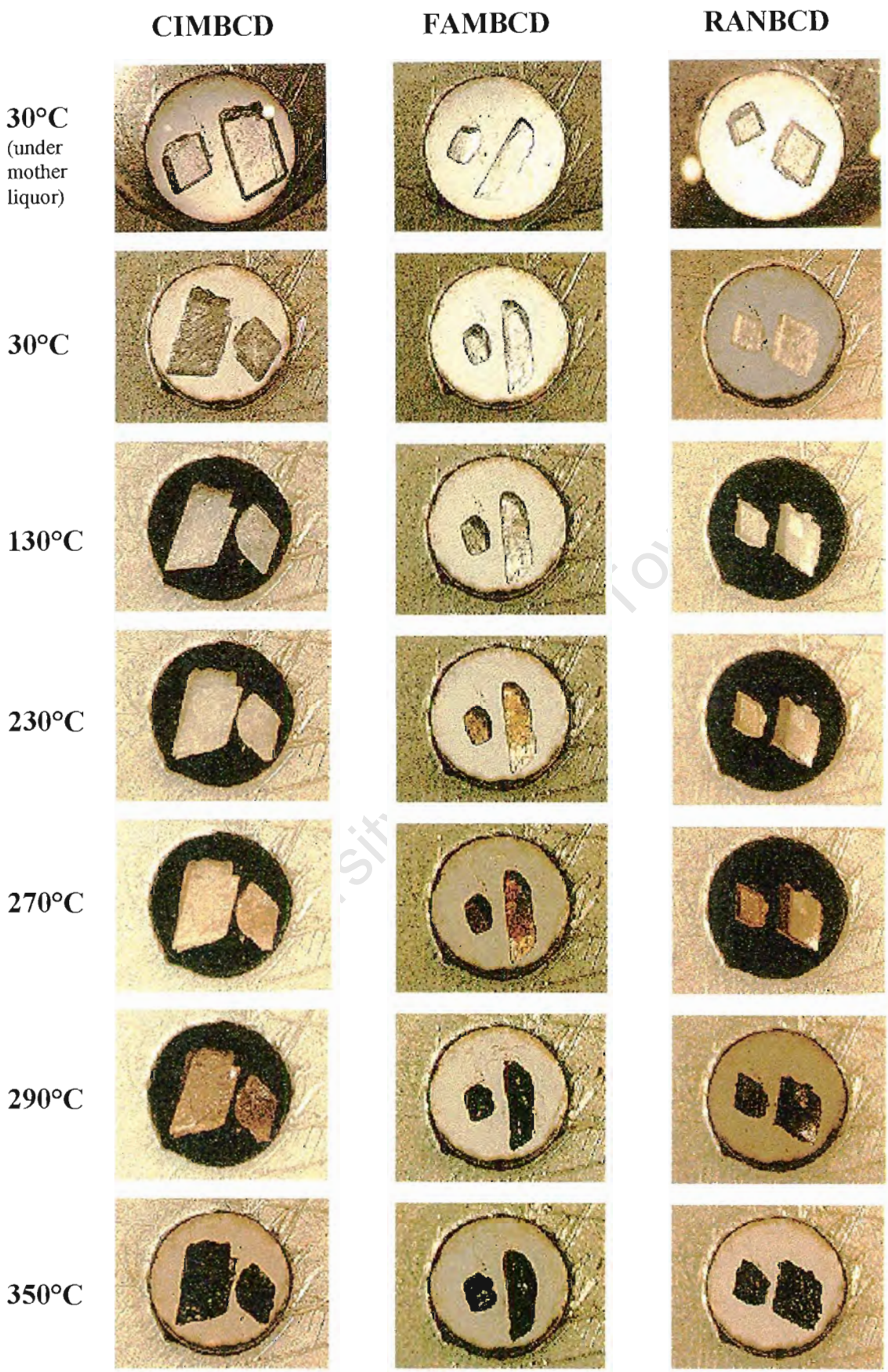

Figure 4.4 HSM photographs taken at various temperatures for crystals of the CIMBCD (10x), FAMBCD (10x) and RANBCD (10x) complexes

HSM results for β-CD complexes

The HSM results for CIMBCD, FAMBCD and RANBCD are presented in Figure 4.4. Water loss from the complexes is visible by cracking of the crystals. Water loss occurs over the range 30 to 160°C for the three complexes. The crystals of the complexes are practically opaque following dehydration. The temperature range of water loss is also evident from the TGA traces (Figures 4.5 (a), (b) and (c)). The crystals of the complexes remain visibly unchanged from the end of water loss to the onset of decomposition. The crystals begin to become light brown in colour indicating the onset of decomposition. The latter occurs at 260, 200 and 220°C for the CIMBCD, FAMBCD and RANBCD complexes. Decomposition of the complexes is observed by further mass losses in the TGA traces. At 350°C the crystals are completely black and charred. The CIMBCD complex displays the highest thermal stability of the three complexes.

TGA results for β-CD complexes

The TGA results for the CIMBCD, FAMBCD and RANBCD complexes are shown in Figures 4.5 (a), (b) and (c). A summary of the observed percentage weight losses is presented in Table 4.6. Weight losses from 30 to 160°C represent water loss from the complexes. From 160° to 200°C no significant weight loss is observed for any of the complexes. From 200°C onwards weight losses due to decomposition are observed.

Table 4.6 The percentage weight losses for the CIMBCD, FAMBCD and RANBCD complexes at various temperatures

	CIMBCD		FAMBCD		RANBCD	
Temperature (°C)	Sample weight (%)	ΔWeight loss† (%)	Sample weight (%)	Δ Weight loss† (%)	Sample weight (%)	Δ Weight loss† (%)
30	100	-	100	-	100	-
160	86.4	13.6	87.3	12.7	85.3	14.7
200	86.4	0.0	87.3	0.0	85.3	0.0
220	86.4	0.0	86.8	0.5	85.3	0.0
230	86.4	0.0	85.6	1.2	85.0	0.3
260	86.4	0.0	83.2	2.4	83.9	1.1
270	85.3	1.1	82.2	1.0	82.2	1.7
290	82.5	2.8	65.0	17.2	77.7	4.5
350	28.9	53.6	49.4	15.6	23.9	53.8

† ΔWeight loss (%) = [Sample weight (%) at temperature(n-1)] - [Sample weight (%) at temperature(n)]

Microanalysis

The host:guest obtained from UV were confirmed by the C, H, N and S microanalysis results. The complexes were dried under vacuum for 1 hour and thermogravimetric analysis was used to determine the residual water content of the samples to be analysed (Table 4.4).

Table 4.4 The C, H, N and S microanalysis results for β- and γ-CD complexes with CIM, FAM and RAN

Complex	Calculated (%)				Experimental (%)			
	C	H	N	S	C	H	N	S
CIMBCD.1H_2O	44.13	6.26	3.29	1.25	44.02	6.39	3.61	P†
CIMGCD.1H_2O	44.44	6.26	5.36	2.04	44.30	6.33	5.35	P†
FAMBCD.2H_2O	41.24	6.09	3.66	3.59	41.22	6.08	3.71	3.82
FAMGCD.1H_2O	41.58	5.98	4.26	4.18	41.45	5.99	4.23	4.00
RANBCD.1H_2O	44.46	6.34	2.14	1.22	44.21	6.44	2.28	P†
RANGCD.1H_2O	44.64	6.35	2.46	1.41	44.39	6.48	2.68	1.12

† P = Present in the analysis but the S peak is too broad to be properly integrated

Stoichiometric formulae

The full stoichiometric formulae of the complexes obtained from the TGA, UV and microanalysis results are presented in Table 4.5.

Table 4.5 The H:G:Water ratios and stoichiometric formulae for the β- and γ-CD complexes of CIM, FAM and RAN

Complex	H : G : Water	Stoichiometric formula
CIMBCD	2:1:22	$2(C_{42}H_{70}O_{35})\cdot1(C_{10}H_{16}N_6S)\cdot22(H_2O)$
CIMGCD	3:2:44	$3(C_{48}H_{80}O_{40})\cdot2(C_{10}H_{16}N_6S)\cdot44(H_2O)$
FAMBCD	2:1:21	$2(C_{42}H_{70}O_{35})\cdot1(C_8H_{15}N_7O_2S_3)\cdot21(H_2O)$
FAMGCD	3:2:56	$3(C_{48}H_{80}O_{40})\cdot2(C_8H_{15}N_7O_2S_3)\cdot56(H_2O)$
RANBCD	2:1:25	$2(C_{42}H_{70}O_{35})\cdot1(C_{13}H_{22}N_4O_3S)\cdot25(H_2O)$
RANGCD	3:2:49	$3(C_{48}H_{80}O_{40})\cdot2(C_{13}H_{22}N_4O_3S)\cdot49(H_2O)$

UV Spectrophotometry

The host:guest ratios for the β- and γ-CD complexes were determined by UV spectrophotometry at 201, 207 and 228nm in distilled water for CIM, FAM and RAN. The ratios obtained for the complexes are shown in Table 4.2.

Table 4.2 The host:guest ratios determined from UV spectrophotometry for β- and γ-CD complexes of CIM, FAM and RAN

β-CD Complexes	**CIMBCD**	**FAMBCD**	**RANBCD**
Host : Guest ratio	2:1	2:1	2:1
γ-CD Complexes	**CIMGCD**	**FAMGCD**	**RANGCD**
Host : Guest ratio	3:2	3:2	3:2

Water content

The water content per CD was calculated from the initial mass losses obtained from TGA traces of the β- and γ-CD complexes with CIM, FAM and RAN (Table 4.3).

Table 4.3 The percentage water loss from the β- and γ-CD complexes with CIM, FAM and RAN and the number of water molecules per CD molecule for each complex

Complex	**% weight loss**	**Temperature range (°C)**	**No. of water molecules / CD**
CIMBCD	13.6	30-160	11.0
CIMGCD	15.3	30-160	14.7
FAMBCD	12.7	30-160	10.5
FAMGCD	17.8	30-130	18.7
RANBCD	14.7	30-130	12.4
RANGCD	16.1	30-130	16.3

Complex preparation

The crystalline complexes of cimetidine (CIM), famotidine (FAM) and ranitidine (RAN) with β- and γ-CD were obtained from slow cooling of hot aqueous solutions of CD and drug. The solutions were prepared according to the concentrations and molar ratios listed in Table 4.1. The complexes of β-CD with CIM, FAM and RAN will be referred to hereafter as CIMBCD, FAMBCD and RANBCD. The complexes of γ-CD with CIM, FAM and RAN will be referred to hereafter as CIMGCD, FAMGCD and RANGCD. Photographs of crystals of the complexes are shown in Figure 4.3. The photographs are taken on a microscope under plane polarised light at a magnification of 10x for the β-CD complexes and a magnification of 30x for the γ-CD complexes. Figure 4.3 illustrates the morphologies and sizes of crystals of these complexes.

Table 4.1 Preparation details for the β- and γ-CD complexes with CIM, FAM and RAN

Complex	CD (mmol)	Drug (mmol)	Molar ratio	Water (ml)
CIMBCD	0.46	0.23	2 : 1	4
CIMGCD	0.22	0.22	1 : 1	4
FAMBCD	0.21	0.21	1 : 1	4
FAMGCD	0.44	0.22	2 : 1	2
RANBCD	0.30	0.30	1 : 1	4
RANGCD	0.44	0.44	1 : 1	2

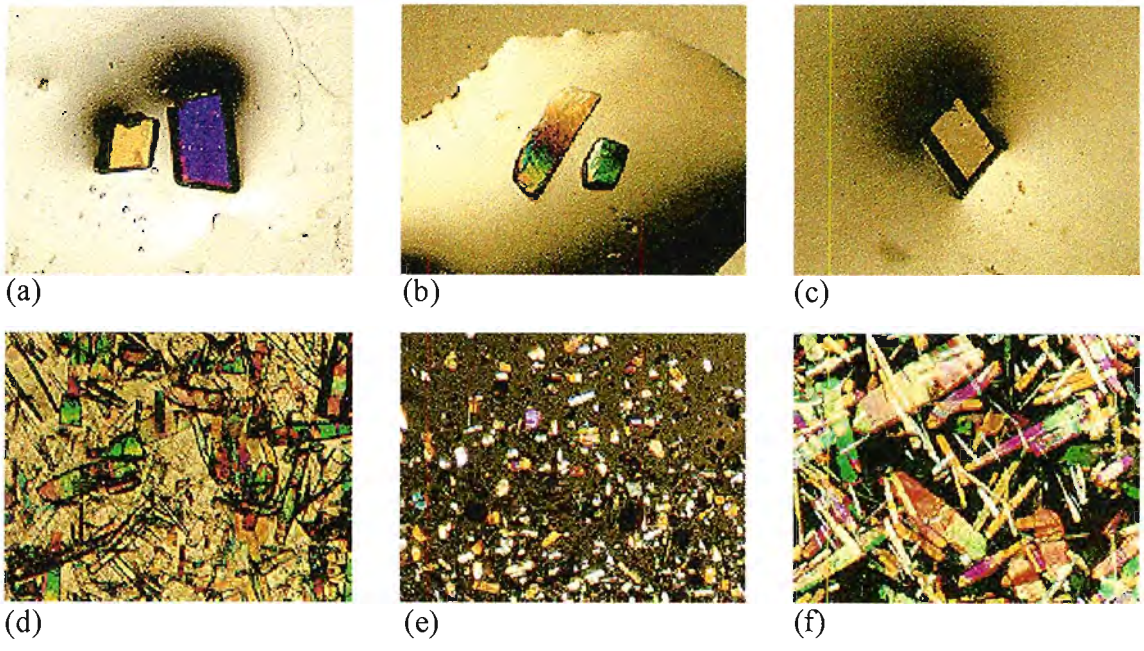

Figure 4.3 Photographs of crystals of the (a) CIMBCD, (b) FAMBCD (c) RANBCD, (d) CIMGCD, (e) FAMGCD and (f) RANGCD complexes under plane polarised light

The preparation and investigation of complexes of CD derivatives with cimetidine have been patented.[6]

The aqueous solubility of famotidine was enhanced in the presence of HP-β-CD.[7] The study reported that cyclodextrin derivatives stabilise famotidine and various other drugs against degradation in aqueous solution. However, it was noted that the stabilising effects are dependent on the chemical structure of the drugs, as well as the nature of the CD in which they are included. A novel method for enhancing the complexation of famotidine and various other chemical substances with HP-β-CD was patented.[8]

Famotidine was reported to form an inclusion complex with HP-β-CD which displayed a phase solubility diagram of the A_L type.[9] The stability constant for complex formation was determined as 100.5 M^{-1} at pH=7.4. The degradation of famotidine by acid catalysis in strongly acidic solutions was shown to be decreased in the presence of HP-β-CD. The dissolution rate of the prepared complex was also shown to be significantly greater than that of the pure drug.

An inclusion complex of famotidine with β-CD was prepared by co-precipitation from hot, distilled water with stirring at room temperature for several days.[10] Phase solubility studies revealed the formation of a 1:1 complex which displayed a phase solubility diagram of the A_L type. The stability constant for the complex was determined as 74.96 M^{-1}. The formation of the complex in the solid state was demonstrated by IR spectroscopy and DSC. The XRD powder pattern of the complex indicated this material to be significantly less crystalline than that of either of the pure components. The dissolution rate of the complex was determined to be double that of the physical mixture and six times higher than that for the pure drug.

The objective of this investigation was to prepare and characterise β- and γ-CD complexes with cimetidine, famotidine and ranitidine in the solid state.

The representation of the possible interaction of ranitidine with β-CD was generated by docking the energy minimised ranitidine conformers, obtained from quenched molecular dynamics simulations, into the β-CD cavity.[4] Figure 4.2 represents the energy minimum which corresponded closely with the solution proton NMR data obtained at 500MHz. The characteristic U-structure of the guest brings the dimethylamino protons in close proximity to the enamine terminal which was confirmed by dipolar coupling between protons associated with these substituents.

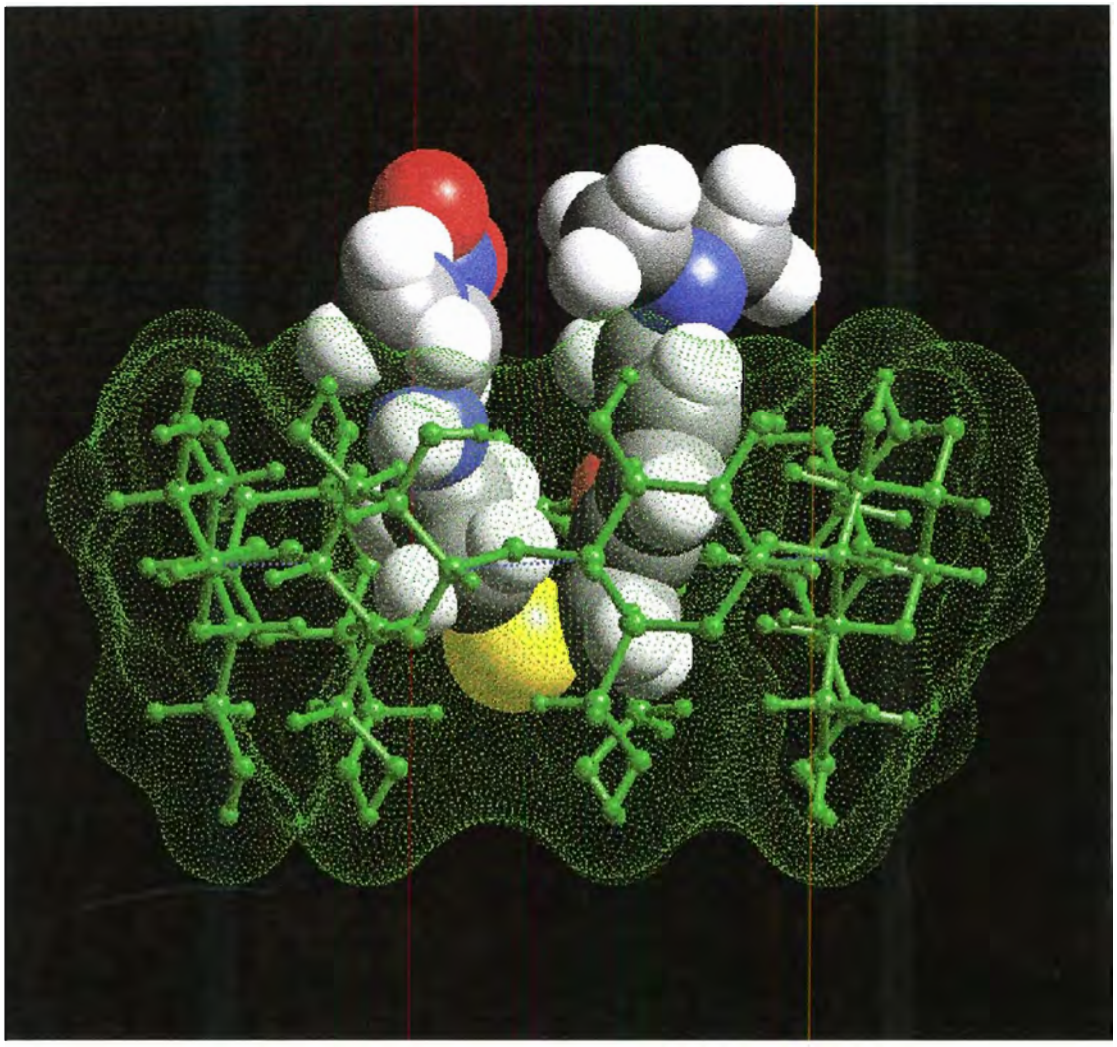

Figure 4.2 Minimised energy structure of the interaction of ranitidine and β-CD

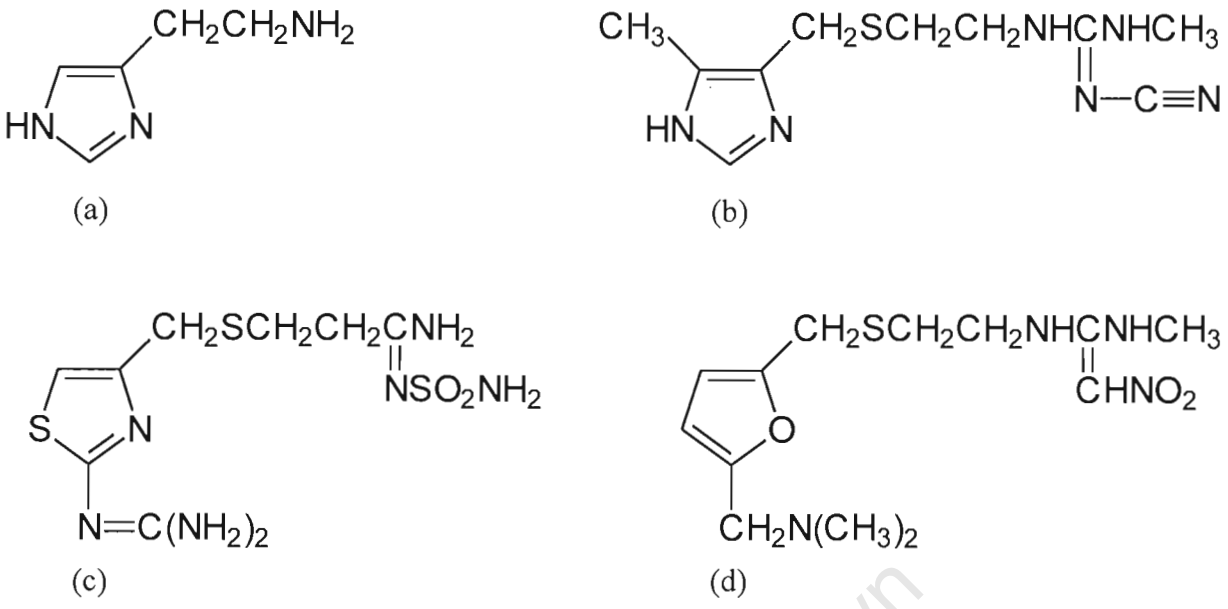

Figure 4.1 Chemical structures of (a) histamine and the three H_2 antagonists (b) cimetidine, (c) famotidine and (d) ranitidine

The preparation and investigation of inclusion complexes of ranitidine hydrochloride with α-, β- and γ-CD and their alkylated and hydroxy-alkylated derivatives have been patented. The inclusion complexes provided ranitidine hydrochloride in a form that was significantly different from Form 1 and Form 2. Preparations of these complexes were formulated for intended pharmaceutical use.[3]

The marketing of the free base of ranitidine was not previously considered because of the chemical instability and hygroscopic nature of the compound. Formulation of this compound as a CD complex could improve certain unfavourable properties.[4]

The preparation and investigation of the inclusion complexes of ranitidine (free base) with the native cyclodextrins and their pharmaceutically acceptable derivatives have been patented.[5] The CD complexes were shown to be tasteless and exhibited improved properties over ranitidine hydrochloride. Improved chemical stability and favourable powdery flow and compaction properties were demonstrated. An α-CD complex with ranitidine was formulated as a tablet intended for pharmaceutical use.

CHAPTER 4 : CD COMPLEXES WITH ANTI-ULCERANTS

Introduction

Cimetidine, Famotidine and Ranitidine are H_2–receptor antagonists which fall into the class of anti-peptic ulcerants.

H_2 antagonists inhibit competitively the interaction of histamine with H_2-receptors. They are highly selective and have little or no effect on H_1- or other receptors. Although H_2-receptors are present in numerous tissues, H_2 antagonists interfere remarkably little with physiological functions other than gastric secretion.[1]

The clinical use of H_2 antagonists is a result of their capacity to inhibit gastric acid secretion, especially in people with peptic ulceration. The H_2 antagonists, cimetidine (TAGAMET™), ranitidine hydrochloride (ZANTAC™), famotidine (PEPCID™) and nizatidine (AXID™) are therefore used in the treatment of peptic ulcer disease, duodenal ulcer, gastric ulcer, hypersecretory states such as Zöllinger-Ellison syndrome, prevention of stress ulcers in critically ill patients and other conditions where it is appropriate to reduce gastric acid secretion.

The H_2-receptor antagonists in clinical use are analogues of histamine that contain a bulky side chain in place of the ethylamine moiety. Early representatives of the group, such as cimetidine (the first of this class of compounds released for general use) retain the imidazole ring of histamine. This ring is replaced in more recently developed compounds by a furan (ranitidine) or a thiazole (famotidine, nizatidine) ring. The structures of histamine and the three H_2-receptor antagonists are shown in Figure 4.1.

Ranitidine is presently marketed as its hydrochloride salt (ZANTAC™) and has been the world's top selling drug for a major portion of the past fifteen years. There are two known polymorphic forms of this drug, namely Form 1 and Form 2.[2] The existence of these two polymorphs was only demonstrated some time after the original patent for ranitidine hydrochloride was issued. The result is an ongoing dispute over the patent rights of ranitidine hydrochloride.

80.) A. Rontoyianni and I. M. Mavridis, *Acta Crystallogr., Sect. C*, **1996**, 52, 2277.

81.) G. M. Sheldrick, *Crystallographic Computing*, ed. G. M. Sheldrick, C. Krüger and R. Goddard, Oxford University Press, **1985**, Volume 3, 175.

82.) E. Egert, *Acta Cryst.*, **1983**, A39, 936.

83.) E. Egert and G. M. Sheldrick, *Acta Cryst.*, **1985**, A41, 262.

84.) G. M. Sheldrick, *SHELXL-93, Program for the Refinement of Crystal Structures*, University of Göttingen, Germany, **1993**.

85.) M. R. Caira, J. J. Gerber and F. N. de Wet, *J. Chem. Crystallogr.*, **1999**, in press.

86.) K. B. Lipkowitz, K. Green and J. Yang, *Chirality*, **1992**, 4, 205.

87.) F. W. Lichtenthaler and S. Immel, *Liebigs Ann.*, **1996**, 27.

88.) K. Harata, in *Inclusion Compounds*, ed. J. L. Atwood, J. E. D. Davies and D. D. MacNicol, Oxford University Press, London, **1984**, Vol. 5, Chapter 9.

89.) K. Lindner and W. Saenger, *Carbohydr. Res.*, **1982**, 99, 103.

90.) K. Harata, K. Uekama, M. Otagiri, F. Hirayama and Y. Ohtani, *Bull. Chem. Soc. Jpn.*, **1985**, 58, 1234.

91.) K. Harata, *Bull. Chem. Soc. Jpn.*, **1982**, 55, 2315.

92.) M. R. Caira, V. J. Griffith, L. R. Nassimbeni and B. van Oudtshoorn, *J. Inclusion Phenom.*, **1994**, 17, 187.

93.) M. R. Caira, V. J. Griffith, L. R. Nassimbeni and B. van Oudtshoorn, *J. Chem. Soc., Chem. Commun.*, **1994**, 1061.

94.) I. Nicolis, A. W. Coleman, P. Charpin and C. de Rango, *Acta Crystallogr., Sect. B*, **1996**, 52, 122.

95.) M. R. Caira, V. J. Griffith, L. R. Nassimbeni, *J. Inclusion Phenom. Mol. Recognit.*, **1998**, 32, 461.

96.) M. Sakurai, M. Kitagawa, H. Hoshi, Y. Inoue and R. Chûjô, *Carbohydr. Res.*, **1990**, 198, 181.

97.) M. Kitagawa, H. Hoshi, M. Sakurai, Y. Inoue and R. Chûjô, *Bull. Chem. Soc. Jpn.*, **1988**, 61, 4225.

98.) M. Sakurai, M. Kitagawa, H. Hoshi, Y. Inoue and R. Chûjô, *Chem. Lett.*, **1988**, 895.

99.) *Chem3D Pro Version 3.5.1* (Copyright **1986-1996** CambridgeSoft Corporation).

100.) F. W. Lichtenthaler and S. Immel, *Starch*, **1996**, 48(4), 145.

101.) F. W. Lichtenthaler and S. Immel, *Starch*, **1996**, 48(6), 225.

102.) E.S. Testa, U.S. US5,866,179, 2 Feb 1999.

58.) G. D. Andreetti, L. Cavalca, P. Domiano and A. Musatti, *Acta Crystallogr. Sect. B*, **1968**, 24, 1195.

59.) K. H. Jogun and J. J. Stezowski, *Nature (London)*, **1979**, 278, 667.

60.) G. Tsoucaris, G. le Bas, N. Rysanek and F. Villain, *J. Inclusion. Phenom.*, **1987**, 5, 77.

61.) I. M. Mavridis and E. Hadjoudis, *Carbohydr. Res.*, **1992**, 229, 1.

62.) A. Rontoyianni and I. M. Mavridis, *J. Inclusion Phenom.*, **1994**, 18, 211.

63.) A. Rontoyianni, I. M. Mavridis, E. Hadjoudis, A. J. M. Duisenberg, *Carbohydr. Res.*, **1994**, 252, 19.

64.) R. K. Tiwari, N. Deo and T. P. Singh, *J. Sci. Res. Bhopal, India*, **1980**, 2, 161.

65.) U. Patel, T. C. Patel and T. P. Singh, *Acta Crystallogr., Sect. C*, **1983**, 39, 1445.

66.) U. Patel, T. C. Patel and T. P. Singh, *Curr. Sci.*, **1983**, 52, 20.

67.) J. J. Stezowski, K. H. Jogun, E. Eckle and K. Bartels, *Nature (London)*, **1978**, 274, 617.

68.) K. Jogun, J. M. Maclennan, J. J. Stezowski, *Eur. Cryst. Meeting*, **1979**, 5, 34.

69.) M. B. Hursthouse, C. Z. Smith, M. Thornton-Pett and J. H. P. Utley, *J. Chem. Soc., Chem. Commun.*, **1982**, 881.

70.) J. A. Hamilton and M. N. Sabesan, *Acta Crystallogr., Sect. B*, **1982**, 38, 3063.

71.) M. Czugler, G. Geiger and J. J. Stezowski, *Z. Kristallogr.*, **1983**, 162, 54.

72.) K. Uekama, F. Hirayama, T. Imai, M. Otagiri and K. Harata, *Chem. Pharm. Bull.*, **1983**, 31, 3363.

73.) K. Uekama, F. Hirayama, T. Imai, M. Otagiri and K. Harata, *Chem. Pharm. Bull.*, **1984**, 32, 1662.

74.) K. Harata, K. Uekama, M. Otagiri and F. Hirayama, *J. Inclusion Phenom.*, **1984**, 1, 279.

75.) I. Nakanishi, M. Arai, T. Fujiwara and K. Tomita, *J. Inclusion Phenom.*, **1984**, 2, 689.

76.) F. Nishioka, I. Nakanishi, T. Fujiwara and K. Tomita, *J. Inclusion Phenom.*, **1984**, 2, 701.

77.) J. J. Stezowski, *Trans. Am. Crystallogr. Assoc.*, **1985**, 20, 73.

78.) T. Fujiwara, K.-I. Tomita, I. Marseigne and J. Vicens, *Mol. Cryst. Liq. Cryst.*, **1988**, 156, 393.

79.) J. Vicens, T. Fujiwara and K.-I. Tomita, *J. Inclusion Phenom.*, **1988**, 6, 577.

40.) E. Testa, **PCT Int. Appl., WO 97 41,843** (Cl. A61K9/68), 13 Nov 1997, US Appl. 646,744, 3 May 1996, 14 pp.

41.) G. Brown, *MSc. Thesis, Cyclodextrin Inclusion Compounds with Non-steroidal Anti-inflammatory Drugs*, University of Cape Town, South Africa, **1997**.

42.) G. M. Sheldrick, *SHELX-76, A system of computer programs for X-ray structure determination*, University of Cambridge, England, **1976**.

43.) M. Haisa, S. Kashino and H. Maeda, *Acta Crystallogr., Sect. B*, **1974**, 30, 2510.

44.) M. Haisa, S. Kashino, R. Kawai and H. Maeda, *Acta Crystallogr., Sect. B*, **1976**, 32, 1283.

45.) I. Moustakali-Mavridis, E. Hadjoudis and G. Tsoucaris, *Mol. Cryst. Liq. Cryst.*, **1990**, 186, 185.

46.) I. Mavridis, E. Hadjoudis and G. Tsoucaris, *Carbohydr. Res.*, **1991**, 220, 11.

47.) J. A. Hamilton and M. N. Sabesan, *Carbohydr. Res.*, **1982**, 102, 31.

48.) C. Betzel, B. Hingerty, M. Noltemeyer, G. Weber, W. Saenger and J. A. Hamilton, *J. Inclusion. Phenom.*, **1983**, 1, 181.

49.) M. Noltemeyer and W. Saenger, *J. Am. Chem. Soc.*, **1980**, 102, 2710.

50.) G. le Bas, C. de Rango, N. Rysanek and G. Tsoucaris, *J. Inclusion Phenom.*, **1984**, 2, 861.

51.) J. A. Hamilton, M. N. Sabesan and L. K. Steinrauf, *Carbohydr. Res.*, **1981**, 89, 33.

52.) J. A. Hamilton, M. N. Sabesan, L. K. Steinrauf and A. Geddes, *Biochem. Biophys. Res. Commun.*, **1976**, 73, 659.

53.) B. Klingert and G. Rihs, *J. Chem. Soc., Dalton Trans.*, **1991**, 2749.

54.) N. Rysanek, G. le Bas, F. Villain and G. Tsoucaris, *Acta Crystallogr., Sect. C*, **1996**, 52, 2932.

55.) D. Mentzafos, I. M. Mavridis and M. B. Hursthouse, *Acta Crystallogr., Sect. C*, **1996**, 52, 1220.

56.) D. Mentzafos, I. M. Mavridis, G. le Bas and G. Tsoucaris, *Acta Crystallogr., Sect. B*, **1991**, 47, 746.

57.) M. M. Harding, J. M. Maclennan and R. M. Paton, *Nature (London)*, **1978**, 274, 621.

19.) S. Y. Lin, J. C. Yang and Y. Kawashima, *T`ai-wan Yao Hsueh Tsa Chih*, **1984**, 36(1), 24.

20.) S. Y. Lin, *Int. J. Pharm. Technol. Prod. Manuf.*, **1983**, 4(4), 14.

21.) S. Y. Lin and J. C. Yang, *Int. J. Pharm. Technol. Prod. Manuf.*, **1984**, 5(4), 19.

22.) S. Y. Lin and J. C. Yang, *Pharm. Acta Helv.*, **1990**, 65(9-10), 262.

23.) S. Y. Lin, Y. H. Kao and J. C. Yang, *Drug Dev. Ind. Pharm.*, **1988**, 14(1), 99.

24.) S. Y. Lin and Y. H. Kao, *Int. J. Pharm.*, **1989**, 56(3), 249.

25.) S. Y. Lin and R. I. Perng, *J. Inclusion Phenom. Mol. Recognit. Chem.*, **1992**, 14(2), 149.

26.) S. Y. Lin and S. S. Lee, *J. Inclusion Phenom. Mol. Recognit. Chem.*, **1989**, 7(5), 477.

27.) S. Y. Lin, *Drug Dev. Ind. Pharm.*, **1990**, 16(15), 2221.

28.) J. Pitha, **U.S. US 4,727,064** (Cl. 514-58; A61K31/70), 23 Feb 1988, US Appl. 603,839, 25 April 1984; 7pp.

29.) I. R. Politzer, K. T. Crago, T. Hollin and M. Young, *J. Chromatogr. Sci.*, **1995**, 33(6), 316.

30.) J. Guo and W. Wang, *Yingyong Huaxue*, **1991**, 8(4), 80.

31.) K. Kralova, L. Mitterhauszerova and A. Stadler-Szoke, *Pharmazie*, **1983**, 38(8), 547.

32.) K. Kralova and L. Mitterhauszerova, *Farm. Obz.*, **1983**, 52(7), 295.

33.) Y. Nozawa and H. Kishimoto, *Funtai Kogaku Kaishi*, **1992**, 29(6), 460.

34.) A. Majid and J. A. Ripmeester, **U.S. US 5,070,081** (Cl. 514-58; A61K9/62), 3 Dec 1991, CA Appl. 564,609, 20 Apr 1988; 4 pp.

35.) S. E. Brown, J. H. Coates, C. J. Easton, S. F. Lincoln, Y. Luo and A. K. W. Stephens, *Aust. J. Chem.*, **1991**, 44(6), 855.

36.) L. J. Tasic, M. D. Jovanovic and Z. R. Djuric, *J. Pharm. Pharmacol.*, **1992**, 44(1), 52.

37.) L. J. Tasic, K. Pintye-Hodi and P. Sabo-Revesz, *J. Incl. Phenom. Mol. Recognit. Chem.*, **1997**, 28, 299.

38.) L. J. Tasic, K. Pintye-Hodi and P. Sabo-Revesz, *Drug Dev. Ind. Pharm.*, **1997**, 23(12), 1153.

39.) V. Weiszfeiler and J. Szejtli, *Proc. Int. Symp. Cyclodextrins, 4th*, Ed. by O. Huber, J. Szejtli, Kluwer, Dordrecht, Netherlands, **1988**, 359.

References

1.) J. E. Fairbrother, *Analytical Profiles of Drug Substances Vol. 3*, K. Florey Ed., Academic Press New York, **1974**, 1.

2.) S. P. Clissold, *Drugs*, **1986**, 32, Suppl. 4 , 46.

3.) A. Szczelik, *Drugs*, **1986**, 32, Suppl. 4, 148.

4.) S. Budavari, M. J.O`Neil, A. Smith, P. E. Heckelman and J. F. Kinneary, Eds., *The Merck Index, 12th Edition*, Merck and Co., Inc., New Jersey, USA, **1996**.

5.) A. J. Repta and J. Hack, *J. Pharm. Sci.*, **1973**, 63, 1982.

6.) A. Hussain, P. Kulkarni, J. H. Fincher and C. W. Hartman, *J. Pharm. Sci.*, **1978**, 67, 545.

7.) K-H. Frömming and J. Szejtli, *Topics in Inclusion Science (Volume 5) : Cyclodextrins in Pharmacy*, Dordrecht, The Netherlands, ~~**1988**~~ **1993**.

8.) B. A. Obiorach, *Int. J. Pharm.*, **1978**, 1, 249.

9.) S. Leight, J. E. Carless and B. W. Burt, *J. Pharm. Sci.*, **1967**, 56, 888.

10.) D. V. Bhalla and J. K. Lalla, *Drug. Dev. Ind. Pharm.*, **1990**, 16(1), 115.

11.) C. T. Bauguess, J. H. Fincher, F. Sadik and C. W. Hartman, *J. Pharm Sci.*, **1975**, 64, 1489.

12.) C. T. Bauguess, F. Sadik, J. H. Fincher and C. W. Hartman, *J. Pharm Sci.*, **1975**, 64, 117.

13.) J. Sztatisz, S. Gal, J. Komives, A. Stadler-Szoke and J. Szejtli, *Therm. Anal., (Proc. Int. Conf. Therm. Anal., 6th)*, Ed. by W. Hemminger, **1980**, 2, 487.

14.) J. Sztatisz, S. Gal, J. Komives, A. Stadler-Szoke and J. Szejtli, *Proc. Int. Symp. Cyclodextrins, 1st, 1981*, Ed. J. Szejtli, Reidal, Dordrecht, Netherlands, **1982**, 237.

15.) F. Giordano, M. Pavan, L. X. Yan, A. La Manna, and G. P. Bettinetti, *Congr. Int. Technol. Pharm.*, 5th, **1989**, 5, 163.

16.) A. Gazzaniga, F. Giordano, M. E. Sangalli, P. Benelli, G. Bettinetti, A. La Manna, *Congr. Int. Technol. Pharm.*, 6th, **1992**, 5, 394.

17.) F. Giordano, G. Bruni and G. P. Bettinetti, *J. Therm. Anal.*, **1992**, 38(12), 2683.

18.) F. Giordano, M. Rillosi, G. P. Bettinetti, A. Gazzaniga, W. Majewski and M. Perrut, *Proc. Int. Symp. Cyclodextrins, 8th*, Ed. by J. Szejtli and L. Szente, Kluwer, Dordrecht, Netherlands, **1996**, 193.

The protrusions of the four guest molecules are seen in CPK diagrams of the dimeric units of the ACEBCD, BROBCD, PHEBCD and DIABCD complexes (left to right) shown in Figure 3.47. These protrusions could be a direct influence on the packing arrangements assumed in each of these dimeric β-CD complexes.

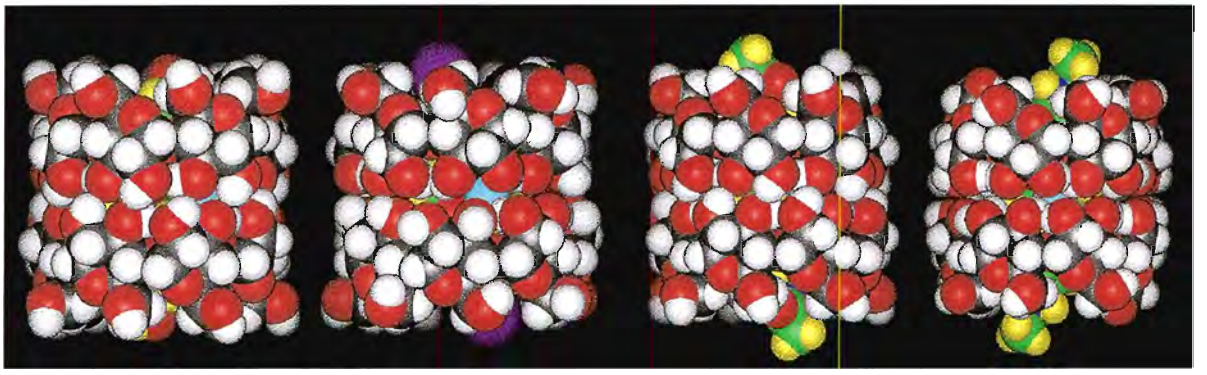

(a) (b) (c) (d)

Figure 3.47 The CPK diagrams of the dimeric unit of the (a) ACEBCD, (b) BROBCD, (c) PHEBCD and (d) DIABCD complexes

B.) Asymmetric volume

The asymmetric volume of a β-CD structure can be defined as the volume of crystal space occupied by a β-CD molecule, its included guest and associated water molecules. This can be computed from the volume of the crystal unit cell and the number of β-CD molecules contained within that cell (*viz.* Asymmetric volume ($Å^3$) = *V*/*Z*). Table 3.66 lists the values of the asymmetric volume, packing type and space group of the four dimeric complexes. It is clear from Table 3.66 in conjunction with Figure 3.47 that there is a direct correlation between the volume of protruding guest and the asymmetric volume of the crystal. Since the water molecules act as more of a "filler" in CD structures, this is an indication that the guest might play a critical role in the determination of the packing arrangement of these β-CD complexes. This issue will be addressed in more detail in the conclusion to this thesis.

Table 3.66 Asymmetric volumes of the ACEBCD, BROBCD, PHEBCD and DIABCD complexes

Complex	Packing Type	*V* ($Å^3$)	*Z*	*V*/*Z* ($Å^3$)
ACEBCD	CH (C2)	6959	4	1740
BROBCD	CH (P1)	3595	2	1798
PHEBCD	IM (P1)	3714	2	1857
DIABCD	DC (C2)	15104	8	1888

In the BROBCD complex the orientation of the substituents is in agreement with the findings of Lichtenthaler et al. with the hydrophobic bromine atom at the primary rim and the hydrophilic acetylamino residue at the secondary rim.

D.) Hydrogen bonding

Certain specific hydrogen bonded interactions between the host and included guest molecule could also play an important role in the orientation of the guest. The guest interactions for the four *para*-subtituted acetanilides have been discussed previously. For all guests, hydrogen bonded interactions were observed for both the acetylamino residue and the *para*-substituent (with the exception of the bromine atom in the BROBCD complex). Therefore, there is no clear distinction for which interactions may be of greater relative importance in determining the orientation of these guests.

In summary, it is likely that the orientations in the β-CD cavity observed for this series of guest molecules are a combination of the various influencing factors listed above and possibly other factors as well. Although it cannot be said that any one of these factors plays a dominant role, the orientations of the acetaminophen and *p*-bromoacetanilide guests allow more efficient inclusion of these guests and closer packing of the host molecules in their respective complexes. This is only made possible by the occurrence of the smaller hydroxy and bromo substituents at the primary rims of the β-CD molecules in which they are included.

Crystal packing

A.) Guest protrusion

The groups occupying the primary hydroxyl ends of the four β-CD dimeric complexes protrude to different extents from the primary rims of the dimers in which they are included. The increasing size of the *para*-substituent results in increasing protrusion of the guest from the primary rim. This is the observed trend for the four β-CD complexes with *para*-substituted acetanilide guests irrespective of whether it is the acetylamino residue or *para*-substituent which occupies the primary hydroxyl rim region.

The extent to which the guests in the four complexes protrude from the dimeric unit follows the order : DIABCD > PHEBCD > BROBCD > ACEBCD.

C.) Hydrophobic attractions

The lack of direct guest to CD interactions in the region of the secondary hydroxyl dimer interface is considered by some researchers to be an indication of the relative hydrophobicity of this region. However, Lichtenthaler et al.[100,101] in their computer-aided visualisation of the molecular lipophilicity patterns have shown that the secondary rim of a β-CD molecule is relatively hydrophilic and its opposite primary rim relatively hydrophobic. They have also shown that the dimeric cavity formed between the two secondary hydroxyl rims of constituent β-CD molecules is a relatively hydrophilic region. This could be viewed as more consistent with the observation that the secondary hydroxyl interface of a β-CD dimer often contains water molecules of crystallisation in addition to portions of a particular guest molecule. Lichtenthaler et al. further suggested that in some cases this difference in relative hydrophobicity between secondary and primary rims can be a determining factor in the orientation of a guest molecule in the CD cavity. In these cases it is suggested that the hydrophilic portions of a guest will align with the hydrophilic portions of the CD and the hydrophobic portions of a guest will align with the hydrophobic portions of the CD. This would imply that the hydrophilic portion of the guest should occur in the vicinity of the secondary rim of the CD and the hydrophobic portion in the vicinity of the primary rim. Figure 3.46 shows the orientation of the four acetanilide guests in the β-CD cavity as determined in this study.

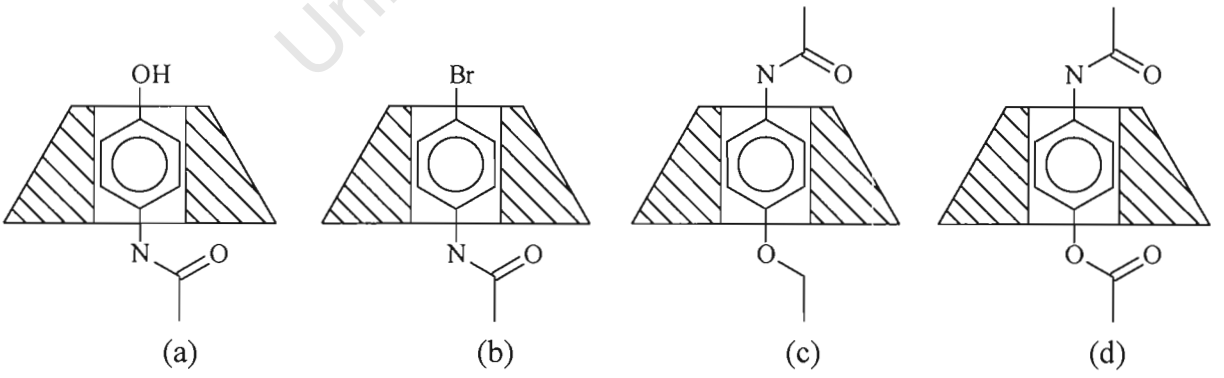

Figure 3.46 Orientation of guest in the β-CD cavity (a) acetaminophen (ACE), (b) *p*-bromoacetanilide (BRO), (c) phenacetin (PHE) and (d) diacetamate (DIA)

For the ACE, PHE and DIA molecules, both substituents on the phenyl rings are relatively polar groups. The only significant difference between the substituents occurs for the BRO molecule between the bromine atom and acetylamino residue.

for the four guests are listed in Table 3.65. The dipole moments were calculated using the MNDO potential function, which is part of the MOPAC utilities of the program Chem3D Pro Version 3.5.[99] The axial reference frame is as illustrated in Figure 3.45, with the *x*-and *y*-axial directions in the plane of the page and the *z*-axial direction coming out of the page. The directions of the dipoles of the four guest molecules in the *xy*-plane are illustrated. In all cases the arrow head is the positive end of the dipole with the arrow tail the negative end of the dipole. The lengths of the illustrated dipoles are proportional to their magnitudes.

Table 3.65 Dipole moments of the uncomplexed *para*-substituted acetanilides

Dipole	Acetaminophen	*p*-Bromoacetanilide	Phenacetin	Diacetamate
x	3.65	3.19	1.45	2.88
y	1.57	1.89	0.08	0.70
z	1.34	0.35	1.59	-1.24
Magnitude	4.19	3.72	2.15	3.21

The acetaminophen and *p*-bromoacetanilide molecules display the largest *y*-components and largest dipole moments of the four guests. The angles which these dipoles make with the direction of the CD dipole (approximated as being parallel to the *y*-direction as indicated in Figure 3.45) is 117° and 121° for acetaminophen and *p*-bromoacetanilide. This conforms somewhat to an anti-parallel orientation of host and guest dipoles. The similarity in conformation and chemical nature of the *para*-substituents of phenacetin and diacetamate result in very weak *y*-components for their dipole moments. It is therefore unlikely that their dipole moments could play any significant role in orientating the respective guests in the CD cavity.

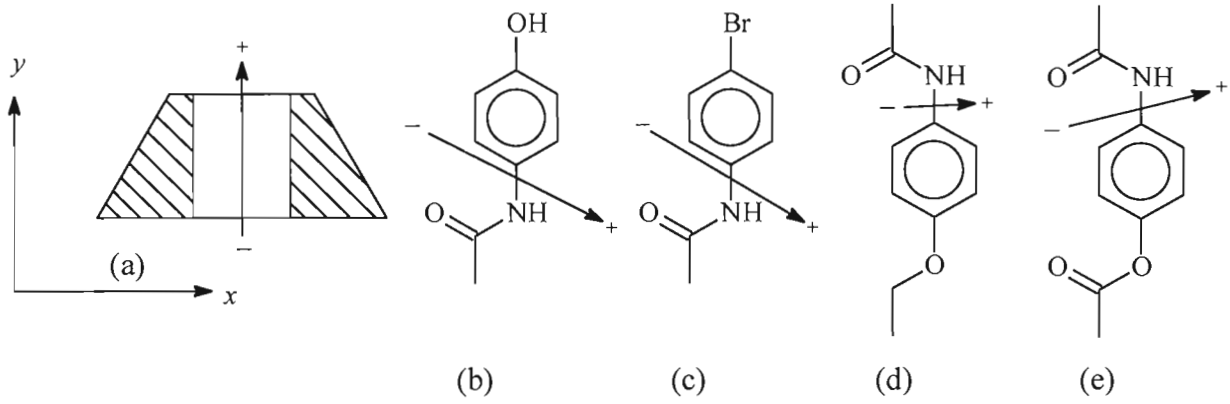

Figure 3.45 Dipole moments of (a) β-CD, (b) acetaminophen, (c) *p*-bromoacetanilide, (d) phenacetin and (e) diacetamate

dimeric β-CD complexes is to include as much of a particular guest within the dimeric unit as possible. This was observed in all complexes by a tilting of the guest molecule within the β-CD cavity. The tilt permits the guests to occupy most of the available space in the cavity and is necessary to avoid abnormally short contacts and steric clashes between the residues in the vicinity of the secondary hydroxyl intradimeric interface. Table 3.64 lists the average tilt angles for the phenyl ring of all four guests relative to the O4 mean planes of the CD. The tilting angle is approximately 65° in all cases (i.e. an angle of approx. 25° with the CD axis).

Table 3.64 Tilt angle of phenyl ring relative to O4 mean plane

Complex	ACEBCD	BROBCD	PHEBCD	DIABCD
Tilt angle (°)	71 (1)	64 (1)	63 (1)	66 (1)

It is noted that for the ACEBCD and BROBCD structures, the *para*-substituents are comparatively significantly smaller than the acetylamino group. In these cases the acetylamino portions are observed to be contained within the secondary rim intradimeric cavity and only very small portions of the hydroxy residue and bromine atom are exposed at the primary rims. In the PHEBCD and DIABCD complexes the ethoxy and acetyloxy substituents are similar in size to the acetylamino group. In these cases the sizes of the substituents may not play a decisive role in determining the orientation of the guest in the β-CD cavity.

B.) Dipole moments

The β-CD molecule displays a large dipole moment (of the order of 10-20 Debye) which is directed with the positive end of the dipole at the primary hydroxyl end and the negative end at the secondary hydroxyl rim. In the inclusion complexes of CDs with aromatic molecules, the guest dipole moment has been noted to adopt an anti-parallel direction to that of the CD.[96-98]

A simplified approach was to calculate the dipole moments for the four *para*-substituted acetanilides from their crystal structures in the uncomplexed state.[44,58,66,85] This approach was taken on account of the disorder of these molecules observed in their respective β-CD complexes and the artificial placement of their hydrogen atoms. The dipole moments calculated in this way would serve as an indication of whether these molecules showed any significant dipole in the direction of their acetylamino or *para*-substituents. The directional components and magnitudes of the dipole moments

E.) Water interactions

The O2, O3 and O6 hydroxyls are involved in contacts with solvent water molecules. Water-water type hydrogen bonds mediate many of the types of interactions that have already been discussed. Table 3.63 shows the normalised number of contacts and their mean O···O contact distances for the various water interactions.

Table 3.63 Water contacts for ACEBCD, BROBCD, PHEBCD and DIABCD

Complex	Water···O2		Water···O3		Water···O6		Water···Water	
	Number	Mean (Å)	Number	Mean (Å)	Number	Mean (Å)	Number	Mean (Å)
ACEBCD	12	2.86	12	2.92	12	2.82	39	2.89
BROBCD	10	2.87	13	2.99	20	2.80	36	2.86
PHEBCD	12	2.87	9	2.98	23	2.80	29	2.84
DIABCD	13	2.79	8	2.93	23	2.80	36	2.85

The dimeric β-CD complexes seem to show many common types of hydrogen bonded interactions and there is a remarkable consistency between the number and lengths of these various contacts despite the differences in packing arrangements of the host molecules that are observed.

Guest orientation

In all four dimeric complexes with the *para*-substituted acetanilide guests investigated in this chapter, the phenyl rings of the guest are centralised in the cavities of the β-CD molecules. The acetanilide group and *para*-substituent must then be located in the vicinity of the secondary and primary rims of the CD. An attempt to explain this orientation of the *para*-substituted acetanilides will be made based on certain criteria which have been suggested to influence this phenomenon. The relative sizes of the *para*-substituents are acetyloxy > ethoxy > bromo > hydroxy, as demonstrated with CPK studies.

A.) Size / shape

In many cases the size and shape of a particular guest molecule may determine its mode of inclusion in a CD cavity. The four *para*-acetanilide derivatives investigated in this study all have their phenyl portions inserted in the β-CD cavity. Although the acetanilide portion of the molecule remains constant in size, the relative sizes of the *para*-substituents differ for these four molecules. A tendency observed for many

The normalised number of contacts suggests that for any one dimer there are on average five such hydrogen bonds with a mean O···O contact distance of 2.89Å.

The direct O6···O6 inter-layer hydrogen bonds show an interesting trend for the four structures. As the columns of dimers become more distorted from the idealised channel structure of a perfect cylinder, so the number of direct contacts between primary hydroxyl groups across the interdimeric interface decreases. The number of these inter-layer contacts decreases in the order ACEBCD (5), BROBCD (3), PHEBCD (2) and DIABCD (1).

D.) Guest interactions

The acetanilide portion of the guest primarily makes contacts to water molecules, either situated in the vicinity of the primary rim (*viz.* PHEBCD and DIABCD complexes) or trapped within the intradimeric region (*viz.* ACEBCD and BROBCD complexes). The only direct contacts between a guest molecule and a CD hydroxyl group are seen for the ACEBCD and PHEBCD complexes. In the ACEBCD structure the hydroxyl group of the acetaminophen molecule is directly hydrogen bonded across the interdimeric interface to a primary hydroxyl group of the adjacent CD of the same dimeric column (Figure 3.10). In the PHEBCD complex a hydrogen bond is formed between the carbonyl oxygen of the acetylamino group of PHE(A) to a primary hydroxyl group of the CD of an adjacent dimeric column (Figure 3.28). The *para*-substituents of the guests are all involved in hydrogen bonding interactions, with the exception of the bromine atoms of the BROBCD complex (Figure 3.19). The hydroxyl groups of the acetaminophen molecule are involved in the only direct guest-to-guest hydrogen bonds observed for the four complexes. They are directly hydrogen bonded to hydroxy groups of acetaminophen molecules included in an adjacent CD of the same dimeric column. These bonds that the hydroxy group makes across the primary interdimeric interface are in addition to the direct contacts it makes to CD hydroxyl groups, as were alluded to earlier. The ethereal oxygen atoms of the ethoxy and acetyloxy groups of phenacetin and diacetamate respectively are involved in hydrogen bonds to water molecules trapped in the secondary intradimeric interface. In many of the guest interactions, water molecules form a link between guest and guest, or guest and CD.

Hydrogen bonding interactions

A.) Cyclodextrin interactions

The nature and contribution of the O2(n)···O3(n-1) hydrogen bonds has been discussed together with their influence on β-CD geometry in the previous section.

B.) Dimer interactions

In all four complexes the principal dimer interactions are the O3···O3 hydrogen bonds. Seven such contacts are made for the dimers of each of the four complexes and their average contact distances are 2.80, 2.84, 2.82 and 2.85Å for the ACEBCD, BROBCD, PHEBCD and DIABCD complexes. The average contact distances of the intradimeric O2···O2 and O2···O3 distances are greater than 3.0 Å in all cases.

C.) Layer interactions

The structure of all dimeric complexes are arranged in dimeric layers and the four complexes investigated in this chapter are no exception. There are two sub-networks of layer interactions that can be distinguished. The intra-layer hydrogen bonds are contacts made between hydroxyl groups of adjacent CDs within the same dimeric layer. The inter-dimeric hydrogen bonds are the contacts made between adjacent dimeric layers. Direct hydrogen bonding between the hydroxyl groups of the CD dimers, as well as hydrogen bonds mediated by water molecules, form a network of these intra-layer and inter-layer hydrogen bonded interactions which form the "glue" which holds the structures together. The O2···O2 and O6···O6 contacts, which were present in all four complexes, are the only direct CD-to-CD intra-layer interactions observed while the O6···O6 contacts provide the only direct CD-to-CD inter-layer interactions observed.

Two intra-layer O2···O2 contacts are observed for each of these four dimeric β-CD structures. The average O···O contact distances of these interactions are 2.83, 2.78, 2.78 and 2.74Å for the ACEBCD, BROBCD, PHEBCD and DIABCD complexes. The BROBCD, PHEBCD and DIABCD each show four O6···O6 intra-layer linkages with average contact distances of 2.86, 2.83 and 2.92Å. Many of the primary hydroxyl groups of ACEBCD were disordered leading to an artificially large number of O6···O6 contacts that are made per dimer.

In general the average side lengths (*l*) of the O4 heptagons are relatively constant; however, the monomeric structures show a wider range of values (the average range for the side lengths is 0.16Å for N=4 dimeric structures and 0.26Å for N=7 monomeric structures in Table 3.62). This, presumably, is the result of elliptical distortions of the macrocycles of monomeric structures to induce a better fit for the guest within the cavity.

The mean and maximum deviations of the individual O4 atoms from the mean O4 plane are significantly larger for the monomeric structures than for the dimeric complexes. The absolute mean deviations for the four dimeric structures are in the range 0.01-0.05Å, while for the monomeric structures the corresponding range is 0.15-0.28Å. The implication is that the conformations of dimeric macrocycles are more planar than those of monomeric structures.

The O2(n)···O3(n-1) hydrogen bonds are on average slightly weaker for monomeric structures versus dimeric structures, and the range of distances is wider. This is again consistent with a more elliptical distortion of the monomeric macrocycles relative to the dimeric macrocycles and the generally less stringent requirements on the conformations of β-CD molecules of monomeric structures.

The tilt angles are on average larger for the monomeric structures, but more significantly, the range of tilt angles for the monomeric structures is significantly larger than for dimeric structures. The narrower range of tilt angles observed for the dimeric structures allows important interdimeric interactions to take place, not otherwise possible.

Whether these distortions of the macrocycle seen for the monomeric structures are caused directly by the nature of the included guest or whether they are the result of a relaxation in the rigid geometrical requirements of β-CD dimers is unclear. However, the uniformly round and regular conformation of the macrocycles of the dimeric structures is vital for the formation of the O3···O3 hydrogen bonds and other intradimeric interactions.

parameters of β-CD molecules of monomeric and dimeric β-CD complexes. A more detailed comparative analysis of the side lengths of the O4 heptagon (*l*), the deviation of the O4 atoms from the mean O4 plane (*d*), the O2(n)···O3(n-1) distances and the tilt angle (τ_2) will be analysed for a number of representative monomeric β-CD structures and the four dimeric structures investigated in this chapter (Table 3.62). The seven monomeric β-CD structures are those for the hydrate[89] (BETACD) and for complexes containing benzyl alcohol[90] (BENBCD), 1,4-diazabicyclo(2.2.2)octane[91] (OCTBCD), sulfathiazole[92] (SULBCD), diclofenac sodium[93] (DICBCD), calcium chloride[94] (CALBCD) and meclofenamate sodium[95] (MECBCD). The dimeric complexes represent two of the four unique dimeric packing arrangements discussed in Chapter 1 and one new class, represented by the DIABCD complex. The seven monomeric complexes represent four of the five unique monomeric packing arrangements discussed in Chapter 1 and one new class, represented by the MECBCD complex.

Table 3.62 Comparative analysis of *l*, *d*, O2(n)···O3(n-1) distance and τ_2 for four dimeric and seven monomeric complexes.

Complex	*l* (Å)		*d* (Å)		O2(n)···O3(n-1) (Å)		τ_2 (°)	
	Mean	Range	Mean	Max.	Mean	Range	|Mean|	Range
ACEBCD	4.37	4.30-4.46	0.05	0.09	2.84	2.76-2.94	10.0	4.2-16.7
BROBCD	4.37	4.26-4.47	0.04	0.07	2.78	2.74-2.83	8.1	4.2-16.2
PHEBCD	4.38	4.28-4.46	0.02	0.04	2.80	2.72-2.84	8.4	5.4-11.9
DIABCD	4.37	4.31-4.40	0.01	0.02	2.80	2.73-2.86	8.4	4.6-11.6
BETACD	4.38	4.25-4.49	0.17	0.28	2.86	2.77-2.96	13.1	-7.1-30.6
BENBCD	4.36	4.17-4.55	0.16	0.23	2.86	2.79-2.93	13.7	-2.2-25.2
OCTBCD	4.36	4.25-4.46	0.15	0.26	2.82	2.69-2.88	11.4	2.8-23.1
SULBCD	4.36	4.25-4.48	0.16	0.32	2.87	2.76-3.13	13.4	3.0-25.7
DICBCD	4.35	4.24-4.50	0.21	0.44	2.84	2.72-3.02	14.6	4.2-31.6
CALBCD	4.35	4.23-4.55	0.28	0.45	2.90	2.71-3.21	17.7	5.8-38.9
MECBCD	4.35	4.28-4.41	0.15	0.23	2.84	2.77-2.89	11.4	2.2-26.4

Table 3.60 The values of the glucose torsion angles (ω, Φ, Ψ, Θ_1, Θ_2) and intersaccharidic angle (φ) for ACEBCD, BROBCD, PHEBCD, DIABCD, their average values and the average values for a number of β-CD structures

Complex	CD	| ω | (°)	Φ (°)	Ψ (°)	Θ_1 (°)	Θ_2 (°)	φ (°)
ACEBCD	A	66	112	127	+51	-52	118
BROBCD	A	67	115	127	+56	-53	118
	B	66	114	127	+55	-53	118
PHEBCD	A	67	113	127	+55	-53	118
	B	66	115	127	+55	-53	118
DIABCD	A	65	114	127	+56	-54	118
	B	66	113	127	+55	-53	118
Average (N=7)		66	114	127	+55	-53	118
All β-CD structures		64	112	128	56	-56	118

Table 3.61 The values of the O4 heptagon parameters (*r*, *l*, *a*, *d*, *t*), the O2(n)···O3(n-1) distances and tilt angle (τ_1) for ACEBCD, BROBCD, PHEBCD, DIABCD, their average values, and the average values for a number of β-CD structures

Complex	CD	*r* (Å)	*l* (Å)	*a* (°)	*d* (Å)	*t* (°)	O2(n)···O3(n-1) (Å)	τ_1 (°)
ACEBCD	A	5.03	4.37	129	0.05	2	2.84	6.2
BROBCD	A	5.04	4.37	129	0.03	1	2.78	4.7
	B	5.03	4.36	129	0.04	3	2.77	4.3
PHEBCD	A	5.04	4.37	129	0.02	1	2.79	4.6
	B	5.05	4.38	129	0.01	1	2.80	5.4
DIABCD	A	5.04	4.37	129	0.01	1	2.80	5.7
	B	5.03	4.37	129	0.01	0	2.79	4.9
Average (N=7)		5.04	4.37	129	0.02	1	2.80	5.1
All β-CD structures		5.1	4.4	129	0.11	5	2.92	10

β-CD complexes can be broadly divided into two classes, namely monomeric and dimeric complexes. In light of the differences observed in the geometrical values of the β-CD molecules between the four dimeric β-CD complexes investigated in this chapter and the average values for all β-CD complexes, a logical follow on to this observation would be to examine the differences between certain geometrical

Discussion of comparative features of ACEBCD, BROBCD, PHEBCD and DIABCD structures

Geometrical features of β-CD host molecules

Tables 3.60 and 3.61 list the average values of the various geometrical parameters of the β-CD molecules for the ACEBCD, BROBCD, PHEBCD and DIABCD complexes as well as average values computed from these four structures. Also included in the tables are the average values of those geometrical parameters computed for β-CD molecules from a number of crystallographic analyses.[86-88]

The most striking characteristic of the data for the four dimeric complexes discussed in this chapter, is that they show a very "round", symmetrical and planar conformation of the macrocycles with closely matching geometrical parameters occurring in a relatively narrow range of values. This can be attributed to the fact that the formation of β-CD dimers does require certain geometrical requirements to be met so that important intra-dimeric hydrogen bonded contacts can be made.

The various torsion angles and the intersaccharidic angle of ACEBCD, BROBCD, PHEBCD and DIABCD were found to closely match the average values obtained for a number of β-CD structures (Table 3.60). This was also found to be the case for the radii, side lengths and O4···O4···O4 angles of the O4 heptagons (Table 3.61).

The most notable differences were observed for the deviation of O4 atoms from the mean O4 plane, the O4···O4···O4···O4 torsion angles, the O2(n)···O3(n-1) hydrogen bonded contact distances and tilt angle.

The average deviation of the O4 atoms from the mean O4 plane and the O4···O4···O4···O4 torsion angles are 0.02Å and 1° respectively for the four β-CD dimeric structures compared to values of 0.11Å and 5° for the averages computed for a number of β-CD structures. This implies that the four dimeric β-CD complexes show a more planar conformation of the macrocycle compared with β-CD structures in general. The O2(n)···O3(n-1) distances and tilt angle (τ_1) were also noted to be smaller for the four dimeric complexes compared to β-CD complexes in general.

C.) Layer interactions

Table 3.57 (a) Intra-layer interactions for the DIABCD structure

Type	Layer	Number / dimer	Range (Å)	Mean (Å)
O2···O2	1	2	2.72	2.72
O6···O6	1	4	2.92-3.04	2.98
O2···O2	2	2	2.75	2.75
O6···O6	2	4	2.81-2.88	2.85

Table 3.57 (b) Inter-layer interactions for the DIABCD structure

Type	Layers	Number / dimer	Range (Å)	Mean (Å)
O6···O6	1-2	1	2.70	2.70
O6···O6	2-1	1	2.70	2.70

D.) Guest interactions

Table 3.58 Guest interactions for the DIABCD structure

Type	Guest	Number / dimer	Number / dimer x N	Range (Å)	Mean (Å)
O3···O33W	A	2	1	2.86	2.86
O4···O23W	A	2	1	2.94	2.94
O4···O33W	A`	2	1	2.66	2.66
O4···O33W	A`	2	1	3.08	3.08
N11···O31W	B	2	1	2.89	2.89
O13···O24W	B	2	1	2.82	2.82
O13···O15W	B`	2	1	3.00	3.00

E.) Water interactions

Table 3.59 Water interactions for the DIABCD structure

Type	Number / dimer	Number / dimer x N	Range (Å)	Mean (Å)
O2···Water	13	11	2.66-3.17	2.79
O3···Water	8	7	2.81-3.11	2.93
O6···Water	23	20	2.66-3.10	2.80
Water···Water	36	28	2.54-3.15	2.85

Hydrogen bonding interactions of the DIABCD structure

Figure 3.44 (a) and (b) show the distribution of water molecules (shown as black spheres in the diagram) in the DIABCD structure.

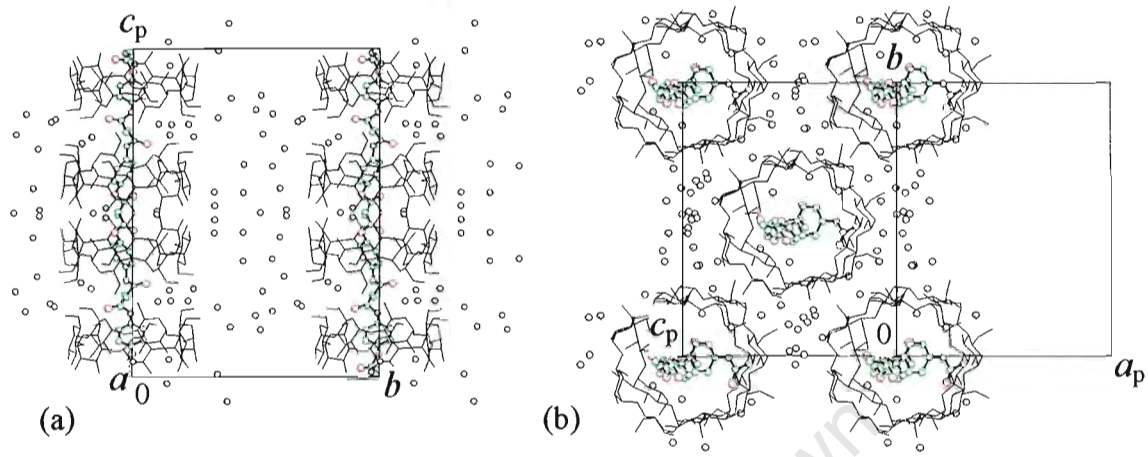

Figure 3.44 Diagrams showing the distribution of water molecules in the DIABCD structure (a) a-axis projection (b) projection down the direction c` (where $c$` = $a + c$)

The listed contact distances for hydrogen bonding interactions are all in the range 2.50 to 3.20 Å and the e.s.d. s are in the range 0.01-0.02 Å for the cyclodextrin, dimer and layer interactions and 0.01-0.08 Å for the guest and water interactions. Tables 3.55, 3.56, 3.57 (a), 3.57 (b), 3.58 and 3.59 list summaries of these interactions for the cyclodextrin, dimer, intralayer, interlayer, guest and water interactions respectively.

A.) Cyclodextrin interactions

Table 3.55 Cyclodextrin interactions for the DIABCD structure

O2···O3	Number / CD	Range (Å)	Mean (Å)
A	7	2.75-2.86	2.80
B	7	2.73-2.86	2.79

B.) Dimer interactions

Table 3.56 Dimer interactions for the DIABCD structure

Type	CDs	Number / dimer	Range (Å)	Mean (Å)
O3···O3	A-A†	7	2.80-2.92	2.86
O2···O2	A-A†	7	2.95-3.13	3.04
O2···O3	A-A†	12	3.14-3.17	3.10
O2···O2	B-B†	7	2.77-2.89	2.83
O3···O3	B-B†	7	3.00-3.05	3.02
O2···O3	B-B†	14	3.02-3.16	3.09

† Two-fold related CD molecules

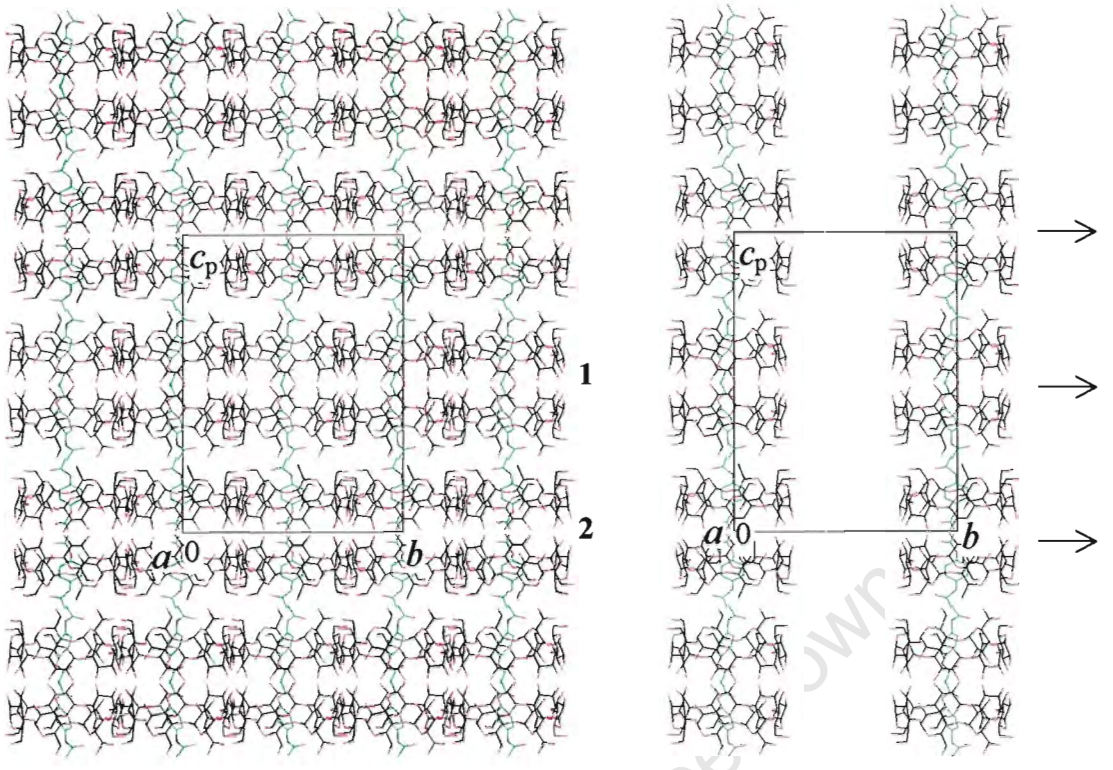

(a) (b)

Figure 3.42 Packing diagram of the *a*-axis projection of the DIABCD structure
(a) C-centred positions included (b) C-centred positions excluded

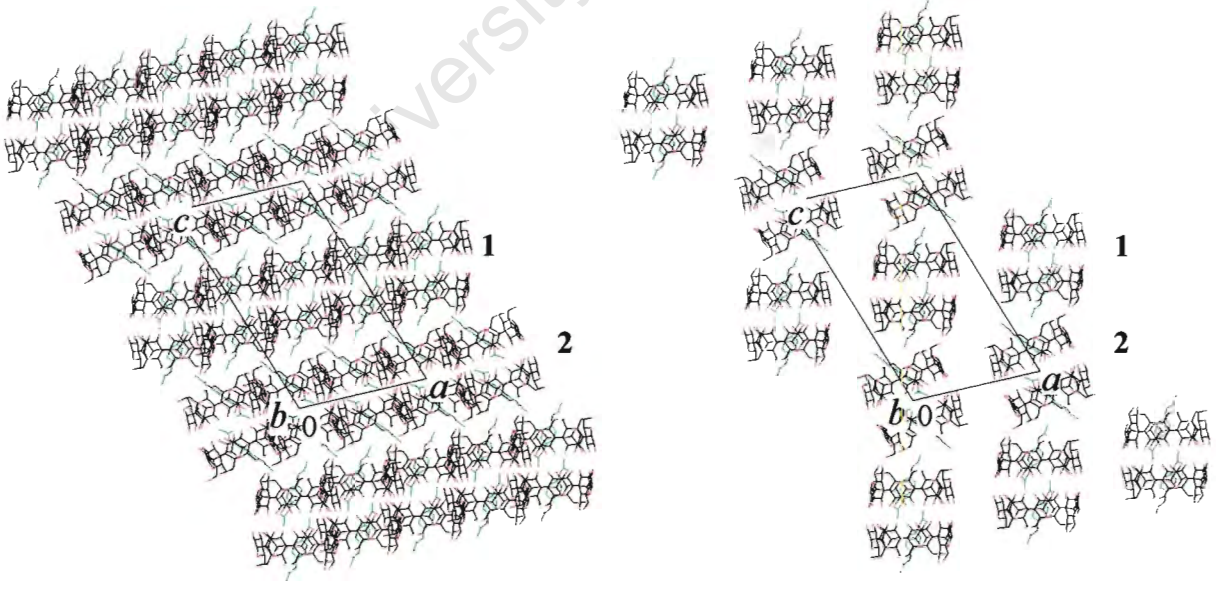

(a) (b)

Figure 3.43 Packing diagram of the *b*-axis projection of the DIABCD structure
(a) C-centred positions included (b) C-centred positions excluded

Figure 3.42 (a) and 3.43 (a) show the packing diagrams for the *a*-axis and *b*-axis projections respectively of the structure while Figure 3.42 (b) and 3.43 (b) show the same projections with the C-centred positions excluded for clarity. The two-fold axes running parallel to the *b*-axis and intersecting the *c*-axis at 0, ½, and 1 are shown in Figures 3.41 and 3.42.

The DIABCD structure is a new type of dimeric packing motif, not yet observed for any β-CD dimeric complexes. Dimeric channels are present and run parallel to the direction *c`* (where $c` = a + c$). The alternative choice of the unit cell for this structure (*viz.* a=19.275Å, b=24.187Å, c=33.381Å and β=103.94°) would have the channels running parallel to the *c*-axis. Every alternate dimer along the channel is tilted at an angle of approximately 45° to the channel axis to form a "disrupted" type of channel. The packing arrangement of the DIABCD complex will be referred to with the abbreviation DC ("disrupted channel"). This is most clearly illustrated in the *b*-axis projection with C-centred positions excluded which is shown in Figure 3.43 (b).

The dimers are arranged in dimeric layers parallel to the *ab*-plane of the structure. There are two distinct dimeric layers (labelled 1 and 2 in Figures 3.42 and 3.43.) which comprise the repeating array of the structure. The dimers of both layers are not parallel to the *ab*-plane but tilted in their respective layer planes.

Further discussion of the DIABCD structure will be included in a comparison of the four β-CD complexes with *para*-substituted acetanilide guests at the end of this chapter.

Crystal Packing of the DIABCD complex

Figure 3.40 shows a stereo diagram of a section of the disrupted channel motif of the DIABCD structure. The dimer is viewed parallel to the mean O4 plane and the positions of DIA(A) and DIA(B) are shown. The dimeric channels are parallel to the direction *c`* (where *c`* = *a* + *c*).

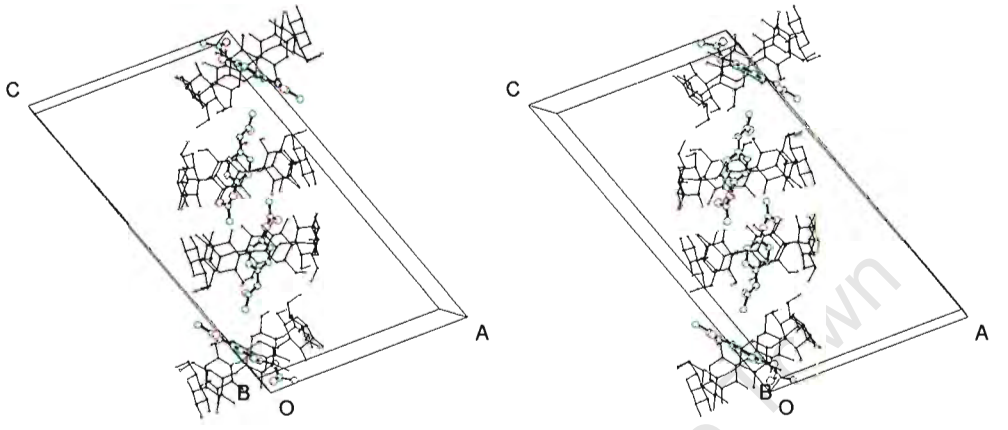

Figure 3.40 Stereo diagram of a section of a channel of the DIABCD complex

Figure 3.41 shows the packing diagram viewed down the direction *c`* (where *c`* = *a* + *c*). This view of the structure illustrates the "endless" channels produced by the cavities of dimeric columns.

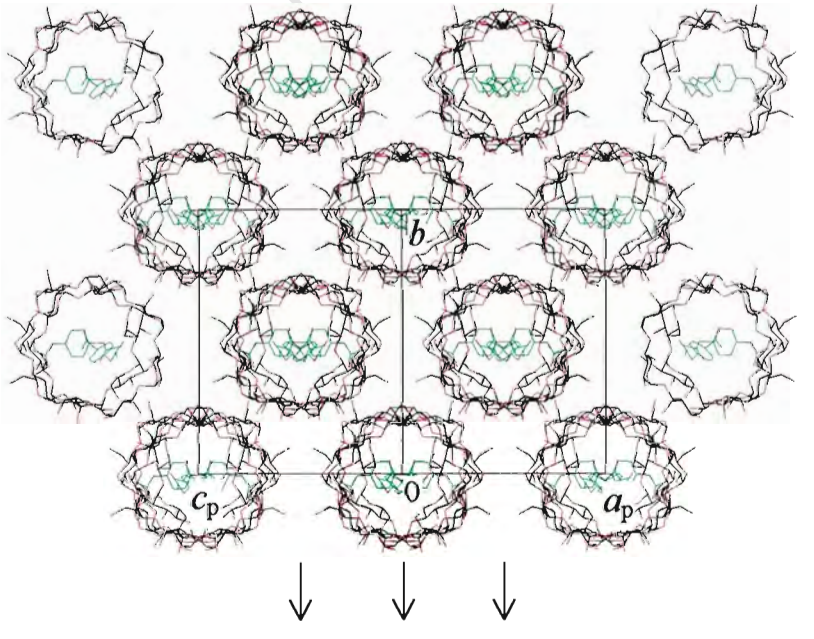

Figure 3.41 Packing diagram of the DIABCD structure viewed down the direction *c`* (where *c`* = *a* + *c*)

Four torsion angles will be used to define the three-dimensional conformation of DIA. These torsion angles define the conformations that can be adopted by the acetamino and acetyloxy residues relative to the phenyl ring. The appropriate torsion angles are illustrated schematically in Figure 3.39. Table 3.54 lists the values of these torsion angles for DIA(A), DIA(A`), DIA(B), DIA(B`) and for the crystal structure of the uncomplexed diacetamate[85] (PARAC) (e.s.d. s are in the range 1-4°).

The observed conformations of the diacetamate molecule included in the β-CD cavity differ from those reported for the uncomplexed drug. The acetamino and acetyloxy residues of uncomplexed diacetamate have torsion angles, δ_1 and δ_3, of approximately 0 and 90° respectively relative to the phenyl ring. The torsion angles adopted by the diacetamate molecules included in the DIABCD complex display variable conformations (Table 3.54). The torsion angles adopted by the uncomplexed diacetamate are imposed by hydrogen bonding and close packing requirements, whereas these requirements are relaxed for the diacetamate molecules included in the DIABCD complex.

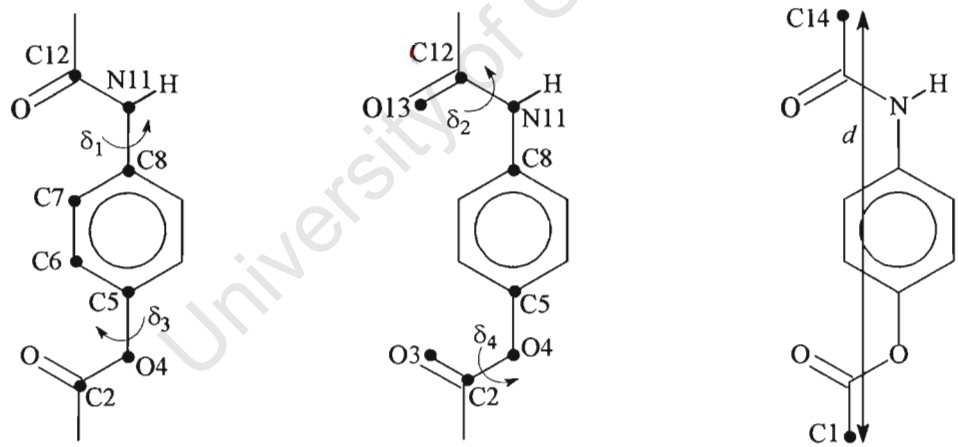

Figure 3.39 Schematic illustration of the torsion angles δ_1, δ_2, δ_3, δ_4 and the distance *d*

Table 3.54 Values of δ_1, δ_2 and *d* for DIA(A), (A`), (B), (B`) and PARAC

Diacetamate	δ_1 (°)	δ_2 (°)	δ_3 (°)	δ_4 (°)	***d*** **(Å)**
DIA(A)	88	48	48	-42	10.07
DIA(A`)	25	-25	33	-29	10.06
DIA(B)	17	-14	64	-33	10.13
DIA(B`)	166	31	164	1	9.95
PARAC	11	-5	-84	-3	10.05

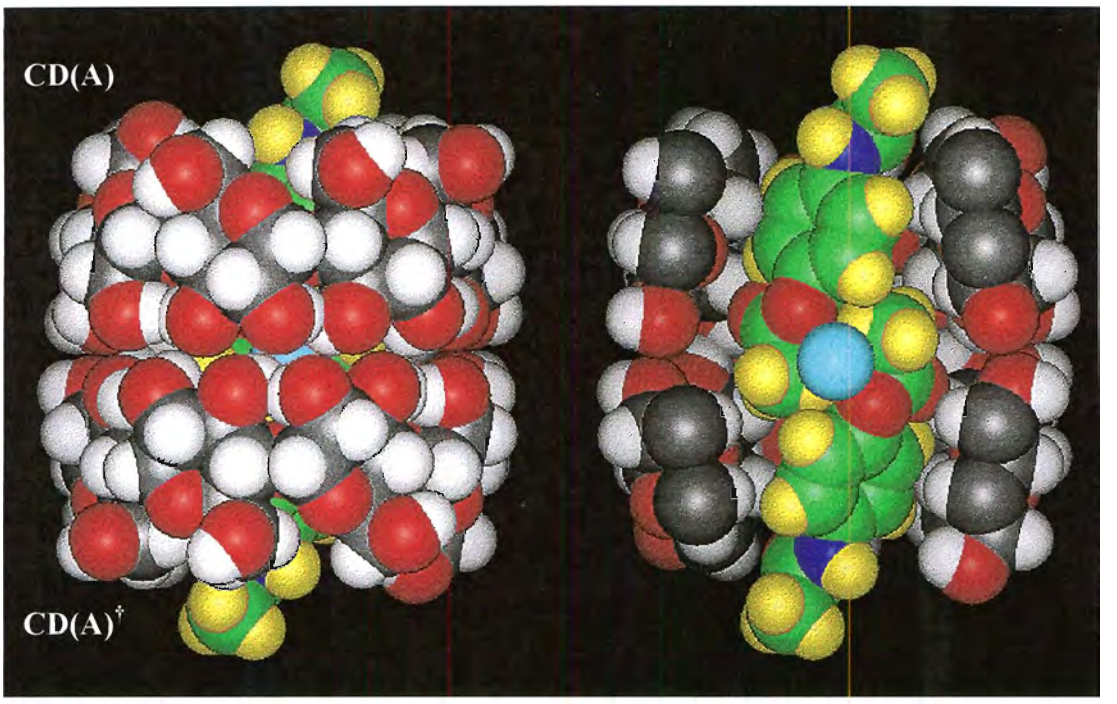

(a) (b)

Figure 3.37 CPK diagram of the CD(A)-CD(A)† dimer of the DIABCD structure (a) side view of dimer (b) sectioned view of the same orientation

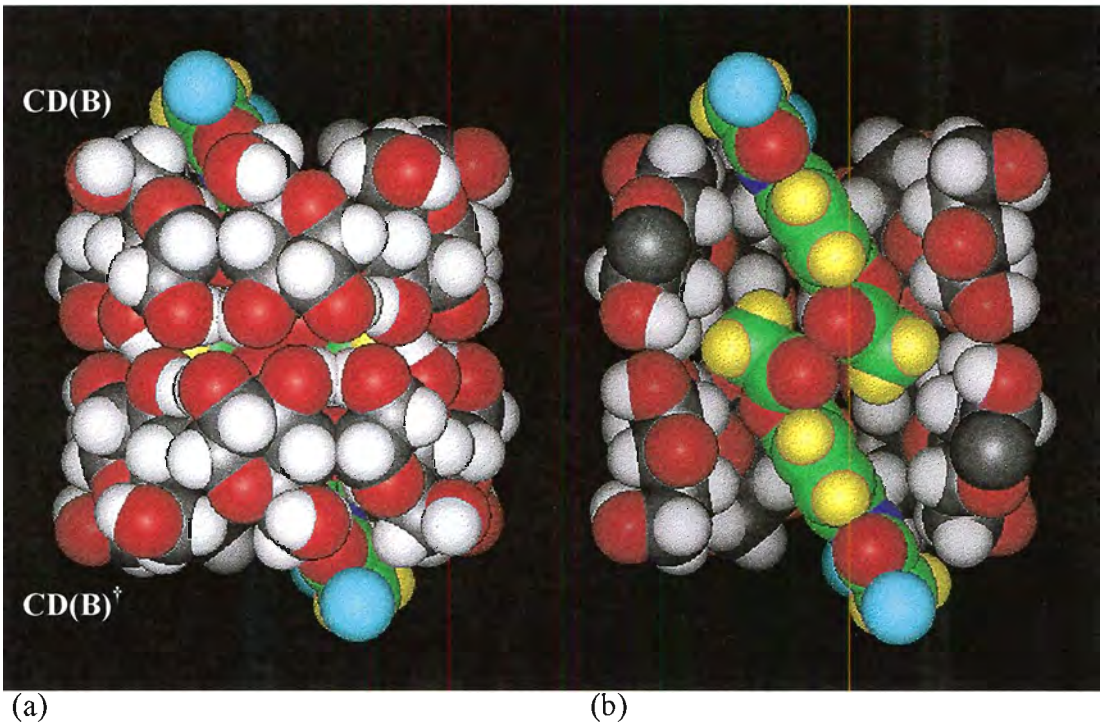

(a) (b)

Figure 3.38 CPK diagram of the CD(B)-CD(B)† dimer of the DIABCD structure (a) side view of dimer (b) sectioned view of the same orientation

† Two-fold related CD molecule

Overall description of the DIABCD structure

Figures 3.37 and 3.38 show CPK diagrams for the two dimeric units of the DIABCD structure. The first dimer includes the positions of DIA(A) (Figure 3.37) while the second dimer includes the positions of DIA(B) (Figure 3.38). The colour codes used in these diagrams are as follows: β-CD: C (grey), O (red), H (white); DIA: C (green), H (yellow), N (blue), O (red); Water: O (light blue). Any hydrogen atoms of the host and guest that were not part of the final refined model have been inserted in geometrically sensible positions for these CPK diagrams.

The acetyl groups of the two guests are situated in the vicinity of the primary rim of the dimer with the acetyloxy groups contained within the secondary hydroxyl interface. It is evident from Figure 3.37 (a) that approximately half of the acetyl group of a DIA molecule protrudes from each of the primary rims of the β-CD dimers. However, the major portions of the DIA guest molecules are contained within the dimer. This is achieved by the tilting of the DIA molecules with respect to the mean O4 planes of the CDs in which they are included. The mean planes of the phenyl rings of DIA(A) and DIA(B) make angles of 70(1)° and 61(1)° with the mean O4 planes of CD(A) and CD(B) respectively. The tilting permits the guest to occupy most of the available space in the intradimeric cavity and is necessary to avoid abnormally close approach of the acetyloxy residues. The tilting of the guest molecules with respect to the mean O4 planes of the CDs in which they are contained has been a feature of all the β-CD complexes that have been investigated in this chapter. This is considered to be an optimal mode of inclusion of *para*-substituted acetanilide guest molecules within a β-CD dimer. The hydrophobic phenyl rings can be centralised in the hydrophobic CD cavity while the more polar substituents can occupy the regions of the primary and secondary rims, where they can interact with CD hydroxyl groups and solvent water. The tilting allows almost complete containment of the guests within the dimer and thereby promotes efficient packing of the β-CD molecules.

The association of O23W with the O4A atom of the acetyloxy group of DIA(A) can be seen (Figure 3.37 (b)). The association of O24W and O31W with the carbonyl oxygen and amino nitrogen atoms of the acetamino residue of DIA(B) is evident from Figure 3.38 (b).

The O13B and O13B` atoms make bridging links through water molecules O24W and O15W respectively to primary hydroxyl oxygen atoms of adjacent CDs. O13B hydrogen bonds to O24W, which in turn bonds to a primary hydroxyl of an adjacent CD of the same dimeric column. O13B` hydrogen bonds to O15W, which in turn bonds to a primary hydroxyl of a CD molecule of another dimeric column.

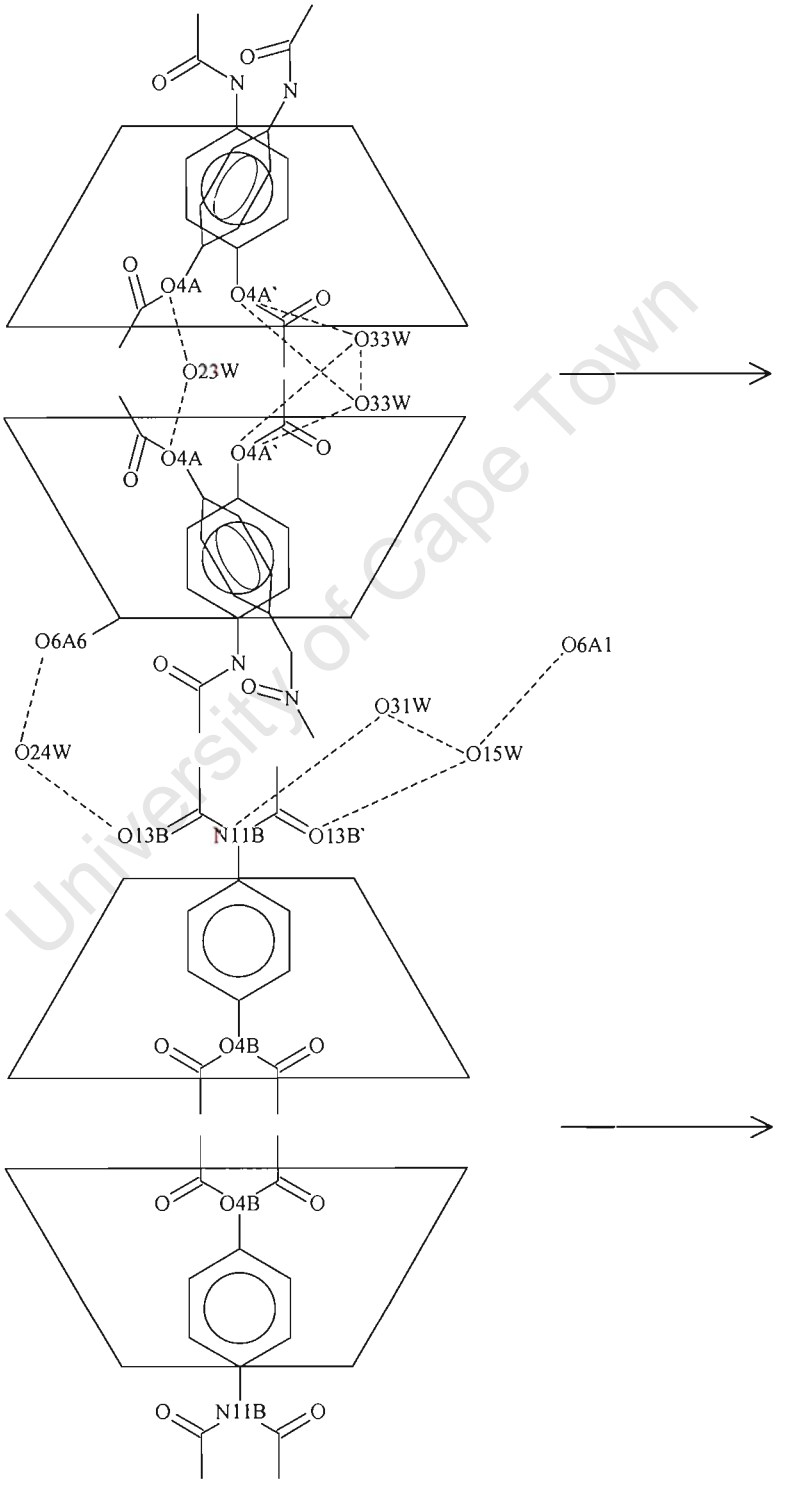

Figure 3.36 Schematic diagram of the guest interactions in the DIABCD complex

Guest interactions for the DIABCD structure

Details of the disorder and guest interactions for the DIABCD structure are shown schematically in Figure 3.36. Table 3.53 lists the contact distances for the relevant interactions associated with the guest molecules (e.s.d. s are in the range 0.02-0.08Å).

The O4 atoms of both of the disordered positions of DIA(A) are within hydrogen bonding contact of water molecules trapped in the intradimeric interface. The O4A atom makes a contact with a water molecule, O23W, positioned on the two-fold axis. This results in the water molecule acting as a bridging link between O4A atoms in opposite halves of the two-fold related CD(A)-CD(A) dimer.

Similar bridging links are made between the O4A` atoms across the two-fold axis, in this case involving the water molecule, O33W. The O4A` atom makes contacts with this water molecule as well as its symmetry related position.

O31W makes a hydrogen bonding contact with the N atom of the acetylamino group. However, this linkage is only present together with the B position of the acetyl group, as this water molecule makes an unacceptably short contact with the primary C atom of the B` position of the acetyl group.

Table 3.53 Guest interactions for the DIABCD structure

Guest interaction	Distance (Å)	Equivalent positions
O3A···O33W	2.86	
O4A···O23W	2.94	
O4A`···O33W	2.66	
O4A`···O33W	3.08	-x+1,y,-z+1
O33W···O33W†	2.93	-x+1,y,-z+1
N11B···O31W	2.89	
O13B···O24W	2.82	
O24W···O6A6	2.78	
O13B`···O15W	3.00	
O15W···O31W	2.87	
O15W···O6A1	2.77	x-1/2,y+1/2,z

† Two-fold related counterpart atom

Table 3.51 Geometrical parameters of the O4 heptagon of the DIABCD structure

Glucose unit	*r* (Å)†	*l* (Å)†	*a* (°)†	*d* (Å)†	*t* (°)†
A1	5.04	4.40	128	-0.01	-2
A2	5.07	4.35	129	+0.02	+2
A3	5.02	4.39	129	-0.02	-1
A4	5.01	4.35	128	+0.01	+1
A5	5.07	4.37	129	-0.01	0
A6	5.03	4.36	128	+0.01	-1
A7	5.02	4.38	129	0.00	+2
A | mean |	**5.04**	**4.37**	**129**	**0.01**	**1**
B1	5.00	4.37	126	-0.01	0
B2	5.11	4.34	130	+0.01	0
B3	5.00	4.40	129	+0.01	0
B4	5.01	4.33	128	-0.01	-1
B5	5.05	4.41	128	-0.01	+1
B6	5.05	4.31	129	+0.02	0
B7	5.02	4.41	130	-0.01	0
B | mean |	**5.03**	**4.37**	**129**	**0.01**	**0**

† Refer to page 6,7 (Chapter 1) for definitions and descriptions of these quantities

Table 3.52 φ , O2(n)···O3(n-1) distances, τ_1 and τ_2 for the DIABCD structure

Glucose unit	φ (°)	O2(n)···O3(n-1) (Å)	τ_1 (°)	τ_2 (°)
A1	118	2.75	2.4)	5.9
A2	119	2.86	8.4	11.6
A3	118	2.78	3.5	7.2
A4	118	2.85	9.2	12.1
A5	118	2.80	5.3	10.0
A6	117	2.83	6.2	9.3
A7	118	2.76	4.7	8.4
A | mean |	**118**	**2.80**	**5.7**	**9.2**
B1	117	2.73	3.0	6.2
B2	120	2.80	5.7	7.7
B3	118	2.79	2.4	6.9
B4	117	2.84	9.0	10.4
B5	118	2.79	5.4	8.4
B6	118	2.80	6.7	9.9
B7	118	2.77	2.3	4.6
B | mean |	**118**	**2.79**	**4.9**	**7.7**

† Refer to page 8,9 (Chapter 1) for definitions and descriptions of these quantities

Geometrical analysis of the DIABCD structure

The asymmetric unit of the DIABCD structure contains two crystallographically independent β-CD molecules, their associated guests and 28.4 water molecules. The two CDs will be referred to as CD(A) and CD(B). The glucose residues of each of the CDs are numbered from one to seven, so that the glucose residues of CD(A) are A1, A2, A3, A4, A5, A6 and A7. The guest molecules associated with CD(A) and CD(B) will be referred to as DIA(A) and DIA(B) respectively. Atoms of the two disordered positions of DIA(A) will be referred to with the suffixes A and A`. Atoms of the disordered acetamino and acetyloxy groups of DIA(B) will be referred to with the suffixes B and B`. Tables 3.50, 3.51 and 3.52 list the geometrical data for the two independent β-CD molecules of the DIABCD structure (e.s.d. s are of the order of 0.01Å for distances and 1° for angles). The geometrical data for the DIABCD complex closely resemble those of the ACEBCD, BROBCD and PHEBCD structures. The D-glucopyranose rings are all in the $^4C_1$ conformation and their torsion angles are consistent with the average values obtained for β-CD structures. All primary hydroxyl groups adopt the (-)-*gauche* orientation, with the notable exception of the primary hydroxyl of A2 which adopts a (+)-*gauche* orientation. This primary hydroxyl group is involved in the only direct inter-layer hydrogen bonded contact of the structure.

Table 3.50 Selected torsion angles for the DIABCD structure

Glucose unit	ω (°)†	Φ (°)†	Ψ (°)†	Θ_1 (°)†	Θ_2 (°)†
A1	-60	114	124	55	-52
A2	+69	115	132	56	-57
A3	-64	113	123	54	-52
A4	-75	114	132	55	-53
A5	-69	111	125	54	-51
A6	-67	111	130	57	-55
A7	-68	115	123	54	-53
A | mean |	**67**	**113**	**127**	**55**	**53**
B1	-62	120	127	56	-52
B2	-69	119	128	53	-51
B3	-70	113	126	55	-53
B4	-70	116	131	56	-55
B5	-64	112	125	54	-52
B6	-66	114	130	57	-57
B7	-63	113	123	54	-51
B | mean |	**66**	**115**	**127**	**55**	**53**

† Refer to page 4,5 (Chapter 1) for definitions and descriptions of these quantities

Modelling of diacetamate (DIA) guest

The modelling of the two DIA guests [referred to as DIA(A) and DIA(B)] proved to be a most challenging task but one which was facilitated by the experiences of disorder in the previously solved ACEBCD and BROBCD structures. At an early stage of refinement a single phenyl ring of DIA(B) was recognisable in the centre of the cavity of one of the two CDs. The atoms of the acetamino and acetyloxy groups were finally located after the examination of many successive difference electron density maps. The assignment of the acetylamino versus the acetyloxy groups was based on the known geometry of the uncomplexed diacetamate molecule.[85] The assignment focussed on the angles around the nitrogen atom (N11) of the acetamino group and the oxygen atom (O4) of the acetyloxy group (indicated with red arrows in Figure 3.35), which have values of 117° and 129° respectively for the uncomplexed diacetamate molecule. These groups were found to be disordered over two positions [labelled B (black) and B` (red) in Figure 3.35] and were assigned s.o.f. s of 0.5 each based on the peak heights in the difference map. This was an analogous type of disorder to that seen for the acetamino groups of the guest molecules of the BROBCD structure. A common isotropic temperature factor, which refined to a final value of 0.15Å^2, was assigned to the non-hydrogen atoms of this group. At an advanced stage of the refinement it became clear that the DIA molecule contained in the second CD cavity was disordered over two distinct sites [labelled A (black) and A`(red) in Figure 3.35] having intersecting phenyl rings almost orthogonal to one another. The non-hydrogen atoms of the guest were located using similar techniques to those used for the ACEBCD structure where a similar type of disorder of the guest was observed. The acetyloxy and acetamino groups were assigned as for DIA(B). The two positions were assigned s.o.f. s of 0.5 each and were refined with a common isotropic temperature factor for each position to values of 0.16 and 0.21 Å^2 for the A and A` positions respectively. Hydrogen atoms were added in geometrically calculated positions and various distance constraints were applied to the model.

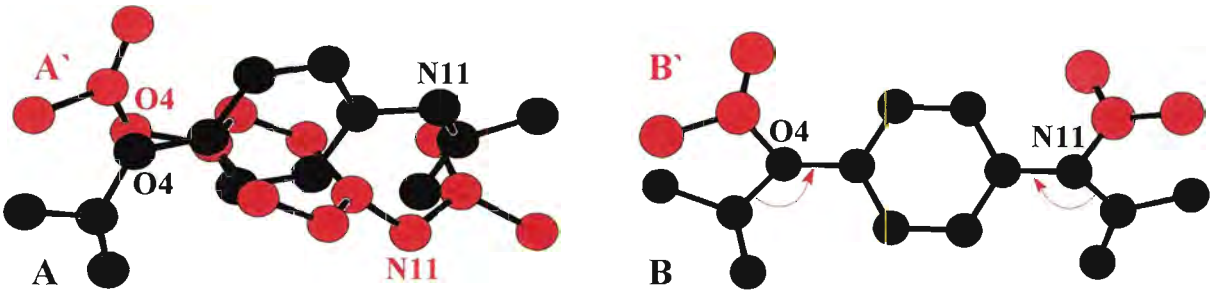

Figure 3.35 The disordered positions of the guest molecules of the DIABCD structure

primary hydroxyl oxygen atoms. Further refinement enabled the location of the remaining primary hydroxyl oxygen atoms. All 14 of these atoms were assigned full site-occupancy and refined with anisotropic temperature factors with U_{eq} values in the range 0.06 to 0.16Å^2. No significant electron density corresponding to disordered primary hydroxyls was present. Refinement proceeded with the placement of water molecules, addition of geometrically fixed hydrogen atoms attached to the CD carbon atoms and the placement of all CD hydroxyl hydrogen atoms using the rotating group refinement (AFIX 147) strategy. The hydrogen atoms of each CD were refined using common isotropic temperature factors to final values of 0.07 and 0.05Å^2 for the two independent CDs. After many successive refinements, 14 water molecules with full site-occupancy were placed, having final anisotropic temperature factors with U_{eq} values in the range 0.10 to 0.20Å^2. A further 18 water molecules with site-occupancy of less than one were refined with fixed isotropic temperature factors of 0.17Å^2 and varying site-occupancy. The site-occupancies of these water molecules varied from 0.37 to 0.95 and they amounted to a further 9 water molecules in the asymmetric unit. The 25.0 water molecules located compared favourably with the 28.4 water molecules expected from TGA analysis.

Table 3.49 Refinement parameters for the DIABCD structure

Refinement	
Refinement program	SHELXL-93
Max 2θ	48.89
Index range	h : 0,22; k : -28,0; l : -39,35
No. of reflections collected	27593
No. of unique reflections	12741
R_{int}	0.047
Reflections with $F_o>4\sigma F_o$	10738
Number of L.S. parameters	1352
R_1 ($F_o>4\sigma F_o$)	0.1012
R_1 for all reflections	0.1119
wR_2	0.2969
w	$[\sigma^2(F_o^2) + (0.2487 \times P)^2 + (48.35 \times P)]^{-1}$
S	0.886
$\Delta\rho$(max) final, $\Delta\rho$(min) final (eÅ^{-3})	0.73, -0.84

Table 3.48 Data-collection parameters for the DIABCD structure

Data-collection		
Diffractometer	Nonius Kappa CCD	
Temperature	293 K	
Radiation λ	Mo Kα (0.71069 Å)	
	Set 1	**Set 2**
ϕ	0.0°	0.0°
θ	0.0°	0.0°
κ	0.0°	-134.75°
ω	0.0°	-160°
Dx	33mm	35mm
Number of frames collected	360	74
Rotation axis / angle	ϕ rotations ($\Delta\phi = 0.5°$)	ω rotations ($\Delta\omega = 0.5°$)
Exposure time / frame	40 sec (x 2)	40 sec (x 2)
Reflections collected	19875	7718

Structure solution and refinement

The solution of the DIABCD structure represented a difficult challenge in view of the fact that the cell parameters did not directly match any of the known β-CD structures and the structure required the location of a large number of non-hydrogen atoms. Two β-CD molecules, two guest molecules and 28.4 water molecules comprised the asymmetric unit of the structure. The magnitude of such a problem and the chemical nature of the species investigated meant that direct method techniques alone were unlikely to provide the structural solution. After the failure of a number of direct methods attempts in SHELXS,[81] the structure was solved using the program PATSEE.[82,83] This program uses Patterson and direct methods to position a fragment of known geometry in a unit cell. The search model, which consisted of a single β-CD molecule, produced favourable statistics from the initial PATSEE run (RFOM = 1.000, TFOM = 1.000, CFOM = 1.532, TPRSUM = 0.798, R_E = 0.249). Partial structure expansion of the correctly positioned β-CD molecule in SHELXS produced most of the atoms of the CD backbone of a second cyclodextrin molecule. The two independent CD molecules were not arranged in a head-to-head dimer but were each half of two separate dimers. The other halves of each dimer were produced by the two fold-axes in the space group C2. The coordinates of the two CD molecules excluding the primary hydroxyl oxygen atoms were successfully refined in SHELXL-93.[84] Difference electron density maps based on initial refinements revealed many of the

X-ray crystallographic analysis of the DIABCD structure

Data-collection

The preliminary cell parameters and space group for the DIABCD structure, containing diacetamate as guest, were determined by x-ray photographic techniques. Laue 2/m symmetry and reflection conditions *hkl* : $h + k = 2n$, *h0l* : ($h = 2n$), and 0*k*0 : ($k = 2n$) indicated the monoclinic space groups C2, C*m* or C2/*m*. The chiral nature of the β-CD molecule determined the space group as C2. The crystals of the complex were mounted under mother liquor in Lindemann capillaries on account of the instability of the crystals when removed from that medium. The data were collected at 273K on a Nonius Kappa CCD diffractometer. All data were corrected for Lorentz-polarisation effects but not for absorption. The absorption effects were considered negligible for the size of the crystal used. Crystal data are listed in Table 3.47 while data-collection parameters are listed in Table 3.48. The space group and cell parameters, with the exception of the *c*-axis length, corresponded closely with those of the ACEBCD structure. The length of the *c*-axis of the DIABCD structure was more than double that of the ACEBCD structure (where $c = 15.700$ Å).

Table 3.47 Crystal data for the DIABCD structure

Crystal Data	
Molecular formula	$2(C_{42}H_{70}O_{35})\cdot 2(C_{10}H_{11}NO_3)\cdot 28.4(H_2O)$
M_r (g.mol^{-1})	3172.06
Crystal system	Monoclinic
Space group	C2
Z	4
a (Å)	19.275 (1)
b (Å)	24.187 (1)
c (Å)	34.289 (3)
α (°)	90
β (°)	109.12 (1)
γ (°)	90
V (Å^3)	15104 (2)
μ (Mo Kα) (cm^{-1})	1.262
D_c (g.cm^{-3})	1.3949
F (000)	6784
Crystal dimensions	0.4 x 0.4 x 0.3 mm

B.) Dimer interactions

Table 3.43 Dimer interactions for the PHEBCD structure

Type	Dimer	Number / dimer	Range (Å)	Mean (Å)
O3···O3	A-B	7	2.77-2.90	2.82
O2···O2	A-B	7	2.94-3.07	3.00
O2···O3	A-B	12	2.83-3.20	3.08

C.) Layer interactions

Table 3.44 (a) Intra-layer interactions for the PHEBCD structure

Type	Number / dimer	Range (Å)	Mean (Å)
O2···O2	2	2.75-2.80	2.78
O6···O6	4	2.74-2.94	2.83

Table 3.44 (b) Inter-layer interactions for the PHEBCD structure

Type	Number / dimer	Range (Å)	Mean (Å)
O6···O6	2	2.92-2.94	2.93

D.) Guest interactions

Table 3.45 Guest interactions for the PHEBCD structure

Type	Guest	Number / dimer	(Number / dimer) x N	Mean (Å)
N11···OW	A	1	1	2.83
O12···O6B2	A	1	1	2.76
N11···OW	B	1	1	2.96
O12···OW25	B	1	1	2.86
O3···O29W	B`	1	0.5	2.58

E.) Water interactions

Table 3.46 Water interactions for the PHEBCD structure

Type	Number /dimer	(Number/dimer) x N	Range (Å)	Mean (Å)
O2···Water	12	11	2.66-3.17	2.87
O3···Water	9	8	2.81-3.15	2.98
O6···Water	23	21	2.63-3.15	2.80
Water···Water	31	29	2.50-3.20	2.84

Hydrogen bonding interactions of the PHEBCD structure

Figure 3.34 (a) and (b) show the distribution of water molecules (shown as black spheres in the diagram) in the PHEBCD structure.

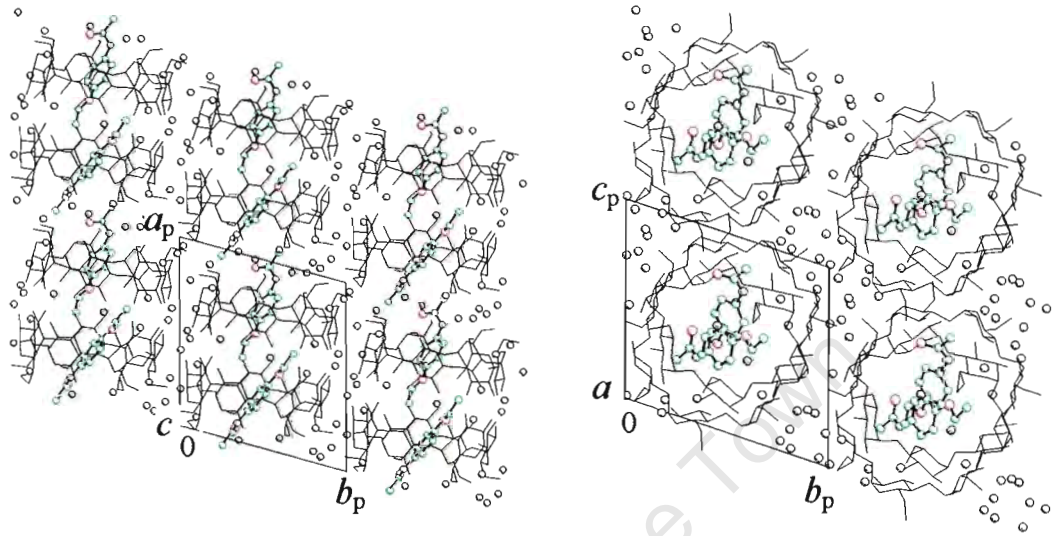

(a) (b)

Figure 3.34 Diagrams showing the distribution of water molecules in the PHEBCD structure (a) *c*-axis projection (b) *a*-axis projection

The interatomic and intermolecular contacts between the known hydrogen bond acceptors and donors are shown in the proceeding tables for the PHEBCD complex. The listed contacts are all in the range of 2.50 to 3.20 Å and the e.s.d. s are in the range 0.01-0.03 Å for the cyclodextrin, dimer and layer interactions and in the range 0.01-0.08 Å for the guest and water interactions. Tables 3.42, 3.43, 3.44 (a), 3.44 (b), 3.45 and 3.46 list summaries of these interactions for the cyclodextrin, dimer, intralayer, interlayer, guest and water interactions respectively.

A.) Cyclodextrin interactions

Table 3.42 Cyclodextrin interactions for the PHEBCD structure

O2···O3	Number / CD	Range (Å)	Mean (Å)
A	7	2.75-2.84	2.79
B	7	2.72-2.84	2.80

The PHEBCD structure consists of a single dimeric layer which forms the repeating array of the structure by stacking along the *a*-axis of the structure. Further discussion of the PHEBCD structure will be included in a comparison of the four β-CD complexes with *para*-substituted acetanilide guests at the end of this chapter.

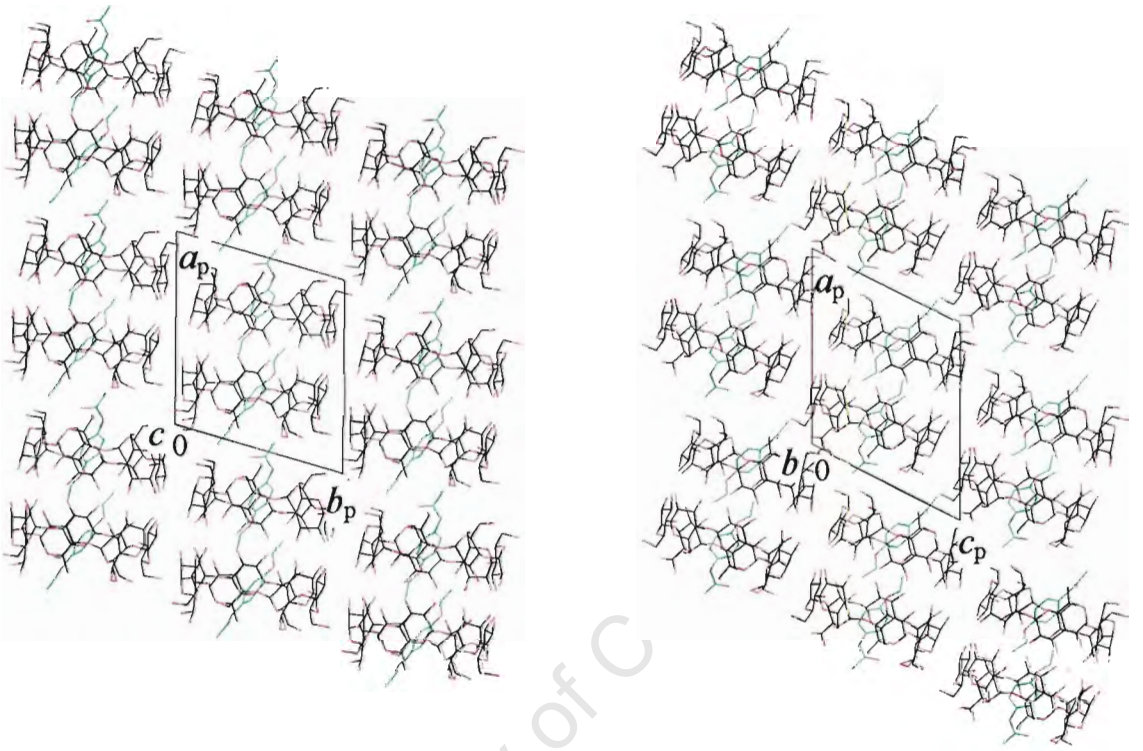

(a) (b)

Figure 3.32 Packing diagrams of the (a) *c*-axis (b) *b*-axis projections of the PHEBCD structure

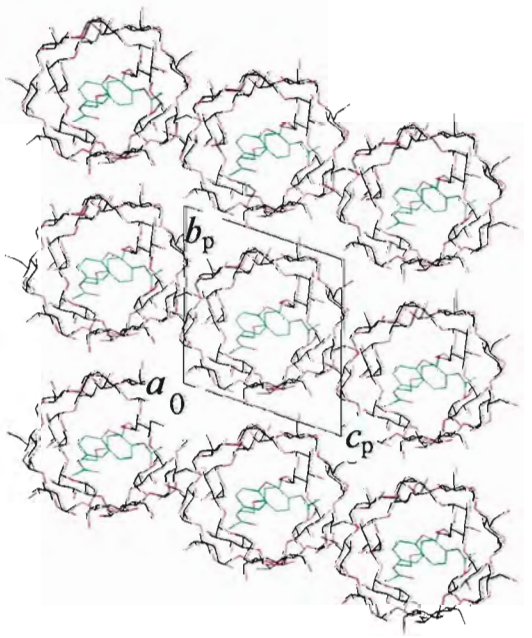

Figure 3.33 Packing diagram of the *a*-axis projection of the PHEBCD structure

Crystal Packing of the PHEBCD structure

Figure 3.31 shows a stereo diagram of a dimer of the PHEBCD structure. The dimer is viewed parallel to the mean O4 planes of the CDs.

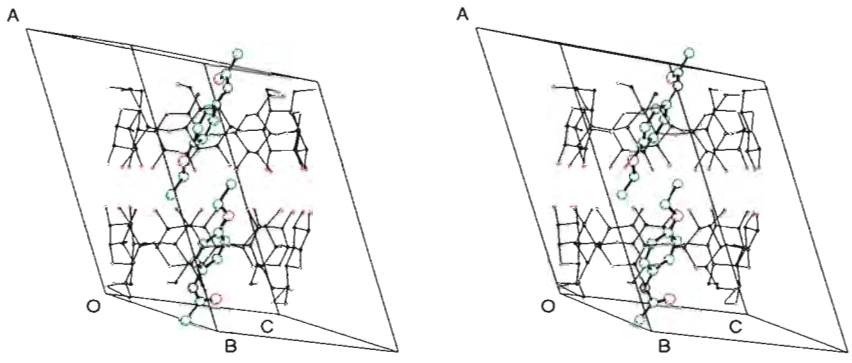

Figure 3.31 Stereo diagram of a dimer of the PHEBCD complex

Figures 3.32 (a) and (b) are extended packing diagrams of the PHEBCD structure showing projections as viewed down the *c*- and *b*-axes. These figures illustrate the stacking of the dimers in columns parallel to the *a*-axis. This stacking mode has been classified as type IM (for 'intermediate'), which is characteristic for β-CD complexes crystallising in the space group P1 with cell dimensions similar to those reported here (viz. with *a* approximately 18Å and *b*, *c* approximately 15Å each).[56] A number of structures with this IM packing motif have been described in the space group P1.[59,63,67-80] The packing of the β-CD dimers is analogous for the PHEBCD structure and these isomorphous structures.

The channels are more deformed at the interdimeric interface than for the CH type structures. The relative average shift of consecutive dimers, when the dimers were viewed perpendicular to their mean O4 planes is 6.0(2) Å for IM type structures crystallising in the space group P1.[56] This value is almost equal to the inner diameter of the β-CD molecule at the primary rim and is slightly larger then the average radius of the O4 heptagon. Figure 3.33 shows the "endless" channels produced by the cavities of the dimers.

From the packing diagrams it is evident that the dimers are arranged in dimeric layers parallel to the *bc*-plane of the structure. These dimeric layers are a characteristic feature of all dimeric β-CD structures.

Four torsion angles will be used to define the three-dimensional conformation of PHE. These torsion angles define the rotational orientations that can be adopted by the acetamino and ethoxy residues relative to the phenyl ring. The appropriate torsion angles are illustrated schematically in Figure 3.30. Table 3.41 lists the values of these torsion angles for PHE(A), PHE(B), PHE(B`) and for the crystal structure of the uncomplexed phenacetin molecule[64-66] (PYRAZB) (e.s.d. s are in the range 1-3° for angles). It is noted from Table 3.41 that the conformations of the acetamino group and ethoxy groups of PHE(A) and PHE(B) are not significantly different from those of the uncomplexed phenacetin. The C1 to C13 distance (*d*) is remarkably constant for phenacetin molecules included in the PHEBCD complex and uncomplexed phenacetin (PYRAZB) (Table 3.41). A feature of the crystallographic analysis is the finding that the ethyl portion of the ethoxy residue of PHE(B) is disordered in two orientations. The torsion angle δ_3 (Figure 3.30) has values of 31° and 164° for the two disordered sites.

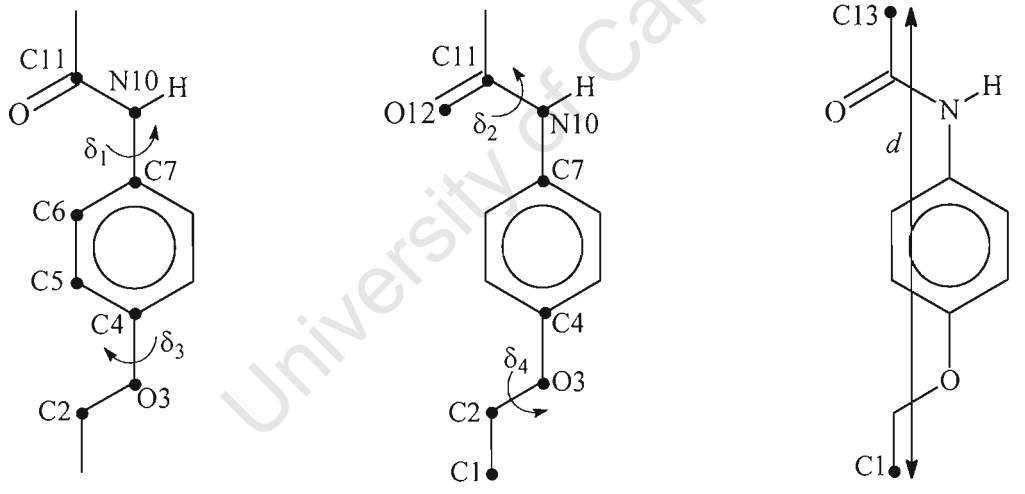

Figure 3.30 Schematic illustration of the torsion angles δ_1, δ_2, δ_3, δ_4 and the distance *d*

Table 3.41 Values of δ_1, δ_2 and *d* for PHE(A),(B),(B`) and PYRAZB

Phenacetin	δ_1 (°)	δ_2 (°)	δ_3 (°)	δ_4 (°)	*d* (Å)
PHE(A)	46	-19	9	178	10.03
PHE(B)	26	-15	31	164	10.04
PHE(B`)	-	-	164	-169	10.10
PYRAZB	30	-1	7	172	10.05

Overall description of the PHEBCD structure

Figures 3.29 (a) and (b) show CPK diagrams for a dimer of the PHEBCD structure. The dimer includes the position of PHE(A) and PHE(B) (where the B` position of the ethyl portion of the ethoxy group is shown). The colour codes used in these diagrams are as follows: β-CD: C (grey), O (red), H (white); PHE: C (green), H (yellow), N (blue), O (red); Water: O (light blue).

The acetyl groups of the two guests are situated in the vicinity of the primary rims with the ethoxy groups contained within the secondary hydroxyl interface of the dimer. It is evident from Figure 3.29 (a) that the entire methyl portions of the acetyl groups of the guests protrude from the primary rims of the β-CD dimer. However, the major portions of the two PHE guest molecules are contained within the dimer. This is achieved by the tilting of the PHE molecule with respect to the mean O4 plane of the CD in which it is included. The mean planes of the phenyl rings of PHE(A) and PHE(B) make angles of 64(1)° and 61(1)° with CD(A) and CD(B) respectively. The tilting prevents abnormally close approach of the ethoxy residues and allows the guests to occupy most of the dimeric cavity. The association of O29W with the O3B atom of the ethoxy group of PHE(B) can be seen in Figure 3.29 (b).

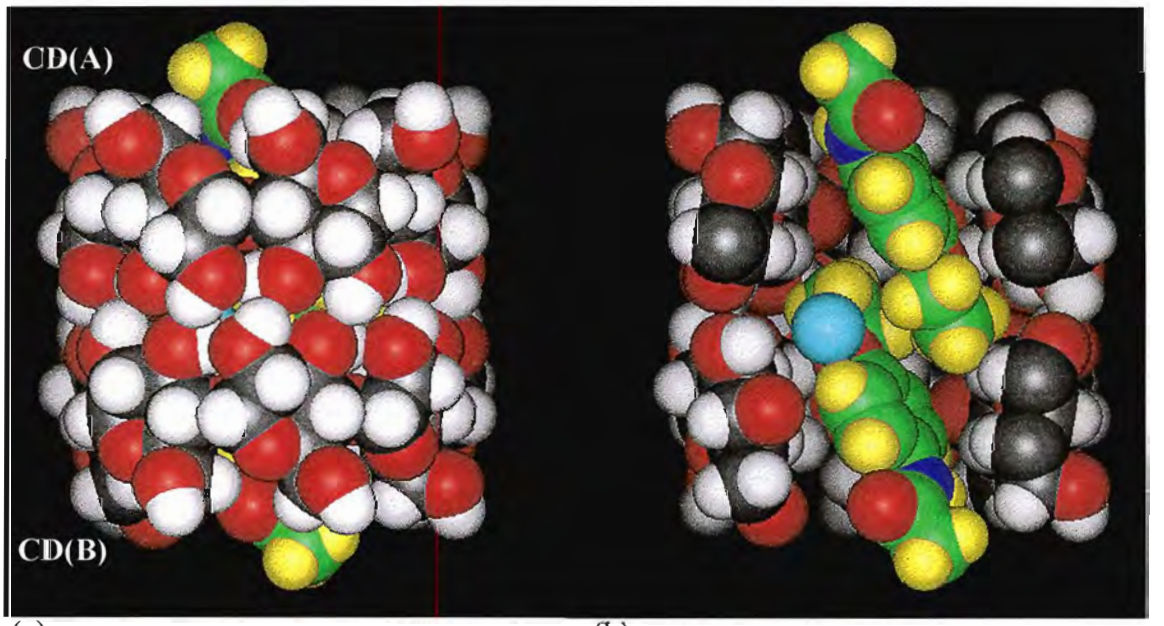

Figure 3.29 CPK diagrams of the dimeric unit of the PHEBCD structure (a) side view of dimer (b) sectioned view of the same orientation

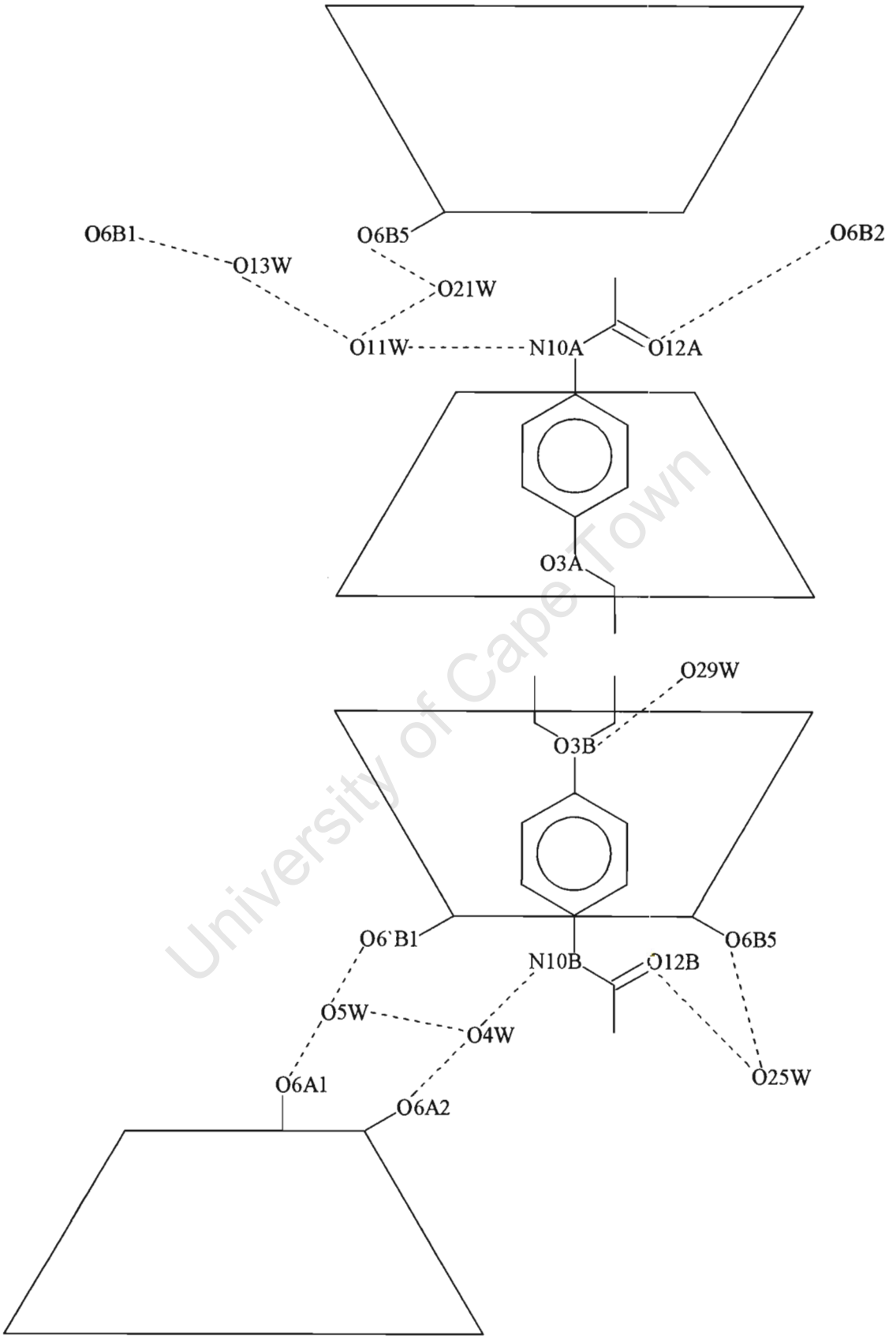

Figure 3.28 Schematic diagram of the guest interactions for the PHEBCD structure

Guest interactions for the PHEBCD structure

Details of the disorder and guest interactions are shown schematically in Figure 3.28. Table 3.40 lists contact distances for relevant interactions associated with the guest molecules (e.s.d. s are in the range 0.01-0.06Å). The carbonyl oxygen atom of PHE(A) is in hydrogen bonding contact with a primary hydroxyl group of a CD belonging to an adjacent dimeric column. The carbonyl oxygen of PHE(B) is linked via a water molecule (O25W) to a primary hydroxyl of the same CD in which it is included. A water molecule (O29W) contained within the intradimeric interface makes a hydrogen bonded contact with the O3B atom of the ethoxy group of PHE(B). However, this contact can only be made when the disordered ethyl portion of the ethoxy group is in the B` position, as the carbon atoms of the B position make unacceptably short contacts with this water molecule. The N atoms of the acetylamino groups of PHE(A) and PHE(B) are involved in hydrogen bonds to water molecules, where the latter are hydrogen bonded to primary hydroxyl O atoms of the same or the adjacent dimeric column.

Table 3.40 Guest interactions for the PHEBCD structure

Guest interaction	Distance (Å)	Equivalent positions
N10A···O11W	2.83	
N10B···O4W	2.96	
O12A···O6B2	2.76	x+1,y,z+1
O12B···O25W	2.86	
O6B5···OW25	2.78	
O3B···O29W	2.58	
O11W···O21W	2.64	
O11W···O13W	2.76	
O21W···O6B5	2.89	x+1,y,z
O13W···O6B1	2.78	x+1,y+1,z+1
O4W···O6A2	2.98	x-1,y,z-1
O4W···O5W	2.79	
O5W···O6A1	2.74	x-1,y,z-1
O5W···O6`B1	2.63	

Table 3.38 Geometrical parameters of the O4 heptagons for the PHEBCD structure

Glucose unit	*r* (Å)†	*l* (Å)†	*a* (°)†	*d* (Å)†	*t* (°)†
A1	5.06	4.38	129	+0.02	0
A2	5.03	4.35	128	0.00	0
A3	5.05	4.40	129	-0.02	-1
A4	5.03	4.32	129	0.00	+2
A5	5.03	4.44	128	+0.03	0
A6	5.05	4.28	129	-0.02	-1
A7	5.01	4.43	128	-0.02	+1
A | mean |	**5.04**	**4.37**	**129**	**0.02**	**1**
B1	5.18	4.31	131	0.00	-2
B2	4.99	4.39	129	+0.04	+1
B3	4.99	4.47	127	-0.01	-1
B4	5.10	4.30	128	0.00	0
B5	5.08	4.43	129	-0.01	+1
B6	4.99	4.29	130	+0.01	-2
B7	5.01	4.46	125	+0.03	+2
B | mean |	**5.05**	**4.38**	**128**	**0.01**	**1**

† Refer to page 6,7 (Chapter 1) for definitions and descriptions of these quantities

Table 3.39 φ , O2(n)···O3(n-1) distances, τ_1 and τ_2 for the PHEBCD structure

Glucose unit	φ (°)†	O2(n)···O3(n-1) (Å)†	τ_1 (°)†	τ_2 (°)†
A1	118	2.76	3.1	6.0
A2	116	2.75	1.2	5.9
A3	119	2.83	8.0	10.5
A4	119	2.79	0.6	6.7
A5	116	2.84	7.3	10.1
A6	118	2.79	4.3	7.2
A7	118	2.80	7.6	10.5
A | mean |	**118**	**2.79**	**4.6**	**8.1**
B1	121	2.79	5.7	9.6
B2	117	2.81	2.3	7.8
B3	118	2.82	9.5	11.6
B4	119	2.83	6.2	8.9
B5	118	2.84	9.0	11.9
B6	118	2.79	2.8	5.9
B7	118	2.72	2.0	5.4
B | mean |	**118**	**2.80**	**5.4**	**8.7**

† Refer to page 8,9 (Chapter 1) for definitions and descriptions of these quantities

Geometrical analysis of the PHEBCD structure

The asymmetric unit of the PHEBCD structure contains two crystallographically independent β-CD molecules, their associated guest molecules and 28.4 water molecules. The two CDs will be referred to as CD(A) and CD(B). The glucose residues of each of the CDs are numbered from one to seven, so that the glucose residues of CD(A) are A1, A2, A3, A4, A5, A6 and A7. The guest molecules associated with CD(A) and CD(B) were PHE(A) and PHE(B) respectively. The atoms of the two disordered ethyl portions of the ethoxy group of PHE(B) will be referred to with the suffixes B and B`. Tables 3.37, 3.38 and 3.39 list the geometrical data for the two independent β-CD molecules of the PHEBCD structure (e.s.d. s are of the order of 0.01Å for distances and 1° for angles). The geometrical data for the PHEBCD structure closely resemble those of the ACEBCD and BROBCD structures. The D-glucopyranose units are in the $^4C_1$ conformation and their torsion angles are consistent with the average values obtained for β-CD structures. The primary hydroxyl groups are all in the (-)-*gauche* conformation with the exception of the major position of the disordered primary hydroxyl group B5 and the minor postions of B1 and B5 which adopt the (+)-*gauche* orientation.

Table 3.37 Selected torsion angles for the glucose residues of the PHEBCD structure

Glucose unit	ω (°)†	ω (°)†	Φ (°)†	Ψ (°)†	Θ_1 (°)†	Θ_2 (°)†
A1	-65	-	114	123	57	-52
A2	-56	-	115	126	56	-53
A3	-65	-	117	133	58	-55
A4	-69	-	114	124	54	-50
A5	-71	-	114	131	58	-60
A6	-64	-	111	125	53	-50
A7	-62	-	116	129	55	-55
A | mean |	**65**	**-**	**114**	**127**	**56**	**54**
B1	-60	+43	117	131	55	-53
B2	-69	-	110	127	52	-50
B3	-63	-	116	131	57	-58
B4	-65	-	111	124	52	-49
B5	+77	+47	113	131	58	-57
B6	-68	-	111	123	54	-51
B7	-59	-	116	125	57	-52
B | mean |	**66**	**45**	**113**	**127**	**55**	**53**

† Refer to page 4,5 (Chapter 1) for definitions and descriptions of these quantities

Modelling of the phenacetin (PHE) guest

Fragments of two PHE guest molecules were apparent in the early stages of refinement and all of the non-hydrogen atoms were located in the initial difference electron density maps. The two guests will be referred to as PHE(A) and PHE(B). At a more advanced stage of refinement it became apparent that the ethyl portion of the ethoxy residue of PHE(B) was disordered over two sites (labelled B and B` in Figure 3.27). The torsion angles around the O3-C4 bond of PHE(B) (shown with a red arrow in Figure 3.27) is approximately 0° for one site and 180° for the other site. Each of the ethyl portions of the ethoxy moieties was included in the model with variable s.o.f. and a sufficient number of distance constraints was applied to ensure reasonable geometry. The final refined s.o.f. s for atoms of the disordered ethyl portions of the ethoxy moiety of PHE(B) were 0.60 and 0.40. Further reduction of the number of least-squares variables was effected by treating the phenyl groups as regular hexagons and assigning two separate common variable U_{iso} values to the C atoms of the two phenyl rings. The guest H atoms were included in geometrically calculated positions at 1.00 Å from their parent atoms and were treated isotropically.

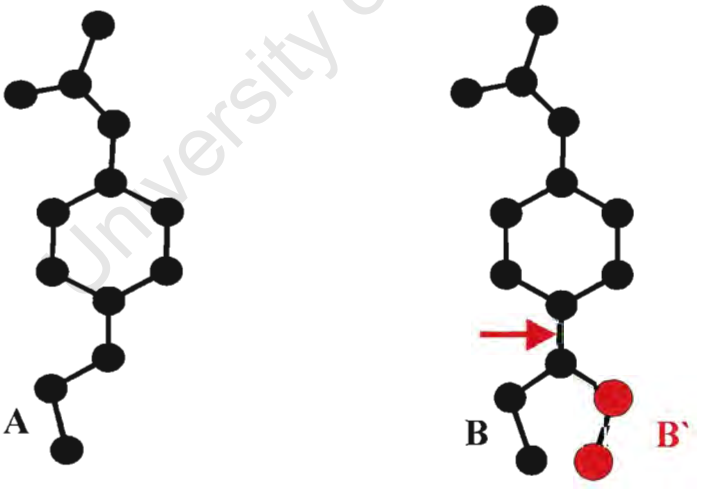

Figure 3.27 Plots of the PHE(A) and PHE(B) guest molecules with disordered portions included

Table 3.36 Refinement parameters for the PHEBCD structure

Refinement	
Refinement program	SHELX-76
No. of reflections collected	13036
No. of unique reflections	12582
R_{int}	0.0595
Reflections with $I > 3\sigma(I)$	10349
Number of L.S. parameters	1103
R_1	0.0994
wR	0.1098
w	$[\sigma^2(F_o) + 3.080 \times 10^{-3} F_o^2]^{-1}$
S	3.39
$(\Delta\rho)_{max}$ final ($eÅ^{-3}$)	0.83
$(\Delta\rho)_{min}$ final ($eÅ^{-3}$)	-0.80

The guest atoms, water molecules and remaining atoms of the host were located in successive difference electron density maps following least-squares refinements using the program SHELX-76.[42] The final cycles involved the blocked full-matrix technique with all atoms refining isotropically except the O2, O3, O4 and O6 oxygen atoms of the two CDs which were assigned anisotropic thermal parameters. The function minimised was $\Sigma w(|F_o| - |kF_c|)^2$ with weights which yielded a constant distribution of $\Sigma(w\Delta F)^2$ with $\sin\theta/\lambda$ and $(F_o/F_{o,max})^{1/2}$. The hydrogen atoms on carbon atoms of the β-CD molecules were inserted in geometrically calculated positions. The oxygen atoms of the primary hydroxyl groups of B1 and B5 were found to be disordered over two sites with final refined s.o.f. s of 0.70 and 0.30 for B1 and 0.67 and 0.33 for B5. The final structural model included 25 water molecules with s.o.f. 1.00 each and 4 with s.o.f. in the range 0.40-0.70, accounting for a total of 27.2 H_2O molecules, or an average of 13.6 H_2O molecules per β-CD molecule, in close agreement with the estimate of 14.2 H_2O per β-CD molecule obtained from thermogravimetric analysis.

Table 3.35 Data-collection parameters for the PHEBCD structure

Data-collection	
Diffractometer	Enraf-Nonius CAD4
Range scanned θ (°)	$1 \leq \theta \leq 25$
Index range	h : -17,17; k : -14,14; l : 0,14
Scan width (°)	0.8 + 0.35 tan θ
Aperture width (mm)	1.12 + 1.05 tan θ
Temperature	273 K
Radiation (λ)	Mo Kα (0.71069 Å)

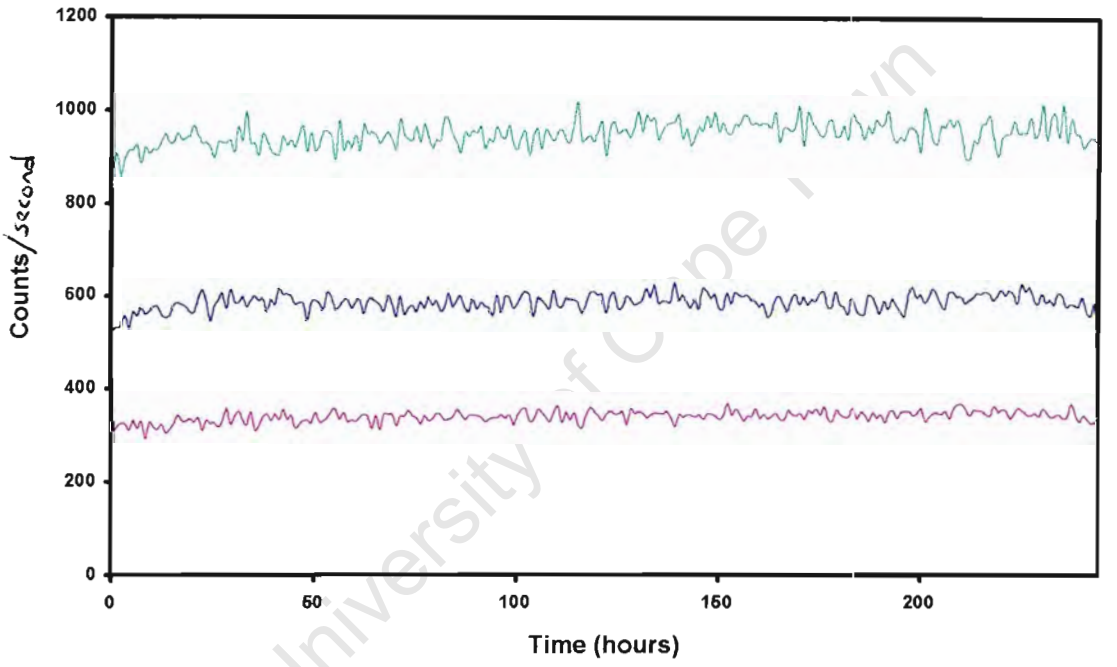

Figure 3.26 Plot of the intensities of the three reference reflections over the 245 hour period of the data-collection of the PHEBCD structure

Structure solution and refinement

The PHEBCD complex crystallises in the triclinic space group P1 with two β-CD molecules, two guest molecules and 28.4 water molecules comprising the asymmetric portion of the structure. The two β-CD molecules are arranged as a dimer. The structure was solved using the published coordinates for the non-hydrogen CD atoms (excluding primary hydroxyl oxygen atoms) of the isomorphous 4-*t*-butylbenzoic acid complex.[63] The final refinement parameters are listed in Table 3.36.

X-ray crystallographic analysis of the PHEBCD structure

Data-collection

The preliminary cell parameters and space group for the PHEBCD structure, containing the phenacetin guest, were determined by x-ray photographic techniques. Laue symmetry $\overline{1}$ indicated the triclinic crystal system. The chiral nature of the β-CD molecule determined the space group as P1. The crystals of the complex were unstable when removed from mother liquor. Therefore, a crystal of the complex was mounted under mother liquor in a Lindemann capillary. The data were collected at 273K on an Enraf-Nonius CAD4 diffractometer. Three reference reflections were measured every hour to monitor crystal decay which was not observed over the 245 hour duration of the data-collection (Figure 3.26). All data were corrected for Lorentz-polarisation effects but not for absorption. The absorption effects were considered negligible for the size of the crystal used. Crystal data are listed in Table 3.34 while data-collection parameters are listed in Table 3.35.

Table 3.34 Crystal data for the PHEBCD structure

Molecular formula	$2(C_{42}H_{70}O_{35})\cdot 2(C_{10}H_{13}NO_2)\cdot 28.4(H_2O)$
M_r (g.mol^{-1})	3140.06
Crystal system	Triclinic
Space group	P1
Z	1
a (Å)	17.979 (4)
b (Å)	15.437 (3)
c (Å)	15.559 (5)
α (°)	103.42 (3)
β (°)	113.22 (3)
γ (°)	98.75 (2)
V (Å^3)	3714 (2)
D_c (g.cm^{-3})	1.4039
F (000)	1680
μ (Mo Kα) (cm^{-1})	1.266
Crystal dimensions (mm)	0.4 x 0.45 x 0.3

B.) Dimer interactions

Table 3.30 Dimer interactions for the BROBCD structure

Type	CDs	Number / dimer	Range (Å)	Mean (Å)
O3···O3	A-B	7	2.79-2.99	2.84
O2···O2	A-B	7	2.93-3.18	3.04
O2···O3	A-B	11	2.99-3.20	3.08

C.) Layer interactions

Table 3.31 (a) Intra-layer interactions for the BROBCD structure

Type	Number /dimer	Range (Å)	Mean (Å)
O2···O2	2	2.77-2.78	2.78
O6···O6	4	2.79-2.92	2.86

Table 3.31 (b) Inter-layer interactions for the BROBCD structure

Type	Number / dimer	Range (Å)	Mean (Å)
O6···O6	3	2.63-3.07	2.83

D.) Guest interactions

Table 3.32 Guest interactions for the BROBCD structure

Type	Guest	Number / dimer	(Number / dimer) x N	Mean (Å)
N8···OW	A	1	0.58	3.19
N8···OW	A`	1	0.42	2.95
O10···OW	A	1	0.58	2.61
O10···OW	A`	1	0.42	2.35†
N8···OW	B	1	0.59	3.02
N8···OW	B`	1	0.41	3.03
O10···OW	B	1	0.59	2.66
O10···OW	B`	1	0.41	2.81

† disordered atoms involved in contact

E.) Water interactions

Table 3.33 Water interactions for the BROBCD structure

Type	Number / dimer	(Number / dimer) x N	Range (Å)	Mean (Å)
O2···Water	12	10	2.63-3.18	2.87
O3···Water	15	13	2.78-3.17	2.99
O6···Water	23	20	2.62-3.19	2.80
Water···Water	44	36	2.52-3.19	2.86

CHAPTER 5 : SALBUTAMOL LAURATE COMPLEXES WITH HP-β-CD BY CO-GRINDING AND KNEADING

Introduction

Salbutamol is one of a large and important group of drugs in use in clinical practice that act on the sympathetic nervous system. The sympathetic nervous system is vitally involved in the homeostatic regulation of a wide variety of functions, among which are heart rate, force of cardiac contraction, vasomotor tone, blood pressure, bronchial airway tone and carbohydrate and fatty acid metabolism. Because the functions that are mediated or modified by the sympathetic nervous system are diverse, agents that mimic or alter its activity are useful in the treatment of several disorders, such as hypertension, shock, cardiac failure and arrhythmias, asthma, allergy and anaphylaxis. The class of drugs known as the sympathomimetic drugs have been developed to bind as agonists to the α_1-, α_2-, β_1- and β_2-receptors of the sympathetic nervous system and have the general formula and numbering scheme shown in Figure 5.1.

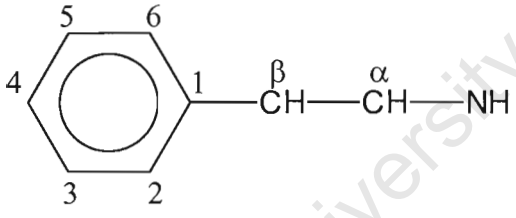

Figure 5.1 General formula and numbering scheme for sympathomimetic drugs

Modifications to this skeleton group are made by substitution on the amino group, aromatic nucleus and α- and β- carbon atoms. These are made in order to regulate the binding such that it may be as specific as possible for certain receptors. The receptors which control the stimulation of bronchial musculature are the β_2-adrenergic receptors. Some of the major adverse side effects of a non-selective adrenergic agonist in the treatment of asthma are caused by stimulation of the β_1-adrenergic receptors in the heart which could result in arrhythmias and other adverse side effects. Accordingly, drugs with preferential affinity for β_2-receptors have been developed.

Salbutamol (or albuterol) is a representative of this group of compounds which are known as the selective β_2-adrenergic agonists. Salbutamol is indicated for the relief of reversible airway obstruction, status asthmaticus and other conditions that require the symptomatic relief of bronchospasm. The drug is available for oral administration as tablets, as a syrup or as an aerosol. The most common form of salbutamol used in clinical practice is the sulphate salt which is marketed as PROVENTIL™ or VENTOLIN™. Preferential activation of the pulmonary β_2-receptors is achieved by inhalation of small doses of the drug in the aerosol form. This approach typically leads to effective activation of the β_2-receptors in the bronchi but very low systemic drug concentrations and thus there is less potential to produce the adverse side effects that can be caused by activation of the cardiac β_1-receptors.

The phenyl ring of salbutamol is substituted by hydroxymethyl and hydroxy groups at the 3 and 4 positions respectively (Figure 5.2). The β-carbon of the aliphatic portion is substituted with a hydroxy group while the amine is substituted with a *t*-butyl group. Salbutamol is a chiral drug with its chiral centre at the β-carbon. In clinical practice it is found that the (*R*)-enantiomer of the drug is the useful one for the treatment of respiratory disorders. In recent years there have been many concentrated efforts to provide a simple and cost-effective method of resolving the two enantiomers.[1]

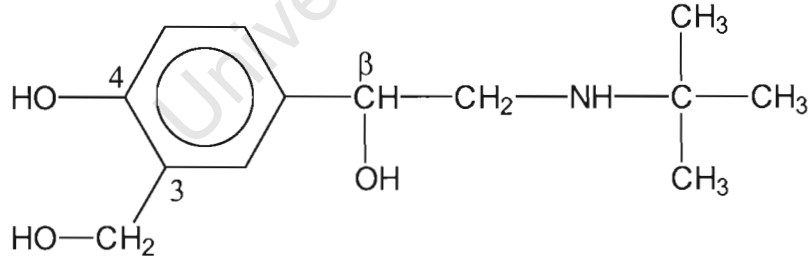

Figure 5.2 Chemical diagram of the structure of salbutamol

A thorough search of Chemical Abstracts from 1972 to July 1998 produced 27 papers reporting the study and applications of salbutamol with various CDs. Many of the papers (16 in all) are concentrated on enantiomeric separation of the (*R*)- and (*S*)-enantiomers of of the drug using various CDs and their derivatives as chiral separating agents in capillary zone electrophoresis.[2-17]

A method for solubilizing salbutamol by combining it with β-CD as well as with a selected hydroxycarboxylic or polycarboxylic acid in the form of an effervescent tablet has been investigated and patented.[18]

The incorporation of salbutamol in a matrix containing a water-soluble CD has been investigated and patented.[19]

β-CD and ethylated-β-cyclodextrin complexes with salbutamol were prepared in a 1:1 molar ratio by the freeze-drying method for an *in vitro* evaluation of the sustained-release behaviour of these formulations. Complex formation in the solid state was confirmed by DSC and the dissolution rates of salbutamol from the inclusion complexes were determined in water. The ethylated-β-cyclodextrin complexes displayed the slowest release of salbutamol and therefore the most favourable potential for the development of a sustained-release salbutamol-CD formulation.[20]

A determination of the stability constants of the salbutamol complexes with β-CD and ethylated-β-cyclodextrin by capillary zone electrophoresis showed that the ethylated-β-cyclodextrin has a higher affinity for salbutamol than β-CD. [21,22] It was determined in a high resolution NMR study that the substitution patterns of the ethylated-β-CD molecules influenced their affinities for salbutamol.[23]

The association constants for 1:1 complexes of salbutamol with α-, β- and γ-CD were determined by phase solubility studies and found to be 1.1, 69.3 and 5.1 M^{-1} respectively.[24] The complexes with α- and β-CD showed A_N solubility behaviour while the γ-CD complex showed B_S solubility behaviour. The association constants for these salbutamol-CD complexes are extremely low relative to binding constants obtained with many other substances. A solid state complex with β-CD was also prepared by freeze-drying and was characterised by DSC. The elimination of the endothermic peak of salbutamol for the inclusion complex was noted and was attributed to the incorporation of salbutamol in the β-CD cavity.

The hydrophobicity of the anion will increase the lipophilicity of this salbutamol dosage form and therefore increase the sublingual absorption. The apparent partition coefficient across the membranes of the sublingual mucosa is increased from <1 for salbutamol to 3-10 for salbutamol laurate.[30] However, by providing a dosage form of salbutomol laurate complexed with HP-β-CD, the solubility of the formulation may once again be increased to a sufficient level such that its delivery at the sublingual mucosa is not hindered by low aqueous solubility. The formation of a high affinity complex between HP-β-CD and salbutamol laurate therefore provides the lipophilic salbutamol laurate with a hydrophilic CD carrier for delivery of the drug to the membranes of the sublingual mucosa where it can be partitioned directly into the circulation for rapid action. The development of such a sublingual form of salbutamol with a rapid onset of action is useful for an emergency response to an asthma attack.

Energy-minimised structures of the interaction of salbutamol laurate with β- and γ-CD are illustrated in Figures 5.5 and 5.6.[30] The Cerius2 package from MSI was used for all calculations and the charge equilibration method was employed for determining electrostatic contributions. The structure of salbutamol laurate was prepared by calculating the lowest energy conformation with automatic repositioning of the fatty acid chain while retaining the critical distance between the carboxylate anion and the salbutamol cation. The CD structures were obtained from the published crystallographic coordinates and torsional restraints were applied to conserve the toroidal structure during minimisations. The lowest energy salt structure was then manually docked into the CD cavities. For the β-CD complex, the best fit was obtained for complexation of the fatty acid rather than the salbutamol ring. The minimised structure is stabilised by hydrogen bonding between a secondary hydroxyl group of the β-CD molecule and the primary hydroxyl group of salbutamol (magenta dotted line in Figure 5.5). For the γ-CD complex, the best fit was obtained for the inclusion of both the salbutamol and fatty acid in the cavity (Figure 5.6).

The aim of this work was to prepare and characterise HP-β-CD complexes with salbutamol laurate in the solid state for possible applications as a sublingual dosage form of salbutamol.

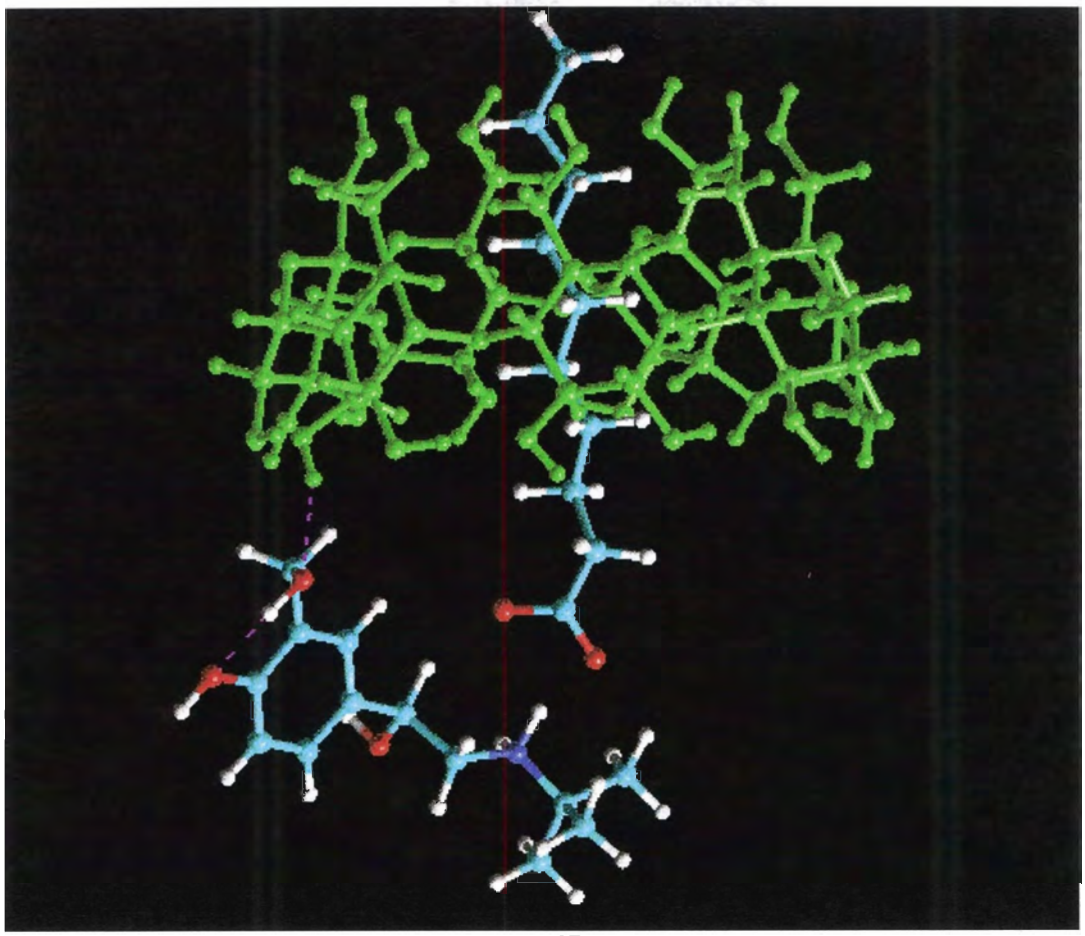

Figure 5.5 Minimised energy structure obtained for the complexation of salbutamol laurate with β-CD

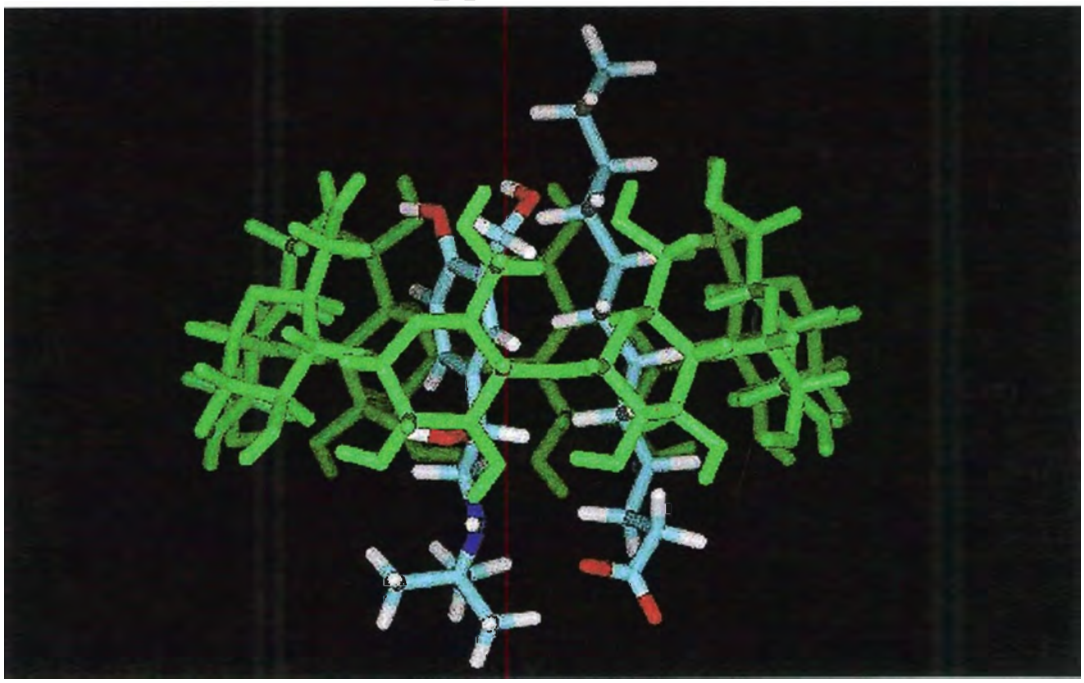

Figure 5.6 Minimised energy structure obtained for the complexation of salbutamol laurate with γ-CD

Polymorphism of salbutamol laurate

From the different batches of salbutamol laurate supplied, two polymorphic forms of the salt were identified. The two polymorphs were characterised by the physical techniques of differential scanning calorimetry (DSC), thermogravimetric analysis (TGA), hot stage microscopy (HSM), infrared spectroscopy (IR), elemental analysis and scanning electron microscopy (SEM). The two polymorphs are hereafter referred to as Form 1 and Form 2.

Microanalysis and IR

The microanalysis and IR results (Tables 5.1 and 5.2 respectively) indicate that the chemical composition of the two polymorphs is identical.

Table 5.1 C, H and N microanalysis results for the Form 1 and Form 2 polymorphs of salbutamol laurate

Element	Calculated %	Form 1	Form 2
C	68.34	68.33	68.50
H	10.25	10.50	10.55
N	3.19	3.40	3.33

Table 5.2 Principal peaks and their intensities for the IR spectra of the Form 1 and Form 2 polymorphs of salbutamol laurate

	Peak wavenumbers (cm^{-1}) with percentage transmission (%) in brackets						
Form 1	722 (70)	1036 (70)	1083 (69)	1152 (69)	1377 (45)	1458 (36)	1545 (42)
Form 2	722 (74)	1036 (75)	1083 (75)	1151 (74)	1377 (50)	1459 (40)	1545 (54)

TGA

Thermogravimetric analysis of Form 1 and Form 2 revealed no significant weight loss over the temperature range 30 to 300 $^{\circ}$C (% weight loss < 0.5 %). TGA therefore discounted the possibility that either of the two polymorphic forms was a hydrate or solvate of any sort.

XRD

XRD patterns (CoKα radiation and conditions as stated in Chapter 2) confirmed the presence of the two polymorphic phases of salbutamol laurate. Although the principal peak for both forms occurs at a 2θ value of 8.3°, at higher 2θ angles the differences between the two polymorphic forms are evident. This is particularly clear for the large peak at 2θ = 26.1° for Form 1, which is shifted to 2θ = 26.5° for Form 2 (Figure 5.7).

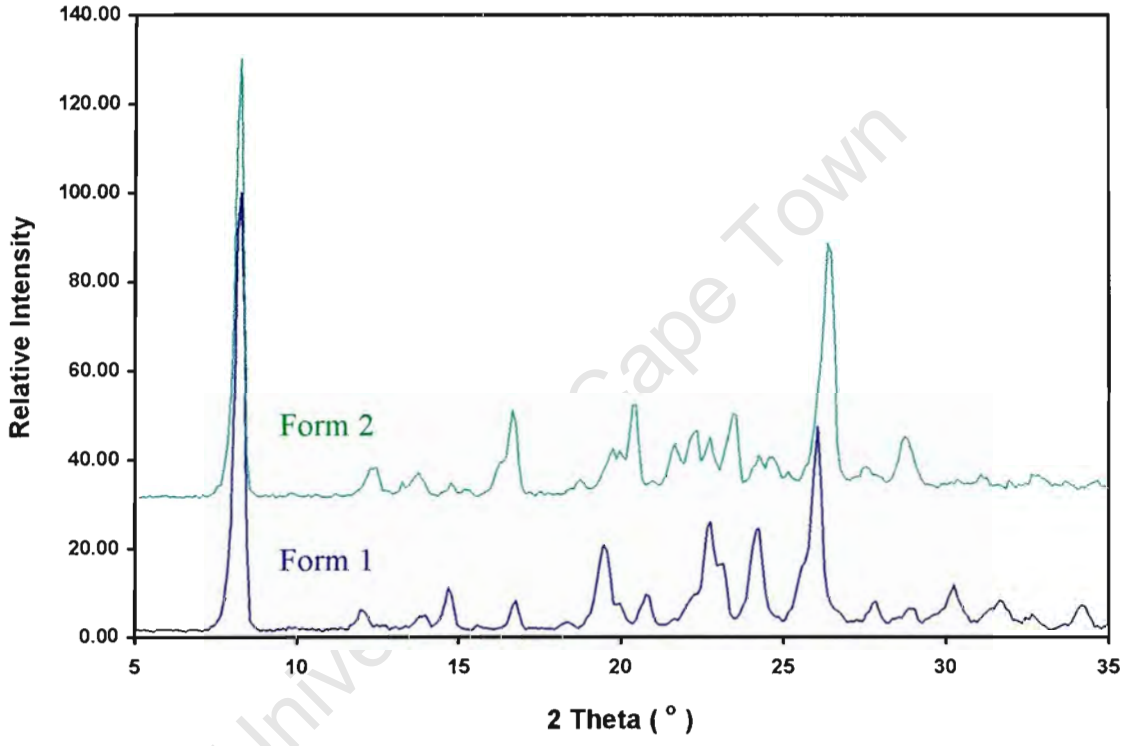

Figure 5.7 The XRD traces of the Form 1 (blue) and Form 2 (green) polymorphs of salbutamol laurate

DSC

DSC traces of the two polymorphs are shown in Figure 5.8 and Figure 5.9. Each polymorph was examined at three different scanning rates of 5, 10 and 20°C/min. At a scanning rate of 20°C/min the DSC trace of Form 1 was characterised by a single endothermic peak at 115°C while the trace for Form 2 shows two peaks at 111 and 115°C. At this scanning rate the two peaks for Form 2 were not clearly resolved. In the traces recorded at 5°C/min, Form 1 shows a single fusion endotherm at 111°C and Form 2 shows two clearly resolved endotherms at 107 and 111°C. The first endotherm is attributed to a phase change from Form 2 to Form 1 followed by the fusion endotherm of Form 1.

HSM

HSM was performed in order to investigate the conversion of Form 2 to Form 1 which was seen for the DSC experiments. The results are shown in Table 5.3. It was observed by HSM experiments that there is indeed a Form 2 to Form 1 conversion taking place upon heating. However, this transition proved very difficult to capture photographically.

Table 5.3 Summary of events observed during HSM analysis of Form 1 and Form 2 polymorphs of salbutamol laurate

Temperature (°C)	Form 1	Form 2
30 – 110	Tiny crystallites and larger clumps of crystalline material; glistening; angular appearance of particles	More fluffy; powdery appearance of particles; no crystalline features; no gloss
110 – 114	Appearance unchanged	Particles become more translucent; texture becomes more angular and smooth; more crystalline appearance
114 – 115	Melting begins	Melting begins
117	Completely melted	Completely melted

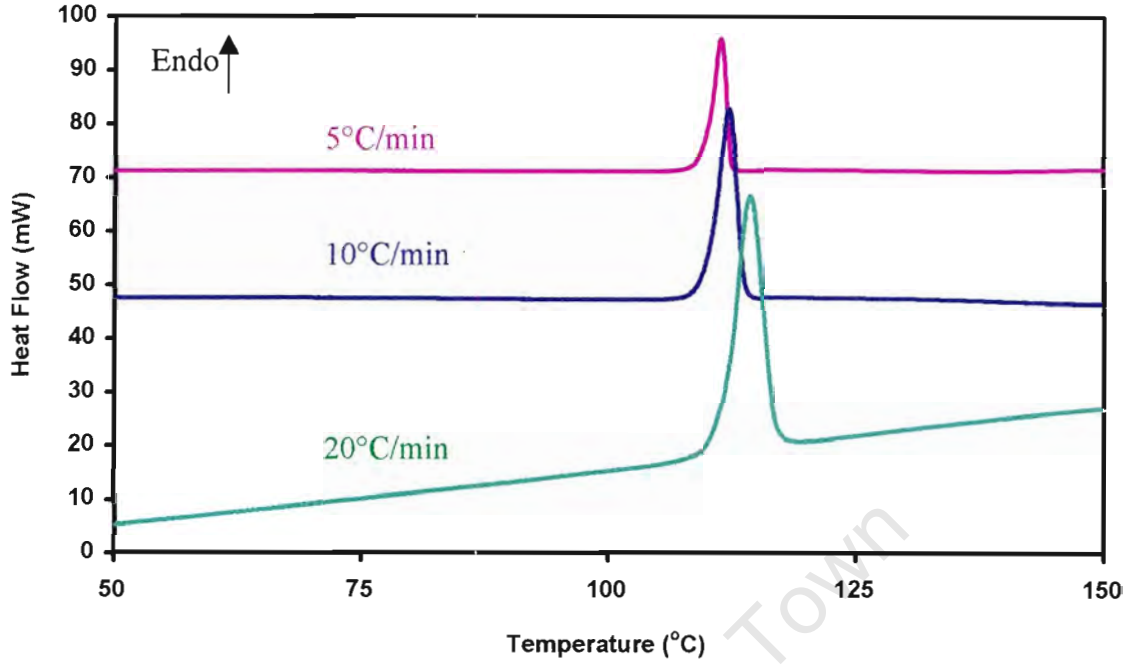

Figure 5.8 DSC traces of the Form 1 polymorph of salbutamol laurate at heating rates of 5, 10 and 20°C/min

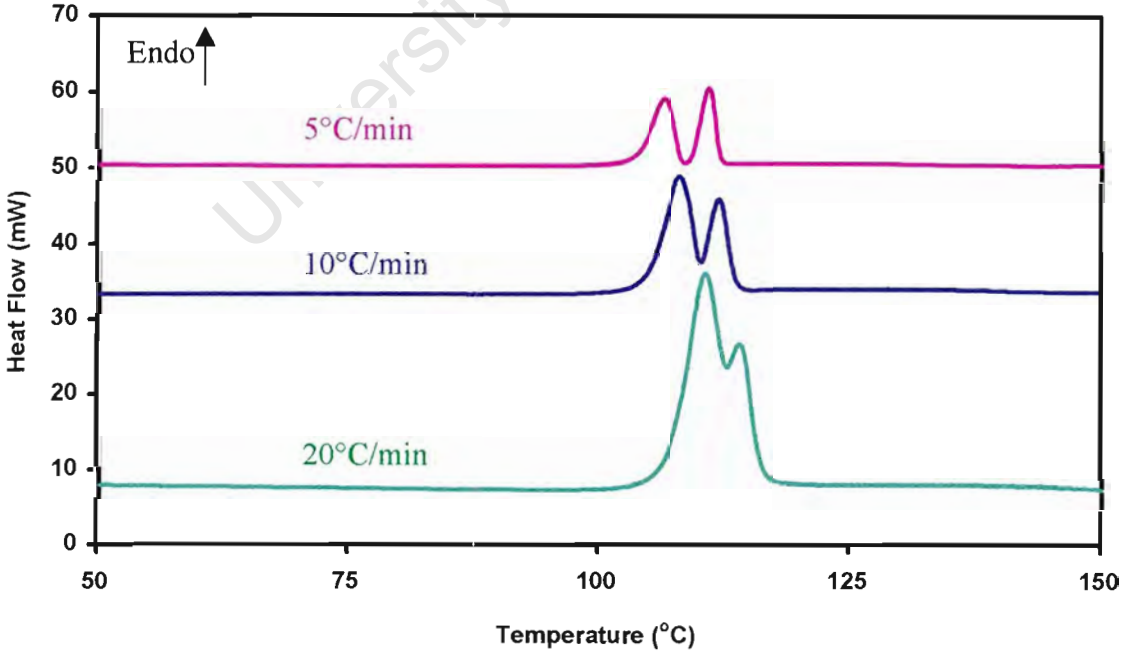

Figure 5.9 DSC traces of the Form 2 polymorph of salbutamol laurate at heating rates of 5, 10 and 20°C/min

SEM

SEM was undertaken in order to examine the differences in morphology, texture and particle size of the two polymorphs (Figures 5.10 and 5.11). It was noted that Form 1 had a crystalline appearance while Form 2 had a more granular appearance. The average particle size of Form 1 was in the range of 10-20μm. The average particle size of Form 2 was considerably larger with most particles in the 200-500μm range.

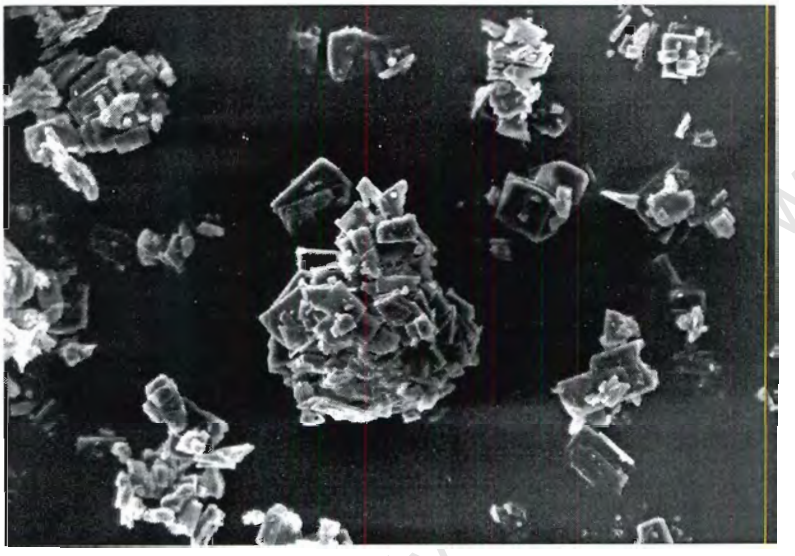

Figure 5.10 SEM photograph of Form 1 of salbutamol laurate (2000x)

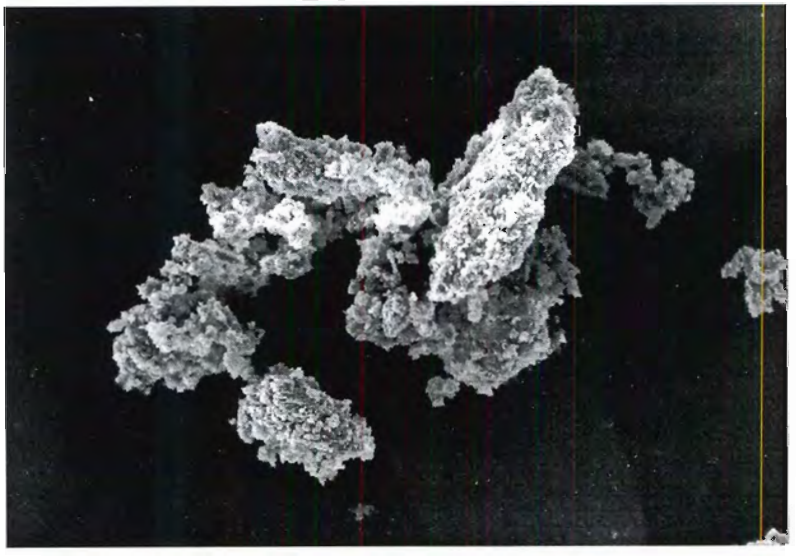

Figure 5.11 SEM photograph of Form 2 of salbutamol laurate (2000x)

Complexation of salbutamol laurate (Form 1) with HP-β-CD

The aim of the investigation was to prepare complexes of salbutamol laurate (Form 1) with HP-β-CD using kneading and co-grinding techniques and using the molar ratios of 1:1 and 1:2 drug:CD. Salbutamol laurate (Form 1) will be referred to as SAL for the remaining portion of this chapter.

Sample preparation:

Samples were prepared in the following ways :

1.) Manual co-grinding using a mortar and pestle
2.) Kneading using a mortar and pestle with small aliquots of water added and then dried in an oven at 60°C for 30min
3.) Mechanical co-grinding using a mechanical grinding apparatus (Wig-L-Bug amalgamator) for 1hr

DSC

DSC experiments were run for all preparations and the melting endotherm for salbutamol laurate was monitored (Table 5.4). DSC conditions were as previously stated (Chapter 2) except that the heating range was 50 to 150°C and the heating rate was 20°C/min. The sample sizes were as follows: SAL (2.0-2.2mg), 1:1 SAL:HP-β-CD preparations (6.0-6.2mg), 1:2 SAL:HP-β-CD preparations (10.0-10.3mg).

The disappearance of the SAL melting endotherm was taken as evidence for complex formation. The presence of uncomplexed, crystalline drug in the preparations was indicated by the presence of the melting endotherm of SAL. The approximate amount of uncomplexed drug was calculated from the heat of fusion of the melting endotherm for SAL. All of the SAL is complexed after manual co-grinding (for 30min), kneading and mechanical co-grinding (for one hour) for both the 1:1 and the 1:2 drug:CD preparations. The melting endotherm of SAL showed a decrease in peak temperature and enthalpy of fusion when the pure drug was ground or kneaded.

Table 5.4 DSC analysis of the SAL melting endotherm

Sample	Conditions	Peak Range (°C)	Onset Temp (°C)	Peak Temp (°C)	Peak Enthalpy J/g (*)	Percentage Uncomplexed Drug (%) (**)
HP-β-CD	As found					
SAL	Raw material	112-126	114	117	103	100
	Co-grnd. 10 min	112-126	114	117	103	100
	Co-grnd. 20 min	105-121	112	114	87	100
	Co-grnd. 30 min	103-120	112	114	84	100
	Kneading	104-121	112	114	85	100
1:1 SAL : HP-β-CD	Phys. mixture	109-125	113	117	88	85
	Co-grnd. 10 min	106-121	110	114	80	78
	Co-grnd. 20 min	100-118	103	110	58	67
	Co-grnd. 30 min	-	-	-	-	0
	Kneading	-	-	-	-	0
	Mech. grnd. 1hr	-	-	-	-	0
1:2 SAL : HP-β-CD	Phys. mixture	90-114	93	102	92	90
	Co-grnd. 10 min	96-112	96	102	53	51
	Co-grnd. 20 min	89-101	89	94	8	9
	Co-grnd. 30 min	-	-	-	-	0
	Kneading	-	-	-	-	0
	Mech. grnd. 1hr	-	-	-	-	0

* Peak enthalpy (J/g) corrected according to the fraction of drug in preparation (correction factor = [mass of drug + mass of CD†] / mass of drug)

** Percentage uncomplexed drug = $\frac{\text{Peak enthalpy of drug endotherm in a preparation}}{\text{Average peak enthalpy of drug alone}}$

† Mass of CD = mass of HP-β-CD (3.2 hydroxypropyls / CD) plus 10% water

Figure 5.12 shows the DSC traces of SAL, HP-β-CD, 1:1 physical mixture of SAL and HP-β-CD and 1:1 kneaded preparation. The disappearance of the SAL melting endotherm is observed for the kneaded preparation.

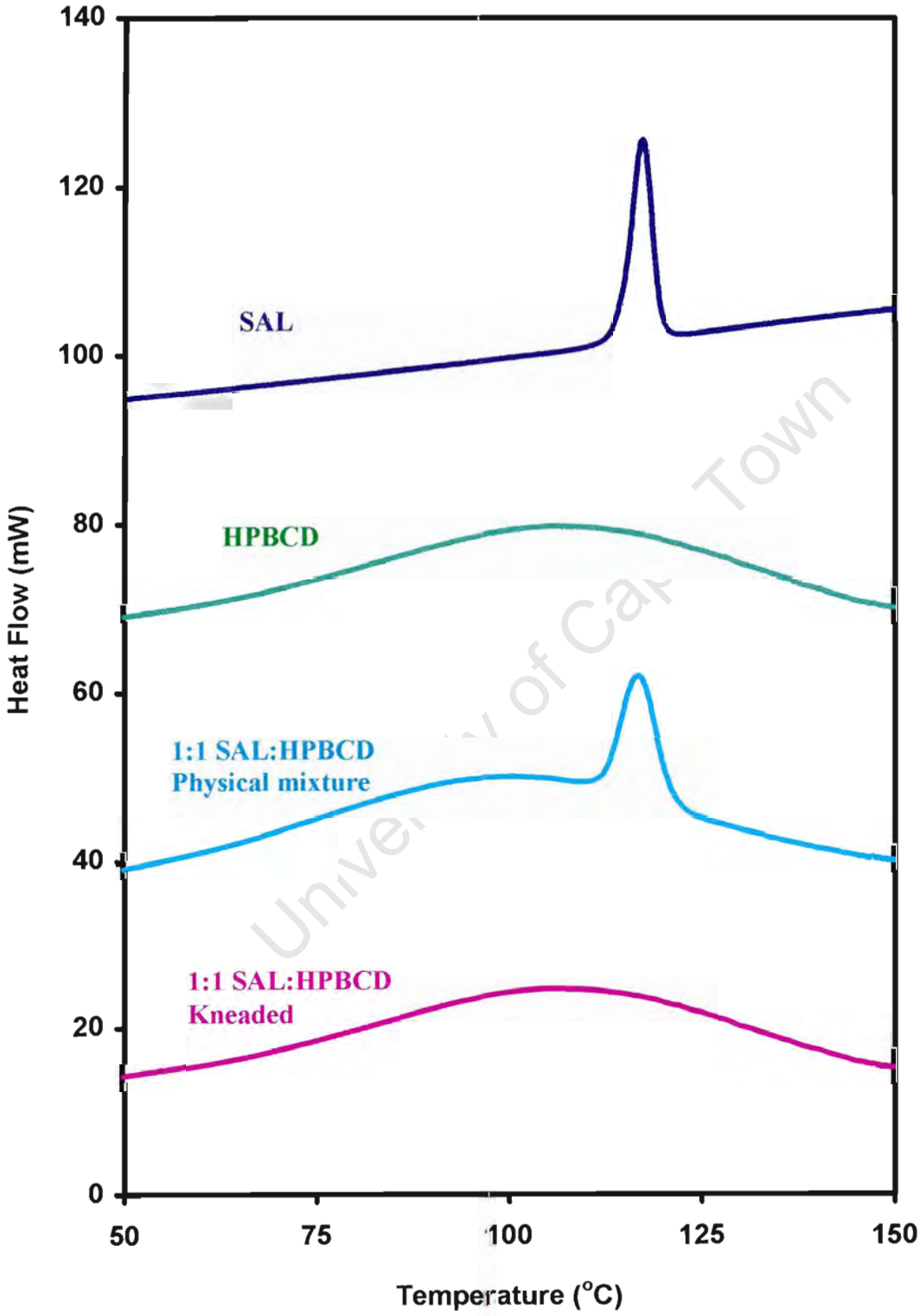

Figure 5.12 DSC traces of SAL, HP-β-CD, 1:2 SAL:HP-β-CD physical mixture and 1:1 SAL:HP-β-CD kneaded preparation

HSM

The various preparations were observed by hot stage microscopy techniques to assess whether differences between complexed and uncomplexed preparations could be detected. HSM conditions are as stated in Chapter 2 with the exception that the heating rate used was 20°C/min. The HSM results for HP-β-CD and SAL are summarised in Table 5.5.

Table 5.5 HSM results for SAL and HP-β-CD

Temperature (°C)	SAL	HP-β-CD
30°C	white powder	white powder
114-115 °C	melting to clear liquid	unchanged
117°C	completely melted	unchanged
170 °C	beginning of decomposition, liquid begins to turn yellow then brown as decomposition continues	unchanged
280°C	completely decomposed	melting to clear liquid

It was noted that physical mixtures as well as the various drug/CD preparations began decomposition at 170°C, which is more than 100°C less than the melting temperature of HP-β-CD (280°C). No drug melt could be observed in physical mixtures of SAL and HP-β-CD or in any other of the SAL/HP-β-CD preparations. However, for the physical mixtures and other preparations where uncomplexed drug had been previously detected by DSC, the white powder of the preparation became speckled with dark yellow patches from 170°C onwards. In contrast, for the preparations that were manually co-ground (for 30 min), kneaded and mechanically co-ground (for 1 hour), the sample became uniformly light yellow from 170°C. All preparations showed discoloration/decomposition from 170°C. The indication was that the interaction with HP-β-CD does not increase the decomposition temperature of SAL.

XRD

XRD powder patterns (CoKα radiation with conditions as stated in Chapter 2) were obtained for all preparations and a number of characteristic peaks of SAL were analysed (Table 5.6). The 2θ range scanned was from 4 to 40° and the sample sizes used were all in the range of 50-52mg.

Table 5.6 Analysis of the characteristic XRD peaks of SAL

Sample	Conditions	2 θ (%I)	2 θ (%I)	2 θ (%I)	2 θ (%I)	2 θ (%I)
HP-β-CD	As found	-	-	-	-	-
SAL	Raw material	8.4 (82)	19.6 (36)	22.9 (47)	24.5 (45)	26.4 (100)
	Co-grnd. 10 min	8.4 (90)	19.6 (53)	22.8 (73)	24.3 (66)	26.2 (100)
	Co-grnd. 20 min	8.4 (44)	19.6 (48)	22.8 (71)	24.3 (62)	26.1 (100)
	Co-grnd. 30 min	8.4 (34)	19.6 (52)	22.8 (70)	24.4 (51)	26.2 (100)
	Kneading	8.4 (47)	19.6 (47)	22.8 (68)	24.4 (49)	26.2 (100)
1:1 SAL:HP-β-CD	Phys. mixture	8.4 (99)	19.6 (48)	22.8 (61)	24.3 (56)	26.1 (100)
	Co-grnd. 10 min	8.4 (69)	19.7 (75)	22.8 (100)	24.4 (79)	26.2 (85)
	Co-grnd. 20 min	8.4 (42)	19.6 (53)	22.8 (100)	24.4 (58)	26.2 (55)
	Co-grnd. 30 min	-	-	-	-	-
	Kneading	-	-	-	-	-
	Mech. grnd. 1hr	-	-	-	-	-
1:2 SAL:HP-β-CD	Phys. Mixture	8.4 (92)	19.6 (62)	22.8 (83)	24.3 (65)	26.2 (100)
	Co-grnd. 10 min	8.4 (56)	19.6 (76)	22.8 (89)	24.3 (77)	26.2 (100)
	Co-grnd. 20 min	8.4 (72)	19.5 (72)	22.8 (100)	24.3 (82)	26.2 (76)
	Co-grnd. 30 min	-	-	-	-	-
	Kneading	-	-	-	-	-
	Mech. grnd. 1hr	-	-	-	-	-

HP-β-CD is a mixture of a number of isomers which have different degrees and patterns of substitution. HP-β-CD is therefore an amorphous substance in the solid state and its XRD trace does not display any characteristic sharp peaks.[31] Any inclusion complex formed with HP-β-CD will likewise be an amorphous substance. Therefore it is not possible to determine a phase change by XRD methods. However, SAL contains a number of relatively sharp and characteristic peaks. The disappearance of these peaks was taken as evidence for inclusion complex formation.

The presence of these peaks in any of the preparations analysed signified the presence of uncomplexed drug and incomplete formation of an inclusion complex of the stoichiometry of the preparation. The characteristic peaks in the XRD trace of SAL occur at 2θ values of 8.4°, 19.6°, 22.8°, 24.4°, 26.2°. XRD proved to be a sensitive technique to detect the presence of uncomplexed SAL. The peak at 2θ = 8.4° is particularly useful for detection of uncomplexed SAL since it is present in a region of the XRD trace where the counts for HP-β-CD are very low. Figure 5.13 shows the XRD traces of SAL, HP-β-CD, a 1:1 physical mixture of SAL and 1:1 SAL:HP-β-CD kneaded preparation. It is evident that the characteristic peaks of SAL are absent from the trace of the kneaded preparation and the pattern resembles that of HP-β-CD.

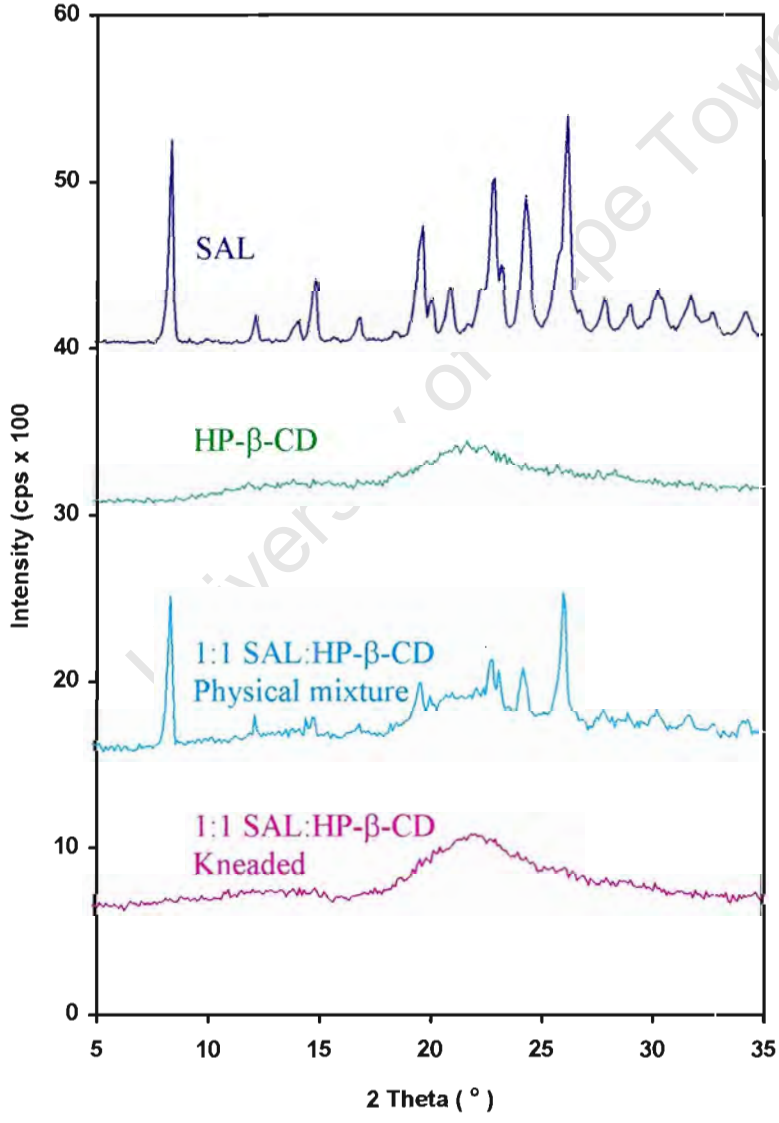

Figure 5.13 XRD traces of SAL, HP-β-CD, SAL:HP-β-CD 1:1 physical mixture and 1:1 SAL:HP-β-CD kneaded preparation

IR

IR spectra were run on all preparations and various IR bands corresponding to HP-β-CD and SAL were analysed (Table 5.7). The IR conditions are as stated in Chapter 2.

Seven of the strongest IR bands common to the various preparations were chosen for analysis. Five of these bands (occurring at wavenumbers of 1032, 1082, 1158, 1377 and 1458 cm^{-1}) were due to overlap of bands from SAL and HP-β-CD; however, these stretches were dominated by the HP-β-CD bands. One of the bands was unique to HP-β-CD (947cm^{-1}). The band at 1545cm^{-1} could be clearly assigned to SAL and is attributed to the C-O asymmetric stretching band for a carboxylate salt.

Table 5.7 Selected IR bands (with percentage transmission in parenthesis) for the various preparations

Conditions	Sample	Peak wavenumbers (cm^{-1}) with percentage transmission in brackets						
HP-β-CD	As found	948 (75)	1032 (42)	1083 (51)	1158 (55)	1376 (53)	1458 (44)	-
SAL	Raw material	-	1036 (84)	1082 (84)	1152 (84)	1377 (60)	1458 (52)	1545 (54)
	Co-grnd. 10 min	-	1036 (69)	1082 (71)	1152 (71)	1376 (61)	1458 (50)	1545 (52)
	Co-grnd. 20 min	-	1036 (78)	1082 (77)	1152 (78)	1377 (58)	1458 (47)	1545 (55)
	Co-grnd. 30 min	-	1036 (72)	1082 (75)	1152 (76)	1377 (57)	1458 (46)	1545 (57)
	Kneading	-	1036 (75)	1082 (77)	1152 (77)	1376 (63)	1458 (53)	1545 (58)
SAL:HP-β-CD 1:1	Phys. Mixture	947 (80)	1034 (62)	1083 (66)	1157 (68)	1376 (50)	1458 (37)	1545 (80)
	Co-grnd. 10 min	947 (81)	1034 (64)	1083 (68)	1155 (71)	1376 (55)	1458 (43)	1545 (78)
	Co-grnd. 20 min	947 (76)	1033 (59)	1083 (64)	1155 (67)	1377 (47)	1458 (34)	1545 (74)
	Co-grnd. 30 min	947 (79)	1030 (62)	1083 (66)	1157 (67)	1377 (43)	1458 (28)	1551 (77)
	Kneading	946 (73)	1030 (56)	1083 (61)	1157 (63)	1377 (40)	1458 (25)	1556 (76)
	Mech. grnd. 1hr	949 (77)	1033 (54)	1082 (61)	1157 (65)	1376 (55)	1458 (22)	1556 (74)
SAL:HP-β-CD 1:2	Phys. Mixture	947 (73)	1033 (54)	1082 (59)	1156 (60)	1377 (36)	1458 (22)	1545 (79)
	Co-grnd. 10 min	947 (76)	1030 (63)	1082 (67)	1158 (67)	1376 (41)	1458 (26)	1545 (81)
	Co-grnd. 20 min	946 (79)	1030 (72)	1082 (76)	1157 (74)	1377 (46)	1458 (30)	1545 (79)
	Co-grnd. 30 min	947 (59)	1029 (43)	1082 (47)	1158 (47)	1377 (18)	1458 (17)	1554 (72)
	Kneading	947 (63)	1031 (58)	1082 (62)	1158 (61)	1377 (25)	1458 (12)	1561 (77)
	Mech. grnd. 1hr	949 (73)	1033 (53)	1082 (58)	1158 (61)	1377 (47)	1457 (35)	1561 (77)

Analysis of the results in Table 5.7 together with careful inspection of the various spectra suggests that all the bands, with the exception of the band at 1545cm^{-1}, seem to remain at a constant frequency throughout the different sample preparations. The 1545cm^{-1} band shifts to higher frequencies for those preparations which were thought to be completely complexed based on the results of the other techniques already employed.

The band at 1545cm^{-1} shifted to 1551cm^{-1} for the 1:1 co-ground (for 30 min) sample and to 1556 cm^{-1} for the 1:1 kneaded and mechanically co-ground samples. The band at 1545cm^{-1} also shifted to 1554cm^{-1} for 1:2 co-ground (for 30 min) sample and to 1661cm^{-1} for the 1:2 kneaded and mechanically co-ground samples.

The shift in the 1545cm^{-1} band seems to be greater in the kneaded and mechanically co-ground samples than the co-ground (for 30min) samples. The shift seems to be greater for the 1:2 than the 1:1 preparations.

Since grinding of the pure drug does not result in any change in the frequency for this band it is suspected that the frequency change on grinding with HP-β-CD could be due to interaction with the CD and is further evidence that an inclusion complex of SAL with HP-β-CD has been formed. However, the broadening of this band that was observed is an indication of a wider variety of molecular environments for SAL. The implication of this might be that the guest assumes a number of orientations within the CD, or that the guest is present in both the included and amorphous forms.

TGA

TGA traces were run for all preparations to quantify the water content (Table 5.8).

TGA conditions were as stated in Chapter 2 with the exception that the heating range was 30-150°C and the heating rate was 20°C/min. The sample sizes used for TGA were as follows : SAL (2-3mg), 1:1 SAL:HP-β-CD preparations (6-7mg), 1:2 SAL:HP-β-CD preparations (10-11mg).

SAL remains anhydrous when subjected to the same treatments used for complex preparation. HP-β-CD contained 7.2 % water corresponding to 5.7 water molecules

per CD molecule. It was noted that the water content per HP-β-CD molecule remained fairly constant through all of the 1:1 and 1:2 preparations with the exception of the mechanically co-ground preparations. The water content per CD molecule was found to be 5.6 water molecules for the mechanically co-ground samples and approximately seven water molecules for all other preparations.

Table 5.8 TGA data for the various preparations of SAL and HP-β-CD

Sample	Conditions	Weight loss range (°C)	Percentage weight loss (%)	Water molecules / HP-β-CD (*)
HP-β-CD	as found	30-130	7.2	5.7
SAL	Raw material	-	0	0
	Co-grnd. 10 min	-	0	0
	Co-grnd. 20 min	-	0	0
	Co-grnd. 30 min	-	0	0
	Kneading	-	0	0
1:1 SAL : HP-β-CD	Phys. mixture	30-130	6.5	6.8
	Co-grnd. 10 min	30-130	6.3	6.5
	Co-grnd. 20 min	30-130	6.8	7.1
	Co-grnd. 30 min	30-130	6.4	6.7
	Kneading	30-130	6.4	6.7
	Mech. grnd. 1hr.	30-130	6.2	5.7
1:2 SAL : HP-β-CD	Phys. Mixture	30-130	7.5	6.9
	Co-grnd. 10 min	30-130	7.7	7.1
	Co-grnd. 20 min	30-130	7.6	7.0
	Co-grnd. 30 min	30-130	7.6	7.0
	Kneading	30-130	7.4	6.8
	Mech. grnd. 1hr.	30-130	5.4	5.7

* Number of H_2Os / CD = $\frac{(\%H_2O \text{ from TGA}) [M_r \text{ HP-β-CD} + M_r \text{ SAL (SAL / HP-β-CD molar ratio)}]}{(M_r H_2O)(100-\%H_2O \text{ from TGA})}$

Conclusion

The presence of two polymorphic forms of salbutamol laurate was detected and these Form 1 and Form 2 polymorphs were characterised by various physicochemical techniques.

The preparations of SAL and HP-β-CD that were found to contain no significant traces of uncomplexed crystalline drug were identified as preparations of an inclusion complex. This was the case for the 1:1 and 1:2 SAL:HP-β-CD preparations which were manually co-ground (for 30 min), kneaded and mechanically co-ground (for 1 hour).

DSC and XRD were found to be the most useful techniques for determining the presence and quantity of uncomplexed SAL. Disappearance of the crystalline phase of SAL was used as evidence for the formation of a CD complex in this study. However, it must be remembered that amorphization of a drug substance can result from the co-grinding or kneading of drug-cyclodextrin systems and it must be considered when thermal profiles and X-ray diffraction patterns on powder are evoked as evidence of inclusion.[32]

IR spectroscopy provided an alternative method of evaluating the CD-drug preparations. The shift of the C-O asymmetric stretching band of SAL to higher frequencies in preparations was taken as further evidence that inclusion of SAL with HP-β-CD had occurred. HSM also showed that preparations of the inclusion complexes behaved somewhat differently from their corresponding physical mixtures.

References

1.) A. T. Stevens, *MSc. Thesis, The Optical Resolution of Albuterol* , University of Cape Town, February 1998.

2.) B. Koppenhoefer, U. Epperlein, B. Christian, Y. Chen, Y. Ji, and B. Lin, *J. Chromatogr., A*, **1995**, 717(1+2), 181.

3.) B. Koppenhoefer, U. Epperlein, B. Christian, B. Lin, Y. Ji, and Y. Chen, *J. Chromatogr., A*, **1996**, 735(1+2), 333.

4.) B. Koppenhoefer, U. Epperlein, X. Zhu and B. Lin, J., *Electrophoresis*, **1997**, 18(6), 924.

5.) B. Koppenhoefer, U. Epperlein, R. Schlunk, X. Zhu and B. Lin, *J. Chromatogr., A*, **1998**, 793(1), 153.

6.) B. Lin, X. Zhu, B. Koppenhoefer and U. Epperlein, *LC-GC*, **1997**, 15(1), 40, 44.

7.) A. Aumatell and R. J. Wells, *J. Chromatogr., A*, **1994**, 688(1+2), 329.

8.) A. Aumatell, R. J. Wells and D. K. Y. Wong, *J. Chromatogr., A*, **1994**, 686(2), 293.

9.) I. Bjoernsdottir and S. H. Hansen, *Chirality*, **1995**, 7(4), 229.

10.) M. Heurermann and G. Blaschke, *J. Chromatogr.*, **1993**, 648(1), 267.

11.) S. K. Branch, U. Holzgrabe, T. M. Jefferies, H. Mallwitz and M. W. Matchett, *J. Pharm. Biomed. Anal.*, **1994**, 12(12), 1507.

12.) S. K. Branch, U. Holzgrabe, T. M. Jefferies, H. Mallwitz and F. J. R. Oxley, J. *Chromatogr., A*, **1997**, 758(2), 277.

13.) Z. Ruan, M. Yuan, Q. Ou and W. Yu, *Fenxi Huaxue*, **1997**, 25(6), 743.

14.) M. Rogan, K. D. Altria and D. M. Goodall, *Electrophoresis*, **1994**, 15(6), 808.

15.) O. Staalberg, H. Broetell and D. Westerlund, *Chromatographia*, **1995**, 40(11/12), 697.

16.) H. Jakubetz, M. Juza and V. Schurig, *Electrophoresis*, **1997**, 18(6), 897.

17.) Y. Tanaka, M. Yuanagawa and S. Terabe, *J. High Resolut. Chromatogr.*, **1996**, 19(8), 421.

18.) A. Badwan, A. Abumalooh, M. Haddadin and H. Ibrahim, **U.S. US 5,646,131** (Cl.514-58; A61K31/715), 8 Jul 1997, US Appl. 199,523, 22 Feb 1994; 10pp.

19.) G. A. Elger, S. T. Leslie, S. T. A. Malkowska, R. B. Miller and P. J. Neale, **Eur. Pat. Appl. 251,459**, (Cl. A61K9/22), 07 Jan 1988, GB Appl. 86/13,688, 05 Jun 1986, 26 pp.

20.) V. Lemesle-Lamche, D. Wouessidjewe, M. Cheron and D. Duchene, *Int. J. Pharm.*, **1996**, 141(1,2), 117.

21.) V. Lemesle-Lamche, M. Taverna, D. Ferrier, D. Duchene and D. Wouessidjewe, *World Meet. Pharm., Biopharm. Pharm. Technol., 1st*, **1995**, 603.

22.) V. Lemesle-Lamche, M. Taverna, D. Wouessidjewe, D. Duchene and D. Ferrier, *J. Chromatogr., A.*, **1996**, 735(1+2), 321.

23.) D. Wouessidjewe, V. Lemesle-Lamche, D. Duchene and B. Perly, *J. Inclusion Phenom. Mol. Recognit. Chem.*, **1996**, 25(1-3) 109.

24.) H. M. Cabral Marques, J. Hadgraft and I. W. Kellaway, *Int. J. Pharm.*, **1990**, 63(3), 259.

25.) H. M. Cabral Marques, J. Hadgraft, I. W. Kellaway and W. J. Pugh, *Int. J. Pharm.*, **1990**, 63(3), 267.

26.) H. M. Cabral Marques, J. Hadgraft, I. W. Kellaway and G. Taylor, *Int. J. Pharm.*, **1991**, 77(2-3), 303.

27.) F. Hirayama, M. Yamanaka, T. Horikawa and K. Uekama, *Chem. Pharm. Bull.*, **1995**, 43(1), 103.

28.) F. Hirayama and K. Uekama, *Pharm. Tech. Jpn.*, **1995**, 11(1), 19.

29.) F. Hirayama, M. Yamanaka, T. Horikawa and K. Uekama, *Pharm. Sci.*, **1995**, 1(11), 517.

30.) L. J. Penkler, South African Druggists International, personal communication.

31.) C. T. Rao, H. M. Fales and J. Pitha, *Pharm. Res.*, **1990**, 7, 612.

32.) S. Y. Lin, Y. H. Kao and J. Yang, *Drug. Dev. Ind. Pharm.*, **1988**, 14, 99.

CHAPTER 6 : CD-INCLUSION COMPLEXES WITH CYCLIZINE

Introduction

Cyclizine is a member of the group of compounds known as the H_1 antagonists, which are all reversible, competitive inhibitors of the interaction of histamine with the H_1-receptors. The action of histamine on H_1-receptors in the body controls a number of physiological responses, which include smooth muscle responses, capillary permeability changes, immediate hypersensitivity reactions (anaphylaxis and allergy) and central nervous system responses. The mechanism of action of the H_1 antagonists is to inhibit the physiological responses to histamine by binding to the H_1-receptors in the body and limiting the binding of endogenous histamine. The various types of H_1 antagonists are designed to act on different H_1-receptors in the body and consequently have different therapeutic uses.

Most H_1 antagonists have a tertiary amino group linked via a chain to two aromatic substituents to replace the primary amine and single aromatic ring of histamine. The H_1 antagonists in clinical use are grouped according to their structure into the ethanolamine, alkylamine, piperazine, piperidine and phenothiazine classes. Cyclizine is a member of the piperazine class of H_1 antagonists. The cyclizine molecule contains a piperazine ring linked by the amine nitrogen atoms to diphenylmethyl and methyl substituents. The chemical structure and numbering scheme of cyclizine used in the crystal structure analysis are shown in Figure 6.1.

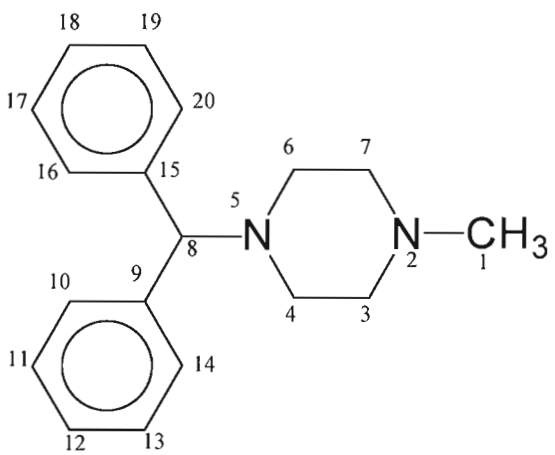

Figure 6.1 The structure of cyclizine and numbering for the structure analysis

As a drug, cyclizine falls more broadly into the category of antiemetics and anti-nauseants and is used to prevent and treat motion sickness, vertigo, nausea and vomiting. The drug is most commonly available for clinical usage in the form of its hydrochloride salt which is marketed as VALOID™.

The hydrochloride salt of cyclizine is moderately soluble in water while the free base has a solubility in water of < 0.001g/ml at 25°C. Both the free base and the hydrochloride salt are light sensitive and therefore the compounds need to be protected from light during storage.[1]

A thorough search of Chemical Abstracts from 1972 to July 1998 produced three papers which dealt with the study and applications of cyclizine with various CDs.

Solution calorimetry was used to evaluate the stability constants and enthalpy changes associated with complexation of 13 amine drugs with the diphenylmethyl functionality with α-, β- and γ-CD.[2] The thermodynamic parameters and binding constants for the interaction of cyclizine hydrochloride, chlorcyclizine.HCl and chlorcyclizine.2HCl with α-, β- and γ-CD in aqueous solution were calculated at 25°C and are presented in Table 6.1.

Table 6.1 Thermodynamic parameters and binding constants for 1:1 complexes of Cyclizine.HCl, Chlorcyclizine.HCl and Chlorcyclizine.2HCl with α-, β- and γ-CD

Compound	CD	ΔH (kJ/mol)	K (M^{-1})	ΔG° (kJ/mol)	ΔS° (J/mol.K)
Cyclizine.HCl	α	-20.04 ± 1.00	48.4 ± 3.65	-9.62	-35.0
	β	-28.83 ± 1.46	1215.2 ± 95.4	-17.61	-37.6
	γ	-4.11 ± 0.03	731.9 ± 18.1	-16.35	41.1
Chlorcyclizine.HCl	α	-24.43 ± 0.80	114.1 ± 66.3	-17.39	-23.5
	β	-24.08 ± 1.25	2461.9 ± 338.0	-19.36	-15.8
	γ	-8.16 ± 0.07	1298.9 ± 51.2	-17.77	32.2
Chlorcyclizine.2HCl	α	-23.44 ± 0.92	1111.6 ± 9.5	-17.40	-20.3
	β	-22.77 ± 0.97	2404.5 ± 96.5	-19.36	-11.4
	γ	-7.21 ± 0.05	1108.5 ± 35.9	-17.38	34.1

The authors drew a number of conclusions from the results presented in Table 6.1 together with results obtained for the interaction of eleven other amine drugs, all containing the diphenylmethyl functionality, with CDs.

Some of these conclusions are summarised below :

1.) β-CD forms the strongest interactions with amine drugs with the diphenylmethyl functionality and the order of stability for the complexes is β-CD > γ-CD > α-CD.
2.) One of the phenyl groups of the diphenylmethyl functionality inserts into the CD cavities.
3.) The amine functional group does not penetrate the CD cavity.
4.) A methyl or halogen substituent on the aromatic ring increases the stability of the complexes.
5.) Van der Waals interactions are important in complex formation for α- and β-CD while complex formation with γ-CD is largely entropically driven.

Conclusions 2, 3 and 4 were also drawn by the same authors when the interactions of HP-β-CD with twelve amine drugs with the diphenylmethyl functionality were investigated.[3]

Molecular modelling techniques were used to study the complexation of cyclizine, as well as ten other amine drugs with the diphenylmethyl functionality, with α-, β- and γ-CD.[4] The computer generated minimum energy structures for the α-CD and β-CD inclusion complexes with cyclizine.HCl are shown in Figure 6.2 and Figure 6.3 respectively. The studies found that the aromatic ring (shaded yellow) was preferentially included in the cavities of α- and β-CD and that only a single aromatic ring could fit into the cavity at one time. It was also found that the phenyl ring does not penetrate as deeply into the α-CD cavity since there is an energy barrier which prevents it from passing through the narrowest part of the cavity. No such energy barrier exists for the inclusion of the aromatic ring into the β-CD cavity. The phenyl ring included in the cavities of both α- and β-CD appears to be tilted somewhat in order to reduce repulsion between the other phenyl ring and the secondary rim of the CDs. It is possible for the cyclizine molecule to have one or both phenyl rings included in the γ-CD cavity.

The two alternative binding possibilities gave similar binding energies and therefore some uncertainty existed over which mode of insertion would be preferred in the γ-CD complexes. The authors concluded that cyclizine.HCl and ten other diphenylmethyl functionalised amines preferentially approach the CD cavities of α-, β- and γ-CD from their more open secondary hydroxyl sides. Insertion from the smaller primary hydroxyl aperture results in more unfavourable contacts between other parts of the guest molecules and the primary hydroxyl groups. Calculations also showed that it was energetically unfavourable to include the protonated amine group into the CD cavity. The calculated binding energies of the complexes of 13 amine drugs with the diphenylmethyl functionality with α-, β- and γ-CD showed good correlation with the stability constants obtained from solution calorimetric titrations.

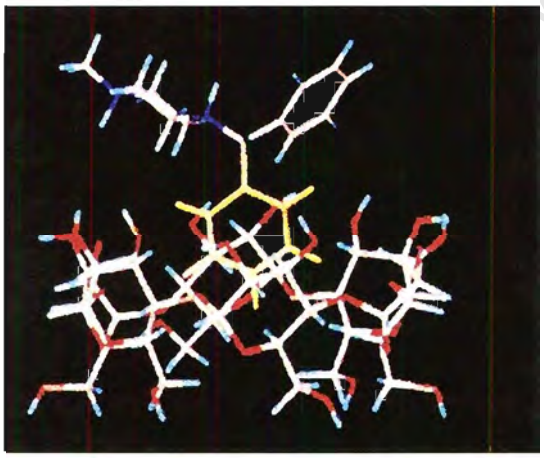

Figure 6.2 Minimum energy structure for the interaction between cyclizine.HCl and α-CD

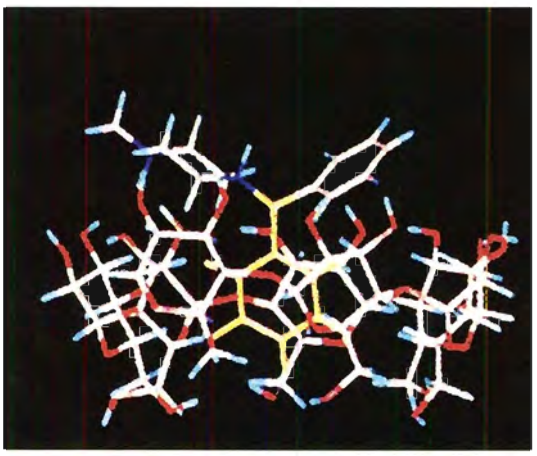

Figure 6.3 Minimum energy structure for the interaction between cyclizine.HCl and β-CD

As the therapeutic use of cyclizine is as an anti-nausea and anti-emetic, a more rapid dissolution and absorption rate for the drug is highly desirable. Administration of cyclizine in the form of a CD dosage form could enhance the dissolution and absorption of the drug, as well as increase the chemical stability. Cyclizine base is less polar than the hydrochloride salt form and is therefore a more suitable candidate for CD complexation. The solubility and dissolution rate from tablets of a CD dosage form of cyclizine base would then need to be compared to that of the hydrochloride powder and tablets to investigate whether CD complexation provides a cyclizine dosage form with enhanced solubility and dissolution characteristics.[5]

The aim of investigation was to prepare crystalline complexes of cyclizine (hereafter referred to as CYC) with β- and γ-CD and characterise them fully in the solid state to provide physicochemical characterisation of the complexes. This would be necessary in order to facilitate the investigation of CD dosage forms of cyclizine with possible application for oral administration in tablet form. It is hoped that such a CD complexed cyclizine formulation would display a much enhanced rate of absorption and dissolution and provide cyclizine in a rapidly acting form.

Preparation of free base of cyclizine from the hydrochloride salt

The hydrochloride salt of cyclizine (5g) was dissolved in distilled water. A saturated solution of sodium carbonate (pH=10) was added and the mixture was extracted with ethyl acetate (x3). The combined organic extract was washed with aqueous saturated sodium chloride (x3), dried over $MgSO_4$, and concentrated under reduced pressure to yield the free base of cyclizine (3.87g, 88% yield).

Complex preparation

The crystalline complexes of CYC with β- and γ-CD were obtained from slow cooling of hot aqueous solutions of CD and CYC. The solutions were prepared according to the concentrations and molar ratios listed in Table 6.2. The complexes of cyclizine with β- and γ-CD will be referred to hereafter as CYCBCD and CYCGCD respectively. Photographs of crystals of the two complexes are shown in Figure 6.4. The photographs are taken on a microscope under plane polarised light at a magnification of 10x and illustrate the morphologies and sizes of the crystals of the two complexes.

Table 6.2 The details of the preparation of the CYCBCD and CYCGCD complexes

Complex	CD (mmol)	Drug (mmol)	Molar ratio	Water (ml)
CYCBCD	0.30	0.30	1 : 1	4
CYCGCD	0.44	0.44	1 : 1	2

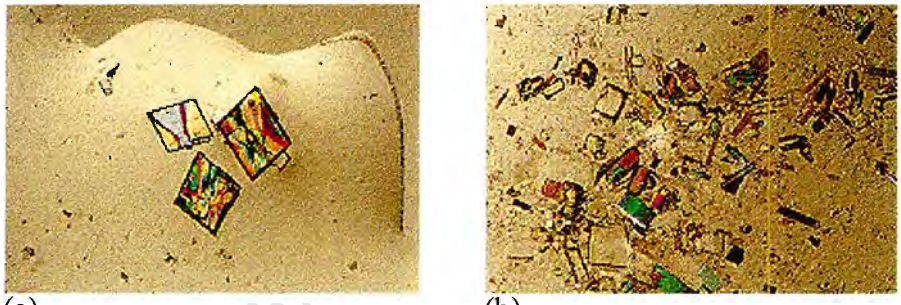

(a) (b)

Figure 6.4 Photographs of the (a) CYCBCD and (b) CYCGCD complexes taken on a microscope under plane polarised light at a magnification of 10x.

UV Spectrophotometry

The host:guest ratios were determined by UV spectrophotometry at 225nm in 0.1M HCl and are shown in Table 6.3.

Table 6.3 The host:guest ratios determined from UV spectrophotometry for CYCBCD and CYCGCD

Complex	CYCBCD	CYCGCD
Host : Guest ratio	4 : 3	3 : 1

Microanalysis

The host:guest ratios were confirmed by C, H and N microanalysis results (Table 6.4). The complexes were dried under vacuum for 1 hour and thermogravimetric analysis was used to determine the residual water content of the samples to be analysed.

Table 6.4 The C, H and N microanalysis results for CYCBCD and CYCGCD

Complex	Calculated (%)			Experimental (%)		
	C	H	N	C	H	N
CYCBCD.4H_2O	47.38	6.72	1.49	47.48	6.66	1.49
CYCGCD.3H_2O	45.02	6.49	0.64	45.30	6.50	0.73

Water content

The total water content of the complexes was calculated from the initial mass losses obtained from TGA traces of CYCBCD and CYCGCD (Table 6.5).

Table 6.5 The percentage water loss from the CYCBCD and CYCGCD complexes and the number of water molecules per CD molecule for each of the complexes

Complex	% weight loss	Temperature range (°C)	No. of water molecules / CD
CYCBCD	14.2	30-130	12.5
CYCGCD	16.7	30-130	16.4

Stoichiometric formulae

The full stoichiometric formulae of the complexes obtained from the TGA, UV and microanalysis results are presented in Table 6.6.

Table 6.6 The H:G:Water ratios and stoichiometric formulae for CYCBCD and CYCGCD

Complex	H : G : Water	Stoichiometric formula
CYCBCD	4 : 3 : 50	$4(C_{42}H_{70}O_{35})\cdot 3(C_{18}H_{22}N)\cdot 50(H_2O)$
CYCGCD	3 : 1 : 49.2	$3(C_{48}H_{80}O_{40})\cdot 1(C_{18}H_{22}N)\cdot 49.2(H_2O)$

HSM

HSM was used to analyse the thermal behaviour of the complexes upon heating at a constant heating rate of 10°C/min. The HSM results for CYCBCD and CYCGCD are presented in Figure 6.5.

After removal from mother liquor, both complexes displayed signs of cracking as the crystals begin to lose their water of crystallisation. At 130°C the complexes have become opaque. TGA results (Figures 6.6 and 6.7) show that water loss is complete by this temperature. The crystals of the two complexes remain unchanged from 130 to 250°C. At 250°C they begin to turn light brown in colour indicating the first signs of decomposition of the complexes. Decomposition begins at a relatively slow rate and accelerates over the intervals 250-270°C, 270-300°C and 300-350°C. This is more clearly shown from the TGA results presented in Table 6.7. At 350°C the crystals of the two complexes are completely black and charred.

TGA

The TGA results for both the CYCBCD and CYCGCD complexes show similar features (Figures 6.6 and 6.7). A summary of the observed percentage weight losses is presented in Table 6.7. Weight losses from 30 to 130°C represent water loss from the complexes. From 130° to 250°C no significant weight loss is observed. From 250°C onwards, weight loss due to decomposition of the complexes is observed. The weight loss due to decomposition accelerates in an exponential manner from 250°C onwards.

Table 6.7 The percentage weight losses for the CYCBCD and CYCGCD complexes at various temperatures

Temperature (°C)	CYCBCD		CYCGCD	
	Sample weight (%)	Δ Weight loss (%)†	Sample weight (%)	Δ Weight loss (%)†
30	100.0	-	100.0	-
130	83.3	16.7	85.8	14.2
250	83.3	0.0	85.8	0.0
270	82.0	1.3	85.0	0.8
300	78.0	4.0	83.0	2.0
350	15.0	63.0	26.0	57.0

† ΔWeight loss (%) = [Sample weight (%) at temperature(n-1)] - [Sample weight (%) at temperature(n)]

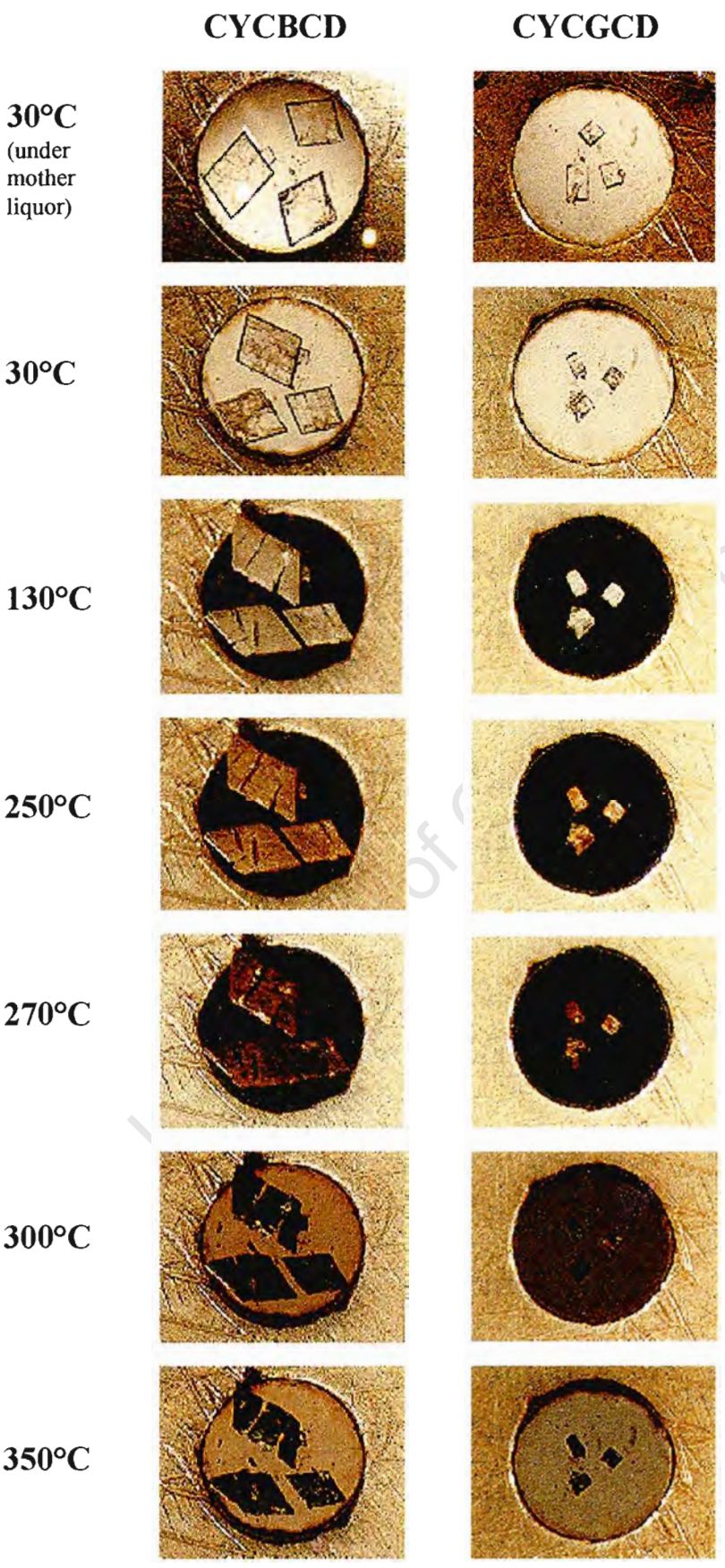

Figure 6.5 HSM photographs taken at various temperatures for crystals of the CYCBCD and CYCGCD complexes

DSC

The DSC traces for the CYCBCD and CYCGCD are fairly similar displaying many common features (Figures 6.6 and 6.7).

Both traces display a fairly sharp endotherm in the temperature range 30°C to 130°C corresponding to water loss from the complexes. The peak of this water loss endotherm (labelled A) occurred at 82°C for CYCBCD with a shoulder at 114°C. The corresponding peak for CYCGCD occurs at 96°C (labelled A) with a weak shoulder at 120°C. The shoulders on the peaks indicate in each case that water loss is a multi-step process. The major peak of the water loss endotherm represents the release of the bulk of the water content of the complexes while the shoulder represents the more tightly bound water which is released only at a higher temperature.

From 130°C to 250°C the DSC traces of both complexes lack any significant endo- or exothermic peaks. For the CYCBCD and CYCGCD complexes a fairly small endotherm (labelled B) with its peak at 250°C indicates the beginning of decomposition for the complexes. This is in agreement with the HSM and TGA results which show decomposition beginning at this temperature (Figures 6.5, 6.6 and 6.7). The onset of decomposition at 250°C is followed by a shallow exotherm at 270°C for CYCBCD (labelled C) and 275°C for CYCGCD (labelled C). This is a further thermal event associated with the continuing decomposition of both complexes.

The final stages of decomposition of these complexes are characterised by a broad exotherm with a bimodal peak at 330°C for CYCBCD and a peak at 333°C for CYCGCD (labelled D). This is followed by endothermic peaks at 342°C for both complexes. Interpretation of the thermal events occurring during the final stages of decomposition is complicated by the significant loss of mass relative to the original sample which affects the baseline of the trace.

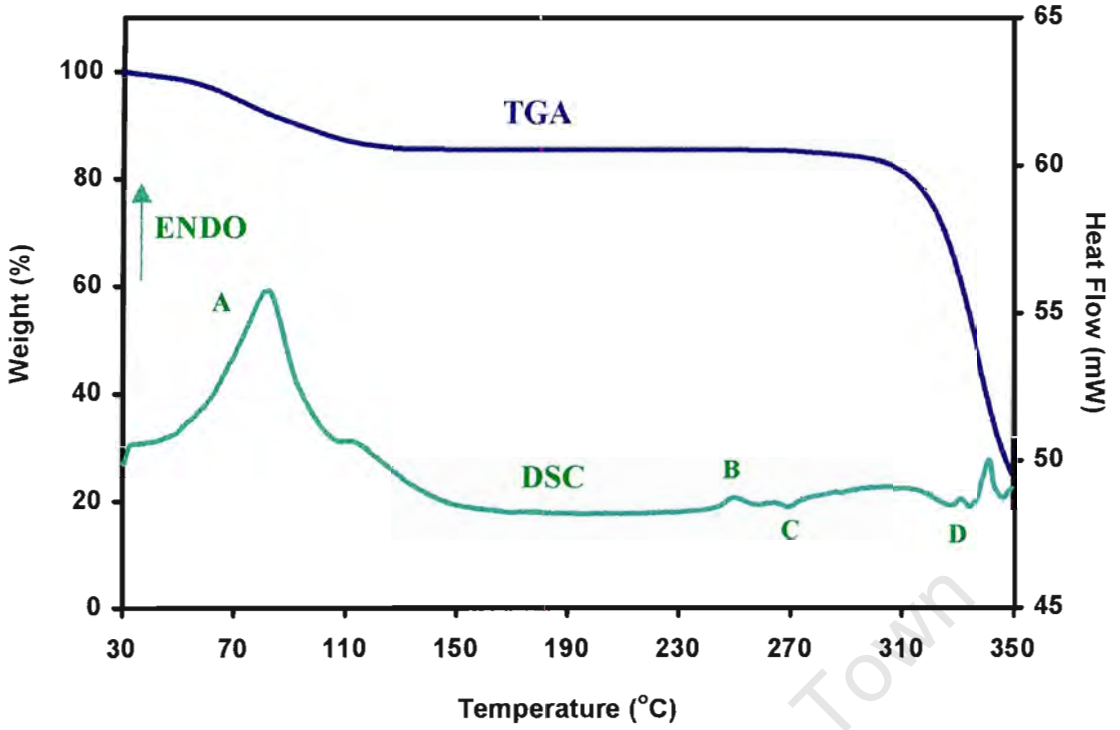

Figure 6.6 DSC and TGA traces for the CYCBCD complex

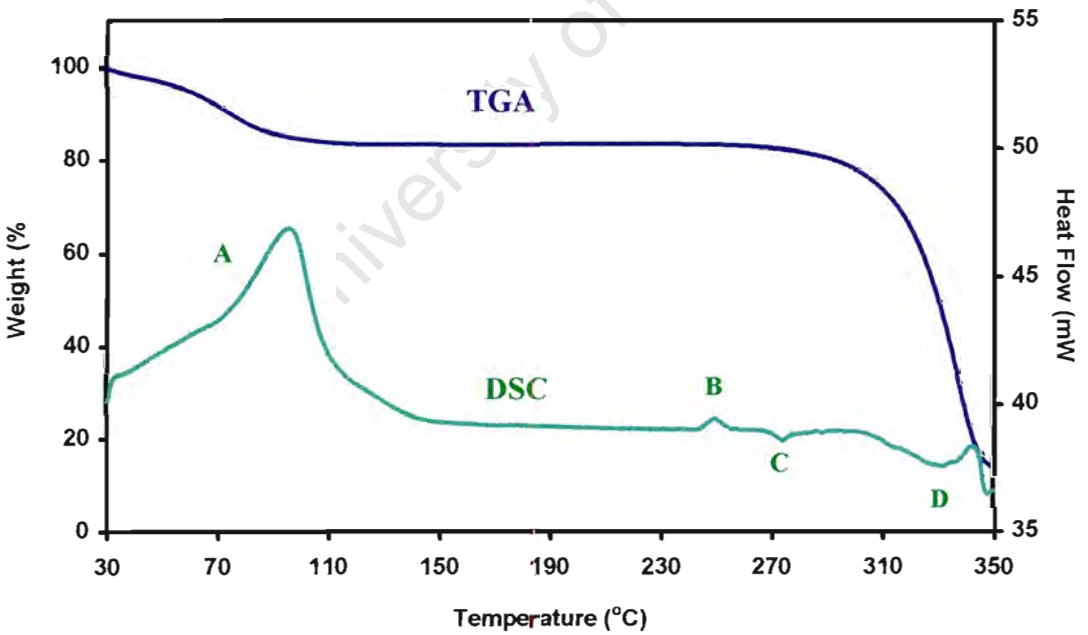

Figure 6.7 DSC and TGA traces for the CYCGCD complex

X-ray crystallographic analysis of the CYCBCD structure

Data-collection

The preliminary cell parameters and space group for the CYCBCD structure were determined by x-ray photographic techniques. The later revealed Laue 2/*m* symmetry and reflections condition $0k0$: k = 2n which indicated the monoclinic space groups $P2_1$ or $P2_1/m$. Since the host is chiral the former space group was chosen. A crystal of the complex was mounted under mother liquor in a Lindemann capillary tube and data were collected at 293K on a Nonius Kappa CCD diffractometer. The long crystal axis of 65Å created certain problems with the resolution of the frames. The data-collection strategy was optimised empirically by the author to achieve the best possible resolution over all frames. Data were corrected for Lorentz-polarisation effects but not for absorption, since μ = 1.209cm^{-1} represented negligible absorption for the size of crystal used. The crystal data parameters are listed in Table 6.8 and details of the data-collection strategy are given in Table 6.9.

Table 6.8 Crystal data parameters for the CYCBCD structure

Crystal Data	
Molecular formula	$4(C_{42}H_{70}O_{35}).3(C_{18}H_{22}N_2).50(H_2O)$
M_r (g.mol^{-1})	6238.92
Crystal system	Monoclinic
Space group	$P2_1$
Z	2
a (Å)	15.246 (1)
b (Å)	65.075 (5)
c (Å)	15.609 (1)
α (°)	90
β (°)	102.62 (1)
γ (°)	90
V (Å^3)	15112 (2)
D_c (g.cm^{-3})	1.3713
μ (Mo Kα) (cm^{-1})	1.207
F (000)	6680.0
Crystal dimensions (mm)	0.4 x 0.4 x 0.3
Temperature	293 K
Radiation, λ	Mo Kα (0.71069 Å)

Table 6.9 Data-collection parameters for the CYCBCD structure

Data Collection	
Diffractometer	Nonius Kappa CCD
Set 1	
ϕ	0.0°
θ	18.0°
κ	0.0°
ω	180.0°
Dx	70mm
Number of frames collected	400
Rotation axis / angle	ϕ rotations, $\Delta\phi = 0.5°$
Exposure time / frame	40 sec (x2)
Number of reflections	31843
Set 2	
ϕ	57.0°
θ	18.0°
κ	-134.75°
ω	-140°
Dx	70mm
Number of frames collected	110
Rotation axis / angle	ω rotations, $\Delta\omega = 0.5°$
Exposure time / frame	40 sec (x2)
Number of reflections	10061
Set 3	
ϕ	-122.0°
θ	18.0°
κ	-134.75°
ω	-140°
Dx	70mm
Number of frames collected	110
Rotation axis / angle	ω rotations, $\Delta\omega = 0.5°$
Exposure time / frame	40 sec (x2)
Number of reflections	9795

Refinement and structure solution

The solution of the CYCBCD structure represented a highly complex crystallographic problem mainly because of the large number of non-hydrogen atoms which needed to be located. Eight CD molecules are contained in the unit cell (which had dimensions of approx. *a,c* =15Å and *b* = 65Å). In the monoclinic space group $P2_1$, this represented four crystallographically independent CD molecules. According to the stoichiometric formula, three CYC molecules and 50 water molecules also needed to be located for the complete structure solution.

The structure was solved using the program PATSEE[6] which uses Patterson and direct methods to position a fragment of known geometry in a unit cell. Initial attempts using a single β-CD molecule as the molecular fragment failed to produce a model which could be refined successfully. Further attempts using a search model of two β-CD molecules arranged in a head-to-head dimer produced a starting model with favourable statistics from the PATSEE run (*viz.* RFOM = 0.435, TFOM = 1.000, CFOM = 0.963 and R_E = 0.259). Partial structure expansion of the correctly positioned dimer in SHELXS[7] produced most of the atoms of the CD backbones of two further cyclodextrin molecules. The coordinates of the four CD molecules excluding the primary hydroxyl oxygen atoms were successfully refined in SHELXL-93.[8] Difference electron density maps based on initial refinements revealed many of the primary hydroxyl oxygen atoms as well as fragments of the cyclizine molecules. Further refinement led to the placement of all the non-hydrogen atoms of three cyclizine molecules and the remaining primary hydroxyl oxygen atoms. All 28 of the primary hydroxyl oxygen atoms were assigned full site-occupancy and refined with isotropic temperature factors in the range 0.05 to 0.17Å^2. No significant electron density corresponding to disordered primary hydroxyls was present. This was a fairly unusual feature of the structure as disorder of the primary hydroxyl groups of the native CDs is fairly common. Refinement proceeded with the placement of water molecules, addition of geometrically fixed hydrogen atoms to CD carbon atoms, the placement of all CD hydroxyl hydrogen atoms using the rotating group refinement (AFIX 147) strategy and the addition of idealised hydrogen atoms for the guest molecules. The hydrogen atoms of each CD and each guest molecule were refined using a common isotropic temperature factor. After many successive refinements, 31 water molecules with full site-occupancy were placed with final isotropic temperature

factors in the range 0.08 to 0.20Å^2. A further 14 molecules with site-occupancy of less than one were refined with fixed isotropic temperature factors of 0.20Å^2 and varying site-occupancy. The site-occupancies of these water molecules varied from 0.55 to 0.95 and they amounted to a further 10.5 water molecules in the asymmetric unit. The 41.5 water molecules located compared favourably with the 50 water molecules expected from TGA analysis. Refinement was isotropic for all 413 non-hydrogen atoms.

Anisotropic refinement was not considered as it would have produced an unfavourable data to parameter ratio. The latter stages of refinement were performed using the blocked mode in SHELXL-93, with the parameters divided into two blocks. This was because the maximum limit of refinable parameters (1500) had been exceeded with the 1747 parameters used in the final refinement. Details of the final refinement parameters are listed in Table 6.10.

Table 6.10 Refinement parameters for the CYCBCD structure

Refinement	
Refinement program	SHELXL-93
Index range	h : 0 to18 ; k : 0 to 77 ; l : –18 to 18
Max 2θ	52.67°
R_{int}	0.053
Absorption correction	None
Measured reflections	51699
Rejected reflections	18
Unique reflections	22576
Reflections suppressed	0
Number of reflections used in refinement	22576
Reflections with $F_o>4\sigma F_o$	8806
R_1 ($F_o>4\sigma F_o$)	0.0937
R_1 for all reflections	0.2039
wR_2	0.2863
S = GooF	0.853
Number of parameters used in refinement	1747
Optimised weighting parameters	a = 0.1670, b = 0.00
Δρ(max)	0.75 e/Å^3
Δρ(min)	-0.42 e/Å^3

Geometrical analysis of the CYCBCD structure

The four crystallographically independent cyclodextrins are designated CD(A), CD(B), CD(C) and CD(D) and the guest molecules associated with the later three CD molecules will be referred to as CYC(B), CYC(C) and CYC(D). The glucose residues are numbered from one to seven, so the glucose residues of CD(A) are A1, A2, A3, A4, A5, A6 and A7. The glucose residues of all four CDs are in the $^4C_1$ chair conformation. The geometrical parameters defining the CD macrocycles are listed in Tables 6.11, 6.12 and 6.13 (e.s.d. s are of the order of 0.01Å for distances and 1° for angles).

The values of the CD torsion angles (Table 6.11) reveal that all the glucose residues display similar pyranoid ring conformations. The geometrical parameters of CD(A) do not show any significant variations from those of CD(B), CD(C) and CD(D) despite the fact that this CD is essentially unoccupied by a guest molecule as revealed in the structure solution

The primary hydroxyl groups all have the (+)-*gauche* conformation with only two exceptions, namely for glucose units A3 and B7 which are found in the (-)-*gauche* conformation. The intersaccharidic torsion angles display a narrow range of values close to the mean value for all β-CD structures indicating that tilting of the glucose units with respect to the CD mean planes are likely to fall in a narrow range too. The geometrical data for the O4 heptagons of the four CDs reveal that the macrocyclic structure is very symmetrical. The radii and side lengths of the O4 heptagons are both within a narrow ranges. The deviations of the O4 atoms from the mean O4 planes and the values of the O4···O4···O4···O4 torsion angles are indicative of a planar O4 heptagon. The overall geometrical features of the CDs suggest that the nature (size, shape and chemical functionalities) of the included guest does not cause large distortions of the macrocycle conformation. The O2(n)···O3(n-1) distances range from 2.70 to 2.88 Å and indicate that strong hydrogen bonds are responsible for the conformational rigidity of the macrocycles. The narrow ranges and symmetrical distributions of the geometrical indicators suggest largely undistorted macrocyclic structures for the four β-CD molecules.

Table 6.11 Selected torsion angles for glucose units of the CYCBCD structure

Glucose unit	ω (°)†	Φ (°)†	Ψ (°)†	Θ_1 (°)†	Θ_2 (°)†
A1	-60	110	125	56	-53
A2	-66	116	126	55	-48
A3	+65	116	132	52	-49
A4	-66	116	124	53	-50
A5	-69	113	132	63	-59
A6	-70	112	126	53	-50
A7	-65	111	132	56	-55
A | mean |	**66**	**113**	**128**	**55**	**-52**
B1	-67	115	126	58	-53
B2	-65	116	133	56	-55
B3	-66	109	125	54	-54
B4	-65	111	126	51	-49
B5	-61	115	125	52	-50
B6	-64	116	121	56	-53
B7	+65	115	128	56	-53
B | mean |	**65**	**114**	**126**	**55**	**-52**
C1	-61	116	127	53	-51
C2	-69	114	130	57	-57
C3	-66	114	128	52	-47
C4	-69	113	131	59	-60
C5	-66	111	124	53	-54
C6	-68	112	128	55	-54
C7	-69	116	118	54	-53
C | mean |	**67**	**114**	**127**	**55**	**-54**
D1	-68	111	123	54	-48
D2	-66	116	135	59	-60
D3	-65	111	124	54	-53
D4	-68	111	130	54	-53
D5	-64	110	122	56	-54
D6	-66	117	126	56	-55
D7	-65	116	131	54	-54
D | mean |	**66**	**113**	**127**	**55**	**-54**

† Refer to page 4,5 (Chapter 1) for definitions and descriptions of these quantities

Table 6.12 Geometrical data for the O4 heptagons of the CYCBCD structure

Glucose unit	r (Å)†	l (Å)†	a (°)†	d (Å)†	t (°)†
A1	4.47	4.93	129	0.00	+4
A2	4.39	4.99	126	-0.04	-3
A3	4.27	5.18	128	+0.05	0
A4	4.48	5.07	133	-0.01	+2
A5	4.37	4.88	126	-0.03	-1
A6	4.37	5.13	127	+0.02	+1
A7	4.33	5.16	131	+0.01	-2
A | mean |	**4.38**	**5.05**	**129**	**0.02**	**2**
B1	4.49	4.91	130	-0.03	+2
B2	4.33	4.97	124	+0.02	-1
B3	4.32	5.23	130	0.00	+2
B4	4.44	5.01	132	+0.01	-2
B5	4.39	4.89	127	-0.03	+1
B6	4.38	5.13	126	+0.03	+2
B7	4.31	5.16	132	+0.01	-2
B | mean |	**4.38**	**5.04**	**129**	**0.02**	**2**
C1	4.41	4.94	125	-0.04	0
C2	4.24	5.22	129	+0.03	-2
C3	4.50	5.05	132	+0.03	+1
C4	4.34	4.87	126	-0.03	+2
C5	4.40	5.13	127	-0.02	-2
C6	4.31	5.15	130	+0.04	-1
C7	4.46	4.96	131	-0.01	+2
C | mean |	**4.38**	**5.05**	**129**	**0.03**	**1**
D1	4.49	4.87	131	0.00	+3
D2	4.29	4.93	124	+0.03	-2
D3	4.31	5.25	129	-0.04	0
D4	4.40	5.03	133	+0.01	0
D5	4.49	4.84	126	+0.01	0
D6	4.32	5.16	125	-0.01	0
D7	4.35	5.24	132	-0.02	-2
D | mean |	**4.38**	**5.05**	**129**	**0.02**	**1**

† Refer to page 6,7 (Chapter 1) for definitions and descriptions of these quantities

Table 6.13 Values of intersaccharide bond angles (φ), the O2(n)···O3(n-1) distances and the tilt angles (τ_1 and τ_2) for the CYCBCD structure

Glucose unit	φ (°)†	O2(n)···O3(n-1) (Å)†	τ_1 (°)†	τ_2 (°)†
A1	118	2.84	+2.6	+6.2
A2	118	2.70	+0.7	+4.4
A3	117	2.84	+8.0	+9.9
A4	118	2.86	+3.8	+9.6
A5	118	2.85	+7.0	+10.5
A6	115	2.79	+4.2	+8.3
A7	119	2.84	+10.6	+13.4
A | mean |	**118**	**2.82**	**5.3**	**+8.9**
B1	118	2.85	+2.5	+7.4
B2	118	2.85	+9.5	+12.9
B3	118	2.86	+5.0	+10.6
B4	119	2.81	+3.8	+7.4
B5	117	2.80	+3.0	+7.0
B6	119	2.78	+5.0	+5.0
B7	117	2.86	+4.9	+7.9
B | mean |	**118**	**2.83**	**4.8**	**8.3**
C1	120	2.74	+1.2	+6.4
C2	118	2.81	+6.8	+9.7
C3	119	2.86	+4.2	+8.7
C4	114	2.85	+9.3	+11.6
C5	118	2.81	+5.0	+9.3
C6	119	2.86	+8.5	+9.3
C7	118	2.77	+1.2	+4.3
C | mean |	**118**	**2.81**	**5.2**	**8.5**
D1	120	2.88	+0.2	+4.5
D2	118	2.87	+11.5	+14.0
D3	115	2.86	+5.9	+10.8
D4	119	2.88	+7.9	+11.3
D5	119	2.82	+2.1	+4.8
D6	117	2.74	+2.5	+5.4
D7	119	2.87	+7.5	+11.8
D | mean |	**118**	**2.85**	**5.4**	**8.9**

† Refer to page 8,9 (Chapter 1) for definitions and descriptions of these quantities

Overall description of the CYCBCD structure

The crystal structure of the CYCBCD complex will be discussed firstly in terms of the inclusion of the three cyclizine guests in their respective CDs, followed by a discussion of the CD(A)-CD(B) and CD(C)-CD(D) dimers and completed with a description of the complete structure and its packing arrangement.

Figures 6.8 6.9 and 6.10 show CPK models of the inclusion of the three cyclizine molecules, CYC(B), CYC(C) and CYC(D) in the cyclodextrins CD(B), CD(C) and CD(D) respectively. For all proceeding these diagrams the colour codes are: β-CD: C (grey), O (red), H (white); CYC: C (green), H (yellow), N (blue); Water: O (light blue).

All three cyclizine molecules are inserted into the CD cavity via their piperazine rings leaving their diphenylmethyl portions protruding somewhat from the CD cavity. This is in contrast to the conclusions drawn by Guillory et al.[2,4] for the complexation of cyclizine.HCl with α-, β- and γ-CD, namely that inclusion of one of the phenyl rings was energetically more preferred than inclusion of the piperazine ring. However, in those studies the piperazine ring was protonated and therefore a more polar group, which would explain its decreased affinity for the CD cavity.

Although the piperazine ring is inserted in the CD cavity for all three crystallographically independent guests, their modes of insertion and extent of penetration reveal significant differences. CYC(B) and CYC(C) (Figures 6.8 and 6.9) penetrate the CD cavity from the secondary hydroxyl sides. The modes of insertion of these two guests are very similar with both guests penetrating the CD cavity fairly deeply such that the methyl substituents of their piperazine rings protrude from the primary hydroxyl rim and approximately half of the diphenylmethyl moieties are contained within the CD cavities. CYC(D) (Figure 6.10), on the other hand, penetrates the CD cavity from the primary hydroxyl end and the extent of insertion into the cavity is significantly less. No part of the piperazine ring protrudes from the secondary hydroxyl rim while the diphenylmethyl moiety protrudes almost completely from the primary hydroxyl rim.

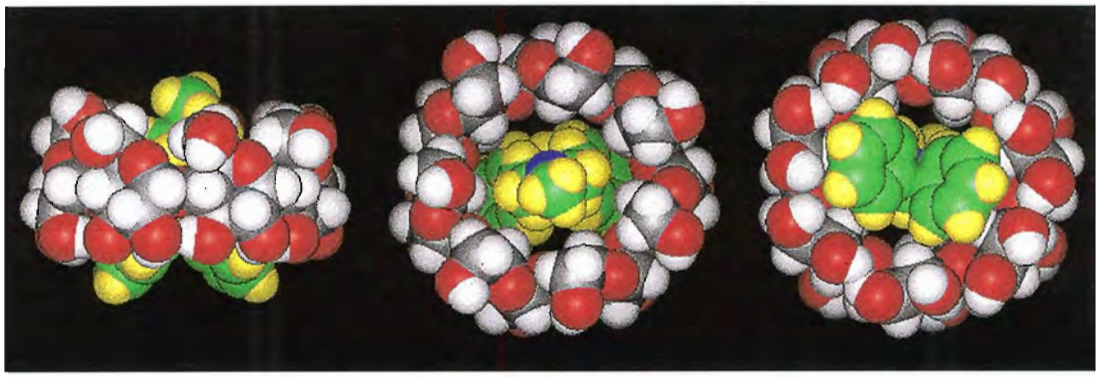

(a) (b) (c)

Figure 6.8 The CPK space filling diagrams for insertion of CYC(B) into the cavity of CD(B) (a) view perpendicular to the CD axis (b) view from primary hydroxyl side of the CD (c) view from the secondary hydroxyl side of the CD

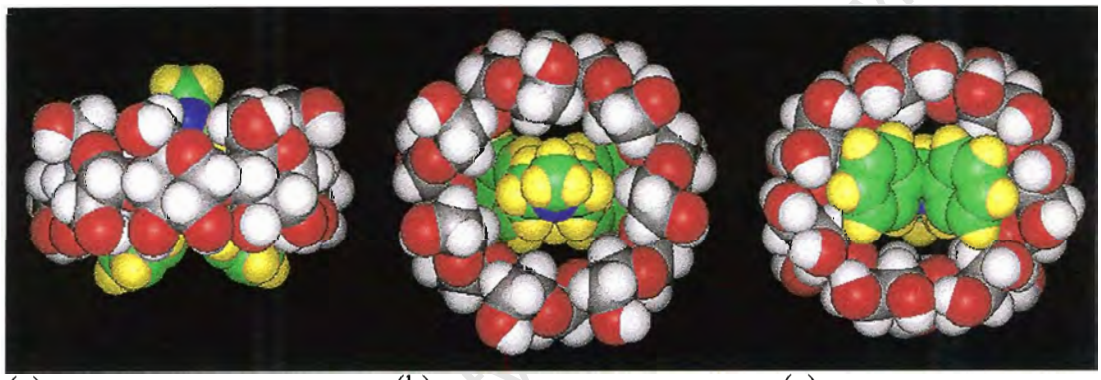

(a) (b) (c)

Figure 6.9 The CPK space filling diagrams for insertion of CYC(C) into the cavity of CD(C) (a) view perpendicular to the CD axis (b) view from primary hydroxyl side of the CD (c) view from the secondary hydroxyl side of the CD

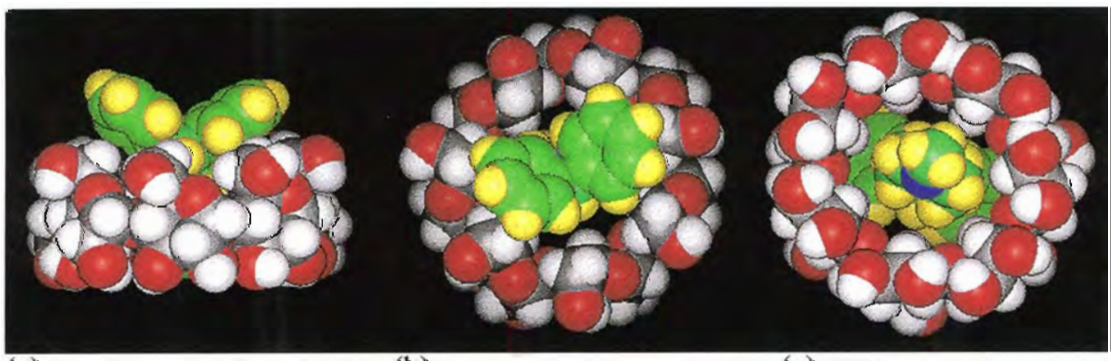

(a) (b) (c)

Figure 6.10 The CPK space filling diagrams for insertion of CYC(D) into the cavity of CD(D) (a) view perpendicular to the CD axis (b) view from primary hydroxyl side of the CD (c) view from the secondary hydroxyl side of the CD

The four CDs and their associated guests are arranged as two crystallographically independent dimers as is shown in Figure 6.11 and Figure 6.12.

The CD(A)-CD(B) dimer (Figure 6.11) contains the CYC(B) molecule of which the major portion is contained within CD(B), with only a portion of the methyl substituent of the piperazine ring protruding from the primary end. It is also noted that in the region of the dimeric interface, just under half of the diphenylmethyl group of CYC(B) protrudes from the secondary hydroxyl face of CD(B) and penetrates CD(A) from its secondary hydroxyl end. The secondary hydroxyl dimeric interface best accommodates the relatively large size of the diphenylmethyl group. A water molecule (O12W), shown as light blue sphere in Figure 6.11 (b), is hydrogen bonded to the N5 atom of CYC(B) with a N5···O12W distance of 2.79 (2) Å for the contact.

The CD(C)-CD(D) dimer (Figure 6.12) contains the CYC(C) and CYC(D) guests. A portion of the methyl substituent of the piperazine ring of CYC(C) protrudes from the primary hydroxyl side of CD(C) and almost the entire diphenylmethyl group of CYC(D) protrudes from the primary hydroxyl end of CD(D). An interesting feature of this dimer is that the two CYC molecules included in it are in van der Waals contact in the region of the secondary hydroxyl interface. Two of the methyl hydrogen atoms of CYC(D) are involved in C-H···π interactions with the two phenyl rings of CYC(C). A water molecule (O25W), shown as a light blue sphere in Figure 6.12 (b), is hydrogen bonded to the N5 atom of CYC(C) with a N5···OW25 distance of 2.88 (2) Å for the contact.

From inspection of the two dimers it is noted that for the CD(A)-CD(B) dimer, a large portion of CD(A) appears largely devoid of a guest or water molecules. It is also noted that the bulk of the diphenylmethyl group of CYC(D) protrudes from the primary hydroxyl face of CD(D). This is partially compensated by a portion of the diphenylmethyl group of CYC(D) being included by the empty primary hydroxyl end cavity of CD(A) (Figures 6.13 and 6.14). This feature of the structure explains the unusual 3:4 guest:CD stoichiometry of the complex. The size and shape of the β-CD dimeric unit is such that it cannot accommodate two CYC molecules in their entirety. Large portions of the guests would protrude from the primary ends of the dimers and they would not be able to pack efficiently.

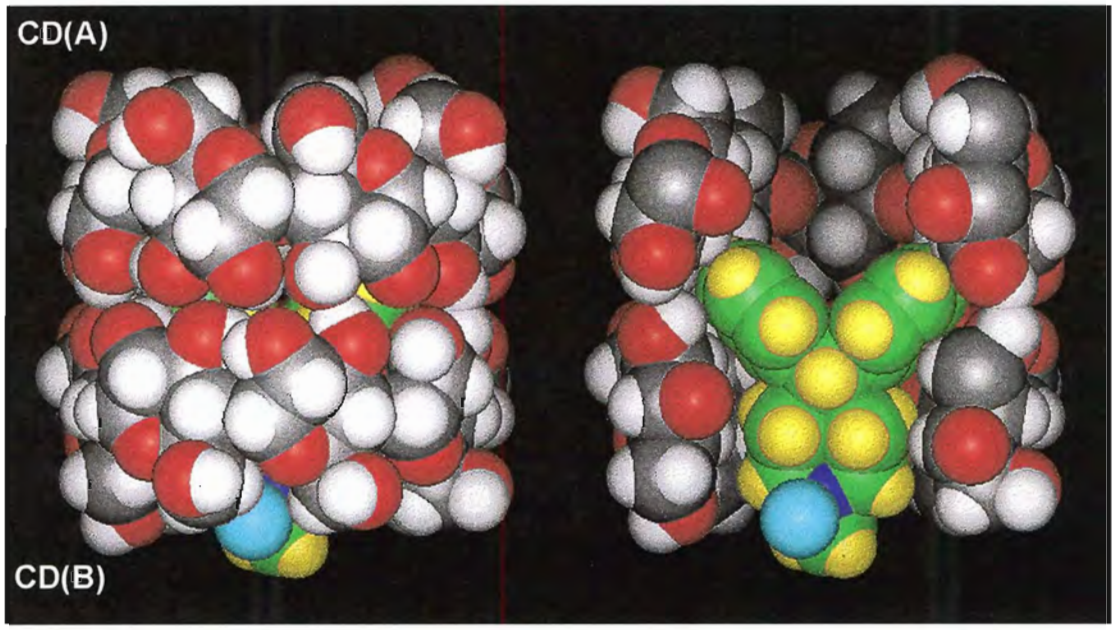

(a) (b)

Figure 6.11 The CPK space filling diagrams for the CD(A)-CD(B) dimeric unit (a) view perpendicular to the CD axis (b) view perpendicular to CD axis with a section of the CD molecules of the dimer removed to show the inside of the cavity

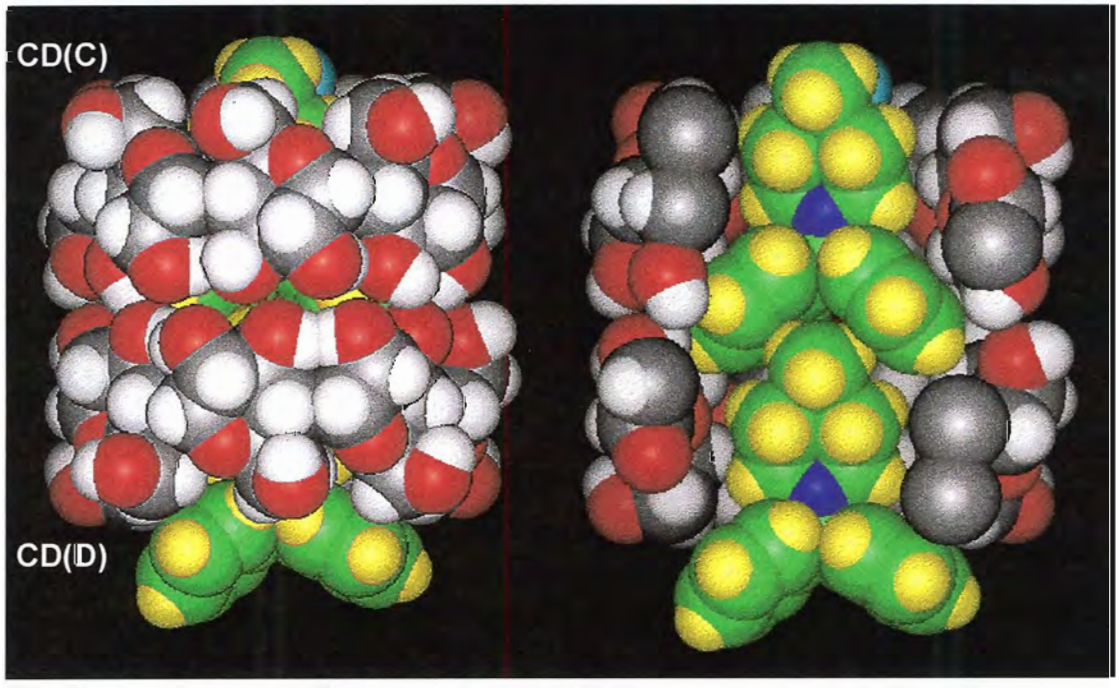

(a) (b)

Figure 6.12 The CPK space filling diagrams for the CD(C)-CD(D) dimeric unit (a) view perpendicular to the CD axis (b) view perpendicular to CD axis with a section of the CD molecules of the dimer removed to show the inside of the cavity

Figure 6.13 shows the position of the CYC(D) molecule relative to the CD layer immediately below, consisting of screw-axis related CD(A) molecules. From Figure 6.13 (a) it is clear that in projection one of the phenyl rings of CYC(D) (labelled A) lies in the interstitial space between four CD(A) molecules. Figure 6.13 (b) shows that ring A rests on the surface of the layer of CD(A) molecules. Figure 6.14 (a) and (b) show the penetration of the other phenyl ring (labelled B) into the primary hydroxyl end of the cavity of a CD(A) molecule.

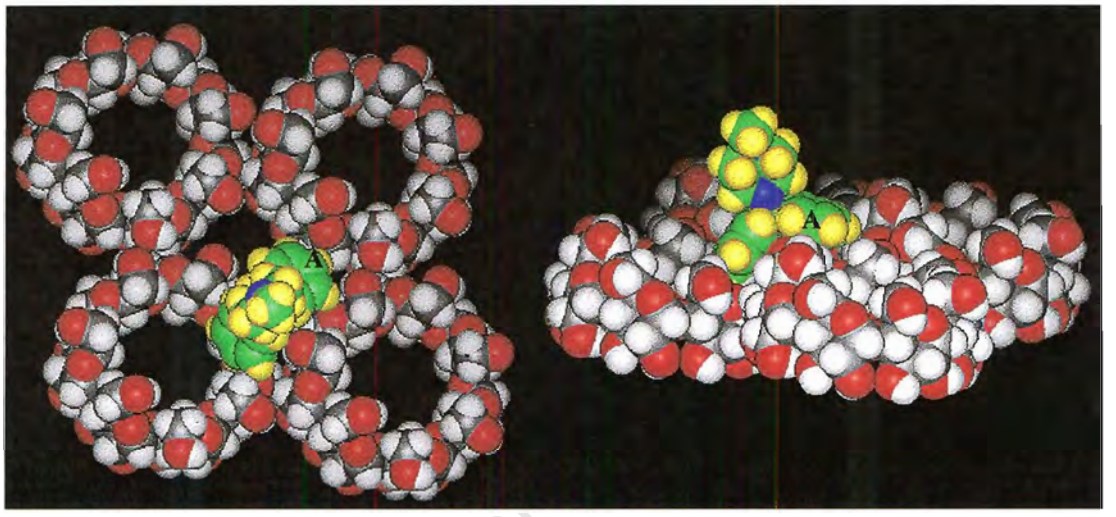

(a) (b)

Figure 6.13 The position of CYC(D) relative to the CD layer below (a) view perpendicular to mean CD plane (b) view approximately parallel to mean CD plane

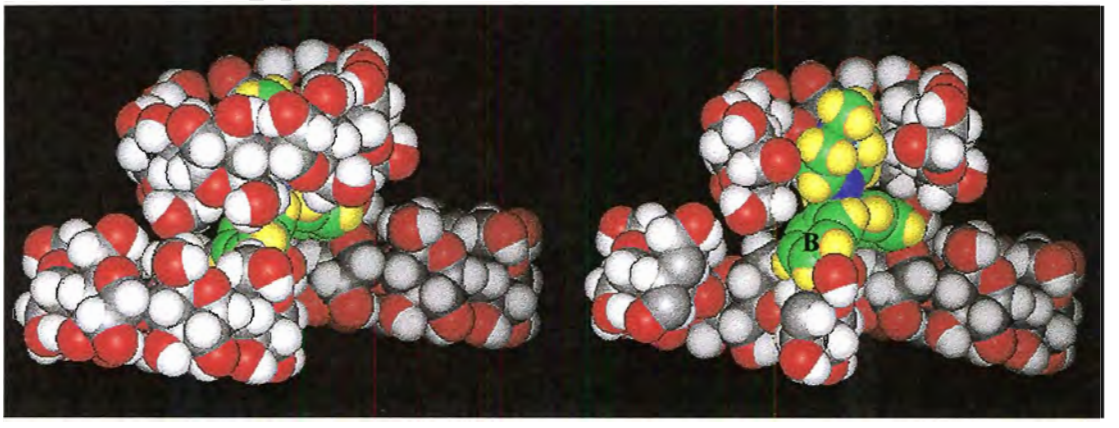

(a) (b)

Figure 6.14 The inclusion of phenyl ring B of CYC(D) (a) view parallel to the mean plane of the CDs (b) the same view direction with some of the CD molecules sectioned to reveal the inclusion of CYC(D)

Guillory et al.[4] in their molecular modelling studies referred to unfavourable steric interactions that occur when a molecule such as cyclizine is included from the primary hydroxyl end of a CD, as is the case for the inclusion of CYC(D). This statement will be discussed in terms of the conformations of the three cyclizine molecules included in the CYCBCD structure. Only two torsion angles define the conformational freedom of the cyclizine molecule. The two torsion angles, which will be referred to as δ_1 and δ_2, are shown in Figure 6.15 and their values are listed in Table 6.14 (e.s.d. s in the range 1-2°) for the three cyclizine molecules of CYCBCD and for the structure of cyclizine hydrochloride, CYCLIZ, determined by Bertolasi et al.[9,10]

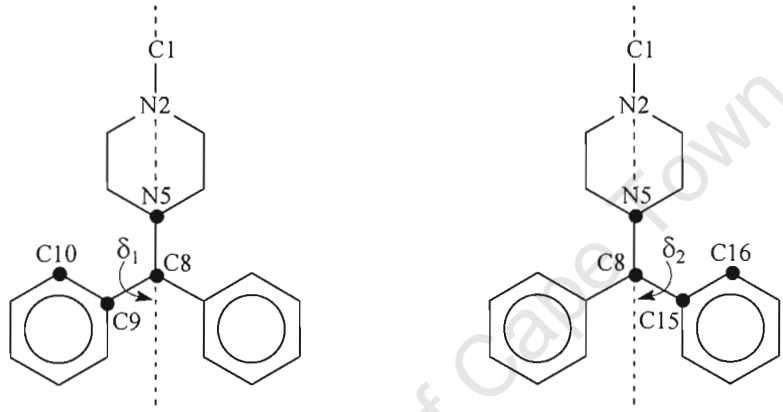

Figure 6.15 Representation of the torsion angles, δ_1 and δ_2 , of the cyclizine molecule

Table 6.14 Torsion angles, δ_1 and δ_2 for CYC(B), CYC(C), CYC(D) and CYCLIZ

Cyclizine	δ_1	δ_2	$(\lvert\delta_1\rvert + \lvert\delta_2\rvert)/2$
CYC(B)	-41	44	42.5
CYC(C)	-43	44	43.5
CYC(D)	-31	53	42.0
CYCLIZ	-43.5	43.5	43.5

In the CYCLIZ structure the two phenyl rings are related by a mirror plane through the C1, N2, N5, C8 atoms[9,10] (Figure 6.15). Therefore, the structure is perfectly symmetrical across this plane and the torsion angles, δ_1 and δ_2, are exactly equal and opposite. The two phenyl rings of CYC(B) and CYC(C) display very similar torsion angles to that of CYCLIZ, and the two phenyl rings are also very symmetrical across the aforementioned plane. The two phenyl rings of CYC(D), on the other hand, are significantly distorted from this symmetrical relationship. The absolute mean torsion angle for CYC(D) is 42°; however, the individual torsion angles show that the phenyl rings have angular deviations of 9.5° and 12.5° away from this mean. The deviations are in opposite directions and represent a non-symmetrical twisting of the two rings.

Crystal Packing of the CYCBCD structure

The asymmetric part of the structure is a tetrameric unit consisting of the CD(A)-CD(B) and CD(C)-CD(D) dimers. This tetrameric unit is rotated and translated by a screw axis along the *b*-axis to produce the contents of a unit cell. The stereo diagram of the *a*-axis projection of the contents of a single unit cell is shown in Figure 6.16. Figures 6.17 (a) and 6.17 (b) are projections viewed down the *c*- and *a*-axes respectively. The structure is extended by translation for four unit cells along the *c*-axis for Figures 6.17 (a) and four unit cells along *a*-axis for Figure 6.17 (b). The structures are also translated one unit cell along the *b*-axis. The extended packing diagrams show how translation in the *ac*-plane produces an array of dimeric layers. Four dimeric layers comprise the repeating array of the structure and these layers are labelled as Layers 1, 2, 3 and 4 in Figures 6.17 (a) and (b). Layers 1 and 2 are related to Layers 3 and 4 by a screw axis along the *b*-axis of the cell. The mean macrocyclic planes of the dimers of Layers 1 and 2 are tilted 10° anti-clockwise in their respective layer planes. The mean macrocyclic planes of the dimers of Layers 3 and 4 are tilted 10° clockwise in their respective layer planes. When viewed in projection down the *b*-axis all layers are laterally displaced from one another by more than the radius of a β-CD molecule. The displacement of Layers 1 and 4 from Layers 2 and 3 is evident in Figure 6.17 (a) while the displacement of Layers 1 and 2 from Layers 3 and 4 is evident in Figure 6.17 (b).

Fujiwara et al.[11,12] described the *S*-(-)-*p*-tolylsulfoxide-β-CD complex (referred to hereafter as TOLBCD (Figure 1.12 (b)) with closely matching cell parameters and the same space group ($P2_1$) as the CYCBCD complex. However, the packing arrangement was not described in detail and the coordinates for this structure were not obtainable. In their review on β-CD dimeric complexes, Mentzafos et al.[13] described the TOLBCD complex as consisting of a tetrameric channel, similar to that found in the β-CD complex with barbital (Form II),[14] with the tetramers packed according to the chessboard mode. The CYCBCD complex has no true tetrameric channel and the packing differs from the description of the packing of the TOLBCD complex. The difference between the two structures is best seen in the packing diagram shown in the papers by Fujiwara et al.[11,12] The orientation and relative positions of the two dimers of the asymmetric unit are significantly different from those for the CYCBCD structure.

The CYCBCD complex therefore represents a new β-CD packing arrangement which differs from the TOLBCD complex by a shifting of the four dimeric layers away from the tetrameric channel motif. This disruption of the tetrameric channel would probably be the result of accommodation of the protruding portions of CYC(D).

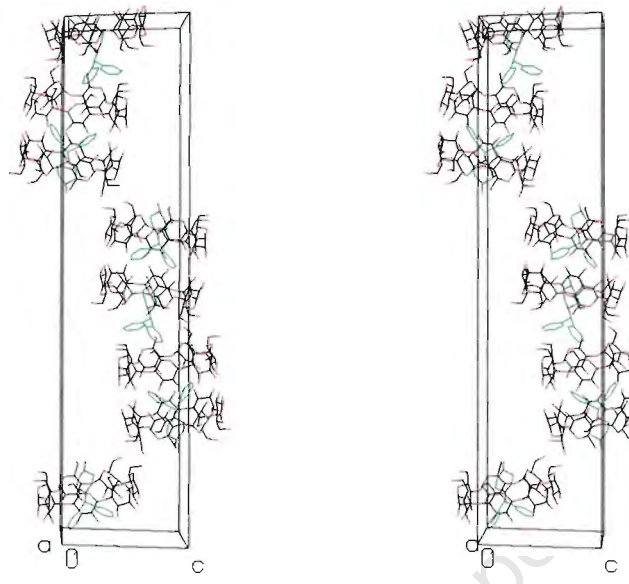

Figure 6.16 Stereo diagram for the CYCBCD structure viewed down the a-axis

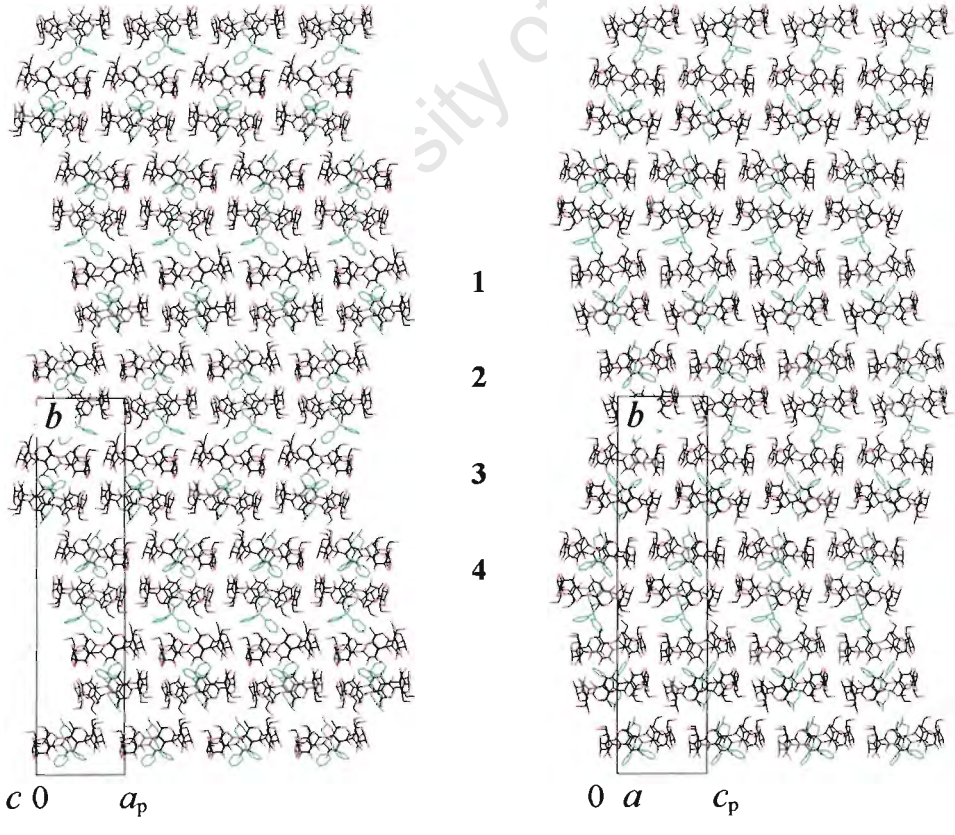

(a) (b)

Figure 6.17 Extended packing arrays of the CYCBCD complex viewed in the *c*-axis projection (b) *a*-axis projection

The rationale for a possible mechanism of crystal formation and an explanation for the unusual stoichiometric ratio of the CYCBCD complex will be discussed in terms of the details of the structure solution and the available literature references to the mode of inclusion of cyclizine by β-CD.

It has been shown via molecular modelling studies that only the piperazine ring or one of the two aromatic rings of cyclizine can be included within the β-CD molecule.[4] It was also shown in the same study that the cyclizine molecule cannot pass through the β-CD cavity because of steric hindrances. It can therefore be concluded with certainty that the mode of insertion of cyclizine is a direct indication as to the direction of approach of the molecule to the β-CD cavity.

A schematic illustration of the proposed mechanism of crystal formation is shown in Figure 6.18 and will be discussed in detail below.

The inclusion of cyclizine from the primary rim of β-CD was reported, from a molecular modelling study, to be significantly less favourable than inclusion from the secondary rim.[4] It is also noted from the inclusion of cyclizine in the CYCBCD complex that there is a preference for the inclusion of the piperazine ring of cyclizine in the CD cavity. Therefore, it is likely that in solution the most stable structure would be that of the piperazine ring of the cyclizine molecule inserted in the β-CD cavity from the larger secondary hydroxyl rim. From empirical observations, the formation of β-CD dimers is also a preferred arrangement for β-CD molecules.[13] Two β-CD molecules with cyclizine included from their secondary hydroxyl ends would be unable to form a stable head-to-head dimer due to steric clashes of the diphenylmethyl groups of the included guests. The result would be expulsion of one of the guests and the formation of a stable dimer with one included cyclizine molecule. However, this would leave a large empty portion of the CD cavity of one CD in the dimer. This can be filled by a cyclizine molecule inserting its piperazine ring from the primary hydroxyl end. During the crystallisation, these dimers would need to pack together in an efficient and stable manner. The diphenylmethyl groups protruding from one of the primary hydroxyl ends of the dimers would prove to be a hindrance to the packing of these dimers. Therefore the dimers could expel all the cyclizine molecules included from the primary hydroxyl ends and form a stable crystal or alternatively, as seen for the CYCBCD crystal structure, some compromise may be reached between (i) trying to keep the guest volume to cavity volume ratio as close to unity as possible and (ii) the formation of a stable CD structure with the highest possible packing efficiency.

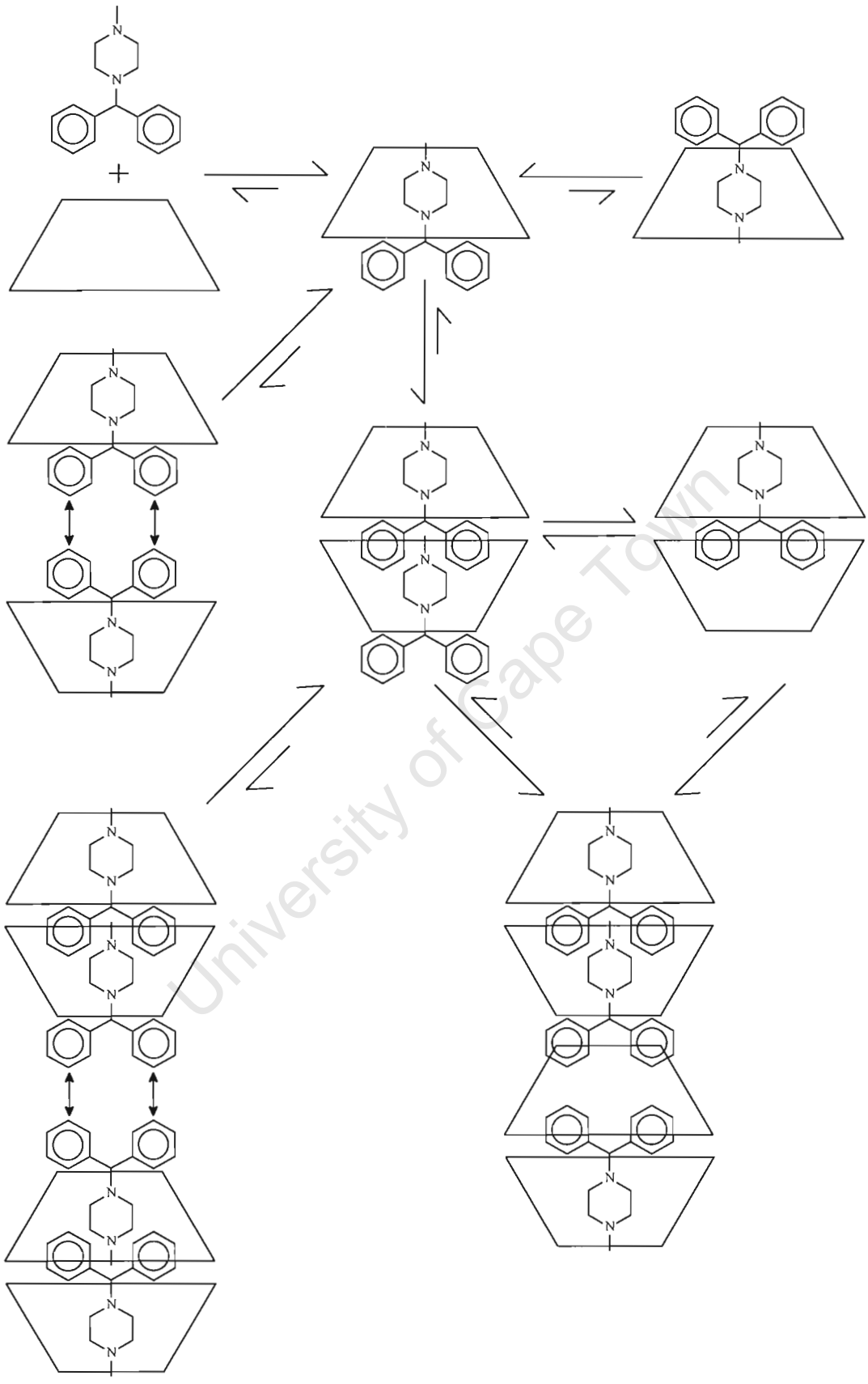

Figure 6.18 Schematic illustration of the proposed mechanism for crystal formation

Hydrogen bonding interactions of the CYCBCD structure

Tables 6.15, 6.16, 6.17 (a), 6.17 (b), 6.18 and 6.19 list summaries of the appropriate contacts for the cyclodextrin, dimer, intralayer, interlayer, guest and water interactions respectively. The listed contacts are all in the range of 2.50 to 3.20Å and the e.s.d. s are in the range 0.01-0.03Å for the cyclodextrin, dimer, layer and guest interactions and 0.01-0.05Å for the water interactions.

A.) Cyclodextrin interactions

The secondary rims of the β-CD molecules of the CYCBCD complex are held together by a ring of hydrogen bonds between the O2 and O3 hydroxyl groups of adjacent glucose units. These hydrogen bonds contribute significantly to the stability of the macrocyclic conformation and are observed from neutron studies to be of a flip-flop nature.[15,16] Table 6.15 lists a summary of the O···O contacts for interactions of this nature for the CYCBCD complex.

Table 6.15 Cyclodextrin interactions for the CYCBCD structure

O2···O3	Number / CD	Range (Å)	Mean (Å)
A	7	2.70-2.85	2.82
B	7	2.78-2.86	2.83
C	7	2.74-2.86	2.81
D	7	2.74-2.88	2.85

B.) Dimer interactions

A large percentage of the known structures of β-CD complexes contain the β-CD molecules linked together by hydrogen bonding at their secondary hydroxyl ends to form characteristic dimeric units.[17] Table 6.16 lists the contacts between the O2 and O3 hydroxyl oxygen atoms of the CD(A)-CD(B) and the CD(C)-CD(D) dimers of the CYCBCD complex. The hydrogen bonds between the O3 secondary hydroxyl groups are evidently the most important of the intra-dimer linkages with O···O contact distances of 2.85Å and 2.89Å for the CD(A)-CD(B) and the CD(C)-CD(D) dimers respectively. The average O···O contacts between CD(C)-CD(D) are in all cases 0.04-0.05Å longer than the corresponding contacts for CD(A)-CD(B). An explanation for this observation could be the more crowded nature of the inter-dimer space of the CD(C)-CD(D) dimer relative to that of the CD(A)-CD(B) dimer.

Table 6.16 Dimer interactions for the CYCBCD structure

Type	Dimer	Number / dimer	Range (Å)	Mean (Å)
O3···O3	A-B	7	2.74-3.04	2.85
O2···O2	A-B	7	2.97-3.14	3.04
O2···O3	A-B	12	3.03-3.18	3.12
O3···O3	C-D	7	2.78-3.15	2.89
O2···O2	C-D	6	3.02-3.16	3.06
O2···O3	C-D	9	3.05-3.19	3.12

C.) Layer interactions

As already mentioned, the structure of the CYCBCD complex consists of four dimeric layers (Layers 1-4). Direct hydrogen bonding between the hydroxyl groups of the CD dimers as well as hydrogen bonds mediated by water molecules form a network of intra-layer and inter-layer hydrogen bonded interactions.[17] O2···O2 and O6···O6 interactions seem to be the principal intralayer interactions, as was observed for the β-CD dimeric complexes investigated in Chapter 3, while a single O6···O6 interaction provides connectivity between each pair of adjacent layers. Tables 6.17 (a) and (b) list the O···O contact distances for the various intra-layer and interlayer interactions respectively.

Table 6.17 (a) Intra-layer interactions for the CYCBCD structure

Type	Layer	Number / dimer	Range (Å)	Mean (Å)
O2···O2	1	2	2.72-2.78	2.75
O6···O6	1	4	2.76-3.01	2.87
O2···O2	2	2	2.76	2.76
O6···O6	2	4	2.80-3.11	2.92
O2···O2	3	2	2.76-2.78	2.75
O6···O6	3	4	2.76-3.01	2.87
O2···O2	4	2	2.76	2.76
O6···O6	4	4	2.80-3.11	2.92

Table 6.17 (b) Inter-layer interactions for the CYCBCD structure

Type	Layers	Number / dimer	Range (Å)	Mean (Å)
O6···O6	1-2	1	2.97	2.97
O6···O6	2-3	1	2.66	2.66
O6···O6	3-4	1	2.97	2.97
O6···O6	4-1	1	2.66	2.66

D.) Guest interactions

One hydrogen bond is made by each of the cyclizine molecules CYC(B) and CYC(C) (Table 6.18). They are both to water molecules situated in the vicinity of the primary hydroxyl rim of the CDs and have been discussed earlier in this chapter.

Table 6.18 Guest interactions for the CYCBCD structure

Guest···Water	Distance (Å)
N2B···O12W	2.79 (2)
N2C···O25W	2.88 (2)

E.) Water interactions

Table 6.19 lists the O···O contact distances for numerous water to water and CD hydroxyl to water interactions which are present in the CYCBCD complex. These interactions form a vast and complicated hydrogen bonded network where water molecules mediate many of the types of the interactions already discussed.[17] For some of the water interactions, disordered water atoms are involved in the interactions and this results in an apparent increase in the number of interactions present. The number of water interactions will be adjusted by multiplication by a normalising factor, N †.

† N = [total occupancy of atoms involved in contacts] / [total number of sites of atoms involved in contacts]

Table 6.19 Water interactions for the CYCBCD structure

Type	Number	Number / dimer	(Number / dimer) x N	Range (Å)	Mean (Å)
O2···Water	20	10	10	2.73-3.05	2.82
O3···Water	16	8	8	2.78-3.18	2.92
O6···Water	34	17	16	2.60-3.15	2.79
Water···Water	43	22	20	2.70-3.15	2.89

X-ray crystallographic analysis of the CYCGCD structure

Data-collection

The preliminary cell parameters and space group for the CYCGCD structure were determined by x-ray photographic techniques. The later revealed Laue 4/*mmm* symmetry and reflection conditions *h*00 : *h* = 2n which indicated the tetragonal space groups $P42_12$ or $P\bar{4}2_1m$. Since the host is chiral the former space group was chosen. A crystal of the complex was mounted under mother liquor in a Lindemann capillary tube and data were collected at 293K on a Nonius Kappa CCD diffractometer. The data-collection strategy was adapted slightly from the strategy suggested by the COLLECT[18] software from Nonius. Data were corrected for Lorentz-polarisation effects but not for absorption, since $\mu = 1.164 cm^{-1}$ represented negligible absorption for the size of the crystal used. The crystal data parameters are listed in Table 6.20 and details of the data-collection strategy are given in Table 6.21.

Table 6.20 Crystal data parameters for the CYCGCD structure

Crystal Data	
Molecular formula	$3(C_{48}H_{80}O_{40})•1(C_{18}H_{22}N_2)•49.2(H_2O)$
M_r ($g.mol^{-1}$)	5044.1
Crystal system	Tetragonal
Space group	$P42_12$
Z	2
a (Å)	23.8240 (3)
b (Å)	23.8240 (3)
c (Å)	23.0830 (3)
α (°)	90
β (°)	90
γ (°)	90
V ($Å^3$)	13101.5 (3)
D_c ($g.cm^{-3}$)	1.2786
μ (Mo Kα) (cm^{-1})	1.164
F (000)	5400
Crystal dimensions (mm)	0.3 x 0.3 x 0.3
Temperature	293 K
Radiation, λ	Mo Kα (0.71069 Å)

Table 6.21 Data-collection parameters for the CYCGCD structure

Data-Collection	
Diffractometer	Nonius Kappa CCD
Set 1	
ϕ	0.0°
θ	7.042°
κ	0.0°
ω	180.0°
Dx	40mm
Number of frames collected	366
Rotation axis / angle	ϕ rotations, $\Delta\phi = 1.0°$
Exposure time / frame	32.9 sec (x2)
Number of reflections	103692

Refinement and structure solution

The CYCGCD complex contains a trimer consisting of three crystallographically independent γ-CD molecules. However, since the γ-CD molecules lie on a four-fold rotational axis, only the coordinates of two glucose units need to be determined for each CD. The final refinement parameters for the CYCGCD complex are listed in Table 6.22. The structure was solved using the published coordinates for the non-hydrogen CD atoms (excluding the primary hydroxyl oxygen atoms) of the isomorphous 12-crown-4-γ-CD complex.[19] After refinement in SHELXL-93[8] the difference Fourier map revealed the positions of the primary hydroxyl oxygen atoms. Three of these atoms were disordered over two positions each with the major positions in each case having site occupancy factors in the range of 0.55 to 0.73. All the primary hydroxyl oxygen atoms were refined isotropically with a mean isotropic temperature factor of 0.13Å^2 for the disordered O6 atoms and 0.11Å^2 for the full site occupancy O6 atoms. The CD non-hydrogen atoms, excluding the O6 atoms were refined with anisotropic temperature factors. Refinement proceeded with the addition of geometrically fixed hydrogen atoms attached to the CD backbone and the placement of O2 and O3 secondary hydroxyl hydrogen atoms using the rotating group refinement strategy (AFIX 147).[8] The hydrogen atoms of each of the three diglucosyl units were refined with a common isotropic temperature factor.

Table 6.22 Refinement parameters for the CYCGCD structure

Refinement	
Refinement programme	SHELXL-93
Index range	h 0,29 ; k 0,21 ; l 0,28
Max 2θ	52.77°
R_{int}	0.057
Absorption correction	None
Measured reflections	103692
Rejected reflections	0
Unique reflections	7456
Suppressed reflections	1
Reflections used for refinement	7455
Reflections with $F_o>4\sigma F_o$	3677
R_1 ($F_o>4\sigma F_o$)	0.1269
R_1 for all reflections	0.1936
wR_2	0.3931
S = GooF	0.934
Number of parameters used in refinement	709
Optimised weighting parameters	a = 0.3135, b = 0.00
Δρ(max)	0.68 e/Å^3
Δρ(min)	-0.54 e/Å^3

After further refinements, 12 water molecules with full site-occupancy were placed and their final isotropic temperature factors were in the range of 0.11 to 0.41Å^2. The number of water molecules placed per CD molecule is therefore 16 which compares well with the 16.4 per CD expected from TGA analysis.

Modelling of the cyclizine (CYC) guest

The centre of the γ-CD molecules of all γ-CD inclusion complexes,[19-23] with the exception of the hydrate,[24-28] lie on a four-fold rotation axis. The four-fold axis runs directly through the γ-CD cavity and any guest included in this cavity will of necessity be disordered by at least four-fold. This will always be true unless the guest has four-fold symmetry (C_4) of its own, as is the case for γ-CD inclusion complexes with 12-crown-4 and its metal ion coordination complexes as guests.[19-21]

Figure 6.19 (a) shows the projection of the γ-CD-12-crown-4 complex down the c-axis of the structure which illustrates the position of the 12-crown-4 molecule in the centre of the γ-CD channel. Figure 6.19 (b) shows a single γ-CD molecule and the corresponding included 12-crown-4 molecule. The C_4 symmetry of both the γ-CD and 12-crown-4 molecules is evident from this figure.

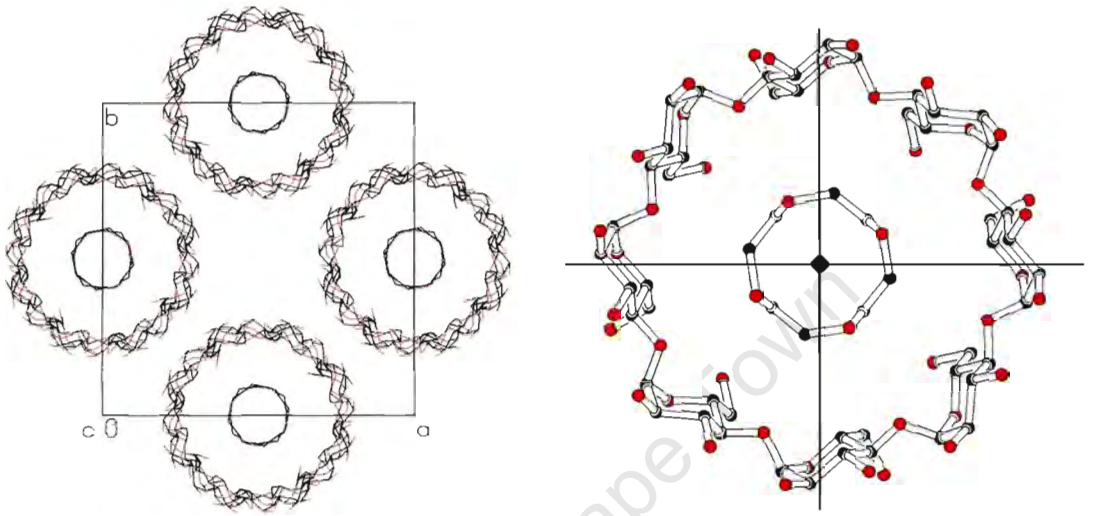

(a) (b)

Figure 6.19 (a) The projection of the γ-CD-12-crown-4 complex down the *c*-axis (b) a single γ-CD molecule and its corresponding included 12-crown-4 molecule

The modelling of the cyclizine molecule in the CYCGCD complex was complicated by the fact that cyclizine cannot adopt C_4 symmetry of its own and would therefore be disordered by at least four-fold around the rotation axis. This made the interpretation of the electron density difference map somewhat confusing.

After the refinement of the host and water molecules was completed, the electron density difference map showed a fairly bipyramidal "cloud" of electron density in the CD channel. This density was confined to the cavities of the CD(A) and CD(B) molecules. The shape and dimensions of this electron density matched the dimensions of two cyclizine molecules positioned in an antiparallel orientation with their diphenylmethyl groups in close contact. Furthermore, the four highest peaks in the electron density map were all positioned on the four-fold axis with two pairs of peaks each approximately 2.8 Å apart. These distances corresponded closely with the N2 to N5 distance in the crystal structure of cyclizine hydrochloride.[9,10]

With the positions of one of the pairs of nitrogen peaks as a starting point, peaks fitting the geometry of a cyclizine molecule were identified from the difference map. The geometry of the cyclizine molecule was maintained by application of various distance restraints and was refined successfully, albeit with a fairly high common isotropic temperature factor of 0.44Å^2. Inspection of the electron density difference map revealed the position of a second cyclizine molecule and it was positioned according to these peaks and the other pair of nitrogen peaks. Refinement of the second guest was successful, again albeit with a common isotropic temperature factor of 0.48Å^2. Inspection of the positions of the two cyclizine molecules revealed that their phenyl rings were in close contact and the terminal atoms were almost overlapping. The close contacts between the two modelled guests suggested that these two cyclizine molecules were two alternate disordered positions. This was in agreement with the stoichiometry of the complex determined from UV and microanalytical techniques which indicated the presence of a single cyclizine molecule per γ-CD trimer. The site occupancy factors of the two guests were adjusted appropriately and the PART instruction was used to differentiate the two portions of the disorder.[8] After refinement, the isotropic temperature factors of the two cyclizine molecules refined to final values of 0.19 and 0.20 Å^2 respectively. The structure solution of the CYCGCD complex is significant as it represents the first successful modelling of a non-symmetrical guest molecule in a γ-CD complex and is also the only other γ-CD complex, besides the 12-crown-4 complexes, where an included guest has been successfully located and modelled in a γ-CD complex. Figure 6.20 (a) shows the two disordered positions of CYC while Figure 6.20 (b) includes their rotated positions.

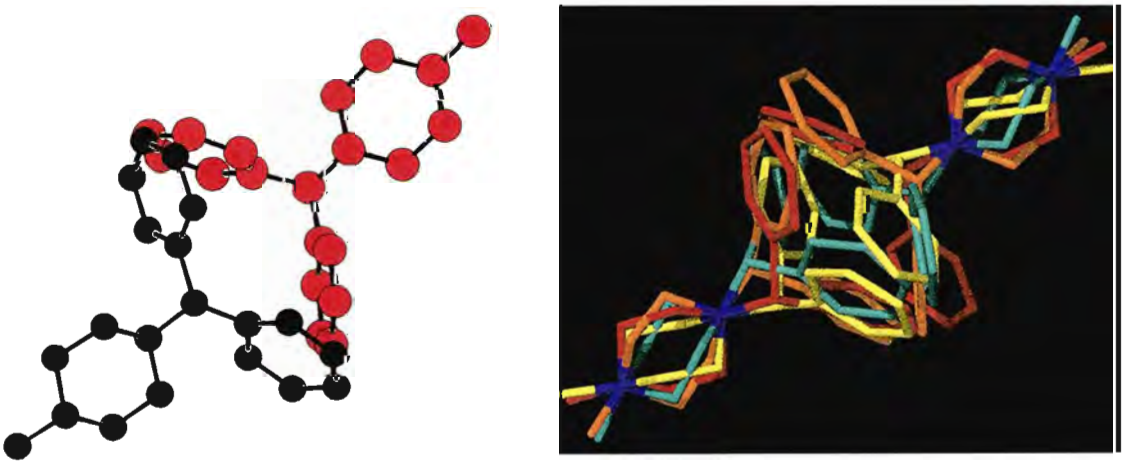

(a) (b)

Figure 6.20 (a) Two disordered positions of CYC, (b) including rotated positions

Geometrical analysis of the CYCGCD structure

The CYCGCD structure, as mentioned previously, consists of three γ-CD molecules arranged to form a trimer. Since the CD molecules lie with their centres on a four-fold axis, only two glucose units from each CD define the host structure. The three CDs will be referred to as CD(A), CD(B) and CD(C) and the glucose units of those three CDs will be designated A1, A2, B1, B2, C1 and C2. The two positions of the cyclizine molecule are designated CYC(A) and CYC(B). The cyclizine molecule is numbered following Figure 6.1 for both disordered positions.

The glucose residues are all in the $^4C_1$ chair conformation and their geometrical parameters are listed in Tables 6.23, 6.24 and 6.25 (e.s.d.s are of the order of 0.01Å and in the range 1-2° for the angles). The three primary hydroxyl groups with full site-occupancy all adopt the (-)-*gauche* orientation with an average value of $\omega = -59°$. The primary hydroxyl groups of A1, A2 and C1 are disordered over two positions each. The major position for each has a primary hydroxyl group in the (-)-*gauche* orientation while the minor positions adopt the (+)-*gauche* orientation.

Table 6.23 Selected torsion angles for glucose units of the CYCGCD structure

Glucose unit	ω_1 (°)†	ω_2 (°)†	Φ (°)†	Ψ (°)†	Θ_1 (°)†	Θ_2 (°)†
A1	- 68	+ 66	110	126	56	-58
A2	- 73	+ 57	110	127	54	-56
A | mean |	**71**	**62**	**110**	**127**	**55**	**-57**
B1	- 59	-	107	131	57	-57
B2	- 59	-	106	130	56	-56
B | mean |	**59**	**-**	**107**	**131**	**57**	**-57**
C1	- 59	+ 82	104	129	57	-60
C2	- 60	-	104	130	55	-57
C | mean |	**60**	**82**	**104**	**130**	**56**	**-59**

† Refer to page 4,5 (Chapter 1) for definitions and descriptions of these quantities

The geometrical parameters of the O4 octagons of the CYCGCD complex are shown in Table 6.24. The γ-CD macrocycles are highly symmetrical with very small deviations from the mean for the radii, side lengths and O4···O4···O4 angles of the O4 octagon. The deviation of the O4 atoms from the mean O4 plane is almost zero and this is further reflected by the near-zero values of the O4···O4···O4···O4 torsion angles. The tilt angles for the glucose residues are positive for the glucose residues of all three γ-CD molecules and are in the normal range for γ-CD structures (Table 6.25).

Table 6.24 Geometrical data for the O4 octagons of the CYCGCD structure

Glucose unit	*r* (Å)†	*l* (Å)†	*a* (°)†	*d* (Å)†	*t* (°)†
A1	4.49	5.89	135	0.00	0
A2	4.52	5.89	135	0.00	0
A | mean |	**4.51**	**5.89**	**135**	**0.00**	**0**
B1	4.47	5.89	136	+ 0.01	- 1
B2	4.53	5.86	134	- 0.01	+ 1
B | mean |	**4.50**	**5.88**	**135**	**0.01**	**1**
C1	4.51	5.91	136	- 0.01	- 2
C2	4.49	5.86	134	+ 0.01	+ 2
C | mean |	**4.50**	**5.89**	**135**	**0.01**	**2**

† Refer to page 4,5 (Chapter 1) for definitions and descriptions of these quantities

Table 6.25 Values of intersaccharide bond distances (φ), the O2(n)···O3(n-1) distances and the tilt angles (τ_1 and τ_2) for the CYCGCD structure

Glucose unit	φ (°)†	O2(n)···O3(n-1) (Å)†	τ_1 (°)†	τ_2 (°)†
A1	117	2.79	+10.0	+13.1
A2	117	2.77	+10.1	+12.9
A | mean |	**117**	**2.78**	**10.1**	**13.0**
B1	118	2.85	+12.2	+17.0
B2	117	2.89	+11.0	+16.6
B | mean |	**118**	**2.87**	**11.6**	**16.8**
C1	119	2.93	+15.1	+17.6
C2	117	2.86	+13.7	+17.6
C | mean |	**118**	**2.90**	**14.4**	**17.6**

† Refer to page 4,5 (Chapter 1) for definitions and descriptions of these quantities

Overall description of the CYCGCD structure

The CPK diagrams (Figures 6.21 and 6.22) show the relative positions of the disordered cyclizine molecule in the trimer formed by CD(A), CD(B) and CD(C). The colour codes used for these figures are: γ-CD: C (grey), O (red), H (white); CYC: C (green), H (yellow), N (blue); Water: O (light blue). The hydrogen atoms on the cyclizine molecules were not part of the refined model, but have been inserted in geometrically fixed positions for these CPK diagrams.

For clarity, a single orientation of the four-fold rotated positions of CYC(A) and CYC(B) is shown in each case and these two positions of the disordered pair are represented in separate figures. The relative positions of CYC(A) and CYC(B) are shown in Figures 6.21 and 6.22 respectively.

It is evident from the figures that the modes of inclusion of both molecules of the disordered pair are quite similar. The piperazine ring of CYC(A) is inserted into the secondary hydroxyl end portion of the cavity CD(A) while the piperazine ring of CYC(B) is inserted into the secondary hydroxyl end portion of the cavity of CD(B). The piperazine ring penetrates deeply into the γ-CD cavity in both cases, such that the methyl substituent of the piperazine ring protrudes from the primary hydroxyl ends. The diphenylmethyl group in both cases occupies the secondary interface between CD(A) and CD(B) (Figures 6.21 (b) and 6.22 (b)).

The mode of inclusion for the cyclizine molecule of CYCGCD is therefore very similar to that of the two cyclizine molecules which are included into the secondary hydroxyl end of the β-CD cavity in the CYCBCD structure (Figures 6.8 and 6.9).

A single water molecule (OW8) is included in the trimer cavity in the vicinity of the primary hydroxyl end of CD(C). The water molecule is in hydrogen bonding contact with the disordered primary hydroxyl group of glucose A1, which has a (+)-*gauche* primary hydroxyl torsion angle, and is therefore orientated towards the inside of the CD cavity.

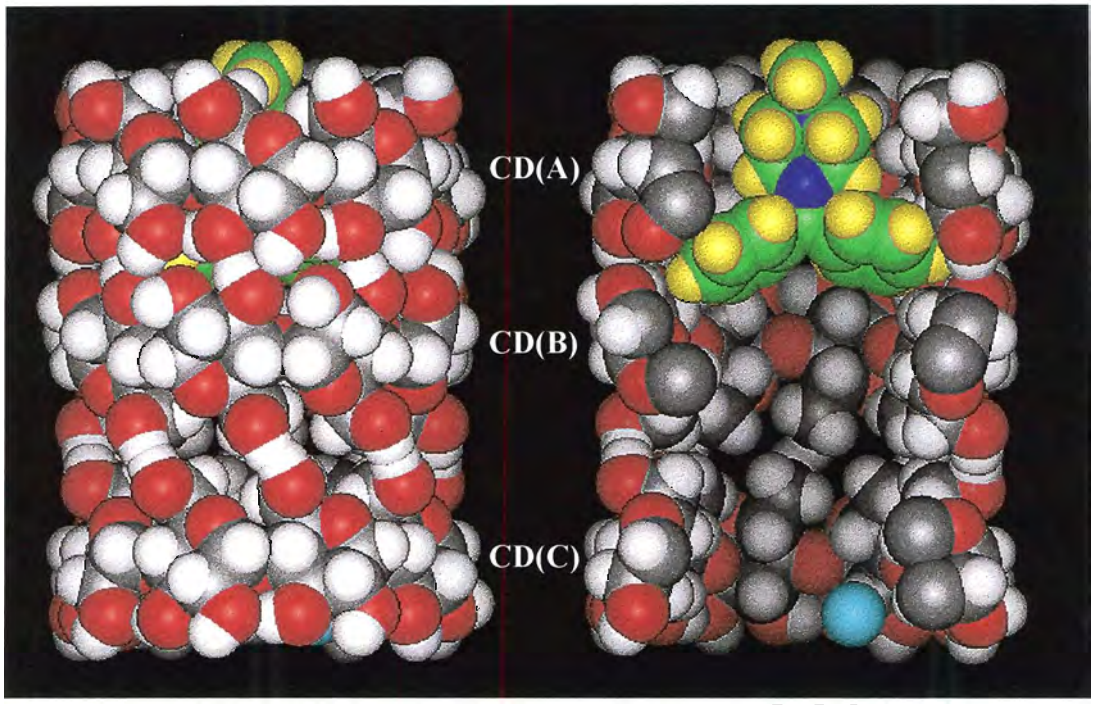

(a) (b)

Figure 6.21 γ-CD trimer with one of the four rotated positions of CYC(A)
(a) view perpendicular to the trimer axis (b) same view with the trimer sectioned

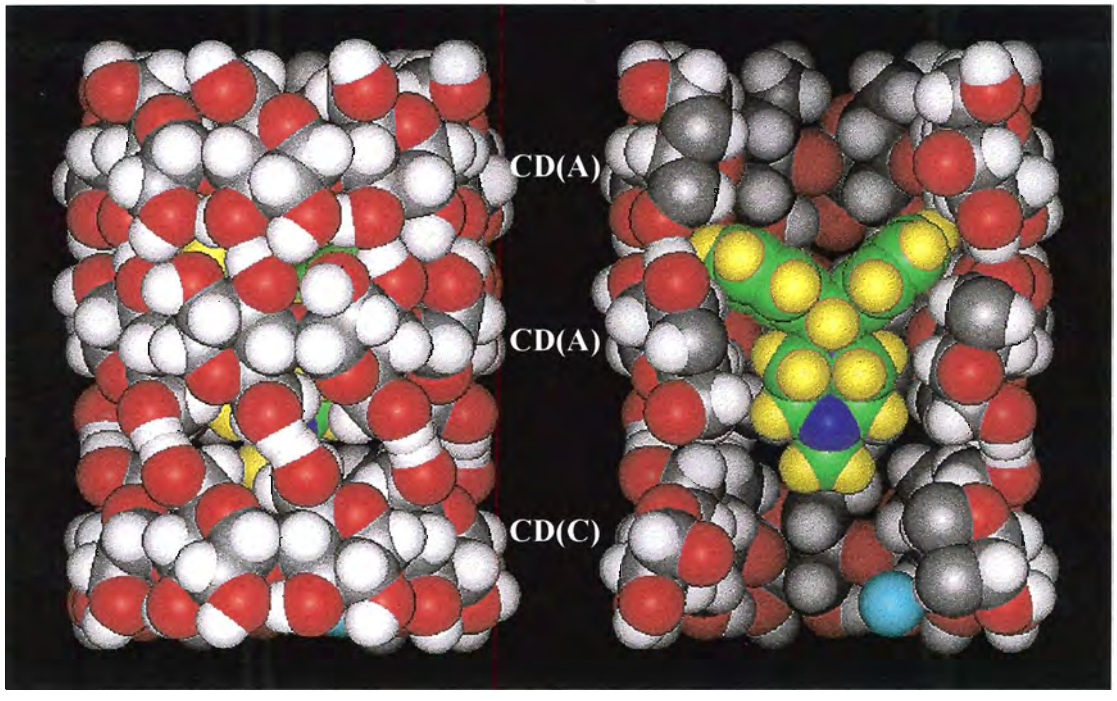

(a) (b)

Figure 6.22 γ-CD trimer with one of the four rotated positions of CYC(B)
(a) view perpendicular to the trimer axis (b) same view with the trimer sectioned

Crystal packing of the CYCGCD structure

Figure 6.23 (a) shows a sectioned view of a γ-CD trimer illustrating the conglomeration and overlap of atomic positions that results from the four-fold rotation of the two positions of the cyclizine guest. Figure 6.23 (b) shows the same trimer viewed down its cavity. A stereo diagram of a γ-CD trimer with a single rotated position of CYC(A) and CYC(B) is shown in Figure 6.24 (a). Figure 6.24 (b) is a projection down the *c*-axis of the structure with all rotated positions of CYC(A) and CYC(B) shown. The water molecules (shown as empty diamonds) are clearly seen to be located in the interstitial channels. Representations of the packing arrangement of the CYCGCD structure are presented in Figures 6.25 (a) and (b) with a single rotated position of CYC(A) shown in each case. Figure 6.25 (a) is a projection down the *a*-axis of the structure and shows the stacking of γ-CD trimers to form "infinite" columns. Figure 6.25 (b) is a projection of the structure down the *c*-axis and illustrates the "endless" channels formed by cavities of columns of γ-CD trimers. Figure 6.25 (a) illustrates an example of one arrangement in the crystal which would maintain the 1:3 CYC:γ-CD stoichiometric ratio observed for the CYCGCD structure.

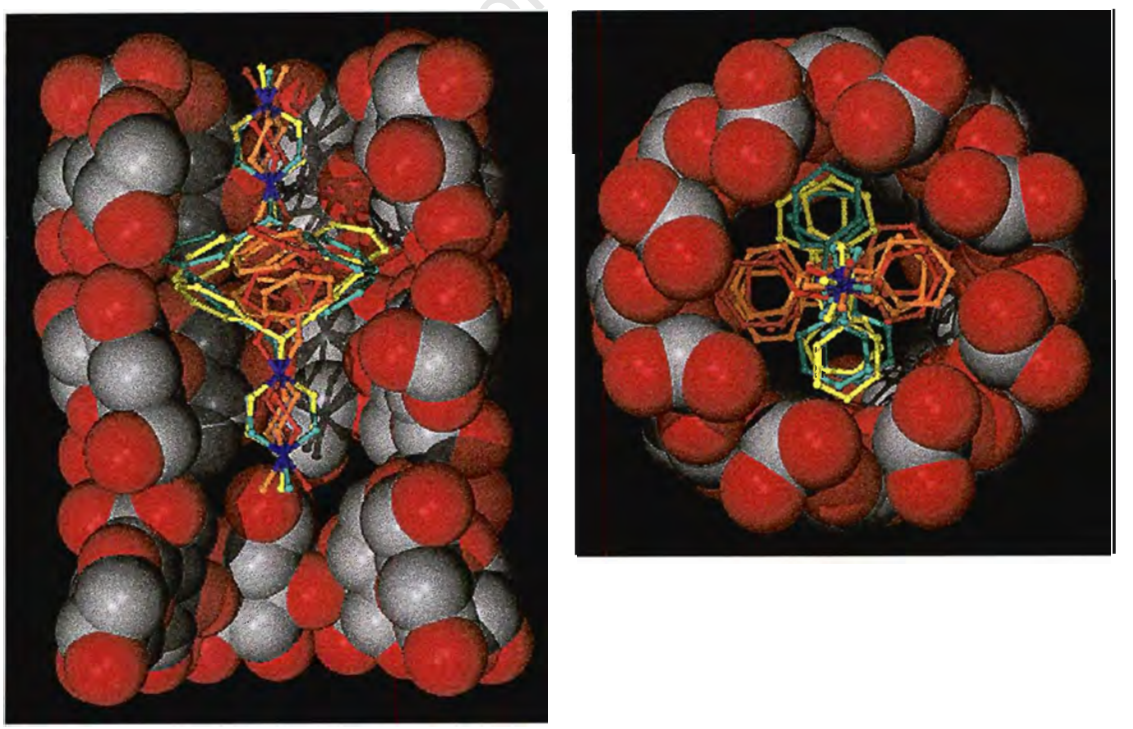

(a) (b)

Figure 6.23 γ-CD trimer showing all rotated positions of CYC(A) and CYC(B) (a) sectioned side view of trimer (b) view down cavity of trimer

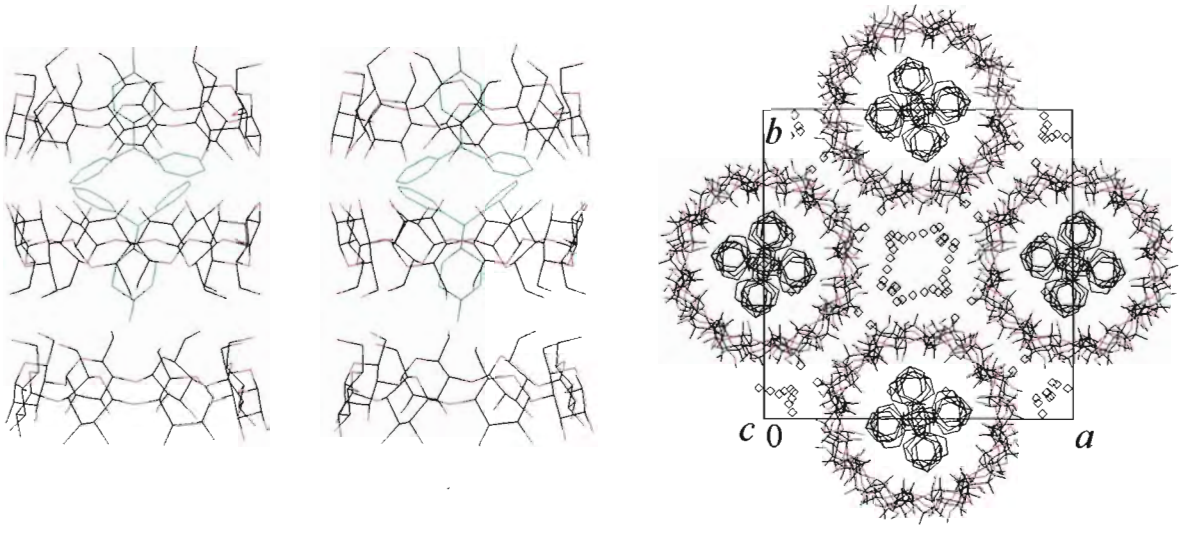

(a) (b)

Figure 6.24 (a) stereo diagram of γ-CD trimer showing a single rotated position each for CYC(A) and CYC(B) (b) *c*-axis projection of the CYCGCD structure showing the positions of the water molecules (all rotated positions of CYC(A) and CYC(B) included and the water molecules are drawn as empty diamonds)

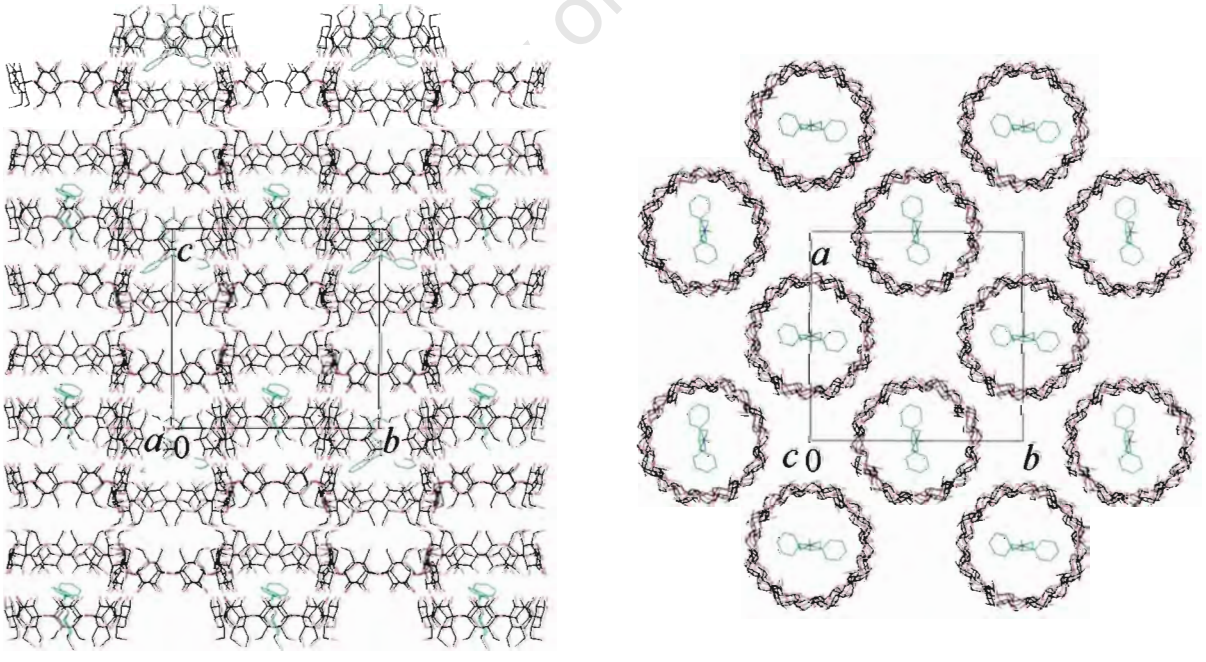

(a) (b)

Figure 6.25 (a) *a*-axis projection of the CYCGCD structure (b) *c*-axis projection of the CYCGCD structure (a single rotated position of CYC(A) is shown)

The CYCGCD complex displays the usual stoichiometric ratio of 1:3 CYC:γ-CD. The stoichiometric ratio of the CYCGCD complex seems to motivate the question of why further cyclizine molecules could not have been included in the structure. An attempt to address this question will be made using the empirical and crystallographic data obtained thus far.

From the results of crystal structure analysis of CYCBCD and CYCGCD and the spatial requirements of the cyclizine molecule, as related to the inclusion space provided by the β- and γ-CD head-to-head dimers, it is evident that only one cyclizine molecule can be completely included within a head-to-head CD dimer.

The CYCGCD structure contains a cyclizine molecule included in the CD(A)-CD(B) head-to-head dimeric portion of the γ-CD trimer. The inclusion of a further cyclizine molecule could occur only from the secondary or primary hydroxyl ends of CD(C), or from one of the primary hydroxyl ends of the CD(A)-CD(B) dimer (Figure 6.26). In all of these cases it would mean that large portions of the additional cyclizine molecule would be left protruding from the CD molecule in which it has been included. This would in all probability cause disruption of the head-to-tail and tail-to-tail interactions that occur for the γ-CD trimeric channel packing arrangement. Since this arrangement with its distinctive head-to-head, head-to-tail and tail-to-tail interactions is seen for all γ-CD structures, with the exception of the hydrate, it very likely represents a preferred arrangement of γ-CD molecules. Any disruption to the stability of this arrangement would therefore be disfavoured during the formation of the crystal of a γ-CD inclusion complex.

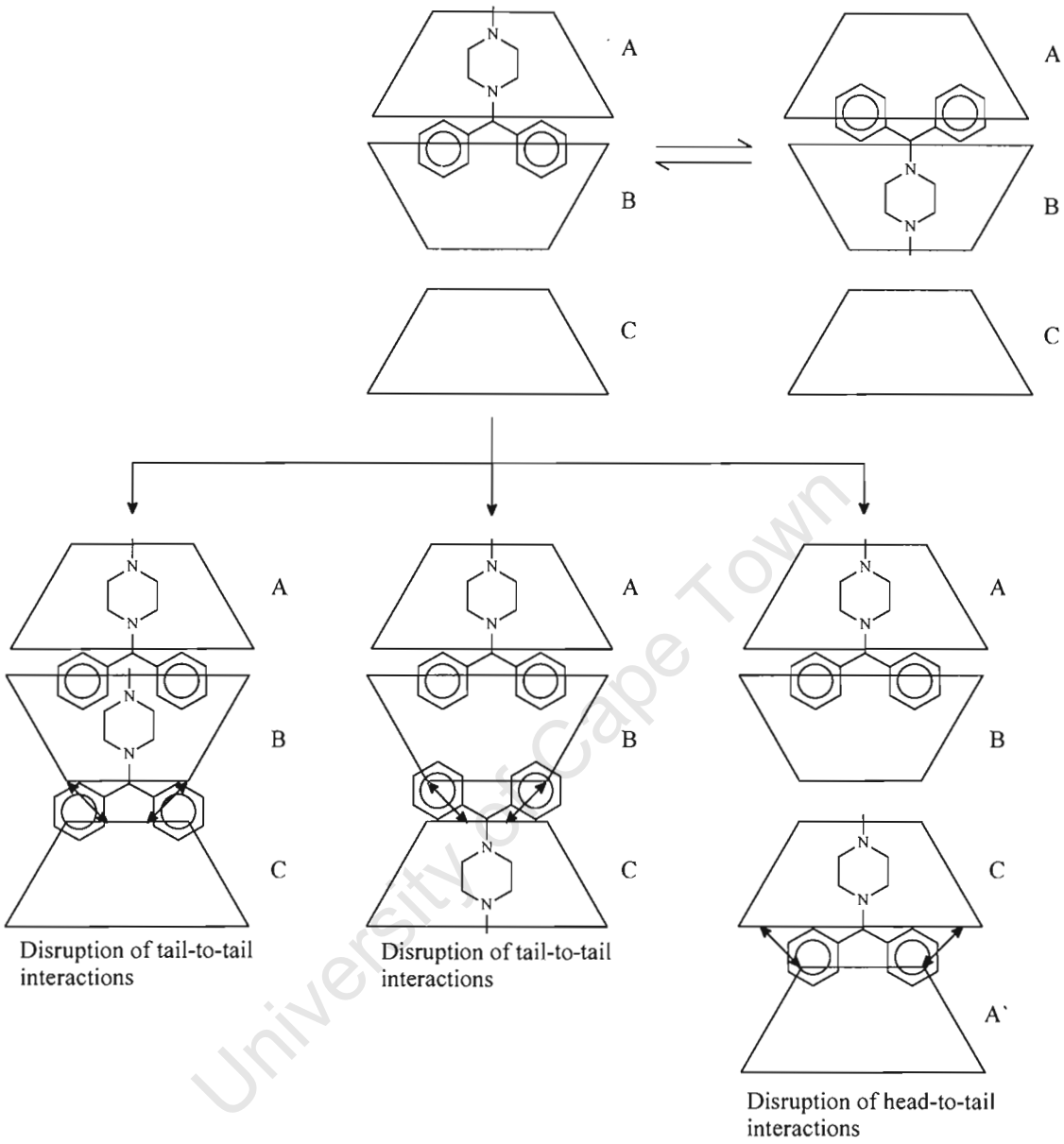

Figure 6.26 A schematic illustration of the inclusion of an additional CYC molecule to the γ-CD timer

Hydrogen bonding interactions of the CYCGCD structure

Tables 6.26, 6.27, 6.28 and 6.29 list summaries of the appropriate contacts for the cyclodextrin, trimer, inter-channel and water interactions. The listed contacts are all in the range of 2.50 to 3.20Å and the e.s.d. s are in the range 0.01-0.02Å for the cyclodextrin, trimer and inter-channel interactions and 0.01-0.05Å for the water interactions.

A.) Cyclodextrin interactions

The hydroxyl groups of the secondary hydroxyl end of the γ-CD molecules of the CYCGCD complex are held together by a ring of hydrogen bonded interactions as has been seen for the β-CD molecules of the complexes discussed so far. This rim of hydrogen bonds is a general feature seen for all β- and γ-CD complexes and serves to stabilise the macrocyclic conformation of the CD. Table 6.26 lists the O···O contacts for interactions of this nature.

Table 6.26 Cyclodextrin interactions for the CYCGCD structure

O2···O3	Number / CD	Range (Å)	Mean (Å)
A	8	2.77-2.79	2.78
B	8	2.85-2.89	2.87
C	8	2.86-2.93	2.90

B.) Trimer interactions

The formation of the γ-CD trimer as a primary building block is seen for all the known complexes of γ-CD, with the exception of the γ-CD hydrate structure. It is evident from this that it is a largely preferred and stable arrangement of γ-CD molecules. The trimer exhibits head-to-head, head-to-tail and tail-to-tail orientations of the γ-CD molecules in the trimer. These orientations are stabilised by direct hydrogen bonded interactions between the CDs and those mediated by water. Tables 6.27 (a), (b) and (c) list the O···O contact distances for head-to-head, head-to-tail and tail-to-tail interactions of the γ-CD trimer.

Table 6.27 Trimer interactions for the CYCGCD structure

(a) Head-to-head trimer interactions

Type	CDs	Number / trimer	Range (Å)	Mean (Å)
O3···O3	A-B	8	2.80	2.80
O2···O2	A-B	8	2.98	2.98
O2···O3	A-B	16	3.19-3.20	3.20

(b) Tail-to-tail trimer interactions

Type	CDs	Number / trimer	Range (Å)	Mean (Å)
O6···O6	B-C	8	2.79-2.81	2.80

(c) Head-to-tail trimer interactions

Type	CDs	Number / trimer	Range (Å)	Mean (Å)
O2···O6	A`-C	12	2.77-2.98	2.87
O3···O6	A`-C	8	3.02-3.06	3.04

C.) Inter-channel interactions

The arrangement of CDs in the CYCGCD complex, as already discussed, consists of endless columns of γ-CD molecules. These columns are held together by direct hydrogen bonds between the CD hydroxyl groups and also those mediated by water. Table 6.28 lists the O···O contact distances for direct inter-channel interactions.

Table 6.28 Inter-channel interactions for the CYCGCD structure

Type	Number / trimer	Range (Å)	Mean (Å)
O2···O3	8	2.75-2.83	2.79
O6···O6	4	3.10	3.10

D.) Water interactions

Water molecules play an important role in the stabilisation of trimeric γ-CD structures. The water molecules lie mainly in the interstitial channels forming a network of hydrogen bonds between the columns of γ-CD molecules. The water molecules are bonded directly to the hydroxyl oxygen atoms of the γ-CD or bonded to other water molecules (Table 6.29).

Table 6.29 Water interactions for the CYCGCD structure

Type	Number / trimer	Range (Å)	Mean (Å)
O2···Water	12	2.73-3.05	2.77
O3···Water	16	2.78-3.18	2.97
O6···Water	36	2.59-3.15	2.86
Water···Water	48	2.55-2.94	2.77

XRD

The experimental and calculated XRD patterns of the CYCBCD and CYCGCD complexes are shown in Figure 6.27. A close match between the experimental and calculated patterns is evident for both complexes.

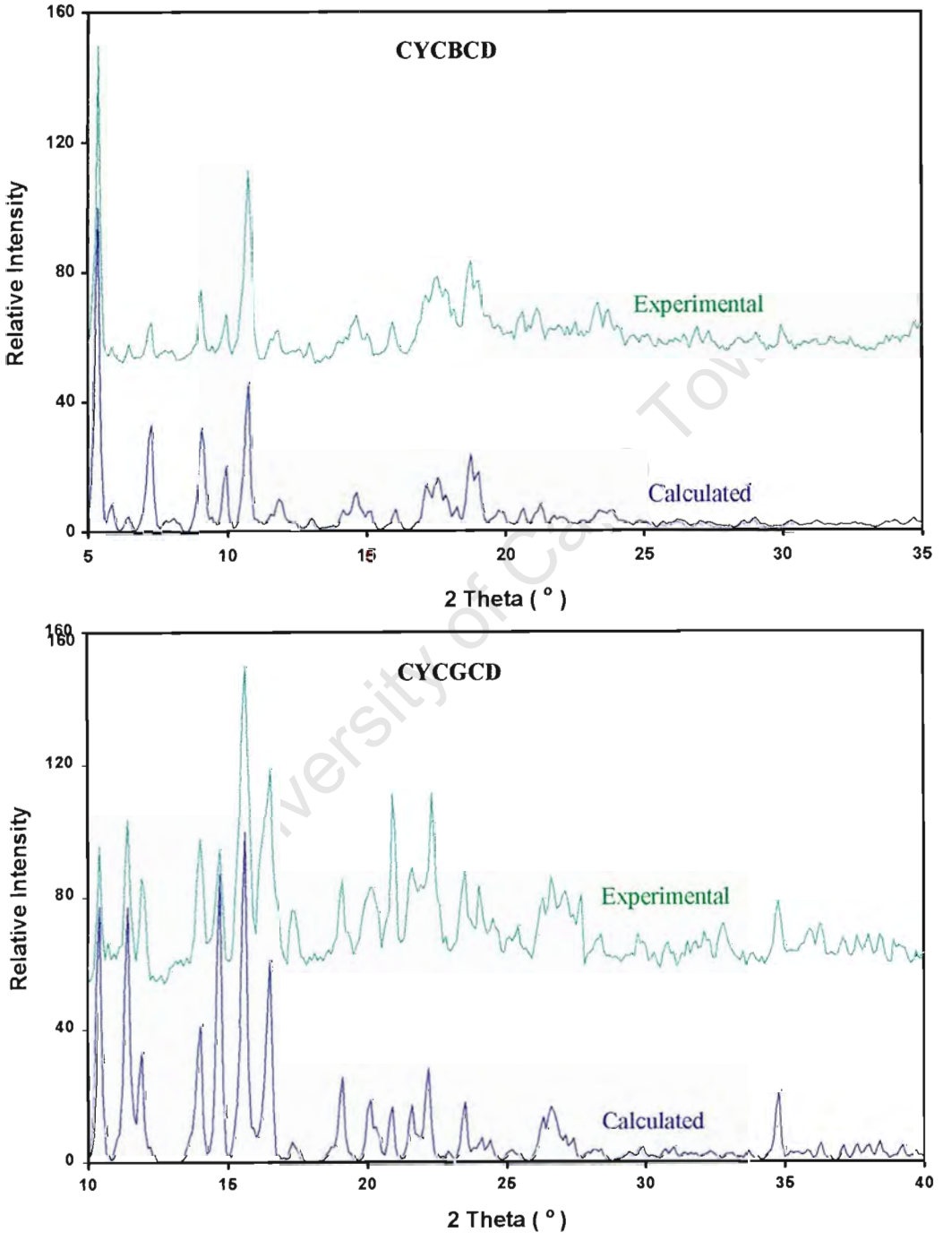

Figure 6.27 Calculated and experimental XRD patterns for CYCBCD and CYCGCD

References

1.) S. Budavari, M. J. O'Neil, A. Smith, P. E. Heckelman and J. F. Kinneary (eds.), *The Merck Index, 12th Edition*, Merck and Co., Inc., New Jersey, USA, **1996**.

2.) W. Q. Tong, J. L. Lach, ~~C. T. Fong~~ T.-F. Chia and J. K. Guillory, *Pharm. Res.*, **1991**, 8(7), 951.

3.) W. Q. Tong, J. L. Lach, ~~C. T. Fong~~ T.-F. Chia and J. K. Guillory, *J. Pharm. Biomed. Anal.*, **1991**, 9(10-12), 1139.

4.) W. Q. Tong, J. L. Lach, ~~C. T. Fong~~ T.-F. Chia and J. K. Guillory, *Pharm. Res.*, **1991**, 8(10), 1307.

5.) L. J. Penkler, South African Druggists International, personal communication.

6.) E. Egert and G. M. Sheldrick, *Acta Cryst.*, **1985**, A41, 262.

7.) G. M. Sheldrick, *Crystallographic Computing*, ed. G. M. Sheldrick, C. Krüger and R. Goddard, Oxford University Press, **1985**, Volume 3, 175.

8.) G. M. Sheldrick, *SHELXL-93, Program for the Refinement of Crystal Structures*, University of Göttingen, Germany, **1993**.

9.) G. Gilli, V. Bertolasi and P. A. Borea, *Eur. Cryst. Meeting*, **1979**, 5, 183.

10.) V. Bertolasi, P. A. Borea, G. Gilli and M. Sacerdoti, *Acta Crystallogr. Sect. B*, **1980**, 36, 1975.

11.) T. Fujiwara, K.-I. Tomita, I. Marseigne and J. Vicens, *Mol. Cryst. Liq. Cryst.*, **1988**,156, 393.

12.) J. Vicens, T. Fujiwara and K.-I. Tomita, *J. Inclusion Phenom.*, **1988**, 6, 577.

13.) D. Mentzafos, I. M. Mavridis, G. le Bas and G. Tsoucaris, *Acta Crystallogr., Sect. B*, **1991**, 47, 746.

14.) I. Nakanishi, M. Arai, T. Fujiwara and K. Tomita, *J. Inclusion Phenom.*, **1984**, 2, 689.

15.) W. Saenger, C. Betzel, G. Hingerty and G. M. Brown, *Nature*, **1982**, 296,581.

16.) W. Saenger, C. Betzel, G. Hingerty and G. M. Brown, *Angew. Chem. Int. Ed. Engl.*, **1983**, 22, 883.

17.) G. le Bas and G. Tsoucaris, *Supramolecular Chemistry*, **1994**, 4, 13.

18.) Z. Otwinowski and W. Minor, *Processing of X-ray Diffraction Data in Oscillation Mode in Methods in Enzymology*, ed. C. W. Carter and R. M. Sweet, Academic Press, New York, **1996**, Vol. 276, 307.

19.) S. Kamitori, K. Hirotsu and T. Higuchi, *J. Chem. Soc.,Chem. Commun.*, **1986**, 690.

20.) S. Kamitori, K. Hirotsu and T. Higuchi, *J. Chem. Soc.,Chem. Commun.*, **1987**, 109, 2409.

21.) S. Kamitori, K. Hirotsu and T. Higuchi, *Bull. Chem. Soc. Jpn.*, **1988**, 61, 3825.

22.) J. Ding, T. Steiner and W. Saenger, *Acta Crystallogr., Sect. B*, **1991**, 47, 731.

23.) K. Lindner and W. Saenger, *Biochem. Biophys. Res. Commun.*, **1980**, 92, 933.

24.) B. E. Hingerty, C. Betzel and W. Saenger, *Am. Cryst. Assoc., Abstr. Papers (Winter)*, **1984**, 12, 37.

25.) K. Harata, *Chem. Lett.*, **1984**, 641.

26.) K. Harata, *Bull. Chem. Soc. Jpn.*, **1987**, 60, 2763.

27.) J. M. Maclennan and J. J. Stezowski, *Biochem. Biophys. Res. Commun.*, **1980**, 92, 926.

28.) Borchert, *Z. Naturforsch., Teil B*, **1948**, 3, 464.

CHAPTER 7 : CONCLUSION

Complex Preparation and determination of stoichiometry

The crystalline phase allows for a definitive characterisation of an inclusion complex, with the x-ray structural solution providing unambiguous proof of complexation. However, with an amorphous substance like HP-β-CD, which is a mixture of a number of isomers, a crystalline phase of an inclusion complex cannot be prepared and characterisation of the complexes is achieved by other criteria. Indications of complex formation are those based on the assumption that the included guest no longer exhibits its bulk crystalline properties when it is interspersed in a CD lattice. Formation of a CD complex is characterised by the disappearance of the fusion event of the guest as well as the disappearance of its XRD profile. Shifts in prominent IR bands of a guest may also serve as an indication that certain interactions of the guest have been altered in the presence of a CD. These trends were all observed for the investigation of the interaction of HP-β-CD and salbutamol laurate effected by co-grinding and kneading (Chapter 5). However, to distinguish between amorphisation of a guest in the presence of a CD and actual complexation in the solid state remains a challenging task.

The combination of UV spectrophotometric analysis, thermogravimetric analysis and microanalysis was the principal means of determining the stoichiometry of a crystalline complex. Before the stoichiometry could be determined it was necessary to demonstrate that the sample consisted of a single phase with no impurities. This was achieved by detailed studies of the thermal properties of the complex, using HSM and DSC techniques, where the behaviour of the complexes was compared with that of the pure CD and drug constituents.

Thermal investigation of CD complexes

A feature of the inclusion complexes investigated in this study was that decomposition of the complexes began at a lower temperature than decomposition of the pure host. This decrease in thermal stability of the inclusion complexes is associated with the thermal stability of the guests they include. The anti-ulcerative inclusion complexes with β- and γ-CD dealt with in Chapter 4 revealed a correlation

between the onset of decomposition of the inclusion complex and the onset of decomposition of the appropriate uncomplexed guest. The implication of these observations was that the inclusion of the guest by the CD does confer additional stability on the particular guest but that the thermal stability of the guest in the uncomplexed state is still an important overall determinant.

The use of XRD to identify CD complexes

Crystalline CD inclusion complexes showed characteristic XRD powder patterns which were distinguishable from those of the uncomplexed guest, pure host or any mixture of the two. However, the XRD trace of a crystalline inclusion complex can in many cases provide additional information on structural characteristics of the CD-complex preparation.

The XRD patterns of the γ-CD complexes with cimetidine, famotidine, ranitidine (Chapter 4) and cyclizine (Chapter 6) were all closely matching implying an isomorphous packing arrangement for the host structures of these complexes. X-ray photography showed a common space group and closely matching cell parameters. These crystallographic features were consistent with structures crystallising in the trimeric channel packing arrangement of γ-CD complexes. The structure solution of the CYCGCD complex confirmed this observation. The CIMBCD complex showed a closely matching XRD pattern and cell parameters to that of the ACEBCD structure, indicating an isomorphous packing arrangement. The XRD pattern of the RANBCD complex showed resemblance to that of the CIMBCD complex and a similar packing arrangement for the two complexes was postulated, despite the differing cell parameters and space groups. The future use of XRD traces as a predictive indicator of structural characteristics of CD complexes may prove very useful.

The XRD patterns calculated from the crystal structure solutions of the β- and γ-CD complexes with cyclizine showed good agreement with their corresponding experimental patterns. The calculated XRD trace can therefore be used to demonstrate the purity and integrity of a crystalline CD inclusion complex. This has implications for the industrial preparation of CD complexes intended for commercial pharmaceutical applications.

X-ray structure solution of CD complexes

Isomorphous replacement techniques proved to be very useful for the structure solution of CD complexes, accounting for the solution of four of the six crystal structures investigated in this study.

Where no isomorphous complex had been reported, the program PATSEE proved to be a powerful tool for solving CD complexes. The power of this approach was evident in the structure solution of the DIABCD (Chapter 3) and CYCBCD (Chapter 6) complexes, which contained two and four CDs respectively within the asymmetric unit. The magnitude of these crystallographic problems proved to be too demanding for conventional direct methods techniques which failed to produce meaningful solutions.

Structural Characteristics of CD complexes

CD Geometry

The β-CD conformation in dimeric structures was noted to be significantly more planar, symmetrical and undistorted compared with the conformations observed in monomer structures. The β-CD molecules of the ACEBCD, BROBCD, PHEBCD, DIABCD and CYCBCD structures showed more symmetrical O4 heptagons, smaller deviations of O4 atoms from planarity with the mean O4 plane and smaller and less variable tilt angles when compared with a wide variety of monomeric β-CD structures. The narrower range of these geometrical parameters is considered necessary to optimise the O3···O3 hydrogen bonds observed for all dimeric β-CD structures.

Hydrogen bonding interactions

The dimeric structures investigated in this study showed a remarkable consistency in the constitution of their hydrogen bonded network. The intra-CD, intra-dimer, intra-layer and CD-to-water interactions of the dimeric structures investigated were all closely matching in the nature of their donors and acceptors and in their observed O···O contact distances. The most notable difference observed was a decrease in the number of direct interactions between primary hydroxyls of adjacent CDs which was correlated with a distortion of the linearity of dimeric columns at the inter-dimer primary interface.

Mode of guest inclusion and orientation

The four *para*-substituted acetanilide guests investigated in Chapter 3 showed very similar modes of inclusion in their respective β-CD complexes. In all cases, two guest molecules were included within a β-CD dimeric unit. The phenyl rings of the guest molecules were centralised in the cavities of the β-CD molecules with the substituents occupying the regions of the primary and secondary rims. The positioning of the relatively polar substituents of the guests at the CD rims allowed for solvation and hydrogen bonding with water molecules and CD-hydroxyl groups respectively. The relatively planar conformations of the uncomplexed *para*-acetanilide guests, which are necessary for the close packing in these structures, were relaxed in their respective β-CD complexes.

The phenyl rings of the guest molecules were tilted by approximately 25° to the dimer axis so that abnormally close approach of substituents in the region of the intradimeric interface could be avoided. This allowed the bulk of all guests to be included in the dimeric unit. However, portions of these guests still protruded to differing extents from the primary ends of the β-CD dimeric unit. The trend of increasing protrusion from the primary faces of the dimer was observed when the guest molecule was varied from : acetaminophen < *p*-bromoacetanilide < phenacetin < diacetamate.

The cyclizine molecule presented an interesting study for the mode of guest inclusion since it can be included in a CD cavity *via* its piperazine ring or *via* either of its two phenyl rings. In both the CYCBCD and CYCGCD complexes, the piperazine ring was inserted in the CD cavity. However, the cyclizine molecule showed different modes of inclusion within the CYCBCD structure with the diphenylmethyl group externalised at both the primary and secondary rims of the macrocycle. The cyclizine guest molecules included from the secondary rim of the β-CD molecules showed very similar conformations to that of uncomplexed cyclizine hydrochloride, where a mirror plane relates the two halves of the molecule. However, for the cyclizine molecule inserted from the primary rim of the β-CD macrocycle a less symmetrical conformation of the guest was observed with the phenyl rings twisted in opposite directions to one another. The twisting of the phenyl rings allowed one of the them to be partially inserted into the cavity of an adjacent CD molecule.

The orientation of a guest was a fundamental question that was addressed for the study of the investigation of the inclusion of the *para*-substituted guests by β-CD. All four guests had *para*-substituents which differed in size and chemical nature. Since in all cases the phenyl rings were observed to be centralised in the β-CD cavities, the orientations were discussed in terms of whether the *para*-substituent would occupy the primary or secondary rim region of the β-CD macrocycle.

For the β-CD complexes with acetaminophen and *p*-bromoacetanilide the acetylamino residues occupied the intradimeric cavity with the hydroxy residue and bromine atom occupying the primary rim region. This orientation was reversed for the β-CD complexes with phenacetin and diacetamate where the acetylamino residues occupied the primary rim regions and the ethoxy and acetyloxy residues occupied the intradimeric cavity.

The anti-parallel alignment of host and guest dipoles[1] and the affinity of hydrophobic portions of guests for the relatively hydrophobic primary rim and hydrophilic portions for the relatively hydrophilic secondary rim[2] have been offered as explanations for the observed orientations of guests within CD complexes.

The dipole moments of the acetaminophen and *p*-bromoacetanilide guests were observed to be tending towards anti-parallel alignment with the CD dipole. However the dipole moments of the phenacetin and diacetamate molecules were more closely aligned with the macrocyclic plane and did not show any dipolarity between the *para*-substituents and acetylamino residues.

The acetylamino, hydroxy, ethoxy and acetyloxy residues are all classed as relatively polar substituents and therefore the differences in their relative hydrophobicities is unlikely to be a significant determinant of orientation. The *p*-bromoacetanilide molecule contains the hydrophobic bromine atom substituent which conformed to the theory proposed by Lichtenthaler et. al[2] and was found situated at the primary rim.

Size of the *para*-substituent was considered an important factor. The position of the bromine atom and hydroxy residue of the *p*-bromoacetanilide and acetaminophen guests at the primary rims allowed for almost complete enclosure of these guests within a β-CD dimeric unit.

Crystal packing of CDs

The packing arrangements of β-CD structures can be examined in terms of their asymmetric volumes (V/Z) (where the asymmetric volume is defined as the cell volume required for a single β-CD molecule, its included guest and its associated water molecules).

The distribution of the asymmetric volumes of all β-CD complexes currently recorded in the Cambridge Crystallographic Database[3] are represented in the form of a scatter diagram in Figure 7.1, with the complexes grouped according to the type of packing arrangement they adopt. Details of the average asymmetric volumes for the various types of β-CD packing arrangements are presented in Table 7.1.

The smaller the asymmetric volume the more efficiently the β-CD molecules can pack. The water molecules in CD complexes are thought of mainly as "space-fillers" and therefore the closeness of packing of CD molecules is directly dependent on the volume of particular guests that interfere with the packing of the CD units in which they are contained (be they monomers or dimers).

From Figure 7.1 it is clear that the different β-CD packing arrangements occur over a fairly wide range of asymmetric volumes and with each arrangement confined to a limited range of values. Further, the asymmetric volumes of the various packing arrangements are only partially overlapping. This would suggest that the packing arrangement adopted by a β-CD structure is dependent on the asymmetric volume.

For the dimeric structures it is noted that an increase in the asymmetric volume is accompanied by a decrease in the linearity of the dimeric columns within those structures. This is the trend observed in going from the CH to IM to SC and CB packing arrangements [diagonal black arrow (labelled 1) in Figure 7.1].

The *para*-substituted acetanilides represent a series of analogous guest molecules with similar modes of inclusion. The extent of protrusion of these guests from their dimeric units follows the order : ACE < BRO < PHE < DIA. The increasing volume of guest protrusion is correlated with an increase in the asymmetric volume of the respective complex [horizontal black arrow (labelled 2) on Figure 7.1] and a change in the packing arrangement.

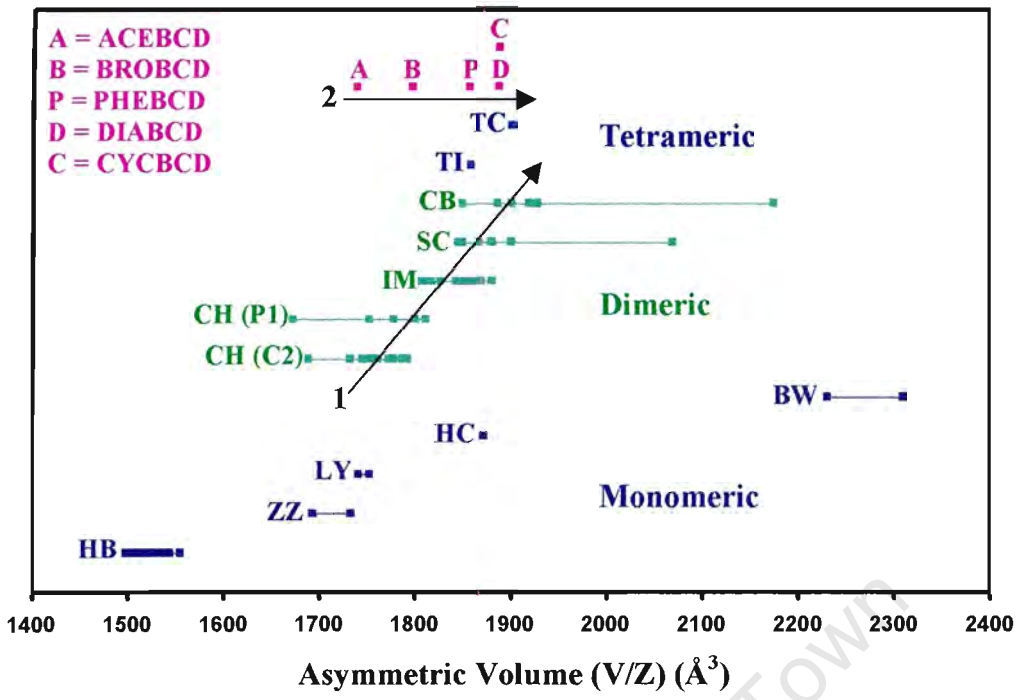

Figure 7.1 Scatter diagram of the asymmetric volumes for the various β-CD packing arrangements

Table 7.1 Details of the asymmetric volumes of the various β-CD packing arrangements

Packing Type†		Space group	Category	Number	Average V (Å^3)	Z	Average V/Z (Å^3)
Monomeric	HB	$P2_1$	1	20	3038	2	1519
Monomeric	ZZ	$P2_1$	1	2	6854	4	1714
Monomeric	LY	$P2_1$	3	2	3494	2	1747
Monomeric	HC	$P6_1$	3	1	11234	6	1872
Monomeric	BW	$P2_1$	3	2	4542	2	2271
Dimeric	CH	C2	2	12	7045	4	1761
Dimeric	CH	P1	2	5	3526	2	1763
Dimeric	IM	P1	2	15	3685	2	1843
Dimeric	SC	$P2_1$	2	7	7596	4	1899
Dimeric	CB	$C222_1$	2	6	15548	8	1943
Tetrameric	TI	P1	2	1	7434	4	1858
Tetrameric	TC	$P2_1$	2	1	15216	8	1902

† Abbreviations for packing type were defined in Chapter 1

The various β-CD packing arrangements recorded in the literature and which featured in this investigation can all be grouped into three basic categories and are discussed below in terms of their asymmetric volumes.

1.) Monomeric cage

This category includes β-CD complexes where the guest is small enough to be completely included in a single β-CD molecule. These complexes tend to prefer the monomeric herringbone packing arrangement, with the smallest asymmetric volume seen for β-CD structures. The zigzag type arrangement of the β-CD molecules for this type of complex, as seen in the packing arrangements of the HB and ZZ type (Chapter 1), allows close approach of β-CD molecules. The fact that no portions of included guests protrude from the monomers allows this efficient packing of the β-CD molecules to be achieved.

2.) Dimeric Layer

This category includes β-CD complexes where the volume of included guest(s) cannot be completely contained in a single β-CD molecule and where no significant distortion of the "roundness" of the β-CD conformation is seen upon inclusion. Fairly rigid geometrical criteria, as discussed earlier, are probably necessary for dimer formation. The volume of a dimeric unit is more than twice that of a monomer since it includes the region of the intradimeric cavity as well as the cavities of the two CDs. In these cases the complexes tend to pack as dimers with the dimers arranged in layers. The dimers are aligned in endless channels when the guest can be almost completely contained within a dimer. As increasingly larger portions of the guests protrude from the β-CD dimers, the asymmetric volume increases accordingly and the channels become more distorted from linearity.

The tetrameric arrangements of the β-CD structures with barbital[4] and *S*-(-)-methyl-*p*-tolylsulfoxide[5] contain two dimers in the asymmetric unit with the dimers forming a tetrameric channel, with these tetrameric units arranged in layers. However, this is still consistent with the dimeric layer classification since the tetrameric layers can be viewed as two dimeric layers with the dimers of adjacent layers arranged such as to produce tetrameric channels. The CYCBCD structure is an interesting example since the asymmetric unit consists of two dimers which do not form a tetrameric channel.

The unusual stoichiometry and mode of inclusion of the guest seem to offer some explanation for why this arrangement is adopted. The modes of guest inclusion and packing arrangement seen for this complex suggest that the efficiency of guest inclusion in β-CD structures is a consideration (i.e. the packing arrangement is "designed" to include the maximum possible number of guest molecules).

3.) Monomeric Layer

This category includes complexes where the guests are too large to be included within a single β-CD molecule and where significant distortion of the β-CD conformation is observed. The distortion in conformation means that many of the favourable head-to-head intra-dimer interactions can no longer be geometrically satisfied. These complexes therefore do not form dimers but pack as monomers and the monomers are arranged in layers.

The β-CD-pyridine structure[6] also packs as monomeric layers; however, it is somewhat of an exception since it is the only known example of a β-CD structure where the guest is not only included in the β-CD cavity but also occupies the interstitial spaces between β-CD molecules. The result is that it displays the largest asymmetric volume yet observed for β-CD structures.

Two recently reported structures of β-CD complexes with meclofenamate sodium[7] and piroxicam sodium[8] are new examples of monomeric layer structures. These two structures and that containing diclofenac sodium[9] represent three of the five known types of packing arrangements that can be classified as monomeric layer and all contain guests which are sodium salts. The influence of the sodium ion on the formation of monomeric layer type complexes is therefore considered to be significant. It is concluded that the strong coordination of the sodium ion to CD hydroxyl groups causes the distortion of the macrocyclic conformation. In all three structures the sodium ion coordinates CD hydroxyls of both the secondary and primary rims of two adjacent CD molecules.

The dimeric layer structures display seven distinct packing types, with the DIABCD and CYCBCD complexes reported in this thesis representing two additional arrangements. The majority of β-CD structures (47 out of 74, or 64%) fall into this category and the number of packing arrangements observed is relatively few in

comparison. On the other hand, only a small number of examples of monomeric layer structures have been reported and the tendency observed is that almost each new structure that falls into this category displays its own unique packing arrangement. This reinforces the notion that the guest may have a more direct influence on the CD conformation and packing arrangement adopted for these structures.

Harata[10] classified the β-CD complexes into 1.) cage, 2.) channel and 3.) layer. The author's classification differs only in that the categories used are 1.) monomeric cage, 2.) dimeric layer and 3.) monomeric layer, where the channel structures are a subset of the dimeric layer category and the layer structures are separated into monomeric and dimeric. Cages, channels and layers are the basic features of all categorisations of β-CD complexes, as is evident from the reviews of Saenger[11,12] and Harata.[10,13]

The distribution of the asymmetric volumes of the known γ-CD structures are illustrated in the form of a scatter diagram in Figure 7.2 with average values of the asymmetric volume for the different γ-CD packing arrangements listed in Table 7.2. The structure of the γ-CD hydrate[14] adopts a herringbone type packing arrangement similar to that observed for the β-CD hydrate[15] and other monomeric cage type β-CD structures. However, most of the γ-CD complexes invariably adopt the trimeric channel structure. The asymmetric volume of the trimeric channel structures is significantly larger than that of the cage type structures. The striking feature is that no intermediate structures have been recorded thus far. This indicates that the trimeric packing arrangement is highly stable and a preferred arrangement for γ-CD complexes and is favoured for the inclusion of all guest molecules within the γ-CD cavity. The arrangement is therefore independent of the nature of the included guest and also does not seem to require efficient guest inclusion.

The number of guest molecules that can be contained within the γ-CD trimer is limited by the non-interference of included guests with the intra-trimer bonds. The γ-CD complexes with cimetidine, famotidine and ranitidine (Chapter 4) contained two guest molecules within the trimer while the complex with cyclizine (Chapter 6) contained only one. It was clear that inclusion of a further cyclizine molecule would inevitably disrupt intra-trimer links and is therefore disfavoured, despite the low guest:host inclusion ratio that results.

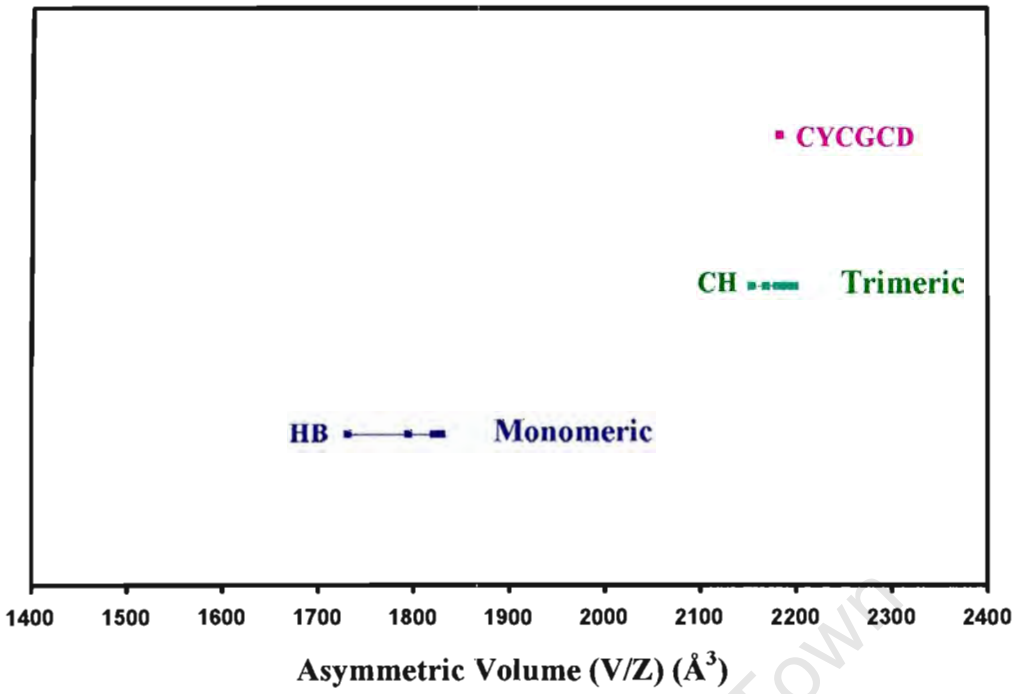

Figure 7.2 Scatter diagram of the asymmetric volumes of the various γ-CD packing arrangements

Table 7.2 Average values of the asymmetric volumes of the various γ-CD packing arrangements

Packing Type†		Space group	Category	Number	Average V (Å^3)	Z	Average V/Z (Å^3)
Monomeric	HB	$P2_1$	1	4	3590	2	1795
Trimeric	CH	$P42_12$	2	7	13097	6	2183

† Abbreviations for packing type were defined in Chapter 1

Pharmaceutical overview

Literature surveys performed for the purposes of this thesis revealed that the CD inclusion of a number of drug substances investigated in this thesis is of great interest to the pharmaceutical community.

Recent patent applications for CD complexes of naproxen,[16,17] ibuprofen[16] and diclofenac sodium[18,19] intended for commercial application were largely based around definitive characterisation of these complexes in the solid state, including the x-ray crystal structures. The use of structural and other physicochemical information in this way continues with the recent patent application lodged for the cyclizine complexes with β- and γ-CD characterised in the present work.[20]

References

1.) M. Sakurai, M. Kitagawa, H. Hoshi, Y. Inoue and R. Chûjô, *Carbohydr. Res.*, **1990**, 198, 181.

2.) F. W. Lichtenthaler and S. Immel, *Starch*, **1996**, 48(4), 145.

3.) *Cambridge Structural Database and Cambridge Structural Database System*, Version 5.12, October **1998**, Cambridge Crystallographic Data Centre, University Chemical Laboratory, Cambridge, England.

4.) I. Nakanishi, M. Arai, T. Fujiwara and K. Tomita, *J. Inclusion Phenom.*, **1984**, 2, 689.

5.) J. Vicens, T. Fujiwara and K.-I. Tomita, *J. Inclusion Phenom.*, **1988**, 6, 577.

6.) C. de Rango, P. Charpin, J. Navaza, N. Keller, I. Nicolis, F. Villain and A. W. Coleman, *J. Am. Chem. Soc.*, **1992**, 114, 5475.

7.) M. R., Caira, V. J. Griffith and B. van Oudtshoorn, *J. Inclusion Phenom. Mol. Recognit.*, 1998, 32, 461

8.) A. Chiesi-Villa, C. Rizzoli, G. Amari, M. Delcanale, E. Rendenti and P. Ventura, *Supramolecular. Chem.*, **1998**, 10, 111.

9.) M. R. Caira, V. J. Griffith, L. R. Nassimbeni and B. van Oudtshoorn, *J. Chem. Soc., Chem. Commun.*, **1994**, 1061.

10.) K. Harata, *Chem. Rev.*, **1998**, 98, 1803.

11.) W. Saenger, J. Jacob, K. Gessler, T. Steiner, D. Hoffman, H. Sanbe, K. Koizumi, S. M. Smith and T. Takaha, *Chem. Rev.*, **1998**, 98, 1787

12.) W. Saenger, in *Inclusion Compounds*, ed. J. L. Atwood, J. E. D. Davies and D. D. MacNicol, Academic Press, London, **1984**, Vol. 2, Chapter 8.

13.) K. Harata, in *Inclusion Compounds*, ed. J. L. Atwood, J. E. D. Davies and D. D. MacNicol, Oxford University Press, London, **1984**, Vol. 5, Chapter 9.

14.) K. Harata, *Bull. Chem. Soc. Jpn.*, **1987**, 60, 2763.

15.) K. Lindner and W. Saenger, *Carbohydr. Res.*, **1982**, 99, 103.

16.) G. R. Brown, M.R. Caira, V. J. Griffith, L. R. Nassimbeni and M. C. Van Oudtshoorn, **SA Pat. Appl. ZA 95/1608**, 27 February 1995.

17.) L. J. Penkler, D. V. Whittaker and L. A. Glintekamp, **PCT Int. Appl. WO 97 18,245** (Cl. C08B37/16), 22 May 1997, 31 pp.

18.) M. R. Caira, V. J. Griffith, L. R. Nassimbeni and M. C. B. Van Oudtshoorn, **SA Pat. Appl. ZA 93/7480**, 10 October 1993.

19.) L. J. Penkler, L. A. Glintekamp, D. G. M. Nicholson and M. C. Van Oudtshoorn, **PCT Int. Appl. WO 96 14,839** (Cl. A61K31/19), 23 May 1996, 20 pp.

20.) L. J. Penkler and D. R. Dodds, **SA Pat. Appl. ZA 99/2097**, 16 March 1999.

Appendix A

The files with the extension SFT contain tables of observed and calculated structure factors as F_o and F_c.

The files with the extension FCF contain lists of the observed and calculated structure factors as F_o^2 and F_c^2.

Disk 1 :	BROBCD.SFT	PHEBCD.SFT
	DIABCD.SFT	CYCGCD.FCF
Disk 2 :	ACEBCD.SFT	CYCBCD.FCF

Appendix B

The files with the extension LST contain tables of atomic coordinates and isotropic displacement parameters, bond lengths, bond angles, torsion angles, anisotropic displacement parameters, hydrogen coordinates and isotropic displacement parameters, least-squared planes and non-bonded contacts.

The files with the extension CIF are the Crystallographic Information Files produced by the PARSTCIF utility of PARST95.

The files with the extension RES are SHELX-type files included for visualisation purposes.

Disk 1 :	ACEBCD.LST	ACEBCD.CIF	ACEBCD.RES
	BROBCD.LST	BROBCD.CIF	BROBCD.RES
	PHEBCD.LST	PHEBCD.CIF	PHEBCD.RES
	DIABCD.LST	DIABCD.CIF	DIABCD.RES
Disk 2 :	CYCBCD.LST	CYCBCD.CIF	CYCBCD.RES
	CYCGCD.LST	CYCGCD.CIF	CYCGCD.RES

Note : The following atoms codes have been changed for the computer files: All structures: O6`→O7; ACEBCD: A`→B; BROBCD: A`→C, B`→D; PHEBCD: B`→D; DIABCD: A`→C, B`→D.

HOST AND GUEST MOLECULES

ACE

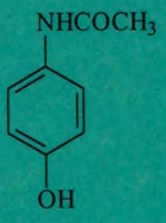

BRO

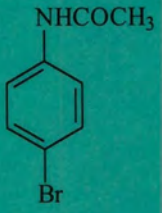

PHE

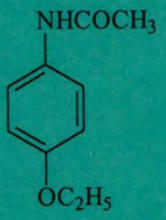

DIA

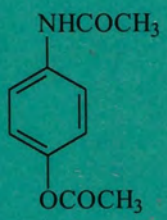

CIM

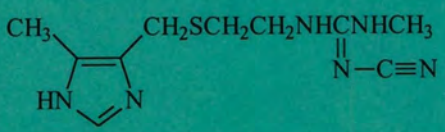

SAL

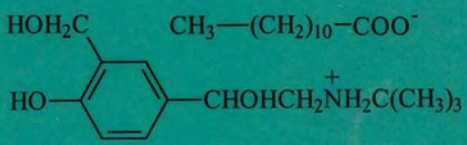

FAM

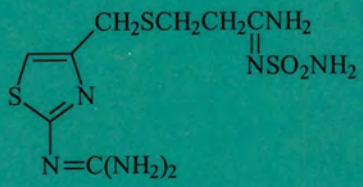

CYC

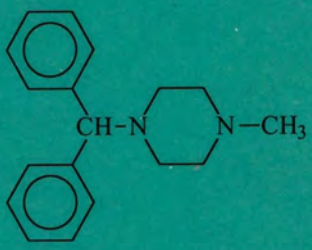

RAN

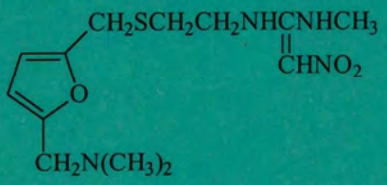

β-CD

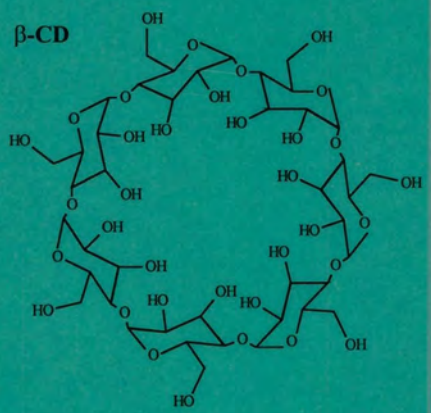

γ-CD

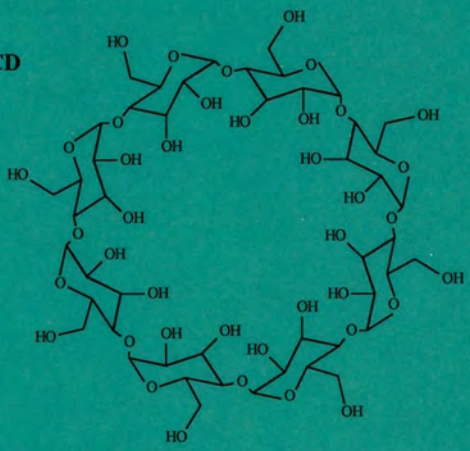

INCLUSION COMPLEXES

HOST	GUEST	H:G	CODE
β-CD	ACE	1 : 1	ACEBCD
	BRO	1 : 1	BROBCD
	DIA	1 : 1	DIABCD
	PHE	1 : 1	PHEBCD
	CIM	2 : 1	CIMBCD
	FAM	2 : 1	FAMBCD
	RAN	2 : 1	RANBCD
	CYC	4 : 3	CYCBCD
γ-CD	CIM	3 : 2	CIMGCD
	FAM	3 : 2	FAMGCD
	RAN	3 : 2	RANGCD
	CYC	3 : 1	CYCGCD

ABBREVIATIONS

ACE	:	Acetaminophen
BRO	:	*p*-Bromoacetanilide
DIA	:	Diacetamate
PHE	:	Phenacetin
CIM	:	Cimetidine
FAM	:	Famotidine
RAN	:	Ranitidine
SAL	:	Salbutamol laurate
CYC	:	Cyclizine
β-CD	:	Beta-cyclodextrin
γ-CD	:	Gamma-cyclodextrin
HP-β-CD	:	Hydroxylpropyl-beta-cyclodextrin